Hughes, Michael Glen
Ph.D; MARCH, 1990.

A Field Study Of Wave - Sediment Interaction In The Swash Zone

Michael G. Hughes

A thesis submitted in fulfilment
of the requirements for the degree of
Doctor of Philosophy

University of Sydney

March, 1989

ABSTRACT

The non-linear shallow water equations are theoretically capable of describing many features of wave motion in the coastal zone. Two sets of solutions exist for the study of swash. The first describes waves which contain bores. The second describes only bore-free waves. Historically, the bore solutions are used to predict swash from breaking waves, and the bore-free solutions are used to predict swash from non-breaking waves. Despite the voluminous literature reporting the application of the theory to idealized swash problems, virtually no study has examined the theory's potential for describing swash on natural beaches.

A framework incorporating the conventions of the shallow water theory is developed to direct the study of natural swash. The assumptions of the theory limit its application to swell wave environments where swash collisions are minimal. Field measurements from such an environment, representing a range of morphologies and sand sizes, are used to test the theory. Least squares regression models fitted to the data match well with most of the theoretical predictions for the swash lens. The following relationships for bore uprush were confirmed:

1) locus of shoreline displacement through time is parabolic,
2) maximum swash height as a function of initial shoreline velocity is quadratic,
3) mean shoreline velocity as a function of initial shoreline velocity is linear, and
4) maximum swash depth as a function of distance is quadratic.

The bore-free solutions could not be compared with the non-breaking waves measured here, as they did not satisfy the theoretical non-breaking criterion. Measurements of swash from non-breaking waves were found to match closely with the theoretical bore solutions. Moreover, no statistical difference between the uprush of bores and non-breaking waves could be discerned from the data. It is hypothesized that some non-breaking waves may contain a virtual bore. A swash continuum is proposed, where the bore and bore-free solutions of the theory describe the end-members. The bore solutions

seem to describe much of the incident swash existing along this continuum, including the non-breaking waves measured here.

The qualitative similarity between the theory and the field data indicates that the gross flow behaviour of the swash is well described. However, the magnitudes of the data are found to be consistently over-estimated by the theory. The nature of this discrepancy suggests the effects of energy dissipation over a natural bed, which are not considered in the inviscid solutions. The equations for swash are re-derived using the original approach of the theory and including a bed shear stress term. The magnitude of the friction factor required to match the data can be suitably predicted using an existing model for shear stress in sheet flow conditions. The effects of infiltration could not be investigated using the available data. It is speculated that they may be second in importance to bed shear, at least for the experimental conditions reported here.

A morphodynamic model is developed to predict natural beach face slopes. The model combines an approximate method for calculating water velocities in the swash with Bagnold's (1963; 1966) sediment transport theory. Reasonable estimates of the sediment flux during the uprush can be obtained from the model. Before realistic estimates of the sediment flux during the backwash can be obtained, a more accurate description of the water velocity than is presently available is needed. Observations made during the course of this study suggest that further research into the effects of infiltration and the backwash bore may be useful in this regard.

ACKNOWLEDGEMENTS

On the completion of this study I extend my thanks to Dr. Peter Cowell, my supervisor, for his guidance throughout the writing of this thesis. In addition, a special vote of thanks is extended to my colleagues Dave Hanslow, Bill Hall, and Marie Ferland, whom provided much companionship in the office and the field throughout many years of studying beaches.

Valuable support during the field programme was provided by Dave Hanslow, Marie Ferland, Bill Hall, Fiona Kotvojs, and Andrew Rawson. Thanks also to Graham Lloyd, Mick Price, Elizabeth Naish, and Nerida Hunt who all contributed in some way to the construction of the instrumentation. The design of the circuitry was provided by John Baird of the Water Resources Laboratory, University of New South Wales.

Additional data used in this study was provided by Troels Aagaard (University of Copenhagen). Various consultations with Stephen Glasby and Barbara Boczar-Karakiewicz (University of Quebec) were very instructive.

Financial support for this study was provided through a Commonwealth Postgraduate Research Award.

I dedicate this thesis to my wife Robin, in warm appreciation for her encouragement, patience, and support throughout those years of toil.

CONTENTS

LIST OF TABLES

LIST OF FIGURES

NOTATION

A_s	cross-sectional area of swash lens [m^2].
B	bore type parameter [*].
C	integration constant.
c	wave crest velocity [m s^{-1}].
D	mean grain diameter [m].
d	water depth at toe of beach face [m].
df	degrees of freedom [*].
E_f	mean energy flux [kg m s^{-3}].
e_b	bedload transport efficiency.
F	defined in (B.11).
f	Darcy-Weisbach friction factor [*].
G	defined in (B.11).
g	acceleration due to gravity [m s^{-2}].
H	wave height [m].
H_b	wave breaker height [m].
h	still water depth [m].
h_i	starting water depth upstream of bore front [m].
h_o	water depth upstream of bore front [m].
h_1	water depth downstream of bore front [m].
h_s	swash depth [m].
$h_{s(max)}$	maximum swash depth [m].
$h_{s*(max)}$	non-dimensional maximum swash depth [*].
h_δ	swash depth in the leading edge [m].
I_b	immersed weight of transported sediment [kg].
I_r	Iribarren number [*].
i_b	immersed weight sediment transport rate [kg s^{-1}].
J_o	zero-order Bessel function.
K_s	total equivalent bed roughness length (movable bed) [m].
k	proportionality constant between u_o and $\sqrt{(gH_b)}$ [*].
k_s	equivalent bed roughness length [m].
$k_{s(f)}$	equivalent bed roughness length (fixed bed) [m].
$k_{s(m)}$	equivalent bed roughness length (movable bed) [m].
L_s	maximum swash length [m].

L_o	deep water wave length [m].
M	Mach number [*].
m	mass of leading 'fluid element' [kg].
n	number of data points.
Q_s	swash discharge [$m^3\ s^{-1}$].
r	sample correlation coefficient.
S	ratio of sediment to fluid density [*].
T	wave period [s].
T_d	duration time of flow down-slope [s].
T_u	duration time of flow up-slope [s].
t	time [s].
t_m	time when $h_{s(max)}$ occurs [s].
$t_{(max)}$	time when maximum shoreline displacement occurs [s].
t_*	non-dimensional time [*].
U_b	bore velocity [$m\ s^{-1}$].
U_s	shoreline velocity [$m\ s^{-1}$].
$\bar{U}_s$	mean shoreline velocity; averaged over L_s [$m\ s^{-1}$].
U_{s*}	shear velocity of the shoreline [$m\ s^{-1}$].
u	horizontal water velocity [$m\ s^{-1}$].
u_b	water velocity immediately behind the bore [$m\ s^{-1}$].
u_o	initial shoreline velocity [$m\ s^{-1}$].
u_s	horizontal water velocity in the swash [$m\ s^{-1}$].
u_*	shear velocity [$m\ s^{-1}$].
V_s	swash volume per unit width of beach [$m^3\ m^{-1}$].
w_b	bore width [m].
X_s	shoreline displacement [m].
X_{s*}	non-dimensional shoreline displacement [*].
x	distance [m].
x_m	position of the mid swash relative to the initial shoreline [m].
x_*	non-dimensional distance [*].
Z	elevation above the bed [m].
Z_s	maximum swash height [m].
z	elevation above still water level [m].
z_o	bed roughness length [m].
α	constant in (5.12) [*].
β	beach slope [rad].
Γ	rate of wave energy dissipation [$kg\ m\ s^{-2}$].
γ	constant of proportionality in (2.4) [*].

δ	length of leading edge [m].
δ_s	thickness of sheet flow layer [m].
ϵ	surf scaling parameter [*].
η	water surface elevation relative to still water level [m].
η_b	bore height [m].
η_s	water surface elevation in the swash zone [m].
θ	Shield's parameter [*].
θ'	skin friction Shield's parameter [*].
θ_c	critical value of Shield's parameter for grain motion [*].
λ	characteristic variable.
ρ	density of seawater [kg m^{-3}].
σ	characteristic variable.
τ	shear stress [N m^{-2}].
Φ	internal friction angle of sediment [rad].
ϕ	potential [m s^{-1}].
Ω	fluid power [N m^{-1} s^{-1}].
ω	radian wave frequency [s^{-1}].

N.B. Unless otherwise indicated, the units used throughout this thesis are consistent with those shown in the square brackets. An asterisk indicates the parameter is non-dimensional.

CHAPTER 1
INTRODUCTION

1.1 Introduction

Wave action on the beach face provides the principle mechanism for sediment exchange between the sub-aqueous and sub-aerial zones of the beach system. Although the fluid mechanics and morphological features of the beach face have been widely studied, very little is known about their interaction in nature. The purpose of this thesis is to examine the interaction of waves and sediment in the swash zone of natural, sandy beaches.

Wave induced changes in the shoreline position relative to the still water level are known as run-up and consist of two components. The first is a quasi-steady super-elevation of the mean water level termed set-up, and the second includes oscillations about this set-up level termed swash (Van Dorn, 1976; Guza and Thornton, 1982). Previously, the approach to studying run-up has been to examine these two phenomenon separately in an effort to simplify the problem (*e.g.* Van Dorn, 1976; Guza and Thornton, 1981 and 1982; Holman and Sallenger, 1985). This study adopts a similar approach, and concentrates on the study of swash.

Swash oscillations occur over a range of frequencies, but can generally be grouped into three categories according to the most energetic wave frequency operating in the surf zone. The first category includes low frequency infragravity waves, believed to arise from non-linear interactions present in the incident wave train (Longuet-Higgins and Stewart, 1964; Gallagher, 1971). Field studies have shown that infragravity waves can be either leaky-mode standing waves (*e.g.* Suhayda, 1974), standing edge waves (*e.g.* Holman and Bowen, 1984), or progressive edge waves (*e.g.* Huntley *et al.*, 1981). Swash motions associated with these waves have periods of 30-300 s (Holman, 1981). The second category includes the higher frequency sub-harmonic edge waves, that sometimes develop due to the reflection and resonance of incident waves (Guza and Davis, 1974). Swash oscillations associated with these waves have periods twice the incident wave period. The third category of swash oscillations are associated directly with the uprush and backwash of incident waves. These occur at frequencies

typically between 5 and 15 s. Previous field experiments have generally concentrated on the first two categories of swash motion (Section 1.3). Since field experiments measuring incident swash are relatively few, this study is concerned with the third category.

The incident swash cycle begins when a wave arrives at the initial shoreline, at which time the shoreline is set in motion and becomes the leading edge of the swash lens (Fig. 1.1). The uprush phase of the swash cycle is completed when the shoreline has climbed to its point of maximum landward displacement. Following the uprush phase, the shoreline begins to return seaward, thus initiating the backwash phase. The backwash phase is completed when the shoreline returns to its initial position. The elevation of the initial shoreline varies with the passage of infragravity waves and tides. Its elevation over a single swash cycle can be regarded as constant however, since the period of these waves are at least an order of magnitude larger than the incident waves.

1.2 Aims And Scope

The major aim of this study is to examine the behaviour of swash on natural, sandy beaches. To achieve the study aim, it is first necessary to find a satisfactory description of the underlying physics of swash. This would enable the apparent effects of a rough and permeable beach to be estimated from field data (Section 1.4). A specific aim of this study is to examine the suitability of the non-linear shallow water theory for the description of swash on natural beaches. Due to the limiting assumptions of this theory, it cannot be expected to provide a complete description of the flow (Section 1.3). However, if it is found to provide a satisfactory description within the imposed limits, then it can be used to quantify the apparent effects of friction and infiltration. A further aim is to refine the theory to include these effects.

Since it is the purpose of this thesis to improve the quantitative description of swash so that the morphological behaviour of beaches can be better understood, the refined theory is applied to the problem of modelling equilibrium beach slopes. This application is only meant to demonstrate the possibility of the theory in this area. It is beyond the feasibility of this study to also provide field data for testing the model results.

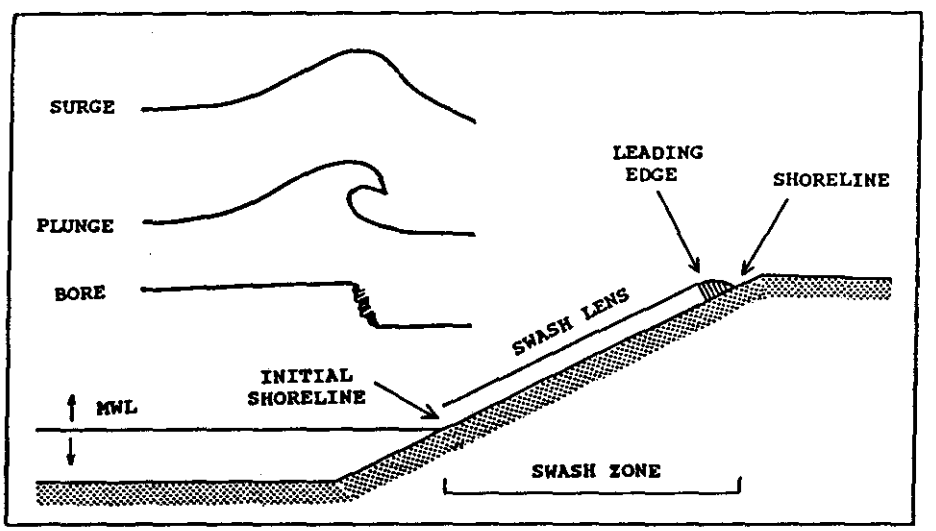

Figure 1.1: Definition of terms that relate to swash processes occurring on a natural beach.

The field data presented in this study is restricted to microtidal, sandy beaches where a clearly distinguishable beach face and swash zone exist (*e.g.* Fig. 1.1). This excludes low gradient, planar beaches that are of the 'dissipative type' described by Wright *et al.*, (1982). This exclusion can be justified on both physical and experimental grounds. It has been shown on these beaches that swash oscillations associated with incident waves are negligible, and consequently have little influence on the morphology. Furthermore, the zone of swash activity on these beaches periodically shifts its position tens of metres laterally, making it difficult to obtain measurements using instruments fixed in space. The exclusion of these beaches does not limit the geographic range of conditions studied here, since each of the beach types for which incident swash exists are examined (Section 2.3).

1.3 Justification and Background

Miche (1951) hypothesized that waves in the surf zone contain both progressive and standing components. In his model he assumed that only the standing component has a finite amplitude at the shoreline; the progressive component is completely dissipated through wave breaking. If this is a reasonable approximation of nature, then the swash amplitude must be proportional to the standing wave amplitude. If breaking is present, then the standing wave amplitude is assumed equal to the maximum that would occur without breaking. The model predicts therefore, that increases in the incident wave height after breaking will produce no change in the incident swash height (*i.e.* the swash is saturated).

In support of Miche's model, Guza and Bowen (1976) showed that standing waves can potentially cross a turbulent surf zone, and Guza and Thornton (1982) provide strong evidence for the saturation of incident swash on a planar, low gradient beach. The complete dissipation of incident wave energy and the saturation of swash is not universal however. Laboratory and field experiments conducted on moderately steep, bar-trough beaches frequently show that wave height in the surf zone can be independent of water depth (*e.g.* Horikawa and Kuo, 1966; Mizuguchi, 1980; Wright et al., 1986). Furthermore, numerical models for bore interaction demonstrate that wave height can ultimately be several times the water depth (Peregrine, 1974a; Bradshaw, 1982). Water surface elevation and velocity spectra measured immediately seaward of the shoreline show significant amounts of energy exist at incident wave frequencies, over a large range of beach morphologies (Bradshaw, 1980; Wright

and Short, 1984; Wright *et al.*, 1986). On many of these beaches cursory observation will demonstrate that the shoreline oscillations associated with incident waves often span the entire beach face, thus suggesting their importance for transporting sediment in this zone.

Most of the existing field studies that focus on swash have directed their attention to infragravity swash. This has been the result of a strong research thrust aimed at establishing the conditions and mechanisms for edge wave generation (*e.g.* Huntley *et al.*, 1977; Bowen and Huntley, 1984; Holman and Bowen, 1984). One of the fundamental requirements for the occurrence of edge waves is the reflection of wave energy from the beach (Guza and Davis, 1974). Since infragravity waves are sufficiently long to be reflected by most typical beach slopes, they are a particularly useful source of information for the study of edge waves. There is little doubt that infragravity waves, if they are of the edge wave type, are responsible for significant changes in morphology during storm events (*e.g.* Holman *et al.*, 1978; Wright, 1980). The resonant nature of these waves causes a substantial increase in elevation of the zone of shoreline activity. Although edge waves are becoming widely studied, their geographic distribution remains to be established. Swash processes related to incident waves are an almost universal phenomena however, and still require further research.

Applied mathematicians working in the field of fluid mechanics have made significant contributions to the study of the underlying physics of swash. Carrier and Greenspan (1958) showed analytically, that the non-linear shallow water theory can describe a number of wave forms capable of climbing a beach without breaking. By proving a set of lemmas and corollaries, Shen and Meyer (1963) also used this theory to obtain solutions for the run-up of a breaking wave. Subsequent researchers have examined the results of this analytical work numerically (*e.g.* Freeman and LeMehaute, 1964; Amein 1966; Gjevik and Pedersen, 1981; Pedersen and Gjevik, 1983), experimentally in wave flumes (*e.g.* Kishi and Saeki, 1966; Miller, 1968; Synolakis 1987a and 1987b), and in the field (Waddell, 1973; Bradshaw, 1982). It should be noted that the field studies are limited, as far as the author is aware, to the two studies listed. They report data from only three experiments, and are restricted to swash following breaking waves.

The shallow water theory provides a particularly attractive framework for the study of swash, since it appears to predict the uprush of both breaking

and non-breaking waves. The basic description of swash derived from the theory assumes however, that the swash is an inviscid fluid moving on a smooth, impermeable beach (see Meyer and Taylor, 1972). The theory is therefore unlikely to provide a complete description of swash on natural beaches. An important area of research requiring further investigation, is the effect of flow resistance due to a rough and permeable bed. These effects have been modelled numerically (*e.g.* Freeman and LeMehaute, 1964; Kirkgoz, 1981; Packwood, 1983) and measured in a number of laboratory experiments (*e.g.* Kishi and Saeki, 1966; Miller, 1968; Kirkgoz, 1981). However, no studies to date have attempted measuring this resistance using field experiments.

The process linking waves and morphological patterns involves the transfer of fluid momentum to the movable bed. The transfer is achieved through a flow induced shear stress at the bed. The magnitude of this stress is a function of the flow characteristics, and the bed roughness and porosity. For this reason, the measurement of flow resistance in the swash zone is expected to provide important insight into the mechanics of morphological change on beaches.

The literature reporting studies of beach face morphology is extensive. Investigations into the relationship between grain size and slope of the primary beach profile (*e.g.* Bagnold, 1940; Bascom, 1951, Wiegel, 1964; Sunamura, 1984) are supplemented by studies of the secondary morphology, such as berms (*e.g.* Bagnold, 1940; Bascom, 1951; Sunamura, 1975) and beach steps (*e.g.* Matsunaga and Honji, 1980 and 1983; Takeda and Sunamura, 1983; Hughes and Cowell, 1987). Patterns of grain size sorting on the beach face have also been studied (*e.g.* Fox *et al.*, 1966; McLean and Kirk, 1969; Richmond and Sallenger, 1984), together with processes of sediment transport in the swash zone (*e.g.* Nelson and Miller, 1974; Richmond and Sallenger, 1984; Howd and Holman, 1987). Although all of these studies allude to the physical processes producing the morphology, with a few notable exceptions (Nelson and Miller, 1974; Richmond and Sallenger, 1984; Howd and Holman, 1987), the direct application of swash mechanics to account for the morphology are rare.

1.4 Approach and Chapter Summary

The non-linear shallow water theory is used to examine the underlying physics of swash, since it is the most appropriate of the available theories for studying wave motion near the shoreline (Section 2.2). This approach necessarily

involves the analysis of swash on a wave by wave basis. At the present level of understanding, there is no method available to extend the results of this single wave analysis to the spectrum of swash motion that occurs naturally. However, Meyer and Taylor (1972) believe that the interaction between swash cycles introduces no new physics to the problem. This suggests that examining processes occurring over a single swash cycle will provide a strong basis for an informed study of swash spectra in the future.

The conceptual framework for this study is presented in Chapter 2. It is shown that incident swash occurs following one of three wave conditions: the arrival of a surf zone bore, plunging breaker, or surging wave at the initial shoreline. The morphology associated with these input waves is classified into three beach types, which are distinguished by their wave conditions immediately seaward of the initial shoreline. It is a premiss of this study, that the wave conditions immediately seaward of the shoreline provide the initial conditions for the swash. It is far too ambitious at this stage, to propose a study of the relationship between swash and waves seaward of the inner surf zone. A theoretical description of swash following breaking and non-breaking waves is presented, together with the underlying assumptions, in the remainder of Chapter 2.

Chapter 3 describes the field sites, instrumentation, and experimental design used to collect data. The sites and methods are chosen to provide data suitable for analysing single swash cycles. A description of the data analysis techniques is provided so that the results presented in Chapters 4 and 5 can be interpreted appropriately.

Field measurements of wave height, initial shoreline velocity, mean shoreline velocity, shoreline displacement, swash depth, swash height, and water surface profiles in the swash zone are presented in Chapter 4. The theoretical predictions presented previously (Chapter 2) are tested using these data for a range of environmental conditions. Since the theory neglects dissipation of energy in the fluid boundary layer, its ability to describe natural swash is expected to be limited. It is found that although the bi-variate relationships suggested by the data have the same functional form as those predicted by theory, the theory consistently over-estimates the magnitude of the data. The qualitative correspondence between theory and data is assumed to indicate that much of the flow mechanics are adequately described by the theory. Several

lines of evidence are then presented to suggest that the discrepancy is due to energy dissipation not previously accounted for.

In Chapter 5, the quantitative discrepancies found between theory and data are used to study the effects of flow resistance in the swash zone. Given that the shallow water theory provides a suitable model for much of the flow behaviour (Chapter 4), the original equations for swash are re-derived to include the effects of energy dissipation in the bed boundary layer. Direct measurements of bed shear and infiltration are prohibitively difficult to obtain in the field. To compare these equations with the field data available, the apparent magnitude of friction and infiltration are assumed to be equal to the quantitative discrepancy found in Chapter 4. This apparent resistance is modelled empirically by a friction factor predicted for the swash zone. While it is recognized that flow resistance also includes infiltration, the data presented only appears to resolve the contribution from bed shear. The refined theory for swash on a natural beach is found to compare well with the data collected in this study.

Chapter 6 is concerned with the morphological implications of the results presented in Chapters 4 and 5. The equations for swash (including friction) are combined with Bagnold's (1963; 1966) approach to sediment transport, to provide a morphodynamic model used for predicting the slope of beach face profiles. At present the model is found to be lacking. However, its poor performance relates to phenomena not yet understood rather than any inadequacy of the theory within its present limitations. Moreover, the application of the model is found to provide some valuable insight into the importance of infiltration, which could not be obtained from the field techniques.

Chapter 7 summarizes the points of discussion raised in previous Chapters, and presents the conclusions of the study.

CHAPTER 2
CONCEPTUAL FRAMEWORK FOR STUDYING THE SWASH ZONE

2.1 Introduction

This Chapter defines in some detail, and within the conventions of the literature, the problem under investigation in this study. It was indicated in Section 1.3 that the study of swash has advanced in several disciplines, with a wide range of objectives pursued. The following discussion integrates much of the multi-disciplinary literature into a framework which will guide the analysis of field data presented in later Chapters. The framework developed below presents no new material, but does provide an original synthesis of the literature designed specifically to address the aims of this study (Section 1.2). The focus of the discussion are those facets of the non-linear shallow water theory which describe swash hydrodynamics, and which are necessary to further the study of beach morphology. The discussion includes both the physical justification, and assumptions of the theory. Although the shallow water theory has occasionally been used in field studies of swash, the rationale and scope for application of this theory that is contained in the following Sections, has generally been absent (Section 1.3).

It is shown below that there are strong contrasts in the predicted flow following breaking and non-breaking waves. Hence, conditions immediately seaward of the initial shoreline are particularly relevant to this study. A brief description of breaker types, and a quantitative method for distinguishing them in the field is presented in Section 2.2. It is demonstrated in Section 2.3 that the wave and morphology combinations which influence the swash can be classified according to three representative *Beach Types*. These *Types* represent most situations where incident swash can be considered important. The three *Beach Types* presented are distinguished according to the breaker types found immediately seaward of the initial shoreline.

Sections 2.4 and 2.5 present the theoretical equations which describe swash following breaking and non-breaking waves respectively. In the presence of breaking waves, wave transformation across the surf zone determines the final wave kinematics at the shoreline. Whereas in the presence of non-breaking

waves, wave reflection determines the conditions at the shoreline. Wave transformation and wave reflection are therefore discussed as precursors to the theoretical descriptions of swash.

2.2 Waves Approaching The Beach

The first-order, non-linear shallow water equations (SWE) are most appropriate for modelling two dimensional water motion in the vicinity of the beach (Stoker, 1957; Peregrine, 1972). Following the notation used in Figure 2.1, the depth integrated equations describing conservation of mass and momentum are

$$\frac{\partial[u(\eta+h)]}{\partial x} + \frac{\partial \eta}{\partial t} = 0 \qquad (2.1)$$

and

$$\frac{\partial u}{\partial t} + u\frac{\partial u}{\partial x} + g\frac{\partial \eta}{\partial x} = 0 \qquad (2.2)$$

(Stoker, 1957); u is the horizontal water velocity, and g is the gravitational acceleration constant. The SWE assume the following.

1) The water surface slope is not much larger than the bed slope (*i.e.* the wave is long).

2) The water pressure is hydrostatic.

3) The vertical distribution of horizontal water velocity is uniform.

4) The fluid is inviscid, incompressible, and irrotational.

Progressive waves that are described by the SWE steepen as they shoal towards the beach (Greenspan, 1958). Consequently, the resultant change in water particle acceleration and surface slope violate the first three assumptions. Analysis of the wave motion beyond the point where the water surface slope becomes steep usually involves the *ad hoc* inclusion of bore theory (Section 2.4.3). The steep wave face physically indicates bore inception, and is frequently followed by wave breaking. Some bore-free solutions of the SWE have been examined by Carrier and Greenspan (1958), however, the physical conditions under which these occur are limited (Greenspan, 1958; Meyer and Taylor, 1972; Sections 2.5.2, 4.4.2, and 4.5).

It should be noted that bore inception before breaking is not often addressed in the experimental literature. The analysis is usually restricted to turbulent bores present inside the surf zone. Much of the discussion in this

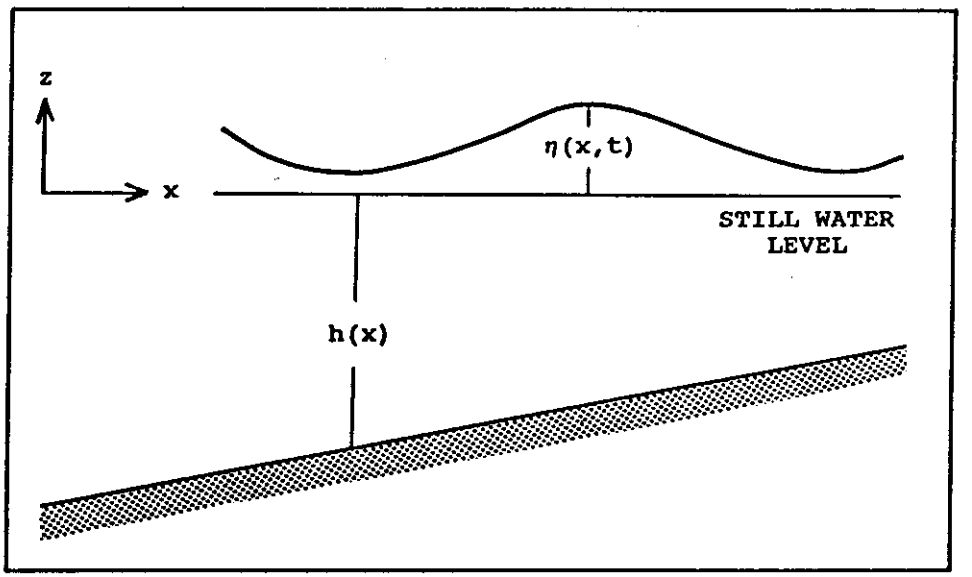

Figure 2.1: Definition sketch showing notation used in the non-linear shallow water equations.

Chapter is also directed towards surf zone bores, since they are most frequently associated with swash motion. However, the understanding that several wave forms can be represented by a bore may have important implications for explaining swash on steep beaches (Section 4.5).

Wave breaking in shallow water begins when either the water velocity exceeds the wave celerity, or the wave face becomes vertical (Ippen and Kulin, 1954; Greenspan, 1958). Empirical studies indicate that the manner in which a wave breaks depends on factors influencing the rate of growth in slope asymmetry; such as wave steepness, and beach slope (see Galvin, 1972). Four common breaker types are shown in Figure 2.2 that represent single points on a continuum of possibilities. Several parameters exist to quantitatively distinguish between these breaker types (see Cowell, 1982 for review), but the most commonly used is the Iribarren number I_r. I_r can be written as

$$I_r = \frac{\tan \beta}{\sqrt{(H_b/L_o)}} \qquad (2.3)$$

(Battjes, 1974), where β is the beach slope, and L_o is the deep water wave length ($gT^2/2\pi$; T is the wave period). The range of I_r associated with each breaker type is shown in Figure 2.2. These ranges must be considered approximate, since they are based on laboratory studies of breakers over planar beach slopes (see Battjes, 1974).

Consideration of (2.3) with Figure 2.2 shows that spilling breakers favour conditions where the beach slope is small, and wave steepness is large. If the wave steepness is reduced or the beach slope increased, the mode of breaking progresses through the plunging and collapsing types towards the surging wave example. This behaviour suggests that breaker types will be associated with particular surf zone morphologies. It is a supposition of this study, that the combination of breaker type and morphology close to the beach defines the initial conditions for the swash.

2.3 Beach Types

Complex three-dimensional variations in morphology and swash flow often occur along a natural beach due to the presence of bars, cusps, and rip channels (Wright and Short, 1984). It can be assumed as a first approximation however, that this three-dimensionality is a spatial along-shore summation of the two-dimensional cases shown in Figure 2.3. This assumption simplifies the

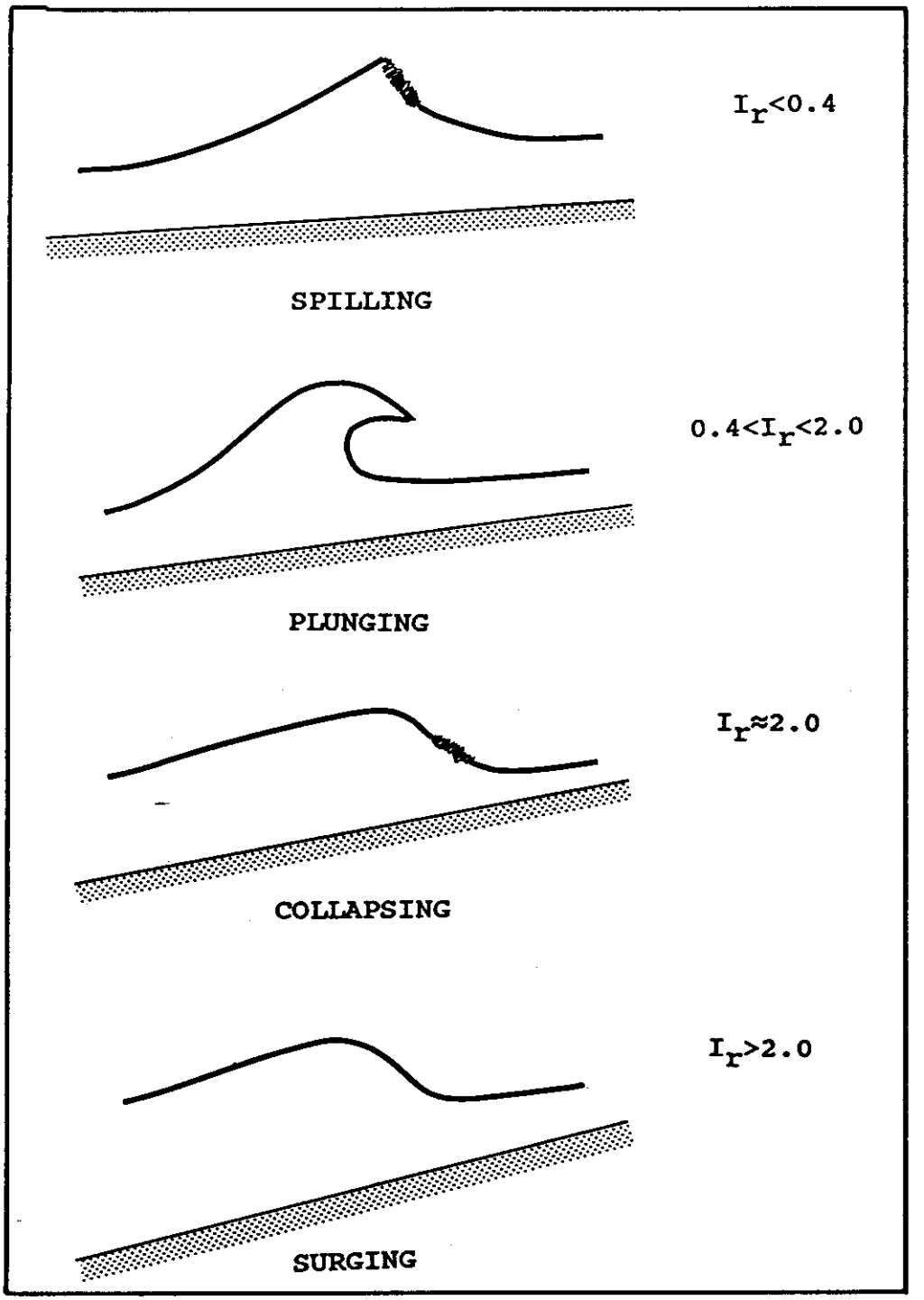

Figure 2.2: Breaker type classification showing water surface profile and I_r value for each type (After Galvin, 1972; Battjes, 1974).

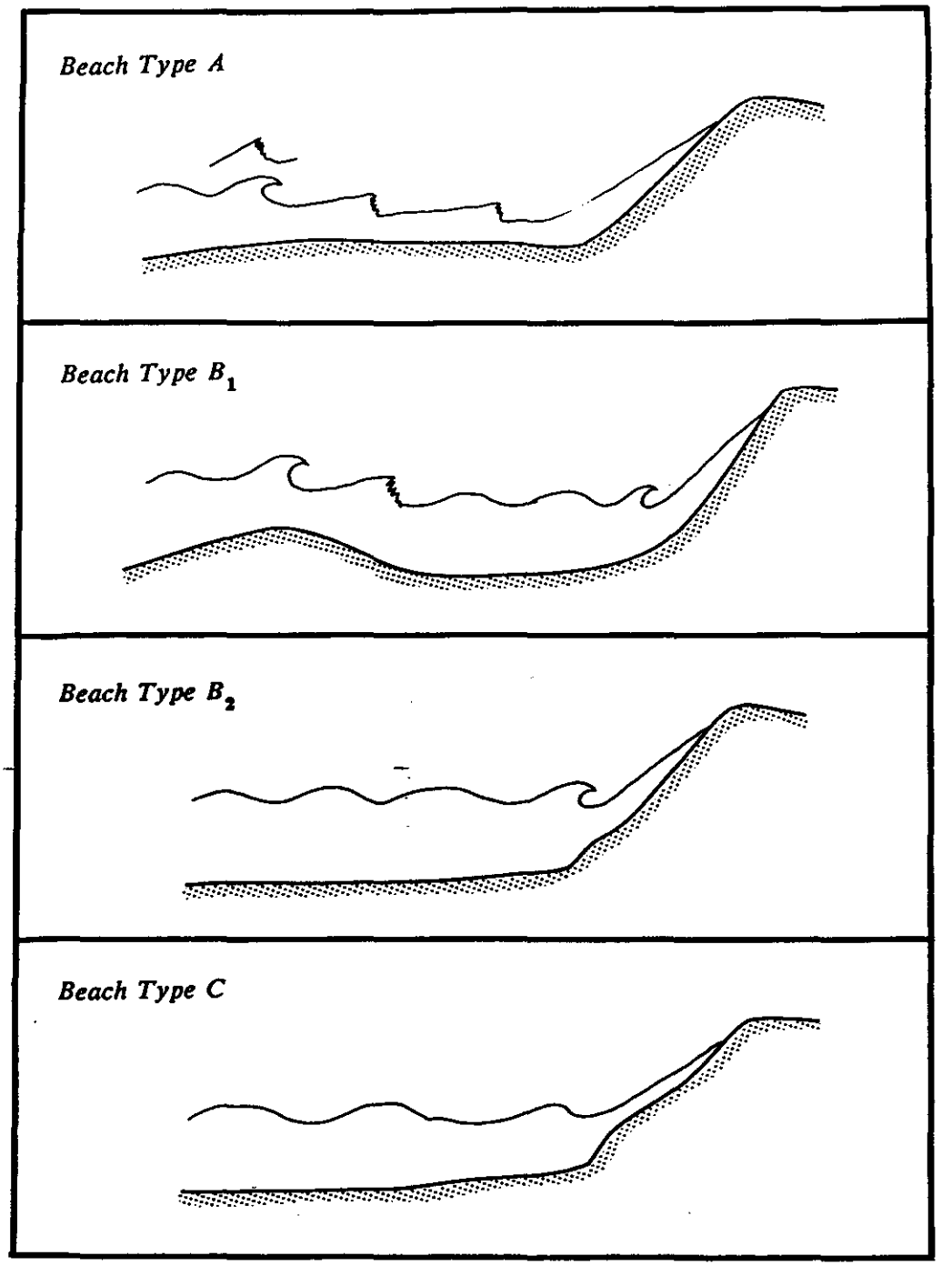

Figure 2.3: Schematic showing morphodynamic details of the three major *Beach Types* commonly referred to in this study.

collection of field data, and permits the application of the two-dimensional theory presented below (Sections 2.4 and 2.5). It does not permit the study of swash in the presence of oblique wave approach, or rhythmic topography with wave lengths of less than about 10 m. For the swell wave environment considered here, this does not pose significant limitations (Section 3.2). The environmental conditions where this assumption is over-restrictive are discussed further in Section 7.2.

The field experiments reported in this study were restricted to the three *Beach Types* shown in Figure 2.3, as they are believed to represent the full range of conditions where incident swash is considered important. *Beach Type A* shows the situation where a welded bar or shallow inner surf zone exists, and waves propagate toward the shoreline as surf zone bores. *Beach Type* B_1 shows the situation where a wave initially breaks over the bar, and then reforms in the trough before plunging again at the shoreline. *Beach Type* B_2 is an equivalent case at the shoreline only the offshore bar is absent. *Beach Type C* shows the situation where waves do not break, but surge up the beach face. It is worth noting that if an unusually large wave occurs on *Beach Type* B_1, it can cross the surf zone as a bore, thus creating similar conditions to those found on *Beach Type A*. Measurements representative of more than one *Beach Type* may therefore occur during a single experiment.

Since I_r distinguishes between breaker types and their associated morphology (Section 2.2), it follows that this parameter is also useful for distinguishing between the *Beach Types* shown in Figure 2.3. Ranges of I_r associated with each *Beach Type*, inferred from the discussion of breaker types contained in Battjes (1974) and Section 2.2, are listed in Table 2.1.

TABLE 2.1
RANGE OF I_r EXPECTED FOR EACH *BEACH TYPE*

Beach Type	Iribarren number
A	$I_r \leq 0.4$
B_1	$0.4 < I_r < 2.0$
B_2	$0.4 < I_r < 2.0$
C	$I_r > 2.0$

As mentioned previously these values are approximate, and are only presented here to show that the *Beach Types* can be sensibly distinguished by a conventional parameter that combines features of both the hydrodynamics, and the morphology. The value of I_r on *Beach Type A* is unlikely to be much less than 0.4, otherwise the wave will remain as a spilling breaker, rather than developing into a surf zone bore. Such a situation precludes the presence of swash at incident wave frequencies (Section 2.4.2). Also, for the higher energy *Beach Type* B_1, values of I_r are expected to be smaller than those present on *Beach Type* B_2.

The following comparison between the *Beach Types* shown in Figure 2.3 and the beach states described by Wright and Short (1984), indicates that the former are very representative of the range of field conditions where incident swash is significant. Wright and Short's beach state model is essentially a classification of the gross, beach-surf zone morphologies typical of a high wave energy, sandy coastline. The model includes three major beach states and four sub-states. The first is their 'dissipative beach state', which displays a very low gradient beach face and surf zone, and a predominance of infragravity wave energy in the swash zone. This beach state is not strongly influenced by incident swash, and is therefore not important to the aims of this study (Wright *et al.*, 1982; Section 1.2). Wright and Short's second major beach state, the 'intermediate beach state', is divided into four sub-states according to the inner bar morphology. Their 'low tide terrace state' is generally uniform along-shore, and conditions adjacent to the shoreline are well represented by *Beach Type A* (Fig. 2.3). Cross-shore profiles along their 'transverse bar and rip state' alternate between welded bars and rip channels. This morphology is an along-shore summation of *Beach Types A* and B_2 respectively (Fig. 2.3). Conditions on their 'rhythmic bar and beach' and 'long-shore bar-trough states' are well represented by *Beach Type* B_1. The along-shore rhythmicity of the former has little effect on incident swash due to the large wave lengths involved. The third major beach state of Wright and Short is the 'reflective beach state', which is well represented by *Beach Type* B_2 or *C*, depending on the wave conditions.

2.4 Breaking Waves And Swash

2.4.1 Introduction.

Breaking waves, either surf zone bores or plunging breakers, produce swash on *Beach Types A* and *B* respectively. The transformation of the wave following incipient breaking is important to this study, because it determines

the wave kinematics at the shoreline that govern the initial conditions for uprush.

The theoretical literature on wave height transformation in the surf zone can be divided according to three approaches. The first is based on a similarity assumption, where the breaker height decays in constant proportion to the mean water depth. Thus

$$H_b = \gamma h \qquad (2.4),$$

where γ is the proportionality constant. Several field studies have shown that this approach adequately describes the wave height transformation on low gradient beaches ($\beta \approx 0.01-0.02$), where $\gamma \approx 0.42$ in the inner surf zone (*e.g.* Thornton and Guza, 1982; Wright *et al.*, 1982). However, other studies have shown that γ is not necessarily constant, but can depend on beach slope, wave steepness, and breaker type (*e.g.* Sallenger and Holman, 1985; Sawaragi and Iwata, 1974). Hence, difficulties arise when applying this approach to the *Beach Types* shown in Figure 2.3.

The second approach, initiated by LeMehaute (1962), is based on the wave energy balance

$$\frac{\partial E_f}{\partial x} + \Gamma = 0 \qquad (2.5)$$

(*ibid.*); E_f is the mean energy flux per unit of wave length, and Γ is the rate of wave energy dissipation. The wave height is usually related to E_f using one of the available wave theories such as small amplitude theory (*e.g.* Mizuguchi, 1980), or solitary wave theory (*e.g.* LeMehaute, 1962). Several theoretical models that use this approach have been tested on laboratory and natural beaches where bar-trough topography occurs, and have proven more satisfactory than the first approach (Battjes and Janssen, 1978; Mizuguchi, 1980; Svendsen, 1984; Battjes and Stive, 1985; Dally *et al.*, 1985; Ebersole, 1987). The gross details of these models differ only in the formulation used to specify the energy dissipation. Some formulations of Γ are based on the effects of turbulent velocity fluctuations (Horikawa and Kuo, 1966), or the turbulent eddy viscosity (Mizuguchi, 1980). Others assume that Γ is adequately represented by that present in a periodic bore (Battjes and Janssen, 1978; Battjes and Stive, 1985; Svendsen, 1984). In a model that permits wave re-formation, Dally *et al.* (1985) assumed that Γ is related to the difference between the actual E_f, and a stable E_f that is proportional to the local water depth (*cf.* (2.4)). Despite the success

of these first two approaches, (2.4) and (2.5), in describing most of the available surf zone data, they share the shortcoming that no energy from the incident waves can exist at the shoreline to produce swash. This is an unrealistic result for the description of most beaches, except those similar to the 'dissipative beach state' of Wright and Short (1984).

Although LeMehaute (1962) initiated the study of surf zone waves based on (2.5), which has been extended to the high degree of sophistication described above, he also recognized that for swash to exist surf zone bores are a necessary condition at the shoreline. The third approach treats waves in the outer surf zone as non-saturated breakers, using (2.5), and when the non-saturated breaker can no longer carry the available energy flux shoreward, bores are introduced *ad hoc* into the analysis (Section 2.4.3). The advantage of this approach over (2.4) and (2.5) is that after the wave crosses the surf zone, it still carries some finite amount of energy at the shoreline to produce swash (see Keller *et al.*, 1960; Freeman and LeMehaute, 1964; Section 2.4.3). This is possible because the energy flux that can be carried by a bore is greater than that carried by a depth-dependant wave of similar height (Svendsen, 1984).

Since it is this third approach which provides the most realistic model of wave height transformation, as far as the swash is concerned, more details are presented in the following Sub-sections (Sections 2.4.2 and 2.4.3). The theory for swash following bore collapse at the shoreline is presented in Section 2.4.4. Swash following plunging breakers has received little attention in the literature, and is therefore discussed only briefly in Section 2.4.5.

2.4.2 Non-saturated breakers.

Non-saturated breakers display a near symmetrical water surface profile, and minor aeration on the upper shoreward face which is the turbulent breaking plume (Fig. 2.4). The essential characteristics of motion for the non-saturated breaker are assumed by LeMehaute (1962) to be approximated by a limiting solitary wave. The maximum amount of energy that such a wave can transmit shorewards is reached, theoretically, when $H_b=0.78h$. Therefore, for the breaker to remain non-saturated, it is required that any excess energy that the solitary wave cannot transmit be dissipated in a manner which does not alter the gross flow characteristics of the wave. This energy dissipation can be achieved through bed friction, and a turbulent breaking plume (*ibid.*). The sum of these dissipation mechanisms is represented by Γ in (2.5). For the purpose

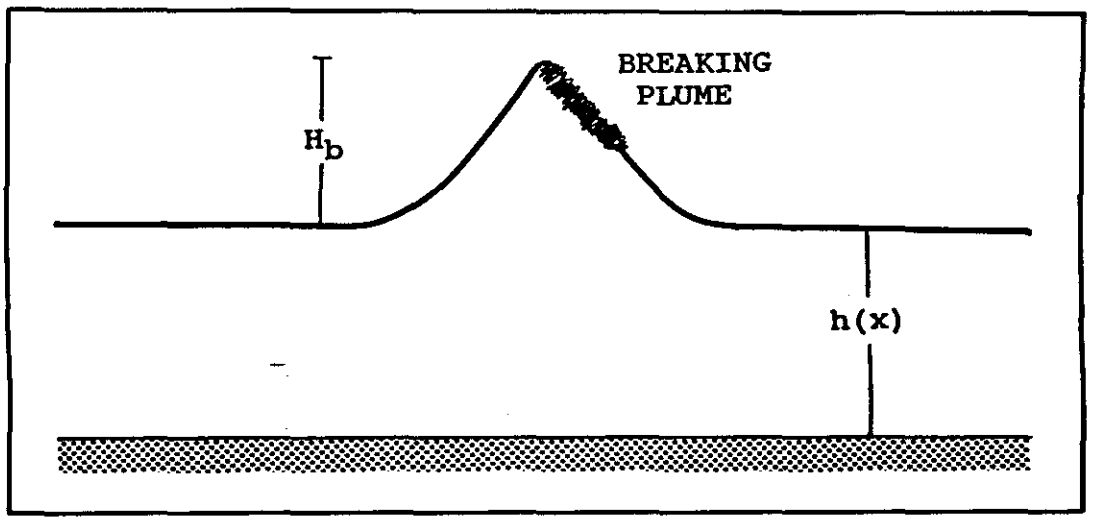

Figure 2.4: Definition sketch showing distinguishing features of the non-saturated breaker (After LeMehaute, 1962).

of analysis, LeMehaute assumed that dissipation due to the former could be described by the quadratic stress law, and dissipation due to the latter was assumed to be similar to that found in a hydraulic jump. Physical justification for these assumptions can be obtained from the original paper.

Theoretically, if non-saturated breakers persist on a beach they must diminish to zero height before reaching the shoreline, and provide no energy to the swash zone at or close to the incident wave frequency (LeMehaute, 1962). These type of waves can only persist near the shoreline when the surf zone slope is almost constant, and very small. On more typical concave-shape profiles, where the slope increases towards the shoreline (see Dean, 1977), the rate of frictional energy dissipation will decline as the shoreline is approached. In such circumstances, LeMehaute's analysis suggests that to remain non-saturated the breaker will steepen in an effort to produce sufficient dissipation in the turbulent breaking plume. If the required dissipation is not reached, the continual steepening of the wave results in eventual loss of symmetry and bore formation. The bore then carries the excess energy to the shoreline to produce swash. This model of the surf zone is very useful because it explains the relative unimportance of incident swash on flat, dissipative beaches (*e.g.* Wright et al., 1982), and recognizes the increased importance of incident swash on steeper beaches where bores occur in the inner surf zone (*e.g. Beach Type A*).

2.4.3 Surf zone bores.

Bores form in the inner surf zone following either a non-saturated breaker, or a plunging breaker. A bore can be considered as a discontinuity that indicates a sharp change in water depth and velocity (Meyer and Taylor, 1972). The traditional treatment of the bore assumes that mass and momentum are conserved through the bore front (*i.e.* the bore condition), and the well known bore equations are used to describe its propagation (*ibid.*; Stoker, 1957). Although the steep slope of the bore front violates the first assumption of the SWE (see Section 2.2), the bore region is very narrow, thus most of the remaining flow can still be described by (2.1) and (2.2).

Surf zone bores are usually defined to be the narrow, steep fronted, foaming turbulent zone at the front of waves in the inner surf zone (Fig. 2.5). Theoretically however, a bore need not be foaming; it is simply that steep part of a wave where the SWE are not valid, and the bore condition is satisfied (Meyer and Taylor, 1972; Stoker, 1957). Several types of surf zone bores are

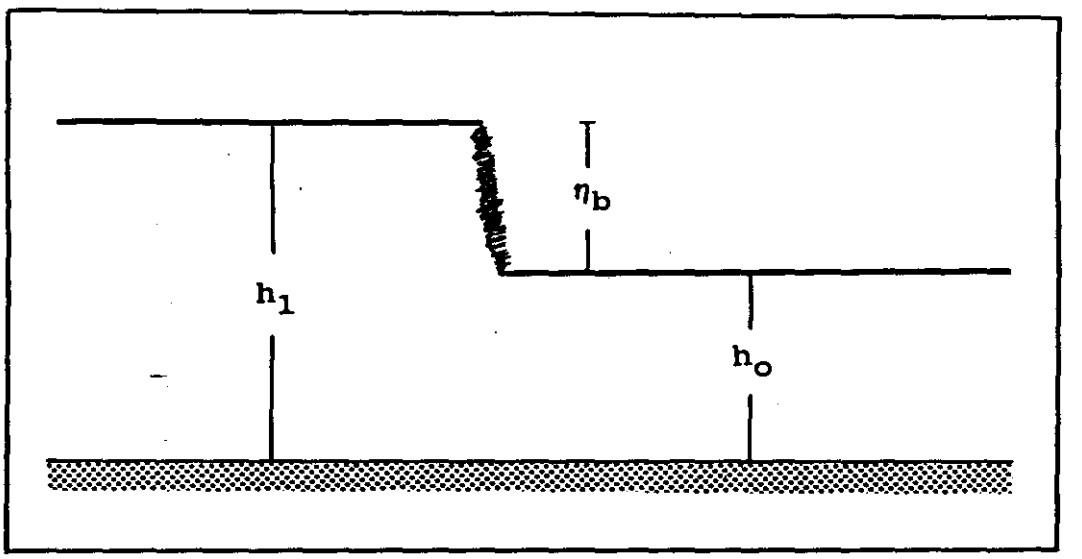

Figure 2.5: Definition sketch showing distinguishing features of the fully developed bore, and notation used in the text (After LeMehaute, 1962).

described in the literature and require recognition, as they behave differently during their approach to the shoreline. Whitham (1958) distinguished between weak and strong bores according to the bore ratio, B, given here as

$$B = \frac{\eta_b}{h_o} \qquad (2.6);$$

the notation is defined in Figure 2.5. Conditions where $B<0.9$ produce weak bores, and where $B>0.9$ produce strong bores (Fig. 2.6; *ibid.*).

Peregrine (1966) also used (2.6), to provide a more detailed classification of bores. Values of $B<0.28$ occur when the bore is undular, and is followed by a series of wavelets radiating seaward from the bore face (Fig. 2.6). For values of $0.28<B<0.75$ trailing wavelets still exist, but the bore front is breaking. For $B>0.75$ the bore is said to be fully developed; with intense breaking occurring at the bore front. Undulations behind the bore arise if the energy flux through the bore exceeds that being dissipated by turbulence at the bore front (Huntley and Bowen, 1975). Both Peregrine's and Whitham's classifications are therefore based on the efficiency of the bore front in dissipating energy, which is dependant on B.

Amein (1966) made a further distinction between bore types according to their water surface profile. Minor bores are recognized as having the bore front preceding the main wave crest, and the bore height being less than the wave height (Fig. 2.6). Major bores have the step-like profile of a fully developed bore, and the bore height equals the wave height (Fig. 2.6). Minor and major bores are expected to occur on steep and gentle beach slopes respectively (*ibid.*).

For a fully developed turbulent bore propagating over a sloping beach, laboratory experiments indicate that as a first approximation, deviations from hydrostatic pressure and the effects of bed friction are negligible compared with other factors (Svendsen and Madsen, 1984; Svendsen, 1987). The velocity of the bore front, U_b, can therefore be given as

$$U_b = \left[\frac{gh_1(h_o+h_1)}{2h_o} \right]^{0.5} \qquad (2.7)$$

(Stoker, 1957), and the water particle velocity, u_b, as

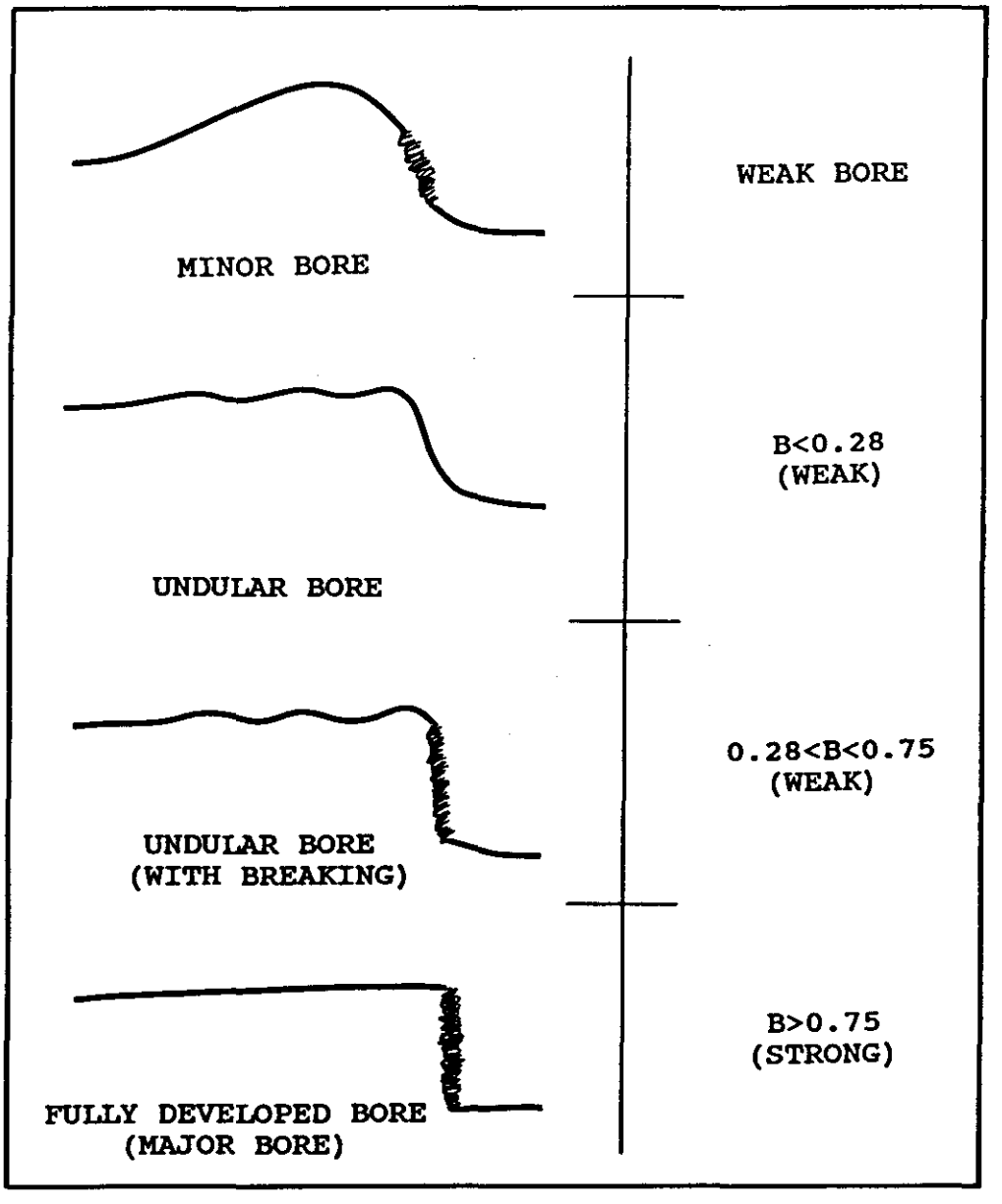

Figure 2.6: Bore classification showing water surface profile and B value for each type (After Amein, 1966; Cowell, 1982; Peregrine, 1966; Whitham, 1958).

$$u_b = \frac{U_b(h_1-h_o)}{h_1} \qquad (2.8)$$

(*ibid.*), where h_o and h_1 are the water depths on the low and high side of the bore respectively (Fig. 2.5). The bore equations, (2.7) and (2.8), are only capable of describing the velocity of the bore front and the water particle velocities immediately behind. All other aspects such as the shape of the bore front and the flow beneath it must be determined by other means (see Madsen and Svendsen, 1983; Svendsen and Madsen, 1984). Semi-empirical corrections to (2.7) and (2.8) have been derived for partially developed or undular bores (see Kishi and Saeki, 1966; Amein, 1966), but are of little consequence to conditions at the shoreline (Keller *et al.*, 1960; Section 4.2.2).

The laboratory and field data shown in Figure 2.7 generally confirms that (2.7) describes the propagation speed of fully developed bores on a range of beach slopes. However, there is some systematic scattering of the data with increasing bore strength. This may be due in part to difficulties of measurement in the presence of strong turbulence (Miller, 1968), but it is also possible that deviations from hydrostatic pressure, which are ignored in the theory, become increasingly important for strong bores (Whitham, 1958).

Whitham (1958) derived an ordinary differential equation that describes the motion of a bore across the surf zone. The Equation can be written as

$$\frac{1}{h_o}\frac{dh_o}{dM} = \frac{-4(M+1)(M-0.5)^2(M^3+M^2-M-0.5)}{(M-1)(M^2-0.5)(M^4+3M^3+M^2-1.5M-1)} \qquad (2.9)$$

(Keller *et al.*, 1960), where M, the Mach number, is

$$M = U_b/(gh_1) \qquad (2.10)$$

(*ibid.*). Integration of (2.9) yields (2.11), which is

$$h_o = \frac{C(M^2-0.5)\exp[0.88\tan^{-1}(M+0.68)]}{(M-1)^{0.8}(M-0.75)^{1.18}(M+2.39)^{1.67}(M^2+1.35M+0.56)^{1.17}}$$

(*ibid.*); C is an integration constant to be determined from the initial strength of the bore. For a given bore where η_b and h_o are known initially, M and C can be calculated from (2.10) and (2.11) respectively. Once these initial quantities are known, η_b, U_b, and u_b can then be calculated for successive values of h_o decreasing towards the shoreline.

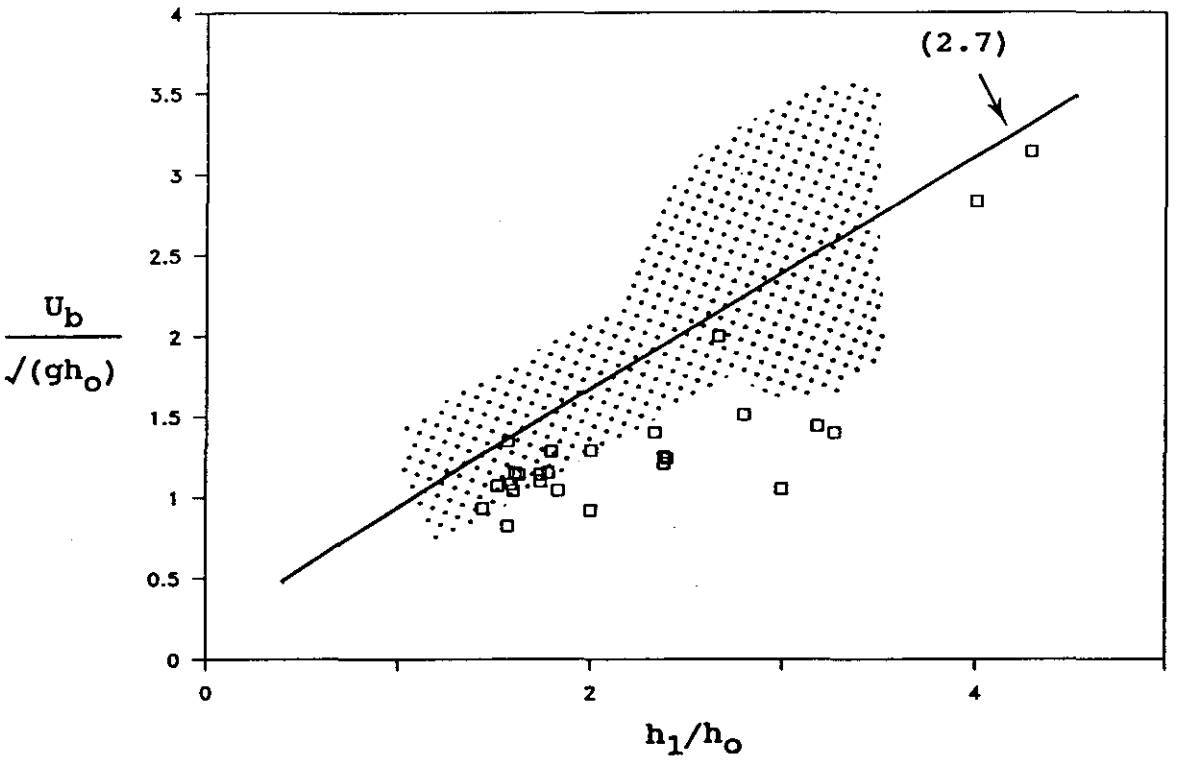

Figure 2.7: Field and laboratory data showing U_b as a function h_1. Dotted area shows the range of laboratory data measured by Miller (1968), and boxes show the actual field data measured by Bradshaw (1982). The range of experimental slopes include $0.03<\beta<0.3$.

Keller *et al.* (1960) used a finite-difference scheme to solve the SWE, and compared the results with the predictions of (2.11). They found excellent agreement for several initial bore strengths. Calculations of η_b, U_b, and B made using (2.11) are shown in Figure 2.8. It is evident that strong bores are predicted to decrease in height and increase in velocity as $h_o \rightarrow 0$, whereas weak bores initially behave *vice versa.* After crossing a threshold however, they behave according to the strong bore solution (Fig. 2.8). This apparent 'forgetfulness' of initial wave conditions as the shoreline is approached (see also Ho and Meyer, 1962), lends support to the supposition of this study, that conditions immediately seaward of the shoreline are the most appropriate to define initial conditions for the swash (Sections 1.4 and 2.3).

Experimental data that bear directly on the theoretical results shown in Figure 2.8 can be found in Bradshaw (1982). Bradshaw obtained measurements of η_b and h_o from a variety of bores at different positions in the surf zone. These data are shown in Figure 2.9. In as far as $h_o \rightarrow 0$ can be taken to indicate the bore approaching the shoreline, the measured B behaves very much according to the predictions shown in Figure 2.8. A more rigourous comparison between theory and data was not possible, as the data set does not contain measurements of the same bore at several positions in the surf zone.

The fact that $h_o \rightarrow 0$ near the initial shoreline implies that U_b and u_b must tend to infinity (see (2.7) and (2.8)). However, for the wave to remain a bore, U_b can never exceed $u_b + \sqrt{(gh_1)}$ measured behind the bore (Freeman and LeMehaute, 1964). This arises from the fact that the bore derives its energy from the wave elements behind, and can therefore never exceed their speed (*ibid.*). It follows then, that $u_b \rightarrow U_b$ as $h_o \rightarrow 0$, and upon arrival at the beach ($h_o=0$) sets the shoreline in motion with an initial velocity $u_o=u_b=U_b$. Hence u_o is finite and can be estimated using (2.11) (Keller *et al.*, 1960; Freeman and LeMehaute, 1964; LeMehaute *et al.*, 1968).

Compared to the traditional approach, recent studies of bores have paid greater attention to the precise details of energy dissipation in the bore front (Madsen and Svendsen, 1983; Svendsen and Madsen, 1984). For example, Svendsen and Madsen (1984) adopted the SWE as a starting point, and introduced two new equations that formulate the free-surface turbulence. Their model provides details of the bore shape and internal flow, which are not available in the classical description. It would appear that Svendsen and

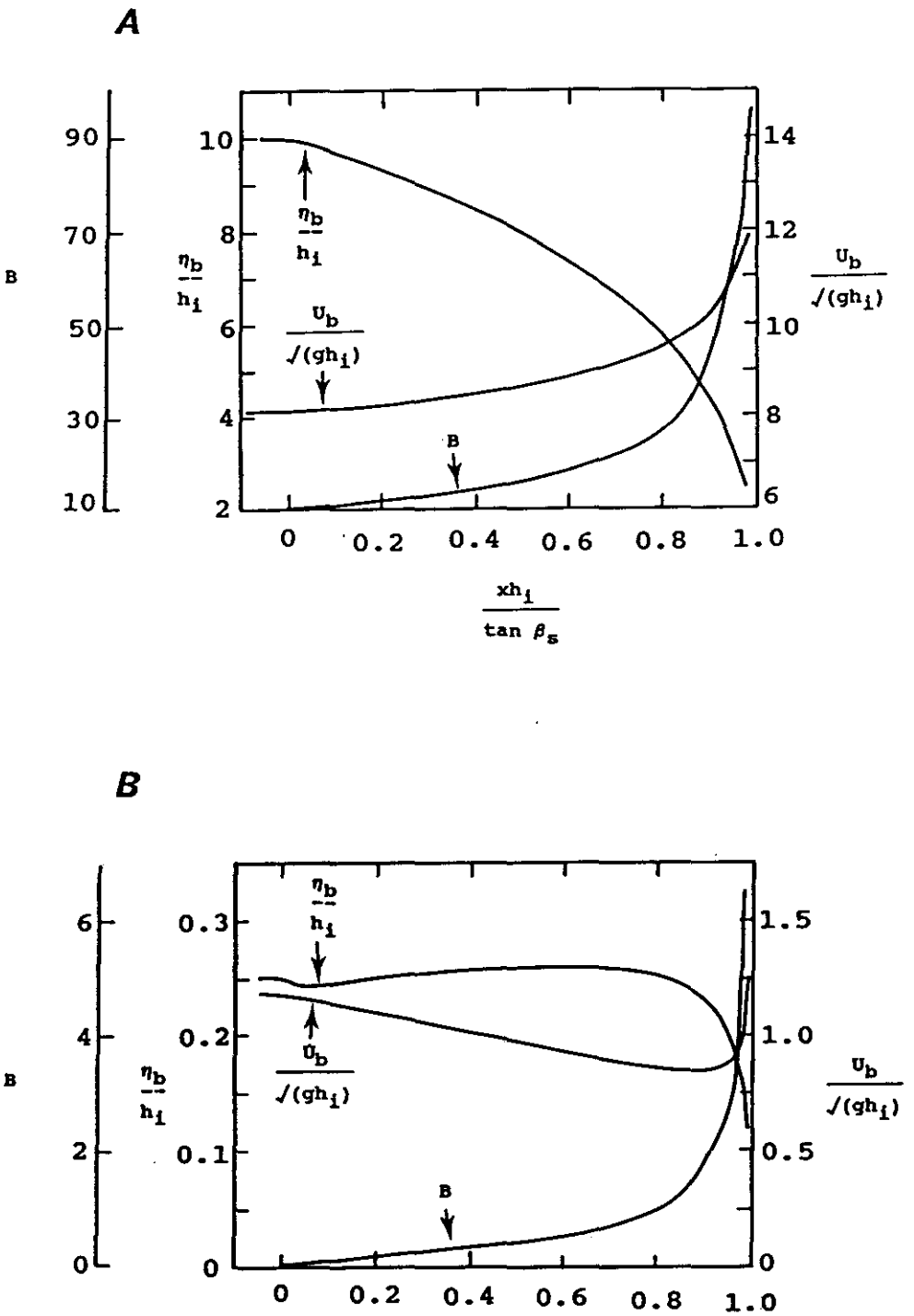

Figure 2.8: *(a)* Predicted behaviour of η_b, U_b, and B for a strong bore approaching the shoreline. Calculations made using (2.9) and the initial conditions η_b=1.0, and h_i=0.1. *(b)* Predicted behaviour of η_b, U_b, and B for a weak bore approaching the shoreline. Calculations made using (2.9) and the initial conditions η_b=0.1, and h_i=0.4 (After Keller *et al.*, 1960).

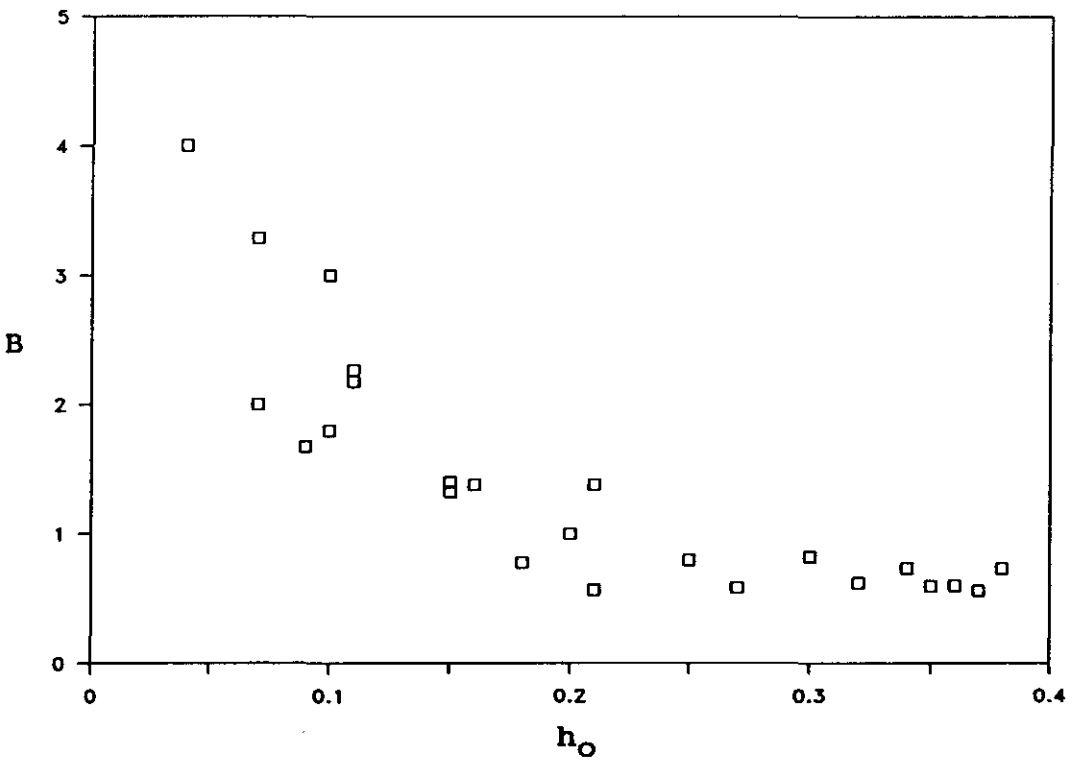

Figure 2.9: Field data from Bradshaw (1982) showing B as a function of h_o. Experimental slope is 0.03.

Madsen's model shows more promise than the traditional approach for the complete description of bores climbing a beach. Unfortunately, their model has not been extended to describe bore collapse at the shoreline. Hence the theoretical description of bore propagation relevant to the swash has not advanced beyond the early work of Keller *et al.* (1960) and Freeman and LeMehaute (1964), described above.

2.4.4 Swash following bore collapse.

During its final approach to the initial shoreline the bore height tends to zero in proportion to the square root of its distance from shore (Fig. 2.8). The rapid decrease in height at the initial shoreline represents bore collapse, and a singularity of water acceleration in the SWE. The advancement of the non-linear shallow water theory to describe swash was only possible after this singularity was re-interpreted both physically and mathematically (Shen and Meyer, 1963; Meyer and Taylor, 1972). It is physically interpreted as a change in wave form from that of a shock to a rarefaction wave, where the initial shoreline becomes the leading edge of the latter (Freeman and LeMehaute, 1964). Mathematically, the re-interpretation of the shore-singularity allows the leading edge to be modelled based on several simple corollaries of the SWE (see Ho *et al.*, 1963).

As stated previously, $u_b \rightarrow U_b$ as the bore approaches the beach. Upon arrival at the beach the bore collapses and sets the shoreline in motion with an initial velocity of $u_o=u_b=U_b$. Since the bore and shoreline represent singularities of the SWE, bore collapse is theoretically instantaneous. Moreover, since the SWE are not valid in the bore region, no details on the mechanism of bore collapse are available from the theory. Despite these limitations at the initial shoreline, the physical problem becomes much simpler in the swash zone. In this zone there is no longer any water upstream of the wave front, hence the free-surface turbulence vanishes, and the problem reduces to that described well by the SWE (Hibberd and Peregrine, 1979; Svendsen and Madsen, 1984).

Ho *et al.*, (1963) presented an interpretation of the corollaries contained in Shen and Meyer's (1963) original analysis of the SWE, to provide a useful physical description of the swash lens on a smooth and impermeable beach. The description assumes that the swash lens can be divided into small 'fluid elements', each containing the same mass of water at all times (Fig. 2.10). The motion of each element in this model depends only on the pressure exerted by

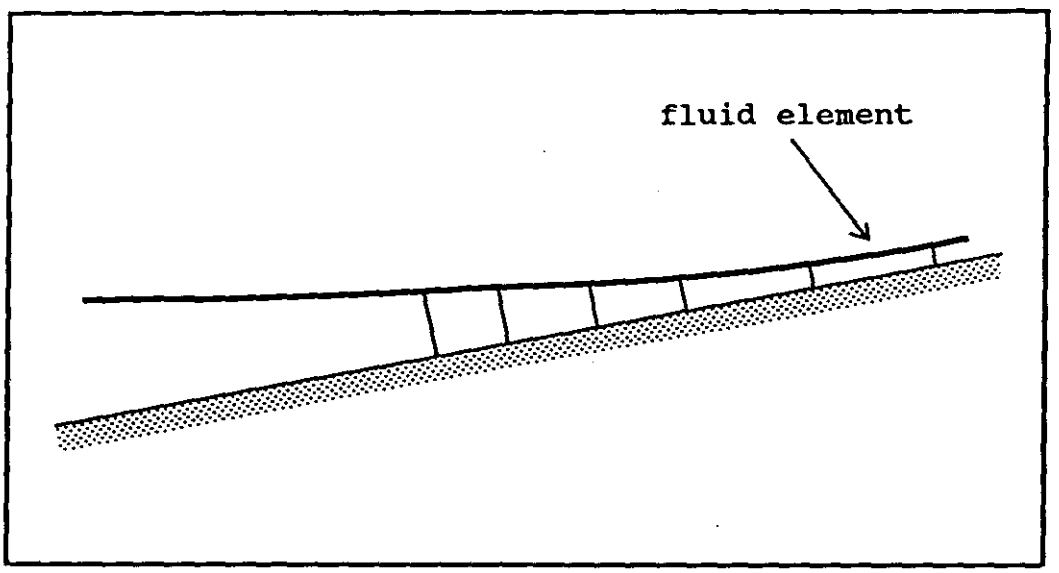

Figure 2.10: Model of the swash lens showing small fluid elements used to analyse the shoreline behaviour (After Ho *et al.*, 1963).

the adjacent elements, and gravity. Since the swash is a rarefaction wave (Stoker, 1957; Freeman and LeMehaute, 1964), the front element is always moving faster than the elements behind. Hence the pressure on this front element will be negligible (Ho *et al.*, 1963). It is assumed here that the leading edge (and shoreline) is an analog of this front element. Thus once the leading edge has been accelerated to its maximum velocity u_o, its motion can be studied by simply considering the balance of forces acting on a 'fluid element' climbing the beach.

Consider the situation shown in Figure 2.11 where a bore propagating shorewards arrives at the initial shoreline $x=0$ at time $t=0$. Assumptions relating to the nature of the fluid are the same as those listed with the SWE (Section 2.2). In addition, it is assumed that the wave period is sufficiently long to ensure no backwash interaction, and that the beach face is smooth and impermeable. The equation of motion for the moving shoreline can now be written as

$$m \frac{dU_s}{dt} + mg(\sin \beta) = 0 \qquad (2.12);$$

m is the mass of the leading wave element. Through integration, and adopting the initial condition that $U_s=u_o$ when $t=0$, the shoreline velocity $U_s(t)$ is obtained;

$$U_s(t) = u_o - gt(\sin \beta) \qquad (2.13).$$

Furthermore, since the shoreline displacement X_s is zero when $t=0$, integration of (2.13) yields

$$X_s(t) = u_o t - 0.5gt^2(\sin \beta) \qquad (2.14).$$

When $U_s=0$ the shoreline is at its maximum displacement, and from (2.13) this occurs when

$$t_{(max)} = \frac{u_o}{g(\sin \beta)} \qquad (2.15).$$

Substituting (2.15) into (2.14) yields the maximum swash length L_s;

$$L_s = \frac{u_o^2}{2g(\sin \beta)} \qquad (2.16).$$

Through trigonometry the maximum swash height Z_s can also be obtained;

$$Z_s = \frac{u_o^2}{2g} \qquad (2.17).$$

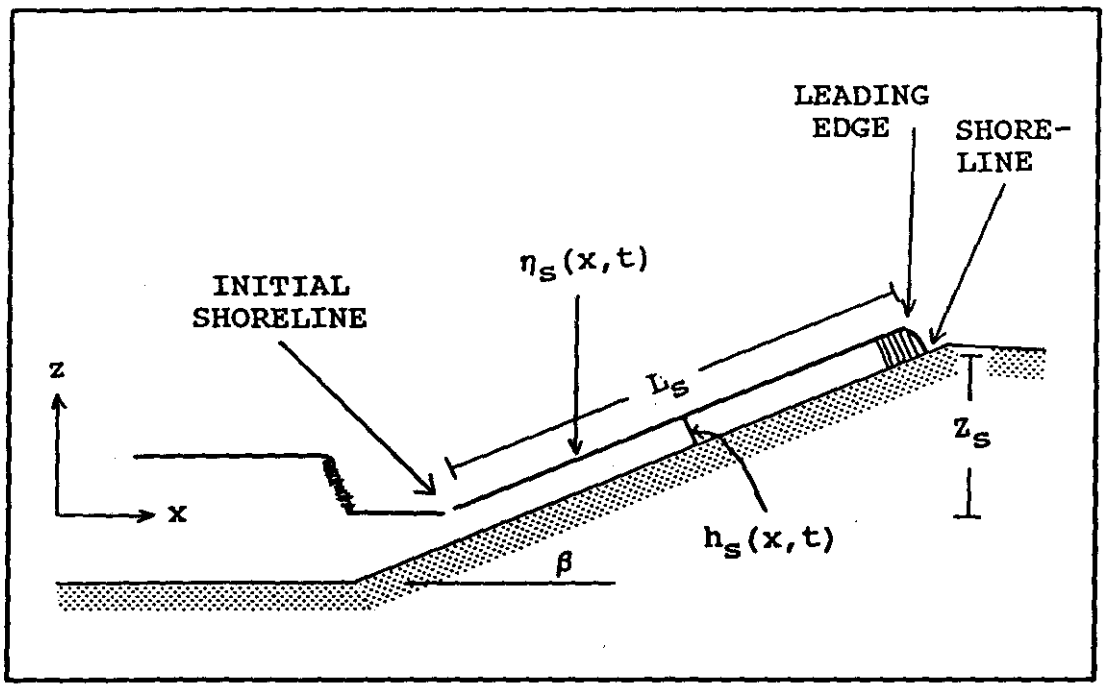

Figure 2.11: Definition sketch showing swash following bore collapse, and notation used in the text.

The mean shoreline velocity $\bar{U}_s$, averaged over the swash length, is

$$\bar{U}_s = \frac{L_s}{t_{(max)}} = \frac{u_o}{2} \qquad (2.18).$$

In addition to the above Equations Shen and Meyer (1963) provide an approximation for the swash depth, $h_s(x,t)$;

$$h_s(x,t) = \frac{(X_s-x)^2}{(3t)^2} \qquad \text{as } (X_s-x)\rightarrow 0 \qquad (2.19)$$

(*ibid.*). The water surface elevation in the swash zone (relative to the initial shoreline) $\eta_s(x,t)$ is therefore

$$\eta_s(x,t) = h_s + x(\tan \beta) \qquad (2.20).$$

The maximum swash depth at any position x along the beach, $h_{s(max)}$, can be obtained by solving $dh_s/dt=0$ for the condition that $d^2h/dt^2<0$. Hence, from (2.19)

$$\frac{dh_s}{dt} = \left[\frac{2u_o t - gt^2(\sin \beta) - 2x}{3t}\right]\left[\frac{x-0.5gt^2(\sin \beta)}{3t^2}\right] = 0 \qquad (2.21).$$

It can be shown that the relevant solution (the right square bracket) gives the time of maximum swash depth as

$$t_m = \left[\frac{2x}{g(\sin \beta)}\right]^{0.5} \qquad (2.22).$$

Substitution of (2.22) into (2.19) yields

$$h_{s(max)} = \frac{g(\sin \beta)(u_o t_m - 2x)^2}{18x} \qquad (2.23).$$

The Equations (2.14), (2.17), (2.18), (2.19), (2.20), and (2.23) describe several features of the incident swash that are readily measurable in the field (Sections 3.4 and 3.5). The relationships given by (2.18) and (2.23) have not been derived previously, and are included here to provide the widest possible description of swash for which field data can be obtained. Graphical representations of these equations are shown in Figure 2.12 to allow later comparison with field data.

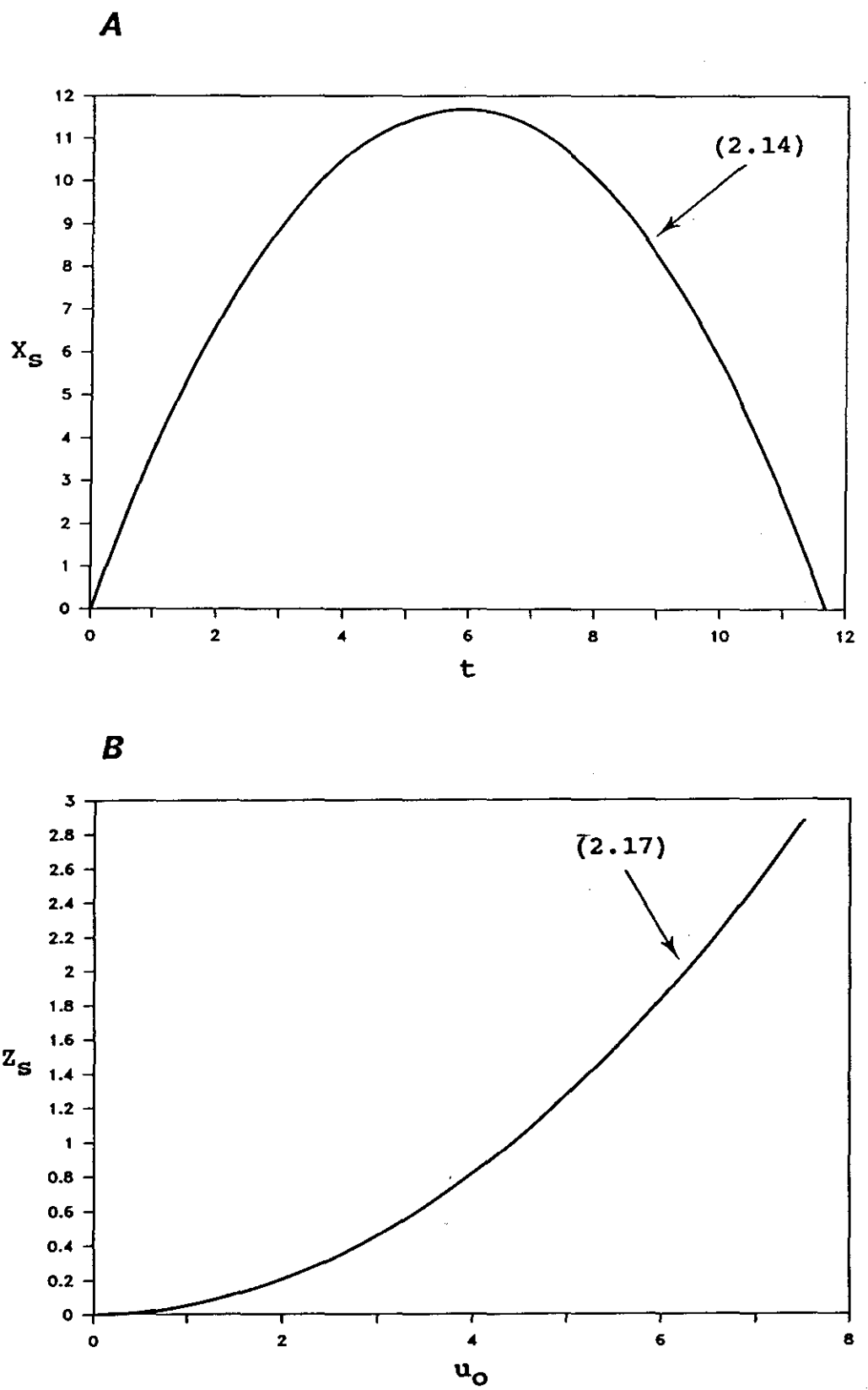

Figure 2.12: *(a)* Predicted $X_S(t)$ for a swash cycle with initial conditions u_o=4, and β=0.07. *(b)* Predicted Z_S as a function u_o.

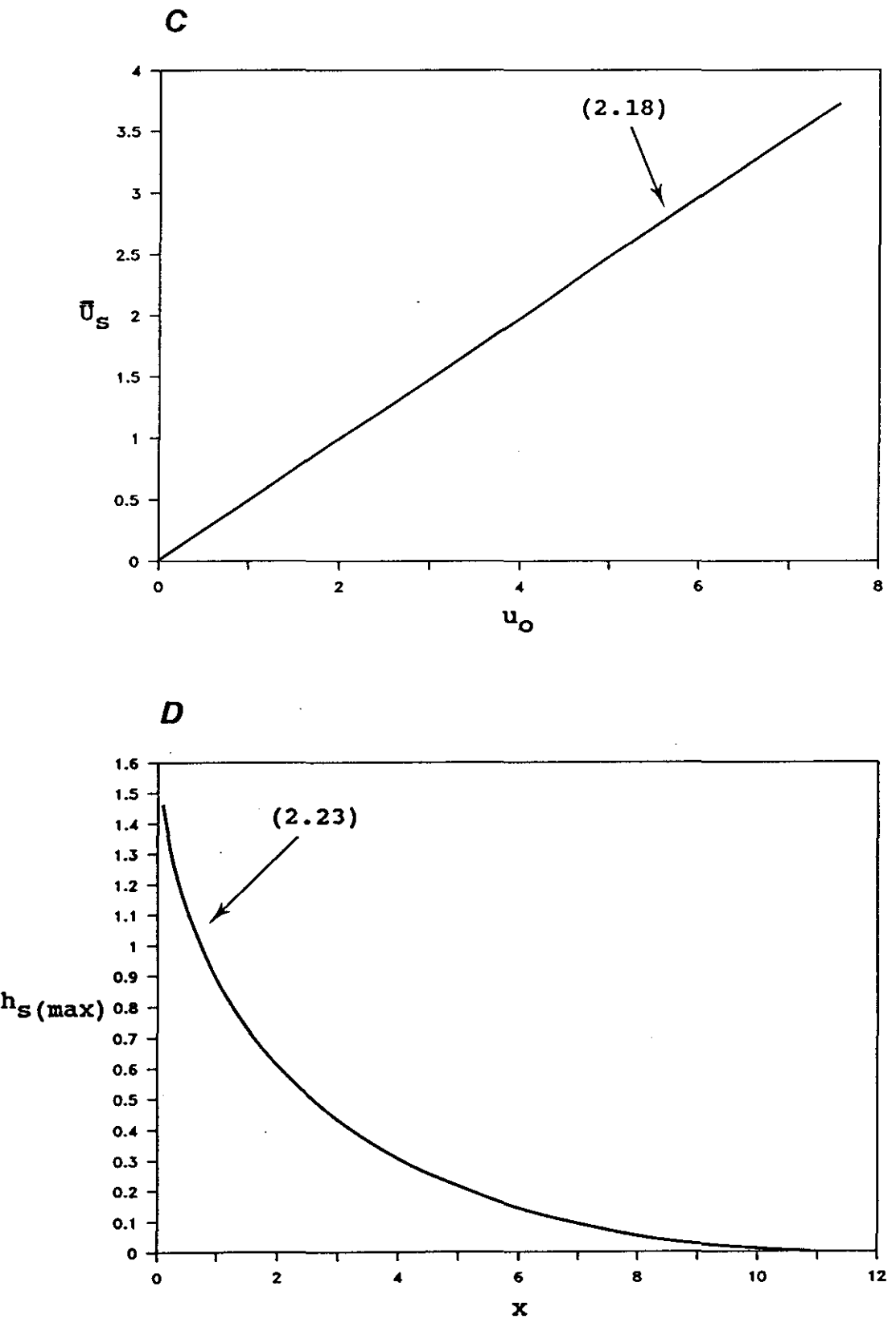

Figure 2.12 contd: *(c)* Predicted $\bar{U}_s$ as a function of u_o. *(d)* Predicted $h_{s(max)}(x)$ for a swash cycle with initial conditions u_o=4, and β=0.07.

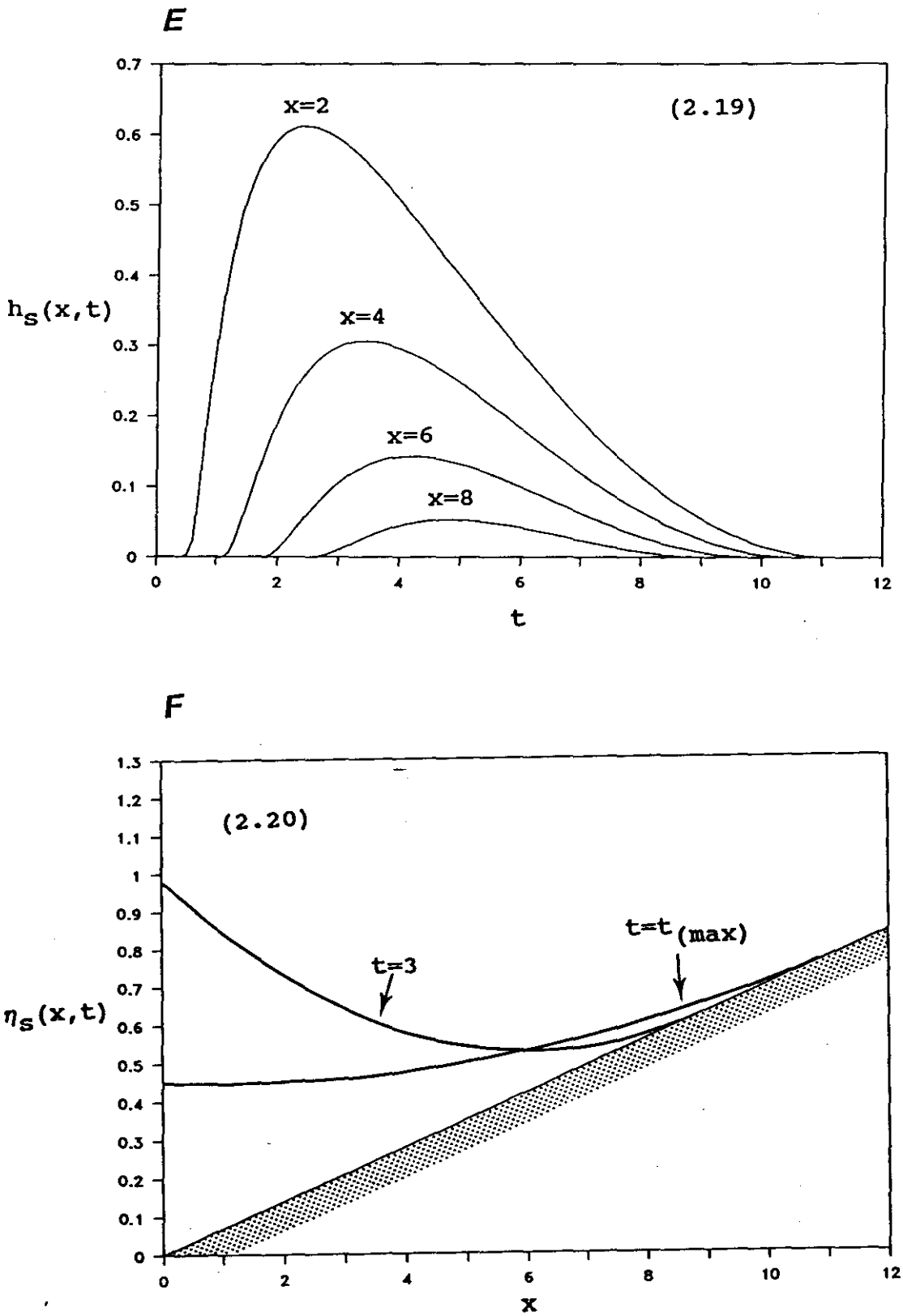

Figure 2.12 contd: *(e)* Predicted $h_s(x,t)$ for a swash cycle with initial conditions u_o=4, and β=0.07. *(f)* Predicted $\eta_s(x,t)$ for a swash cycle with initial conditions u_o=4, and β=0.07.

The detailed analysis of the SWE by Shen and Meyer (1963) indicates that the equations for swash presented above are valid until a singularity of water acceleration occurs in the backwash. The movement of this singularity in the (t,x) plane is represented by a 'limit line', and is shown in Figure 2.13. Shen and Meyer interpreted this 'limit line' to indicate the formation of a landward facing bore. Although the origin and motion of the bore cannot be precisely determined from the theory, it is understood to originate up beach and move seawards within the backwash flow (Fig. 2.13; *ibid.*). At the time that bore inception occurs, the shoreline becomes influenced by processes in the flow interior, and can therefore no longer be described by (2.12).

The principal conclusions of the non-linear shallow water theory for swash following bore collapse on a smooth, impermeable beach are summarised below (*cf.* Fig. 2.12).

1. The behaviour of the swash lens is insensitive to the initial bore type.
2. Once the initial shoreline is accelerated to u_o, the shoreline velocity decreases at a constant rate due to the force of gravity alone. The value of u_o depends on the bore velocity at the shoreline.
3. The time-history of shoreline displacement is parabolic in the (t,x) plane, until the inception of a bore in the backwash.
4. The maximum swash height relative to the initial shoreline is independent of beach slope, and uniquely determined by u_o.
5. The maximum swash depth at any position on the beach occurs before the time of maximum shoreline displacement.
6. As the swash lens climbs the beach it progressively thins with increasing time and distance travelled.

2.4.5 Swash following plunging breakers.

Beach Types B_1 and B_2 display conditions where incident swash is produced directly by plunging breakers. There is very little research reported in the literature that pertains to the complete problem of wave plunge on the beach face and uprush. The only studies of particular relevance include a paper by Hedges and Kirkgoz (1981) that examines the transformation zone of plunging breakers, and a paper by Kirkgoz (1981) on their run-up. Although Kirkgoz (1981) used the predictions of the non-linear shallow water theory for the swash, he was reluctant to adopt bore theory seaward of the shoreline to determine u_o.

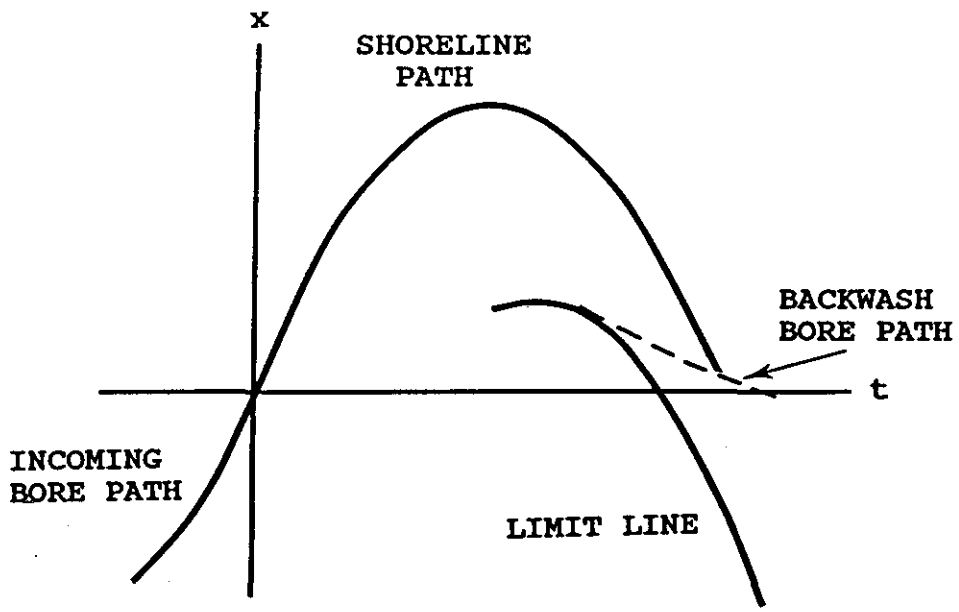

Figure 2.13: Schematic showing inferred behaviour of the backwash bore (After Shen and Meyer, 1963).

The laboratory measurements made by Hedges and Kirkgoz (1981) describe waves in what they term the transformation zone, which is bounded by the point where horizontal asymmetry of the wave profile first occurs, and the point where the wave face becomes vertical. On a natural beach the seaward boundary occurs at approximately $1.4H_b$ (see *ibid.*), or the point of wave reformation in the trough for *Beach Types* B_1 and B_2 respectively. The shoreward boundary usually occurs over the step (see Fig. 2.3).

Hedges and Kirkgoz (1981) found that the crest velocity, c, measured across the transformation zone matched closely with the value of $\sqrt{[g(\eta+h)]}$. Furthermore, the authors noted that as the wave approached the shoreline $u \rightarrow c$, but always remained smaller than c prior to overturning. The behaviour of the wave in the transformation zone appears to follow that expected from the SWE in at least some respects, however, it is unlikely that a complete description is possible once overturning begins. The plunging jet contains large vertical accelerations of water that cause deviations from hydrostatic pressure (see Peregrine *et al.*, 1980), thus precluding the use of the SWE.

It is conceivable that conditions on *Beach Type B* may be studied by applying the SWE and bore equations in the transformation zone, ignoring the details of wave plunge on the beach face, which must represent a singularity of the SWE, and beginning the theoretical treatment again when the uprush begins. This is analogous to the approach described for swash following bore collapse (Section 2.4.4), except here the zone in which the transition to swash occurs is expected to be wider due to the 'breaker travel' (see Galvin, 1972; Section 4.3.2). Also, a method to calculate u_o is not obvious since the plunging jet sets the shoreline in motion in a very different manner to that of bore collapse (Section 4.3.2). Despite these differences in the wave motion at the initial shoreline, it seems reasonable to expect that most of the swash will behave in the manner described in the previous Sub-section.

2.5 Non-Breaking Waves And Swash

2.5.1 Introduction.

Non-breaking or surging waves produce incident swash on *Beach Type C*. For a smooth and impermeable beach, surging waves must be completely reflected from the beach, since dissipation of energy through turbulent breaking is absent. The wave and morphology conditions required to ensure

complete reflection are combined in a surf scaling parameter introduced in Section 2.5.2. The traditional approach used in applying the shallow water theory to the study of swash dominated by reflection of wave energy, is to consider bore-free solutions of the SWE (see Carrier and Greenspan, 1958; Gjevik and Pedersen, 1981; Synolakis, 1987a and b). The important results obtained from this approach are presented in Section 2.5.3.

2.5.2 Wave reflection.

Several parameters exist in the literature that predict the presence of wave reflection (see Bauer and Greenwood, 1988). For instance, Battjes (1974) presents the critical condition $I_r>2.4$, which occurs halfway between complete breaking and complete reflection of the incident wave. He also mentions, however, that the derivation of this threshold is based on unrealistic values for some of the parameters involved. Perhaps a more theoretically sound parameter is that derived from the work of Carrier and Greenspan (1958), which is the surf scaling parameter ϵ;

$$\epsilon = \frac{z_s \omega^2}{g(\tan^2\beta)} \qquad (2.24)$$

(Meyer and Taylor, 1972), and ω is the radian wave frequency ($2\pi/T$). For wave reflection to occur and a standing wave to dominate the swash motion, it is theoretically required that $\epsilon<1$ (*ibid.*). Interestingly, laboratory experiments suggest a less restrictive condition for the occurrence of standing waves, since they have also been observed for $\epsilon<2.0$ to 2.5 (see Guza and Inman, 1975; Guza and Bowen, 1976). The bore-free solutions of the SWE presented in Section 2.5.3 formally require that $\epsilon<1$. The laboratory results indicate therefore, that these solutions may not describe all occurrences of surging waves measured in the field.

2.5.3 Swash following surging waves.

Carrier and Greenspan (1958) were the first to show that if $\epsilon<1$ then solutions to the SWE included non-breaking, bore-free waves climbing a beach. By applying a non-linear transformation to (2.1) and (2.2) they derived a single linear equation that can be used to predict several features of the swash.

Consider the problem of a wave surging up a smooth, impermeable beach such as that shown in Figure 2.14. Assumptions relating to the flow are the same as those listed with the SWE (Section 2.2). In order to solve the SWE for

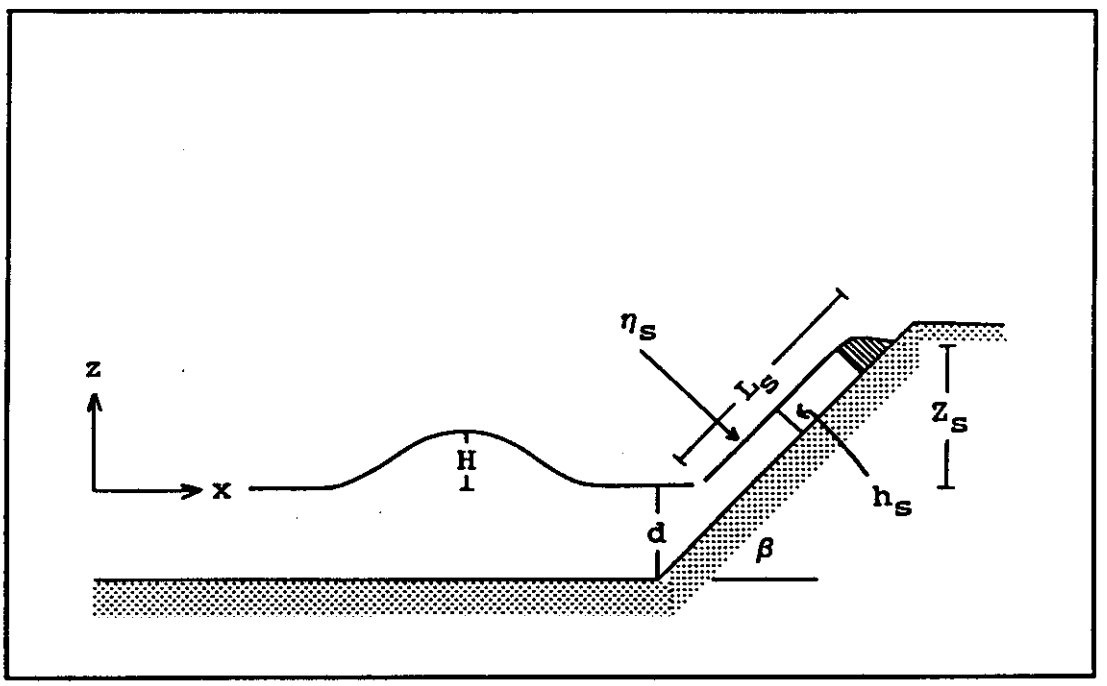

Figure 2.14: Definition sketch showing swash following a surging wave, and notation used in the text.

the problem shown in Figure 2.14, Carrier and Greenspan (1958) transformed the hyperbolic system (2.1) and (2.2) to its characteristic equations. Once this transformation was made the independent variables x and t were defined as functions of the characteristic variables of the system. With this change of variables (2.1) and (2.2) could be reduced to the single linear equation

$$\frac{\partial}{\partial\sigma}\left[\sigma\frac{\partial\phi}{\partial\sigma}\right]-\sigma\frac{\partial^2\phi}{\partial\lambda^2}=0 \qquad (2.25)$$

(Carrier and Greenspan, 1958). The characteristic variables λ and σ are defined by:

$$\lambda = 2[u+(\tan\beta)gt] \quad \text{and} \quad \sigma = 4\sqrt{[g(h+\eta)]} \qquad (2.26)$$

respectively (see *ibid.* for full details).

If the $\phi(\lambda,\sigma)$ chosen to describe the initial wave form satisfies (2.25), then u, x, η, and t in the (λ,σ) plane are written as:

$$u = \frac{1}{\sigma}\frac{\partial\phi}{\partial\sigma} \qquad (2.27)$$

$$x = \left[\frac{1}{4}\frac{\partial\phi}{\partial\lambda} - \frac{\sigma^2}{16} - \frac{u^2}{2}\right] \qquad (2.28)$$

$$\eta = \left[\frac{1}{4}\frac{\partial\phi}{\partial\lambda} - \frac{u^2}{2}\right] \qquad (2.29)$$

$$t = (\lambda/2-u) \qquad (2.30)$$

(*ibid.*).

Carrier and Greenspan (1958) solved (2.25) for η_s, X_s, and U_s using several initial wave forms. The simplest is that of a wave of unit frequency travelling shoreward and being completely reflected from the beach. In this case ϕ can be written as

$$\phi(\lambda,\sigma) = AJ_o(\sigma)(\cos\lambda) \qquad (2.31)$$

(*ibid.*), where J_o is the zero order Bessel function. It can be shown that

$$\frac{\partial \phi}{\partial \lambda} = -AJ_o(\sigma)(\sin \lambda) \qquad (2.32).$$

Thus, combining (2.32) with (2.28) and setting the moving shoreline at $\sigma=0$, $X_s(\lambda)$ for the standing wave (2.31) is

$$X_s(\lambda) = \left[-\frac{A(\sin \lambda)}{4} - \frac{U_s^2}{2} \right] \qquad (2.33).$$

An example of X_s, and η_s at the time of maximum uprush and backwash is shown in Figure 2.15. The maximum swash height occurs when $U_s=0$ and $\lambda=3\pi/2$, so from (2.33)

$$Z_s = A/4 \qquad (2.34).$$

Unless the wave form chosen to represent that observed in the field matches one analysed by Carrier and Greenspan (1958), the transformation of boundary and initial conditions from the (t,x) to (λ,σ) plane is exceedingly complex. This presents difficulties when the aim is to compare theoretical predictions with field data. Fortunately, Synolakis (1987a and b) has obtained solutions for the run-up of a non-breaking solitary wave which compare well with his laboratory experiments. Solitary wave theory has previously been used to successfully describe many features of waves approaching the shoreline (Munk, 1949), and is therefore assumed to be appropriate here.

It should be mentioned that although Synolakis (1987a and b) used a solitary wave as the input wave in both his theoretical and experimental work, it cannot remain a solitary wave and also produce swash (Section 2.4.2). In reality, the wave motion must deviate from the solitary wave description as it climbs the beach. This deviation is sufficiently small however, for the theoretical analysis to continue.

Synolakis (1987a and b) adopted the Boussinesq solution for the surface profile of the solitary wave, and derived a formulation of ϕ that satisfied (2.25). This enabled him to obtain Z_s;

$$Z_s = 2.831/(\cot \beta)\left[\frac{H}{d}\right]^{5/4} \qquad (2.35)$$

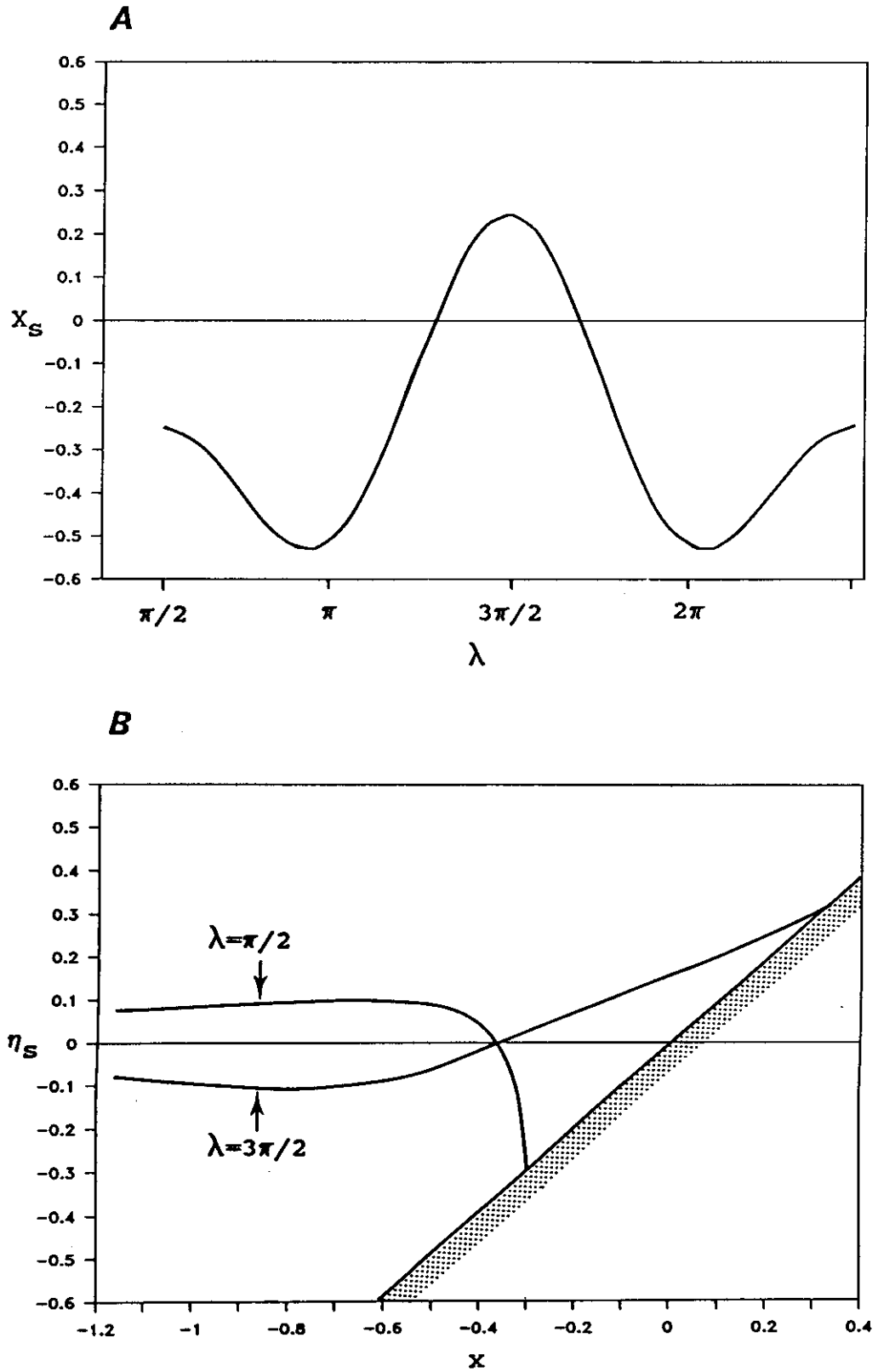

Figure 2.15: *(a)* Predicted $X_S(\lambda)$ for a standing wave with initial condition A=1. (b) Predicted $\eta_S(\sigma,\lambda)$ for a standing wave with initial condition A=1 (After Carrier and Greenspan, 1958).

(*ibid.*), where H is the solitary wave height, and d is the depth at the toe of the beach face (Fig. 2.14). X_s and η_s in the (t,x) plane can also be obtained by using Synolakis' formulation of ϕ, and solving (2.28) and (2.29) using Newton's method of iteration (see Synolakis 1987a and b for full details). An example of $X_s(t)$ and $\eta_s(x,t)$ for a solitary wave climbing a beach without breaking is shown in Figure 2.16.

Synolakis' formulation of ϕ, and the solutions derived from it are formally valid provided that

$$\frac{H}{d(\tan \beta)^{1.11}} < 0.8183 \qquad (2.36).$$

The principle conclusions of the non-linear shallow water theory for the swash motion of non-breaking, bore-free waves on a smooth and impermeable beach are summarised below (*cf.* Fig. 2.15 and 2.16).

1. The behaviour of the swash lens is very sensitive to the initial wave form.
2. The shoreline experiences smooth changes in acceleration during the uprush and backwash.
3. The maximum swash height is directly proportional to the wave height, and inversely proportional to the beach slope.
4. The maximum swash depth at any position on the beach occurs at the time of maximum shoreline displacement.
5. As the swash lens climbs the beach it maintains a wedge shape profile where the swash depth is almost linear in x.

2.6 Summary

The preceding discussion has served to demonstrate the broad scope of the non-linear shallow water theory, especially in its ability to describe waves approaching the beach. The literature contains many examples of the theory's use in hypothetical problems of wave motion both seaward, and landward of the initial shoreline. In synthesizing this literature within the guidance of the study aims, a framework has evolved that now enables application of the shallow water theory to the problem of swash on natural beaches.

The scheme of *Beach Types* presented in Section 2.3 adequately describes conditions relevant to the swash on most natural beaches. The use of this scheme simplifies the study to three general cases. Namely, swash following

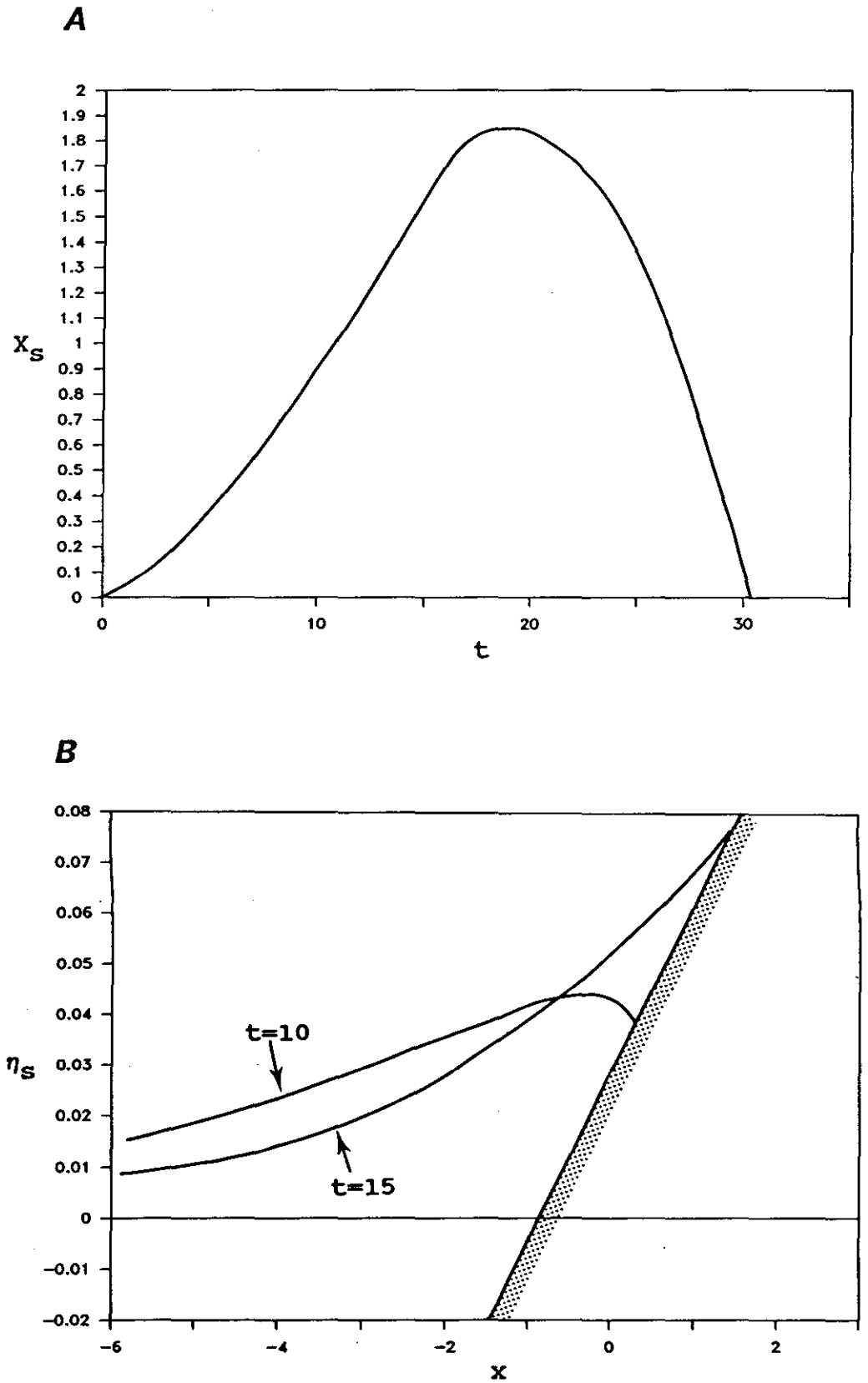

Figure 2.16: *(a)* Predicted $X_s(t)$ for a solitary wave with initial condition H/d=0.019. (b) Predicted $\eta_s(x,t)$ for a solitary wave with initial condition H/d=0.019 (After Synolakis, 1987a and b).

surf zone bores, plunging breakers, and surging waves. Theoretical descriptions of two-dimensional swash on a smooth and impermeable beach have been presented for each of these cases (Sections 2.4.4, 2.4.5, and 2.5.3). Particular care has been taken to describe the assumptions and rationale upon which the theory is based, to enable a meaningful analysis of any discrepancy that may arise when comparing the theory with field data.

Traditionally, application of the shallow water theory in problems relating to swash has involved two approaches: solutions of the SWE that permit bores, and solutions that are bore-free. These two approaches provide different results, and infer that there will be significant differences in the behaviour of swash between *Beach Types*. The solutions for swash following bore collapse are theoretically applicable to *Beach Type A* and *B*, and are found to be insensitive to the bore type far from shore. The bore-free solutions for swash following surging waves are theoretically applicable to *Beach Type C*, provided that (2.24) or (2.36) are satisfied.

CHAPTER 3
FIELD SITES AND METHODOLOGY

3.1 Introduction

The field sites and methodology used in this study were chosen to provide data suitable for analysis using the conceptual framework developed in Chapter 2. The field sites therefore display a range of beach slopes, sediment sizes, and wave breakers that are characteristic of the *Beach Types* shown in Figure 2.3. Some compromises were necessary in the range of data collected. However, the simple methods used provided adequate data on all features of the swash described by the shallow water theory.

Essential details of the field sites and methodology are described in the remainder of this Chapter. Also discussed are estimates of the possible experimental errors that can arise in obtaining and interpreting the data. These estimates are particularly relevant to the interpretation of results presented in later Chapters.

3.2 Field Sites

Within the study region (Fig. 3.1), a suite of natural features combine to provide a very suitable field laboratory in which to obtain data for this study. The amount of deep water wave energy present in the study region is relatively high by world standards (Davies, 1980). Deep water wave heights in excess of 1 m occur 80 % of the time, heights in excess of 4 m occur 1 % of the time, and wave period typically ranges between 6 and 14 seconds (Wright *et al.*, 1980). The modal deep water wave condition, defined as the wave height and period combination at which the product of wave power and frequency of occurrence is maximum, is a 2.5 m swell wave with a 10 s period (*ibid.*). The tides in the region are semi-diurnal, and display a diurnal inequality (Davies, 1980). The spring tide range varies slightly, but is always less than 2 m so that the beach morphology is indicative of wave-dominated processes (Wright *et al.*, 1980; Short and Wright, 1981).

The inner continental shelf along the New South Wales coast line is relatively narrow and steep, with the 30 m depth contour generally lying within

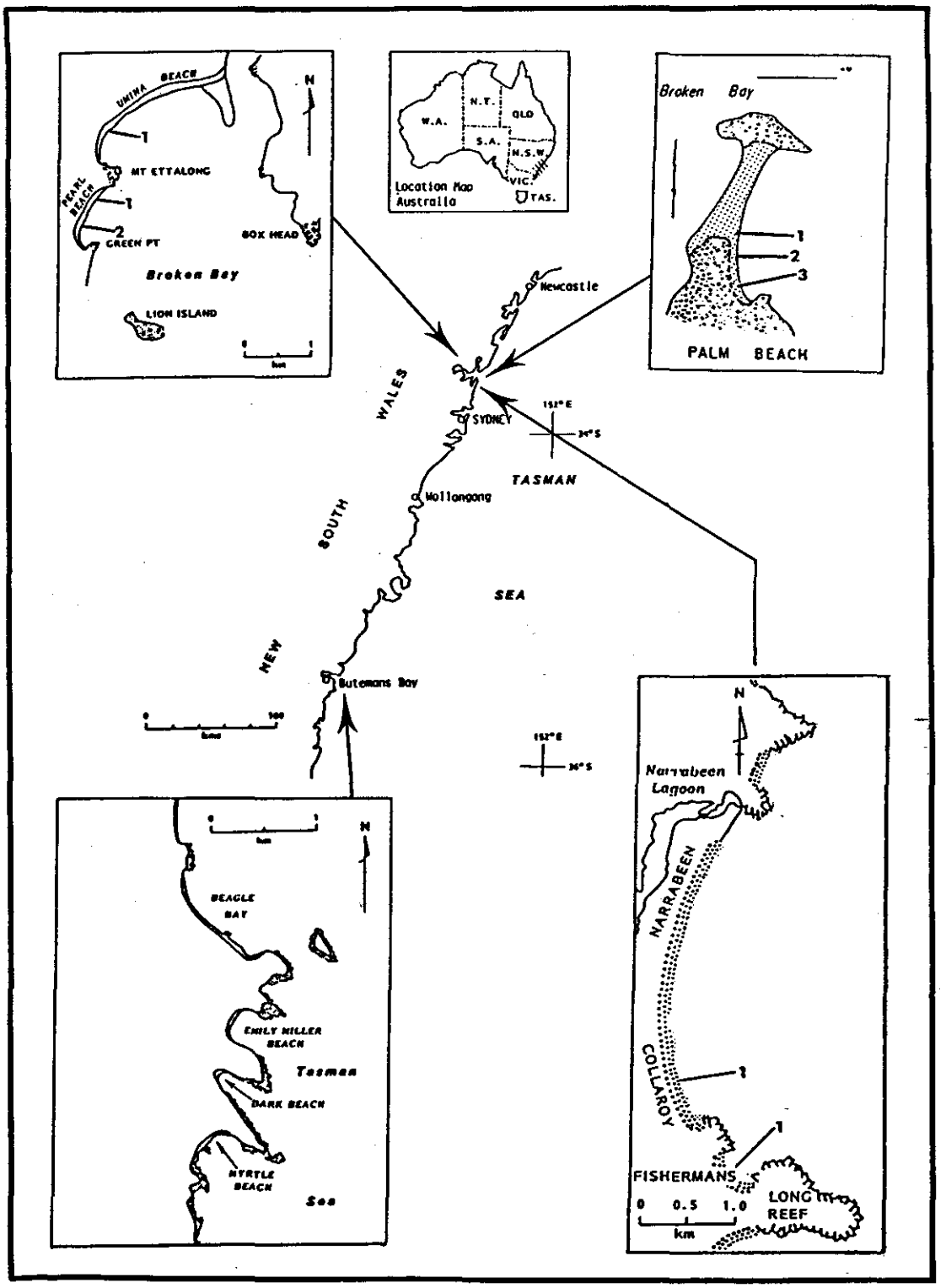

Figure 3.1: **Location maps showing the field sites used in this study.**

2-3 km of the coast (Wright, 1976a). Consequently, on average 96 % of the deep water wave energy reaches the surf zone on the open coast study sites (Fig. 3.1; *ibid.*). However, due to the frictional attenuation of wave energy across Broken Bay, the two field sites located at the back of the bay receive only 75 % of the available energy (Wright *et al.*, 1980).

The compartmentalized nature of the coastline, with alternating rocky headlands and sandy bays, causes variations in the degree of exposure to wave energy within and between embayments. In addition, the diversity of sand grades available (Short, 1984) means a variety of beach and surf zone morphologies exist both spatially and temporally within the study region (Short and Wright, 1981). In particular, the *Beach Types* shown in Figure 2.3 are well represented.

In order to experimentally investigate the theory presented in Chapter 2, two environmental conditions are necessary: large incident wave periods to avoid interference of the backwash by incoming waves, and sufficient levels of wave refraction to ensure that the angle of wave incidence is normal to the shoreline. The wide range of periods associated with natural waves, and the secondary refraction of waves due to surf zone morphology frequently complicates this description. However, the environmental characteristics described above ensured that the field sites satisfied these constraints for periods sufficient to obtain the necessary data.

A total of 25 field experiments were conducted during this study. The site of each experiment, general environmental conditions, and type of experiment performed are listed in Table 3.1. The Table indicates the range of morphodynamic conditions that this study encompasses, and thus the range of conditions for which the study can be considered representative. It is apparent that medium to coarse sandy beaches displaying the morphodynamic conditions schematised in Figure 2.3 are well represented.

3.3 Instrumentation

3.3.1 Introduction.

The small water depths and transient nature of the swash pose significant logistical problems to data acquisition, hence the range of variables which can be measured in the field is limited. A brief summary of previous field methods is presented below to provide a rationale for the choice of

TABLE 3-1
LIST OF FIELD EXPERIMENTS

No.	Date	Beach	Site	ß	H_b	D	Beach Type	Exp. Type
1	11/08/86	Palm	1	0.13	0.30-0.65	0.40	A	1
2	11/08/86	Palm	1	0.13	0.30-0.60	0.39	A	1
3	22/08/86	Warriewood	1	0.11	0.10-0.45	0.49	A	1
4	22/08/86	Whale	1	0.12	0.25-0.70	0.79	A	1
5	16/09/86	Fishermans	1	0.10	0.15-0.65	0.53	B2-C	1
6	16/09/86	Palm	2	0.07	0.15-0.40	0.33	A	1
7	01/12/86	Collaroy	1	0.13	0.20-1.10	0.41	A-B1	1
8	01/12/86	Collaroy	1	0.13	0.20-0.90	0.41	A	2
9	17/12/86	Palm	3	0.13	0.15-0.55	0.29	B2	1
10	17/12/86	Palm	3	0.13	0.20-0.55	0.29	B2-C	2
11	13/01/87	Pearl	2	0.14	0.20-0.50	0.40	C	1
12	13/01/87	Pearl	2	0.14	0.20-0.50	0.43	C	2
13	14/01/87	Ocean	1	0.14	0.20-0.40	0.32	A-B1	1
14	14/01/87	Ocean	1	0.14	0.20-0.40	0.33	A-B1	2
15	14/01/87	Pearl	1	0.15	0.15-0.75	0.40	C	1
16	14/01/87	Pearl	1	0.15	0.20-0.65	0.40	C	2
17	30/01/87	Dark	1	0.13	0.10-0.30	2.00	C	1
18	31/01/87	Dark	1	0.14	0.40-0.60	4.21	C	1
19	31/01/87	Dark	1	0.14	0.20-0.55	4.21	C	2
20	10/02/87	Newport	1	0.15	0.25-0.80	0.44	A	1
21	10/02/87	Newport	1	0.15	0.35-0.70	0.44	A	2
22	13/02/87	Palm	2	0.13	0.30-0.65	0.31	A	1
23	13/02/87	Palm	2	0.13	0.30-0.60	0.31	A	2
24	13/02/87	Whale	1	0.09	0.25-0.55	0.46	A	1
25	13/02/87	Whale	1	0.09	0.25-0.45	0.46	A	2

N.B. The range of H_b refers to that measured near the shoreline.
The parameter D is the mean grain diameter at the mid swash.
D is given in mm.

instrumentation chosen in this study. It will be apparent from this discussion that the choice of instrumentation necessarily depends on the type of analysis proposed. Since this study proposes to analyse field data on a wave by wave basis, the choice of instrumentation was made accordingly.

3.3.2 Previous field methods.

Most of the previous studies that present field measurements of swash have concentrated on time series analysis of the shoreline motion, with many adopting time-lapse photography to obtain their data. This type of data has successfully been used to describe the nature of the swash spectrum (*e.g.* Huntley *et al.*, 1977), and to examine extreme statistics of the maximum swash height (Holman, 1986). Furthermore, photographic techniques have occasionally been used to measure spatial averages of the shoreline velocity (*e.g.* Wright, 1976b; Bradshaw, 1982).

In addition to the camera technique, dual resistance wires have also been used to measure time series of the shoreline position (Guza and Thornton, 1982). This method involves the placement of two parallel wires above the bed at some constant nominal elevation. The shoreline position is indicated by the water level on the wire, which varies the electrical resistance. Although the data collected by this method has principally been used to characterise shoreline spectra (*e.g. ibid.*), it could also be used to provide data for a single wave analysis of shoreline displacement. However, a serious limitation of the method is that the shoreline is defined as the point where the swash depth becomes less than the wire elevation. This may lead to significant errors under a variety of field conditions.

Based on a design initially developed by Schiffman (1965), Kirk (1971) measured the force of swash flows using a dynamometer. This type of instrument can provide data on local flow energy, and water velocity for a single swash cycle. However, measurement of gradients in water velocity cannot be achieved without deploying several instruments. Sonu *et al.* (1974) also measured water velocities, but they used impeller flow meters. Similar attempts were made in this study using the impeller flow meters described in Nielsen and Cowell (1981), but these were unsuccessful due to the small water depths in the swash, and the jamming of the impeller by sand.

In order to obtain spectra of water and bed surface elevations, Waddell (1973) used an array of swash capacitance probes positioned on the beach face in a line normal to the swash flow. Such an array, combined with the appropriate experimental technique, can also provide measurements of swash depth, shoreline velocity, shoreline displacement, and maximum swash height. This type of data is particularly relevant to the approach of this study, as spatially distributed information can be obtained simultaneously over a single swash cycle.

It is clear from the preceding discussion that the choice of instrumentation ultimately depends on the aims of the research. The use of photography is valuable in making measurements of the shoreline position, particularly during high energy conditions when it is desirable for the instrumentation to be isolated from the flow. Frequency analysis of the shoreline motion can be satisfactorily examined using either photography, or resistance wire techniques. However, there are serious problems with using the latter to measure maximum shoreline displacement. For the purposes of this study, swash capacitance probes designed after those of Waddell (1973) were chosen to collect data. This choice was made because they are simple to construct, and are capable of measuring all the features of a single swash cycle necessary to test the theory presented in Chapter 2. It would have been desirable to also measure internal water velocities in the swash, however, the technological constraints did not allow this.

3.3.3 Swash capacitance probes.

Six swash capacitance probes were built to measure water surface elevations on the beach face. Each probe was constructed from brass and perspex rods which support a looped teflon coated wire (Fig. 3.2a). The height of the probe, 1 m, was chosen to permit the measurement of most swash depths when a sufficient length was buried in the sand for support. The wire diameter, 1 mm, was chosen large enough to avoid stretch or breakage, and small enough to avoid the problem of water collecting on the upstream edge. The brass rods were sufficiently spaced to cause no disturbance of the water surface near the wire. The teflon coating on the wire limited the formation of water droplets so that a clearer representation of the water surface could be obtained.

A

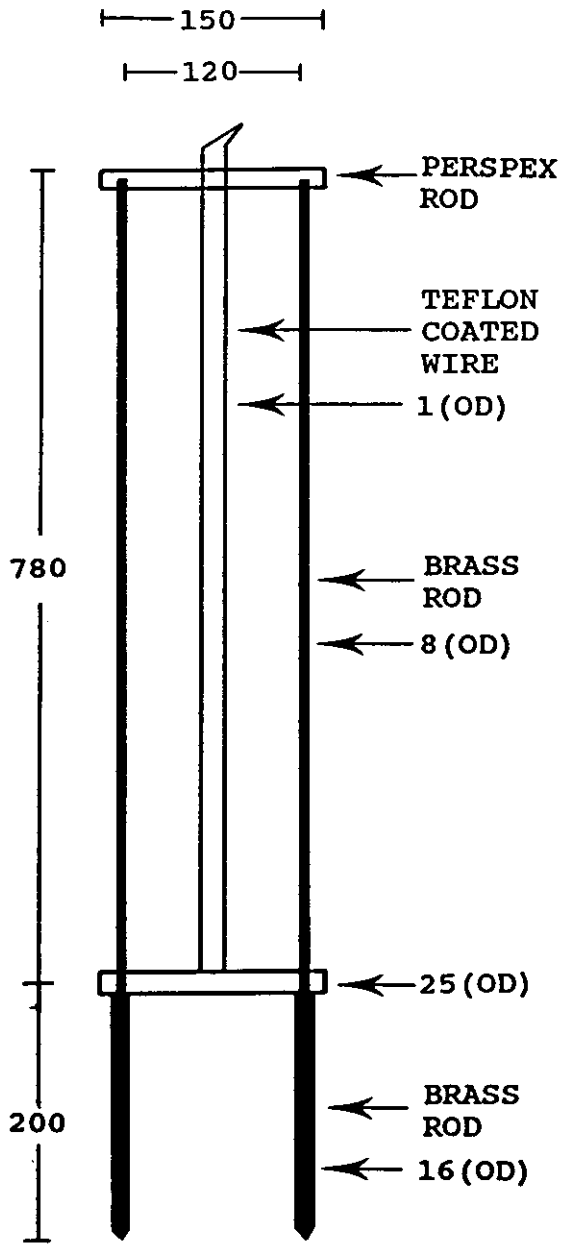

Figure 3.2: (a) Schematic of a swash probe showing dimensions and materials used for construction.

B

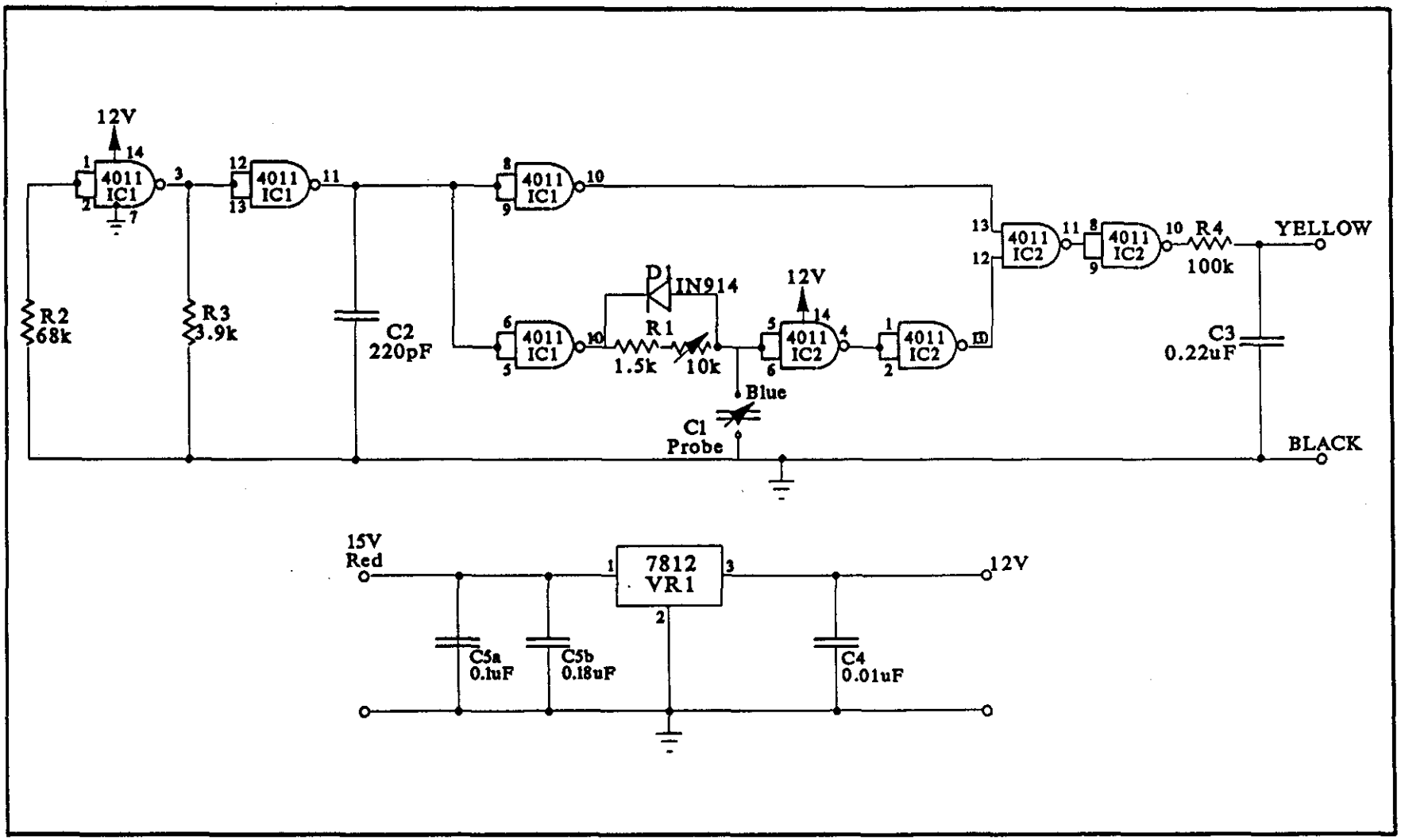

Figure 3.2 contd.: *(b)* Circuit diagram for swash probes.

The water surface elevation is measured by the probe in the following way. The water and wire of the probe act as the two plates of a capacitor, and the teflon acts as the dielectric. Consequently, the capacitance of the probe, which is converted to a DC voltage through the associated circuitry (Fig. 3.2b), is linearly proportional to the immersed length of the probe. The elevation of the bed surface on the probe is easily determined from the ambient capacitance level present between successive swash cycles.

Each probe is self contained and supported by its own circuit board. The boards are housed in water tight containers, and mounted close to the probes to minimise the length of cable sensitive to changes in capacitance. A power box was constructed to distribute 18 V DC power to the probes, and relay variable output DC voltage from the probes to the chart recorders. This box was also designed to enable the synchronised activation and de-activation of the probes.

On site calibration of the probes was carried out after every experiment by lowering each into a container of water at known increments, and recording the corresponding change in output voltage on to the chart. Over the seven months of field use, no maintenance of the probes or circuitry was required, and the calibration information indicated that their response remained linear.

3.3.4 Chart recorders.

The variable output voltage from the swash probes was recorded on two Rikadenki three channel strip chart recorders (R-OX series). These recorders were powered by a portable Dunlite Power Generator (50 Hz, 240 V). Chart recorders were chosen in preference to digital recording to permit immediate on-site assessment of the data, and thus enable greater control over any changes in experimental conditions.

3.3.5 Cine-camera.

The wave conditions seaward of the still shoreline, and the early stages of the uprush were filmed with an Agfa Super-8 cine-camera. The films were analysed using an Agfa movie projector with both freeze-frame and single frame advance capabilities.

3.4 Experimental Design

3.4.1 Introduction.

Two types of experiments were performed to obtain data for this study. Data obtained from the Type 1 experimental design provided most of the information used in later analyses: initial swash velocity, time-history of shoreline displacement, maximum swash height, maximum swash depth, and water surface profiles through time and space. The Type 2 experimental design was only used to obtain detailed measurements of the water surface profile of the leading edge. Both of these experimental designs are described below.

3.4.2 Type 1 experimental design.

An example of the Type 1 experimental design is shown in Figure 3.3a. Range poles marked in 10 cm increments were placed in a line that traversed 5 m of the inner surf zone; immediately seaward of the initial shoreline. Six swash probes were placed in a line across the beach face with their associated circuitry mounted on stakes within close proximity. The probes were positioned to provide good coverage of the prevailing swash length.

As a wave propagated towards the beach face its progress was filmed to provide data on wave height, celerity, and breaker type immediately seaward of the swash zone. Filming continued as the wave crossed the initial shoreline and progressed into the early stages of the uprush. This provided a visual record of the wave transformation across the initial shoreline. At the moment the swash phase began the probes were activated and recorded the progress of the leading edge across the beach, and the time-history of the water surface elevation at each probe. When the point of maximum uprush was reached, the distance of the leading edge from the most landward probe was measured. This provided an estimate of the maximum swash length, and a trigonometric estimate of maximum swash height. At the time of maximum uprush a tic mark was placed on the chart, which required a subjective decision from the operator. This mark enabled the value of $t_{(max)}$ to be estimated. Data recording from the probes continued until the end of the backwash phase.

Following each experiment the beach profile was surveyed to provide the bed slope, and locate the swash probes. Also, sediment samples were collected from the base of the beach, the mid swash, and the approximate limit of maximum uprush. The samples were collected from the top 1-2 cm of the bed to maintain some consistency with the experimental conditions.

A

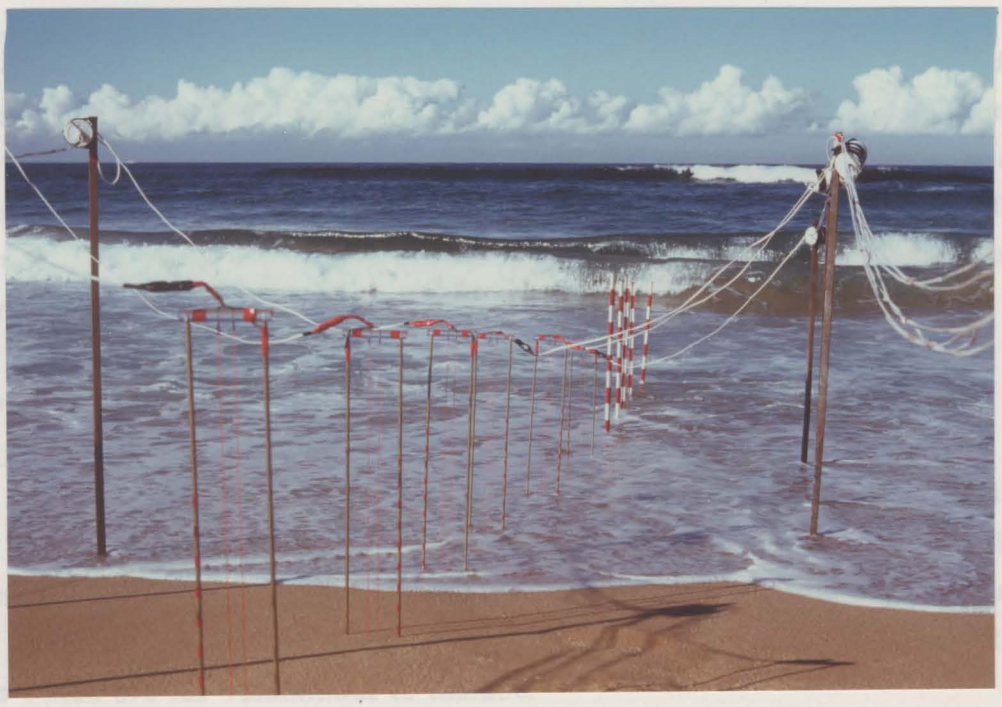

B

Figure 3.3: *(a)* **Photograph showing general configuration of Type 1 experimental design.** *(b)* **Photograph showing general configuration of Type 2 experimental design.**

3.4.3 Type 2 experimental design.

A variation of the instrumentation array described above was used to collect high resolution data on the water surface profile of the leading edge. A Type 2 experiment consisted of six swash probes positioned along a line, and separated by only 2.5 cm (Fig 3.3b). This design provided detailed water surface measurements of the leading 12.5 cm of the swash lens. The remaining experimental procedure was identical to that described above (Section 3.4.2).

3.5 Data Reduction And Laboratory Techniques

3.5.1 Introduction.

The two types of data storage used for the experiments just described were film and chart records. The methods used to extract the required information from these records are described below. All of the experimental data are tabulated in Appendix A, with the exception of the digitized time series which are too voluminous to include.

3.5.2 Analysis of film records.

The film records were analysed using an Agfa movie projector with freeze-frame capabilities. The film records were used to calculate the wave height, wave velocity, initial swash velocity, and to identify the breaker type at the initial shoreline. The wave height was estimated to the nearest 0.05 m from the range poles immediately seaward of the initial shoreline. More accurate measurements were not possible due to the film resolution of the pole markings. The possible error in the measurement of wave height is nominally estimated at 0.05 m, with larger errors probably occurring for the largest wave heights.

The wave velocity measured from the film record was a spatial average between the range poles, which were placed 1 m apart. The velocity was estimated by counting the number of frames required for the wave to advance between two adjacent poles. The camera exposed 18 frames per second, thus yielding a recording interval of 0.056 s. It is worth noting that the instantaneous wave velocity near the shoreline is extremely variable (see Fig. 2.8), and the spatial averages measured here are not representative of the instantaneous value. The initial swash velocity was measured over a much shorter distance, 0.5 m, immediately seaward of the first swash probe. Due to the shorter averaging distance, these measurements are believed to be a reasonably good estimate of the instantaneous velocity.

Errors in estimating velocities from the film are most likely to arise from a miss-count of the number of frames required for the shoreline to advance across the sampling distance. The percentage error due to a miss-count of one frame is shown in Figure 3.4, and was calculated using the following method. For each velocity shown on the abscissa, the number of frames required to measure a propagation length of 1 m was calculated from the film speed of 18 frames per second. One frame was added to each result to simulate an error. The erroneous velocity was then calculated, thus providing the percentage error curve shown in the Figure. For the range of typical swash velocities recorded during the experiments, which is mostly less than 4 m s^{-1}, an error arising from miss-counting will be less than 20 %.

3.5.3 Analysis of chart records.

As a wave climbs the beach the probe records the change in capacitance, and hence water surface elevation with time. Before and after the presence of the swash lens at the probe, the position of the wetted sand surface is represented as a horizontal line on the chart record, indicating the constant capacitance of the emerged bed. Although the bed level is not indicated when the probe is immersed, levels before and after the swash cycle indicate that changes were insignificant over one swash cycle

The record of the bed level is very useful for defining the swash depth, however, some subjective interpretation is required when the wetted sand surface recorded by the probe is below the true bed surface (see Fig. 3.5). This situation occurred when there was infrequent inundation of the upper beach face so that the bed became relatively dry between swash cycles. When this problem was apparent the zero depth level (*i.e.* true bed level) was always chosen to be the level (B) measured at the end of the backwash phase, rather than the level (A) which precedes the arrival of the swash (Fig. 3.5). Level (B) is likely to involve the least error since the level (A) recorded just prior to the uprush may include several minutes of drying time.

In order to obtain true measurements of swash depth and water surface elevation from the chart records, the records were digitized using a Summagraphics digitizing tablet and task specific software run on a Tektronix 4051 micro-computer. The records from Type 1 and Type 2 experiments were digitized at 0.1 s and 0.01 s intervals respectively. The digitized information

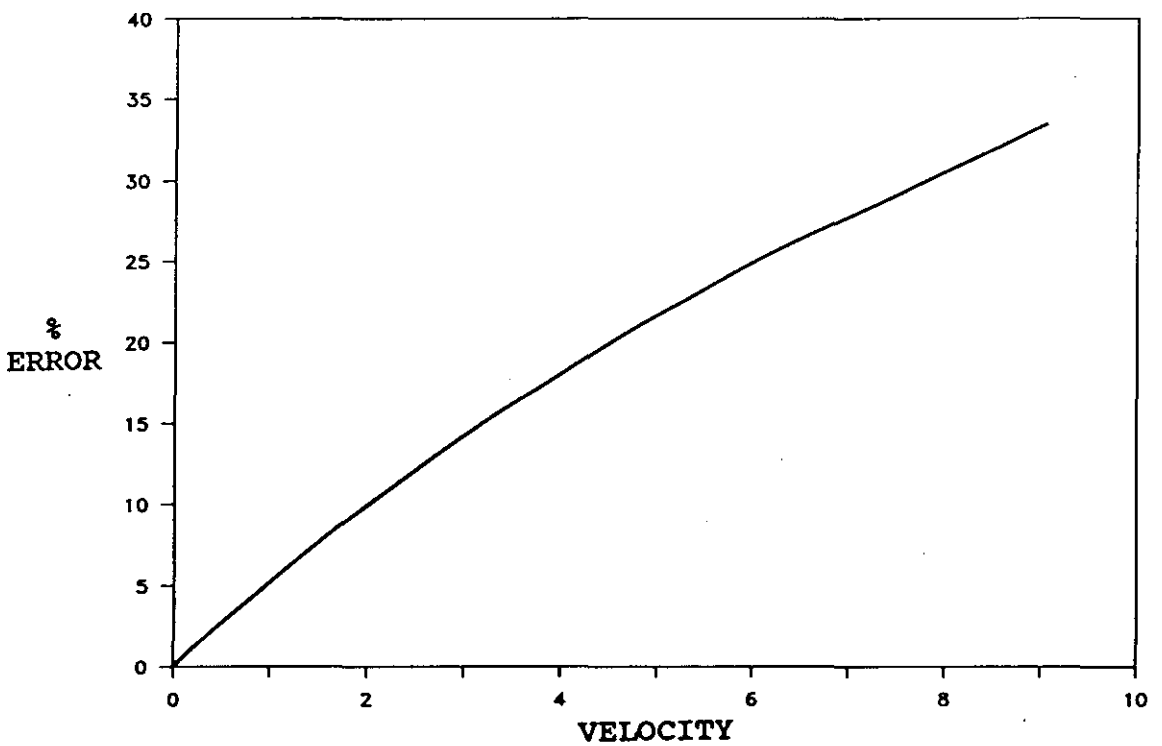

Figure 3.4: Expected error in estimating velocity due to a miss-count of one frame when analysing the film records.

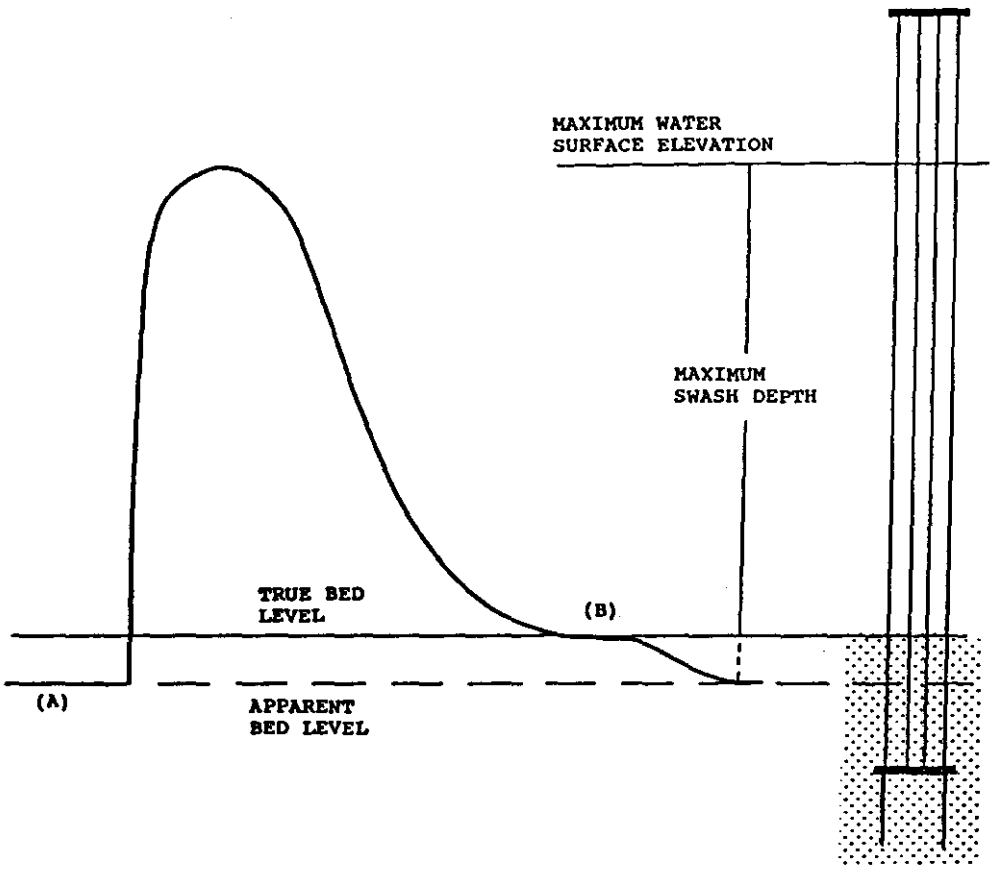

Figure 3.5: Method used for estimating swash depth when the beach surface is subject to drying between swash cycles. (A) indicates the apparent bed level, which is the surface of the wetted sand measured by the probe. (B) indicates the true bed level, which can be recognized in the chart record immediately after the disappearance of the backwash.

was then put through a simple computer algorithm to transfer volts to water surface elevations using the probe calibration data. A total of 1469 time series were digitized. These provided data for 300 individual swash cycles.

The digitized data provided the opportunity to obtain two sets of information. The first set contains measurements of the time-history of shoreline displacement, and the second contains measurements of the swash depth used to re-construct water surface profiles through time and space.

Figure 3.6 illustrates the method for re-constructing the time-history of shoreline displacement relative to the most seaward swash probe. The points (A), (B), and (C) represent the arrival time of the moving shoreline at each probe, and are measured along the abscissa in the Figure. The location of the probes relative to the most seaward probe is determined from the survey, and are measured along the ordinate to map (A'), (B'), and (C'). The time-history of shoreline displacement is thus obtained. The point (0,0) on the mapping represents the arrival time of the shoreline at the first probe, and is taken for the experiments to be the beginning of the swash cycle. Although the swash cycle is defined to begin at the point of collapse of the initial wave type (Section 1.1), this point is difficult to discern in the film records since the transformation to swash is not instantaneous (Sections 4.2.2, 4.3.2, 4.4.2). Consequently, measurements of the swash length, swash height, and shoreline displacement are made relative to the most seaward swash probe; where the initial swash velocity is also measured. The equations presented in Section 2.4.4 indicate that no information is lost using this approach, permitting the removal of any uncertainty in interpreting the exact time at which uprush begins.

Errors involved in obtaining the shoreline displacement from the chart records are believed to be negligible since the arrival of the swash at the probe produces an instantly recognisable increase in capacitance over that associated with the emerged bed (see Fig. 4.11a).

The method used to obtain the maximum swash depth and water surface profiles are shown in Figure 3.7. The maximum swash depths and time of occurrence are identified by (1), (2), and (3), and are measured from the record as shown. The time-history of swash depth at each probe is simply the digitized time series shown in the Figure. The water surface profile of the swash lens at the time of maximum uprush can be re-constructed from the swash depths (A),

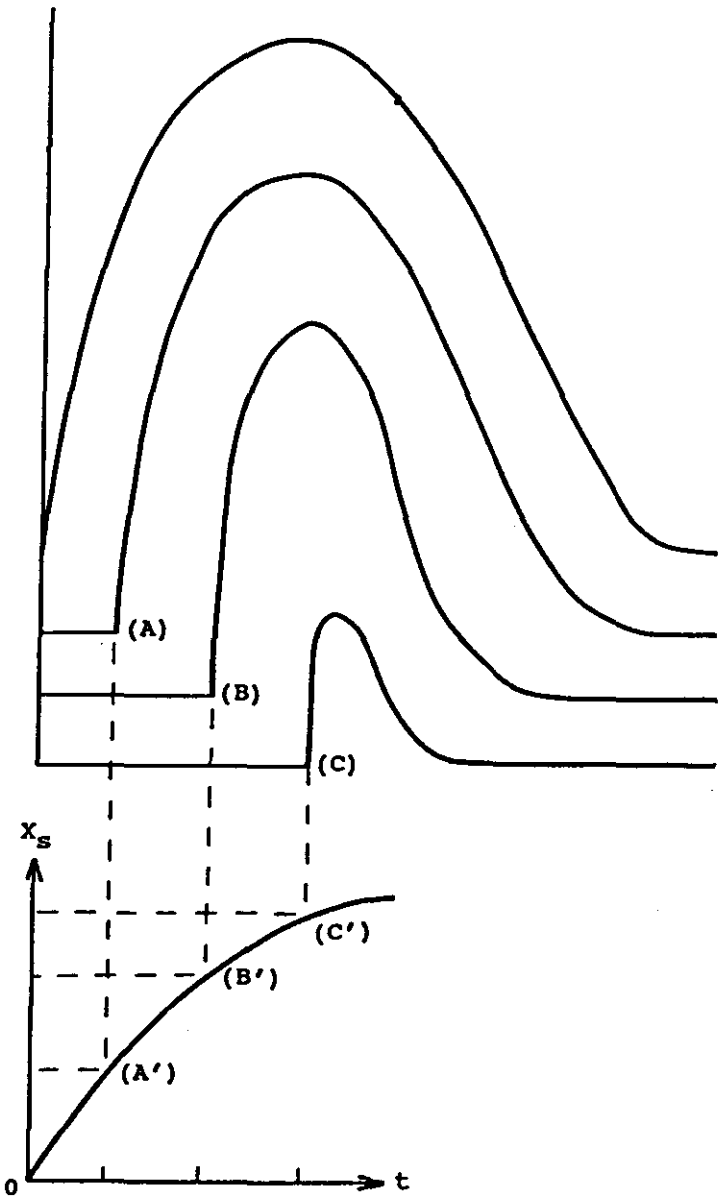

Figure 3.6: Method used for determining the time-history of shoreline displacement from the chart record. The time of arrival of the shoreline at each probe is indicated by (A), (B), and (C). These are combined with the surveyed probe locations to map the locus of shoreline displacement; (A'), (B'), and (C').

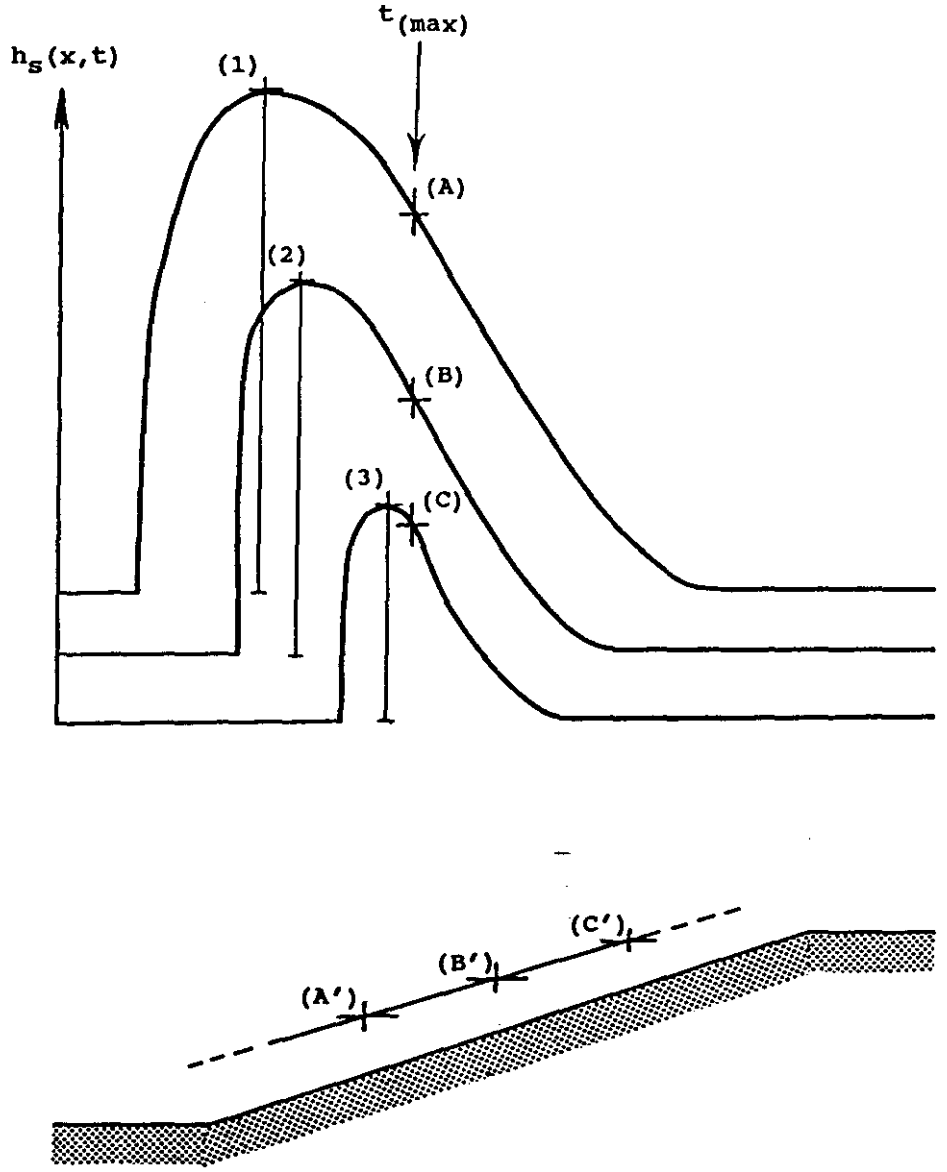

Figure 3.7: Method used for determining the maximum swash depth and water surface profile at the time of maximum uprush. The maximum swash depth and time of occurrence at each probe location is indicated by (1), (2), and (3). The swash depths at the time of maximum uprush are indicated by (A), (B), and (C). These are combined with the surveyed probe locations to produce a profile of the water surface elevation; (A'), (B'), and (C').

(B), and (C), and the surveyed probe locations as shown. In fact, the water surface profile at any time during the swash cycle can be re-constructed using this method.

High resolution water surface profiles of the leading edge were re-constructed from records obtained using the Type 2 experimental design, and the data reduction method just described (Fig. 3.7). In this case however, the time the leading edge arrived at the most landward probe was used for reference. The swash depths were determined at each probe for this reference time, and then combined with the surveyed position of the probes to reconstruct the water surface profile. Typical time intervals of shoreline travel between the two outside probes was of the order of 0.1 s for the Type 2 experimental design. Consequently, the swash depths are measured from the very steep part of the record where large measurement errors can occur if a coarse digitizing interval is used. Thus, a digitizing interval of 0.01 s was applied to obtain these data.

Three possible sources of error relating to measurements of swash depth and water surface elevation are recognized. The first arises from flow interference created by the measuring wire. This was observed to be most problematic near the base of the beach where the largest water velocities occur. The disturbance of the water level occasionally reached 2 cm for the strong deep flows, but was usually of the order of 1 cm. For typical swash depths on the lower beach face, this is likely to produce a maximum error no greater than 10 % of the swash depth. The second source of error relates to the problem of beach drying discussed above (Fig. 3.5). This problem is most apparent on the upper beach face where inundation may be infrequent. When a subjective interpretation of the bed level is necessary, the error may be on the order of 10 % of the swash depth typical on the upper beach, if the maximum depth of drying is assumed to be 1 cm. It should be noted at this point, that it is very unlikely errors due to these two sources will ever arise together, as they are restricted to the lower and upper beach face respectively. The third source of error is the presence of foam floating on the surface of the swash lens. This foam often maintains its thickness for the entire swash cycle. The effect on the measured capacitance may lead to only minor over-estimation of the water depth on the lower beach since depths are relatively large, but on the upper beach the effect is more pronounced since the foam thickness may equal the water depth. Fortunately, foam rarely covered more than 60 % of the swash

lens, and occurred in patches which appear as oscillations in the probe output (see Fig. 4.11a). This enabled some estimation of the foam's thickness. In considering all of these factors it is believed, that for the most part, any errors in estimating the swash depth are unlikely to exceed 50 % and are most likely to be about 15 %.

It is worth noting that the magnitude of these possible measurement errors are largely due to the thin and transient nature of the flow, rather than poor instrument performance. This highlights the principle difficulty encountered with field experimentation in the swash zone, where small measurement errors in terms of absolute magnitude convert to relatively large percentage errors.

3.5.4 Analysis of sediment samples.

The collected sediment samples were washed and dryed in the laboratory. A split of 100 gm from the sample was used for sieving at quarter phi intervals. Retained weights in each of the sieves were used to obtain a frequency distribution of the sample so that statistical moments of the distribution could then be calculated. The mean grain diameter, or first moment of the distribution, was converted from phi scale to mm and is the value used in this study to characterize the size of the bed material.

3.6 Summary

It is apparent from Table 3.1 that the range of experimental conditions offered by the field sites used in this study are very representative of conditions where incident swash predominates (see Section 2.3). The experimental design chosen here has provided data measuring several features of the swash, which can be analysed using the framework developed in Chapter 2. The measurements include wave height, wave velocity, initial swash velocity, maximum swash height, time-history of shoreline displacement, and water surface elevations through time and space.

In describing the experimental method and data reduction techniques, several estimates of possible measurement and interpretation errors have been included. These indicate the confidence that can be placed in the data analysis and results presented in subsequent Chapters. It is noteworthy that data measuring the initial swash velocity, the time-history of shoreline displacement, and the maximum swash height are believed to be very representative.

However, it is possible that significant errors exist in the data describing swash depth and water surface elevation.

CHAPTER 4
FIELD MEASUREMENTS OF SWASH

4.1 Introduction

This Chapter presents original data that describes several features of swash on natural beaches. The features which will be discussed include wave height at the shoreline, initial swash velocity, time-history of shoreline displacement, maximum swash height, mean shoreline velocity, maximum swash depth, and water surface profiles of the swash lens. The ability of the experimental design to provide accurate representation of these characteristics has been discussed in Chapter 3, and should be considered in interpreting the data presented below.

The specific aim of this Chapter is to compare the theoretical solutions for swash presented in Chapter 2, with the field data collected during this study. The comparison is made graphically, and by determining least squares regression models for the data. If the regression models have the same form as the relationships predicted by theory, then it is assumed that the theory is able to qualitatively describe the physics of swash, as far as the assumptions allow. Any quantitative deviations from the theoretical predictions are assumed to be a result of factors not included in the theoretical analysis (see Section 1.4).

Measurements of swash following bore collapse, plunging breakers, and surging waves are presented separately in Sections 4.2, 4.3, and 4.4 respectively. This separation of the analysis conforms to the theoretical framework for study developed in Chapter 2. As this Chapter progresses, it becomes obvious that there is very little difference in the data measured on the three *Beach Types*. Furthermore, it is shown that the solutions of the SWE for bore uprush are successful in describing the swash for both the breaking and non-breaking waves measured in this study. This prompts a new exposition of the non-linear shallow water theory, that contrasts with the traditional view of the theory set forth in Chapter 2 (Section 4.5). A general description of the backwash is presented in Section 4.6. As an introduction to the analysis of flow resistance contained in Chapter 5, evidence existing in the data which suggests the presence of bed friction is outlined in Section 4.7.

4.2 Uprush Following Bore Collapse At The Shoreline

4.2.1 Introduction.

The results reported in this Section relate to data collected on *Beach Type A*. The relevant experimental conditions are listed in Table 3.1 in connection with Experiments 1, 2, 3, 4, 6, 7, 8, 9, 13, 14, 20, 21, 22, 23, 24, and 25. The physical nature of swash following bore collapse on a natural beach is shown in Figure 4.1, and seems to compare well with the theoretical expectations (*cf.* Sections 2.4.3 and 2.4.4). In Figure 4.1a a fully developed bore is shown propagating across a zone of still water towards the initial shoreline. The abrupt changes in water surface elevation and turbulence across the relatively narrow bore front are clearly recognized. When the bore crosses the initial shoreline it collapses, and the free-surface turbulence disappears. The water motion is no longer described by a bore, but a rarefaction wave that climbs the beach. The rarefaction wave appears as a relatively smooth lens of water, the depth of which decreases with time and distance travelled (Figure 4.1b). The foam on the surface of the swash lens is antecedent from the bore phase; it is not generated during the swash cycle. Once the shoreline has reached its maximum height, it begins to move down the beach as backwash. The end of the swash cycle is shown in Figure 4.1c, where the shoreline has returned to its initial position and another bore is seen propagating shorewards.

4.2.2 Bore collapse at the shoreline.

All of the observations of bore collapse reported below relate to fully developed bores. Whenever a partially developed bore was observed in an experiment, the turbulence at the bore front intensified as it propagated shoreward, thus producing a fully developed bore well seaward of the initial shoreline. This observation illustrates the tendency for bores to 'forget' their initial wave form, and is consistent with the theoretical results for sloping beaches proposed by Keller *et al.* (1960) and Ho and Meyer (1962) (Section 2.4.3).

Visually, bore collapse is considered to be complete when there is no longer any water upstream of the bore front, and turbulence generation at the free surface ceases. These conditions correspond to the time when the wave front can no longer be theoretically considered as a bore (see Stoker, 1957). Since in theory the bore is treated as a discontinuity, upon arrival at the initial shoreline its collapse is inferred to be instantaneous (Sections 2.4.3 and 2.4.4).

A

B

Figure 4.1: *(a)* Photograph showing a fully developed bore approaching the initial shoreline. *(b)* Photograph showing the uprush phase of the swash cycle.

C

Figure 4.1 contd.: *(c)* **Photograph showing conditions at the end of the backwash phase.**

On a natural beach however, the fully developed bore has a finite width in the (x,z) plane. Consequently, bore collapse in the field was never observed to be instantaneous. This observation has also been reported by Miller (1968) and Yeh and Ghazali (1988) in reference to their respective laboratory experiments. Despite the theory being inadequate to describe bore collapse, it still describes most of the water motion on the beach face, as the width of the bore collapse zone is very narrow. In accordance with the expectation of Meyer and Taylor (1972), observations from the film records showed that the width of this zone appeared to be positively related to the bore width.

Figure 4.2 shows a schematic of bore collapse that summarizes the pattern of events observed in the film records. In Figure 4.2a the bore is seen travelling toward the shoreline as a quasi-stable form, but decreasing in height and increasing in velocity. This behaviour compares well with Figure 2.8. The width of the bore front and its steepness were observed to be positively related to the bore strength. This observation is consistent with the turbulent energy dissipation model proposed by Svendsen and Madsen (1984). Their model predicts that strengthening bores will increase their surface slope (*i.e.* decrease width) to achieve an increase in energy dissipation sufficient to stabilize the bore shape. Since fully developed bores rapidly increase in strength as they climb the beach (Fig. 2.8 and 2.9), it is expected that the bore front will steepen markedly near the shoreline. This steepening was observed in all the film records, together with an intensification of free-surface turbulence generation (Fig. 4.2a). Immediately seaward of the initial shoreline, instantaneous suspension of large concentrations of sediment in the bore front were also observed (Fig. 4.2b). This was followed by bore collapse and the beginning of uprush (Figure 4.2c).

The steepening of the bore front just seaward of the initial shoreline was also observed by Miller (1968) in his laboratory measurements. These measurements are shown in Figure 4.3. The parameter w_b/η_b, which is inversely related to the steepness of the bore front, decreases sharply near the initial shoreline indicating the steepening of the bore front just described. Once across the initial shoreline w_b/η_b sharply increases again, indicating a rapid flattening out of the bore front and the beginning of uprush. Notice that near the shoreline, the front of the strongest bore steepens the most (Figure 4.3). This confirms both the film observations, and the numerical work of Svendsen and Madsen (1984).

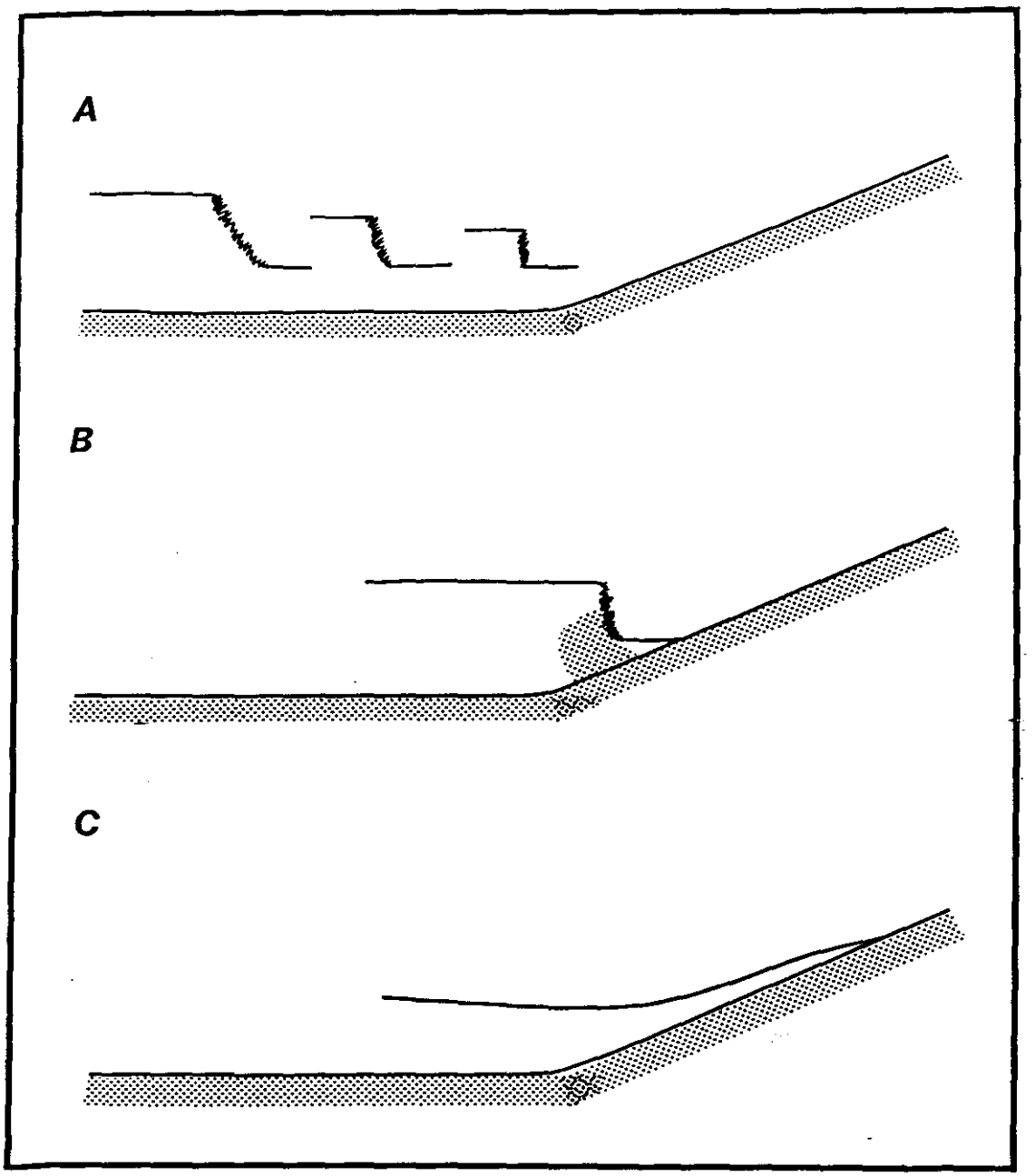

Figure 4.2: Schematic of the transition from bore to swash, which summarizes observations made from the film records.

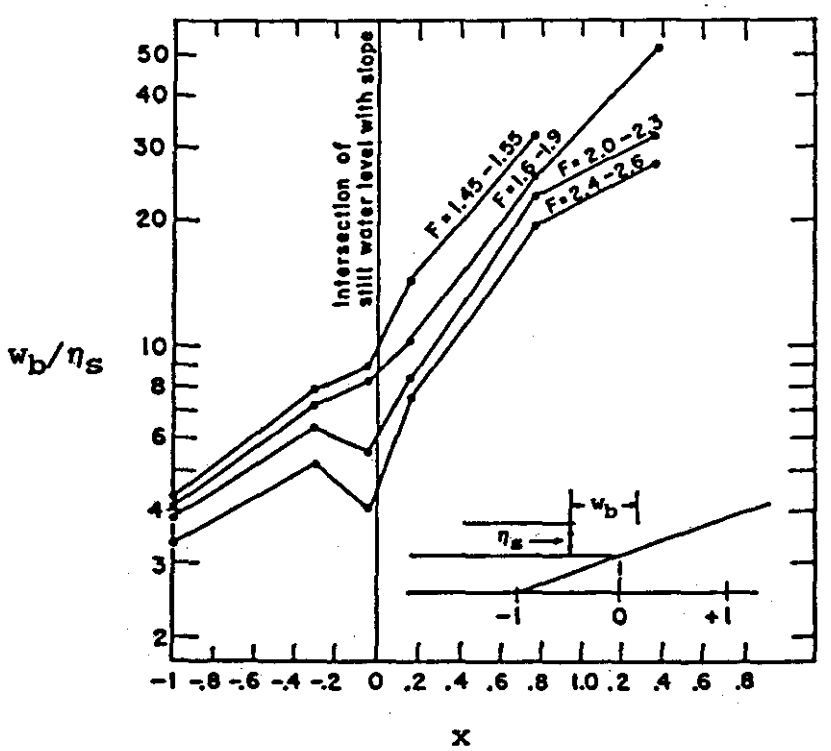

Figure 4.3: Laboratory data demonstrating changes in the bore width as it crosses the initial shoreline (After Miller, 1968).

The instantaneous suspension of large concentrations of sediment in the bore front, near the initial shoreline, is shown in Figure 4.4a. This ubiquitous phenomenon is hypothesized to be a result of the turbulent wake or mixing layer of the bore (see Peregrine and Svendsen, 1978) interacting with the bed. The spread angle of the wake varies directly with the difference in velocity between the bore front and the water upstream (*ibid.*). The wake may not initially extend to the bed for some considerable distance behind the bore (Fig. 2 in *ibid.*). However, since the bore accelerates as it propagates shoreward (Fig. 2.8), the spread angle of the turbulent zone is expected to increase markedly near the shoreline. This effect can be clearly seen in the numerical results of Svendsen and Madsen (1984), which are shown in Figure 4.4b. The collapse of a bore generated in the laboratory, shown in Plate 1 in Yeh and Ghazali (1988), also displays this interaction with the bed.

It is apparent from the preceding discussion that several sources of energy dissipation exist in reality, which are excluded from the theoretical analysis discussed in Section 2.4.3. Unfortunately, a more quantitative assessment of these was not possible due to the difficulties of measuring such processes. Despite recent advances in acoustic and optical back-scatter technology (see Hanes *et al.*, 1988), the measurement of sediment concentrations in highly aerated flow still cannot be achieved without a great deal of uncertainty.

To further advance the understanding of bore collapse, the loss of energy due to turbulence and bottom boundary layer effects may possibly be resolved using the SWE and turbulence model proposed by Svendsen and Madsen (1984). Furthermore, the loss of energy due to bore-backwash interaction can probably be modelled using the standard equations for energy loss in a hydraulic jump (*e.g.* Streeter and Wylie, 1981). For this case, the energy dissipation will be proportional to the Froude number of the backwash flow. Unfortunately, there is very little theoretical understanding of the effects of large sediment concentrations on surf zone wave energy dissipation. A great deal more theoretical and experimental in this area is therefore required, before a complete understanding of bore collapse is possible. The laser techniques now available are already contributing to the experimental study of this problem (*e.g.* Yeh and Ghazali, 1986; 1988).

A

B

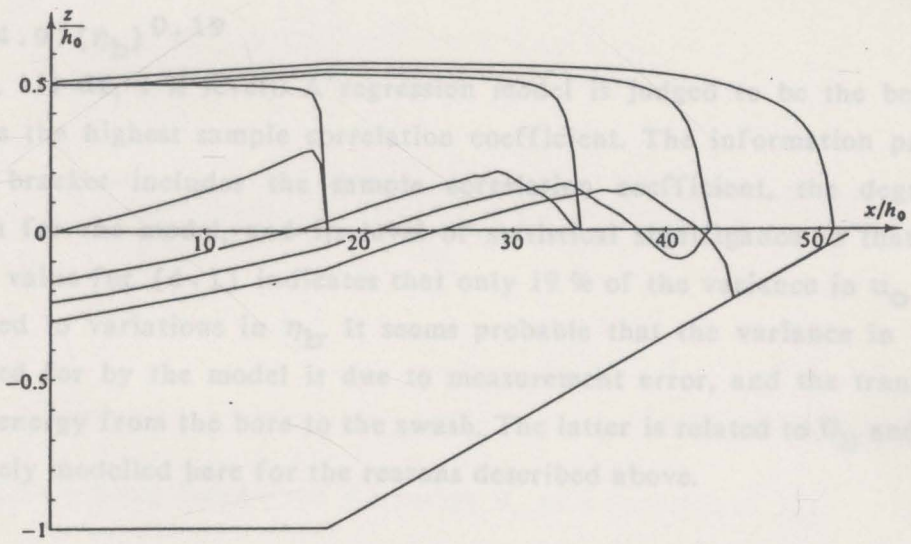

Figure 4.4: *(a)* **Photograph showing large concentrations of suspended sediment in the bore near the time of its collapse (Photo by P. Cowell).** *(b)* **Numerical results from Svendsen and Madsen (1984) showing interaction between the turbulent wake of a bore and the bed. The Froude number of the bore is 1.88.**

In this study, the importance of bore collapse at the initial shoreline arises from its effect on u_o (Section 2.4.4). The dissipation of energy due to the processes just described, which are not accounted for in the bore equations, offer little chance of finding a simple relationship between the terminal U_b and u_o measured in the field. In fact no relationship was found for the data collected in this study. This may be partly explained by the fact that near the shoreline, spatially averaged measurements of U_b are not good estimates of the instantaneous U_b (Section 3.5.2). It seems equally likely however, that boundary layer processes near the shoreline need to be considered in the theoretical model before a quantitative prediction of u_o can be achieved (Section 7.2).

Although no relationship was evident between U_b and u_o, the transfer of potential energy to the swash is certainly indicated in the data. The potential energy is due to the height of the bore above the beach face. The relationship between u_o and η_b is shown in Figure 4.5. The data are aligned parallel to the ordinate, because it was only possible to estimate η_b to the nearest 0.05 m (Section 3.5.2). The best least squares regression model of the data is

$$u_o = 4.97(\eta_b)^{0.19} \qquad (4.1)$$

(r=0.44, 111 df, 1 % level). A regression model is judged to be the best if it provides the highest sample correlation coefficient. The information provided in the bracket includes the sample correlation coefficient, the degrees of freedom for the model, and its level of statistical signifigance in that order. The r^2 value for (4.1) indicates that only 19 % of the variance in u_o can be attributed to variations in η_b. It seems probable that the variance in η_b not accounted for by the model is due to measurement error, and the transfer of kinetic energy from the bore to the swash. The latter is related to U_b and is not adequately modelled here for the reasons described above.

It has previously been suggested that u_o may be proportional to $\sqrt{(gH_b)}$ (Waddell, 1973; Bradshaw, 1982). Since only fully developed bores are considered in this Section, it can safely be assumed that $H_b=\eta_b$. Values reported previously for the constant of proportionality, k, are 3.4 and 1.36 by Waddell and Bradshaw respectively. A frequency histogram of k values measured on *Beach Type A* is shown in Figure 4.6a. The mean value of k lies between those reported by Bradshaw and Waddell. A possible explanation for the range of k is its apparent inverse dependency on η_b, which is shown in Figure 4.6b. Since values of η_b (0.9-1.5 m) contained in Bradshaw's data set are

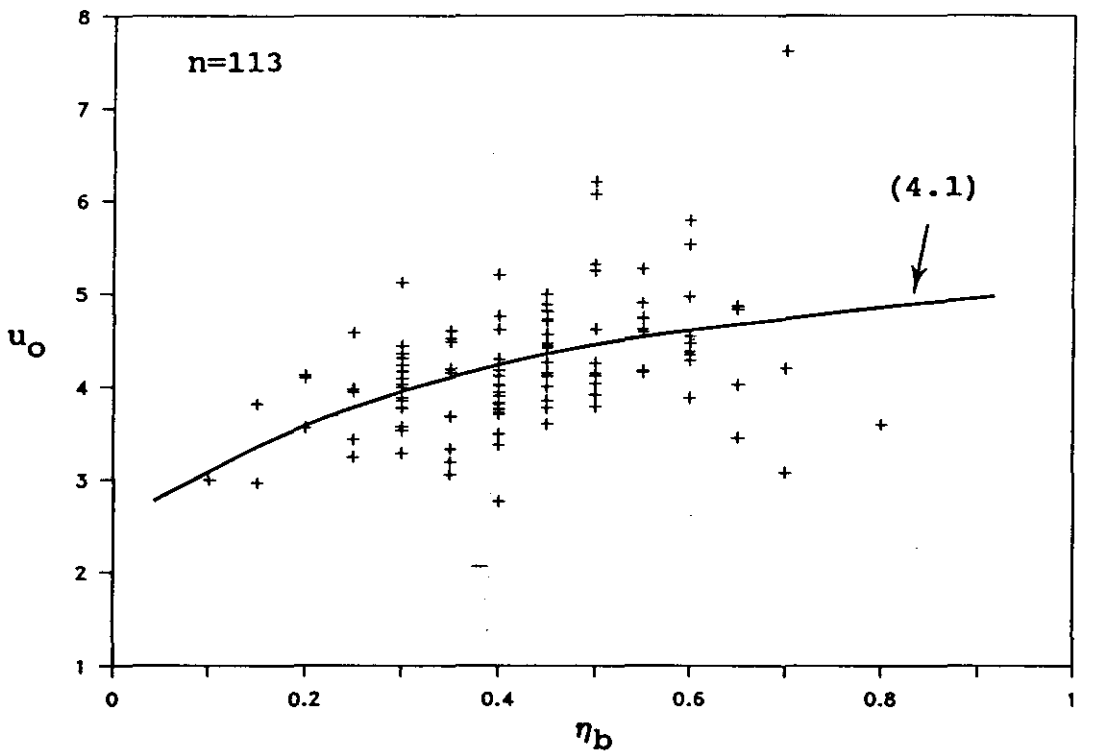

Figure 4.5: Data from *Beach Type A* showing u_o as a function of η_b.

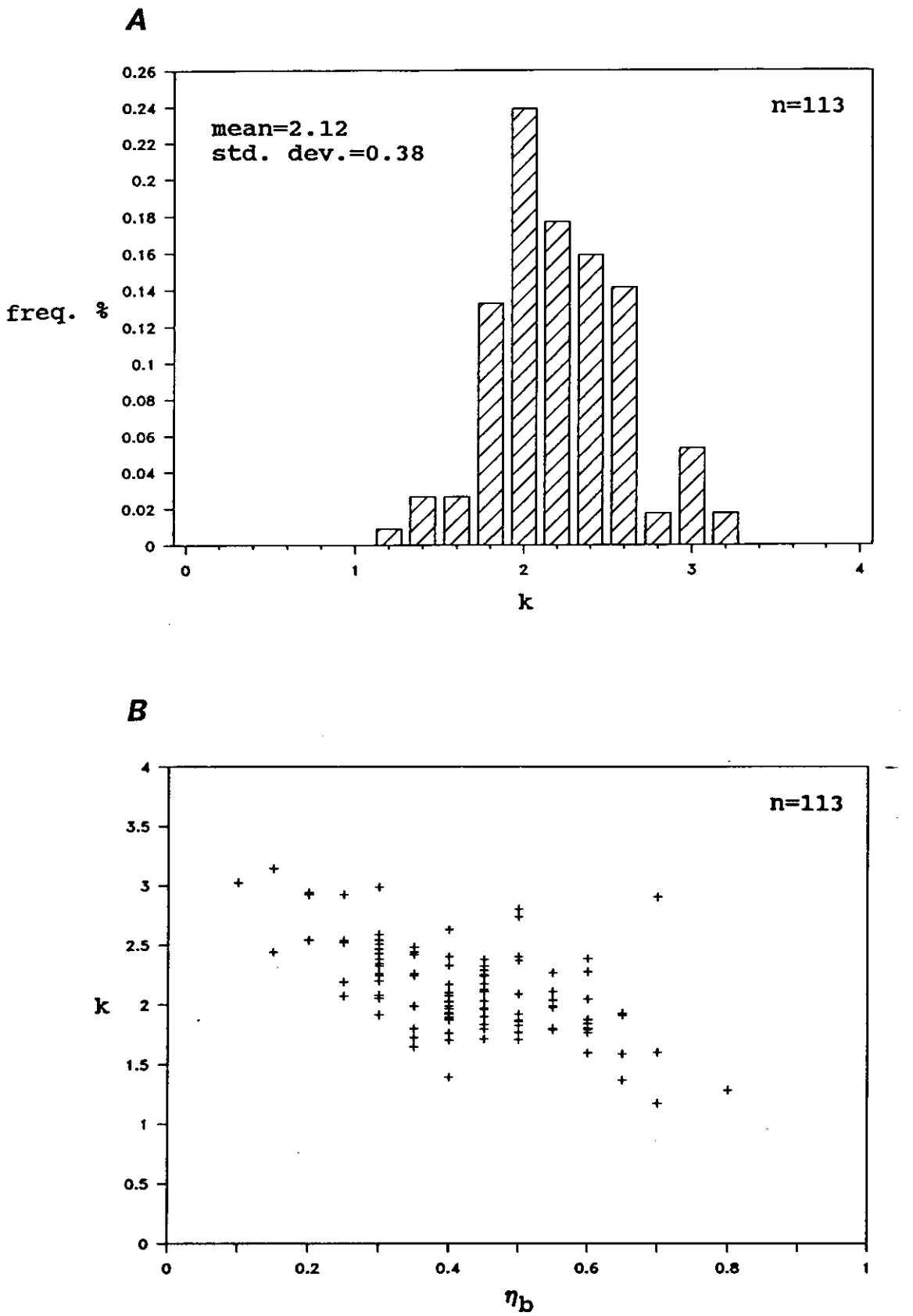

Figure 4.6: *(a)* Frequency histogram of k values measured on *Beach Type A.* *(b)* Values of k as a function of η_b.

at least a factor 3 larger than those measured by Waddell (0.04-0.28 m), his k values are therefore expected to be lower than Waddell's, as indeed is the case. The η_b measured in this study covers the range between these two other studies, and so do the k values. The fact that k>1 indicates that the transfer of energy from the bore to the swash involves more than the potential energy associated with the bore height (Waddell, 1973). The extra energy transferred is the kinetic energy associated with the terminal bore velocity. Stronger bores are expected to dissipate more kinetic energy at the shoreline through the mechanisms described above (see also Svendsen and Madsen, 1984), which may explain why they also have the lowest k values (Fig. 4.6b).

Although some relationship between u_o and η_b is present in the data, the ability to satisfactorily predict the magnitude of u_o is very limited. In the analysis presented in Sections 4.2.3, 4.3.3 and 4.4.3 u_o is therefore taken as the value directly measured (see Section 3.5.2), rather than predicting it from the bore measurements.

4.2.3 Uprush.

In this Section, the theoretical results for swash following bore collapse (Section 2.4.4) are compared with the field data collected on *Beach Type A*. The comparison is made graphically, and through the least squares regression models listed in Table 4.1. In the graphical presentation of the data, only grain size is shown as a third variable in each of the Figures, since the effects of beach slope have been scaled from the data.

According to (2.14) X_s is a quadratic function of t, and dependant on u_o and β. Since the swash probes are stationary, the presence of irregular waves results in a lack of consistency in the location of measurements from one swash cycle to the next. Similarly, the different beach slopes between experiments means that the raw data are not immediately comparable between experiments. For these reasons X_s and t have been non-dimensionalized in the following manner:

$$X_{s*} = X_s/L_s \qquad \text{and} \qquad t_* = t/t_{(max)} \qquad (4.8),$$

where the asterisk denotes the non-dimensional variable, and $t_{(max)}$ and L_s are given by (2.15) and (2.16) respectively. This enables the data for all waves and beach slopes to be compared on the same scale.

TABLE 4.1
LEAST SQUARES REGRESSION MODELS DESCRIBING SWASH ON *BEACH TYPE A*

Model	Eq. no.	r	df	Level
$X_{s*} = 1.44t_* - 0.78(t_*)^2$	(4.2)	0.96	573	1 %
$Z_s = 0.053(u_o)^{1.68}$	(4.3)	0.79	111	1 %
$Z_s = 0.21 + 0.023(u_o)^2$	(4.4)	0.75	111	1 %
$\bar{U}_s = 0.29(u_o)^{1.18}$	(4.5)	0.67	111	1 %
$\bar{U}_s = 0.39u_o$	(4.6)	0.65	112	1 %
$h_{s*(max)} = 0.21 - 0.48x_* + 0.32(x_*)^2$	(4.7)	0.63	426	1 %

The relationship between X_{s*} and t_* is shown in Figure 4.7a, together with the theoretical relationship (2.14) and the regression model (4.2). Only half of the parabola is shown, because only the uprush is considered in this Section. Since the best regression model is a quadratic function, it is inferred that the behaviour of X_{s*} is adequately described by the theory. This is further supported by the fact that 92 % of the variance in X_{s*} is explained by t_* (Table 4.1). However, the measured X_{s*} is consistently over-estimated by the theory for the entire uprush (Fig. 4.7a). Figure 4.7b shows that the degree of theoretical over-estimation is relatively constant, although, there may be a weak tendency for it to increase as $t_* \rightarrow 1$. Similar quantitative discrepancies with the theory are apparent for all the results presented below. The importance of these as indicators of bed friction is discussed further in Section 4.7.

Figure 4.7b shows no obvious arrangement of the data according to the range of grain sizes present between experiments. This does not necessarily preclude grain size from having any effect on the processes measured. It is possible that any effects are either constant for the range of data measured, or small enough to be masked by the experimental error.

The relationship between Z_s and u_o is shown in Figure 4.8a, together with the theoretical relationship (2.17) and the regression model (4.3). Since according to theory Z_s is proportional to u_o^2, a regression model of the form (4.4) is also fitted to the data (Table 4.1; Fig. 4.8a). The difference in variance explained between the two models amounts to 6 % (Table 4.1). It is important to note that although (4.4) is similar to (2.17), the former includes an additional constant which limits its physical interpretation, since for $u_o=0$ it is expected that $Z_s=0$. The magnitude by which the theory over-predicts Z_s seems to increase with u_o (Fig. 4.8b).

The relationship between $\bar{U}_s$ and u_o is shown in Figure 4.9a, together with the theoretical relationship (2.18) and the regression model (4.5). Since a linear relationship is expected from theory, a regression model of the form (4.6) is also fitted to the data (Table 4.1; Fig. 4.9a). The difference in variance explained between the two models is only 3 % (Table 4.1). Given the scatter of the data this difference is insignificant, and it is assumed that (4.6) is the most appropriate model. It is interesting to note that the magnitude of theoretical over-estimation of $\bar{U}_s$ does not change with u_o (Fig.

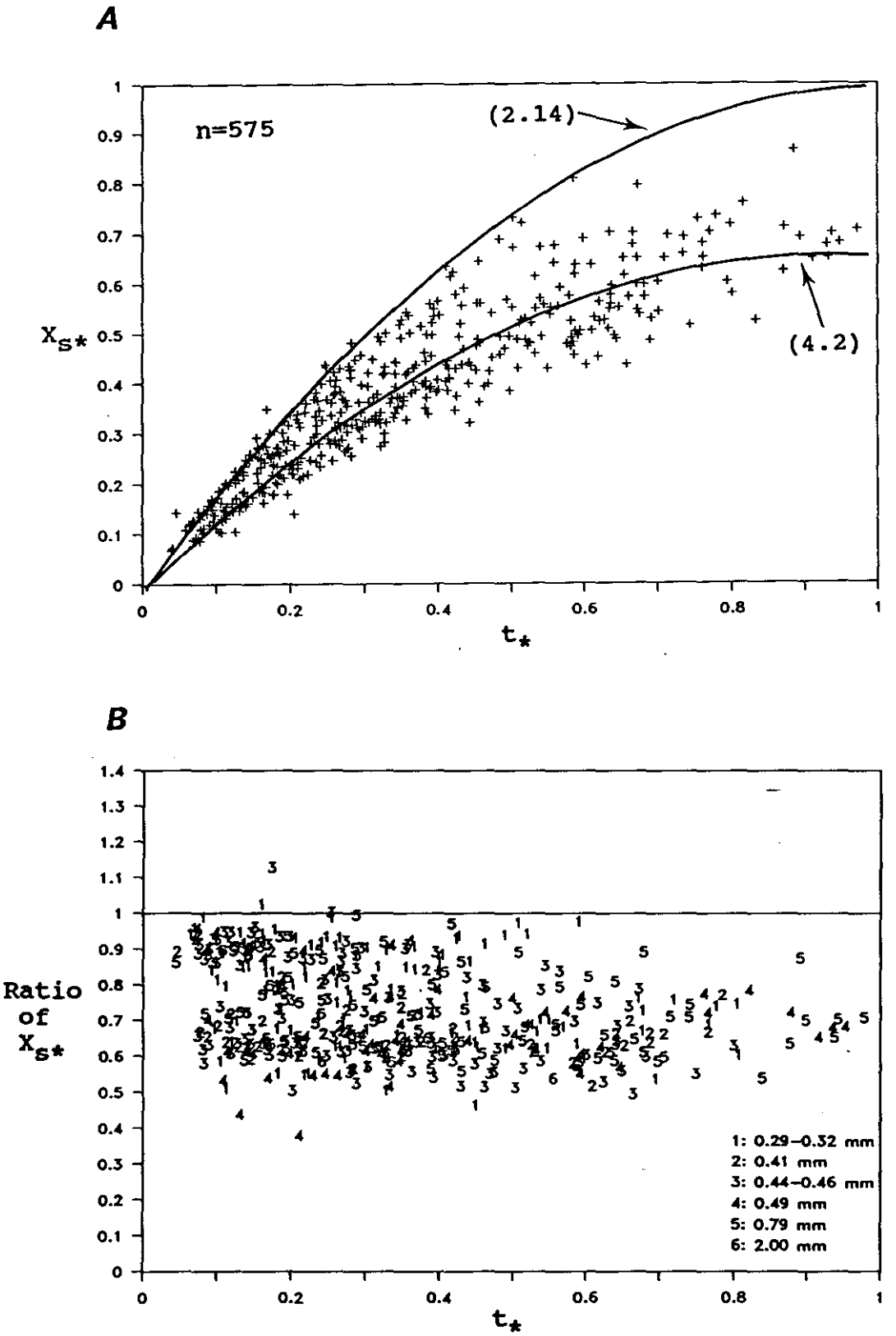

Figure 4.7: *(a)* Data from *Beach Type A* showing X_{s*} as a function of t_*. *(b)* Ratio of measured to predicted X_{s*}, as a function of t_* and D.

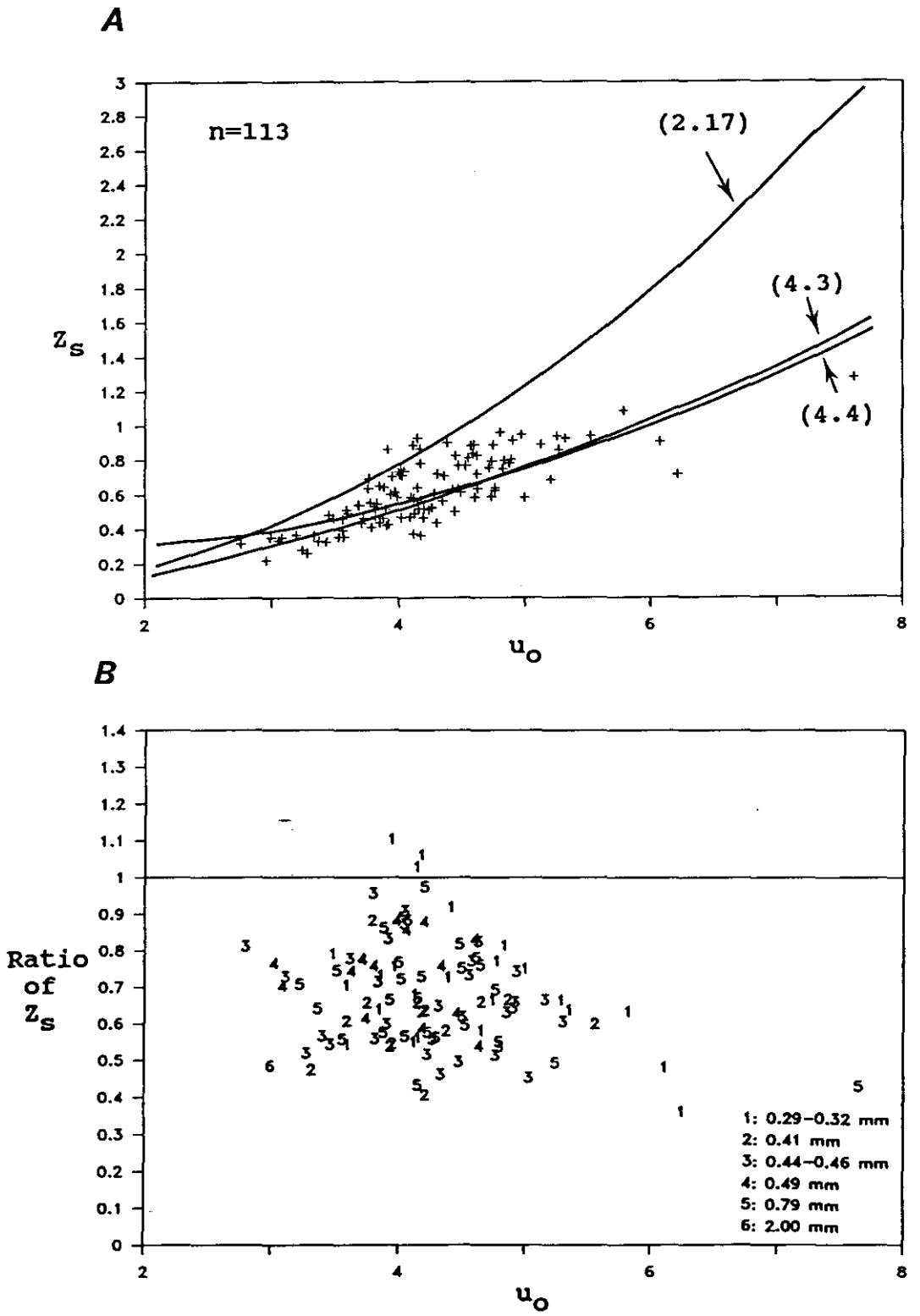

Figure 4.8: *(a)* Data from *Beach Type A* showing Z_s a function u_o. *(b)* Ratio of measured to predicted Z_s, as a function of u_o and D.

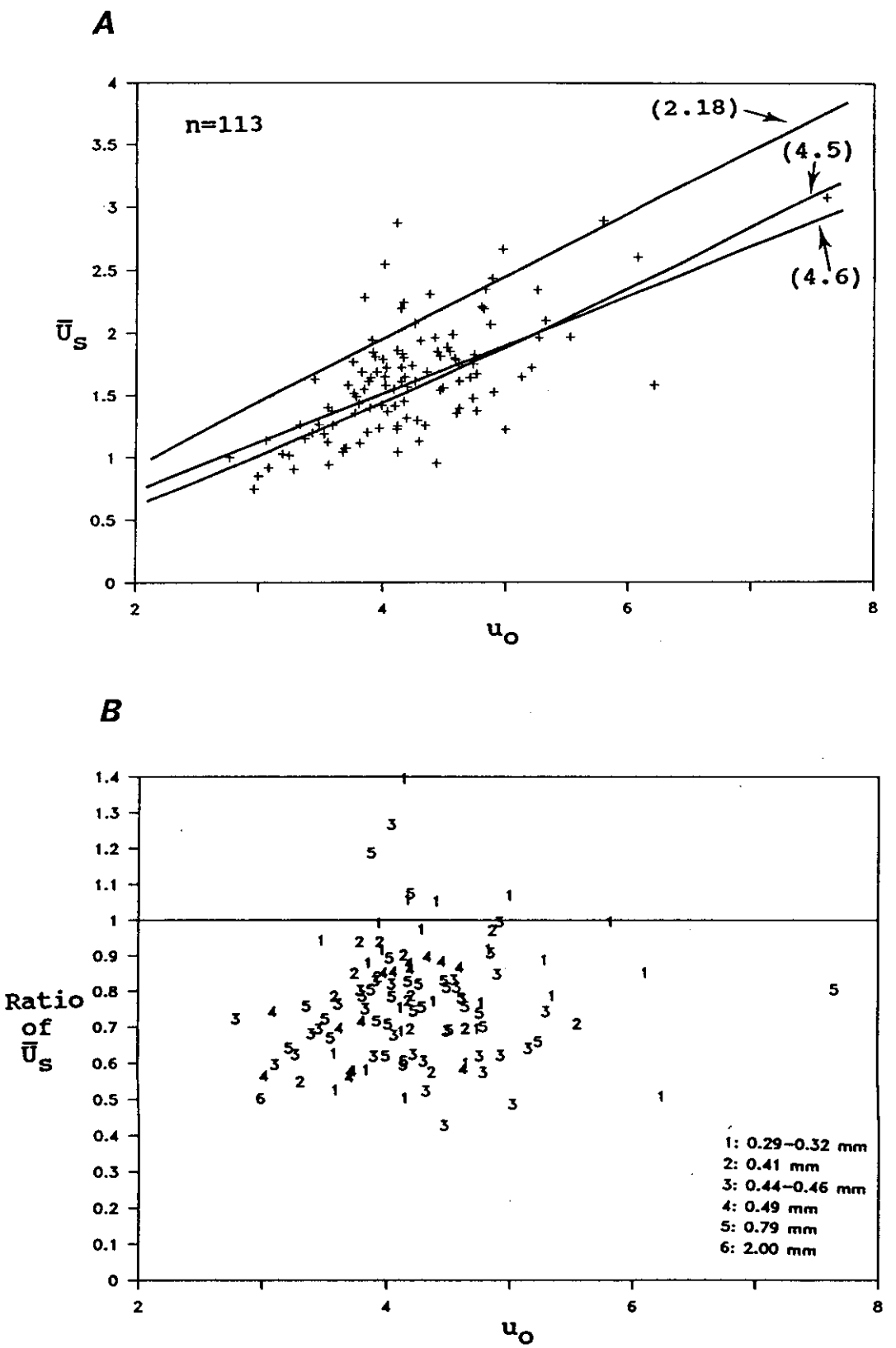

Figure 4.9: *(a)* Data from *Beach Type A* showing $\bar{U}_S$ as a function of u_o. *(b)* Ratio of measured to predicted $\bar{U}_S$, as a function of u_o and D.

4.9b). This is not surprising considering that the measured L_s and $t_{(max)}$ used to calculate $\bar{U}_s$ are both lower than theoretically expected, and are both uniquely determined by u_o (see (2.15) and (2.16)). Only 42 % of the variance in $\bar{U}_s$ is explained by u_o, using (4.6) (Table 4.1). The relatively poorer performance of this model compared to others in the Table does not necessarily suggest that the theory is inappropriate. The large scatter in Figure 4.9a is probably due to the difficulties encountered in recording $t_{(max)}$ (Section 3.4.2).

According to (2.23) $h_{s(max)}$ is a quadratic function of x, and dependant on u_o and β. Thus in order to show the data for all experiments simultaneously, $h_{s(max)}$ and x were non-dimensionalized in the following manner:

$$h_{s*(max)} = h_{s(max)}/Z_s \quad \text{and} \quad x_* = x/L_s \qquad (4.9),$$

where the asterisk denotes the non-dimensional variable, and L_s and Z_s are given by (2.16) and (2.17) respectively.

The relationship between $h_{s*(max)}$ and x_* is shown in Figure 4.10a, together with the theoretical relationship (2.23) and the regression model (4.7). The form of the regression model is again consistent with that expected from theory, but only 40 % of the variance in $h_{s*(max)}$ is explained by this model. Considering the possibility that errors in estimating $h_{s*(max)}$ may reach 50 % due to the presence of foam and beach drying (Section 3.5.3), the fact that a statistically significant relationship exists and is of the correct theoretical form is promising. The most probable explanation for the increase in scatter with distance up the beach lies in the behaviour of h_s near the maximum uprush. It is in this region that h_s is smallest, and if foam is present it can represent a large percentage of the apparent water depth (Section 3.5.3). It is not entirely clear why there is a tendency for the theoretical over-estimation to decrease as x_* approaches unity. A possible explanation is that the shape of the leading edge, which is apparently influenced greatly by friction, results in a larger than expected h_s on the upper beach (see below).

Typical examples of $h_s(t)$ and $\eta_s(x)$ for one swash cycle are shown in Figure 4.11 and 4.12, together with the theoretical predictions given by (2.19) and (2.20). Only selected examples of this type of data are shown, as it was not possible to present the entire set of 1469 time series. It was also not possible to provide an envelope of extremes, due to the non-stationarity of

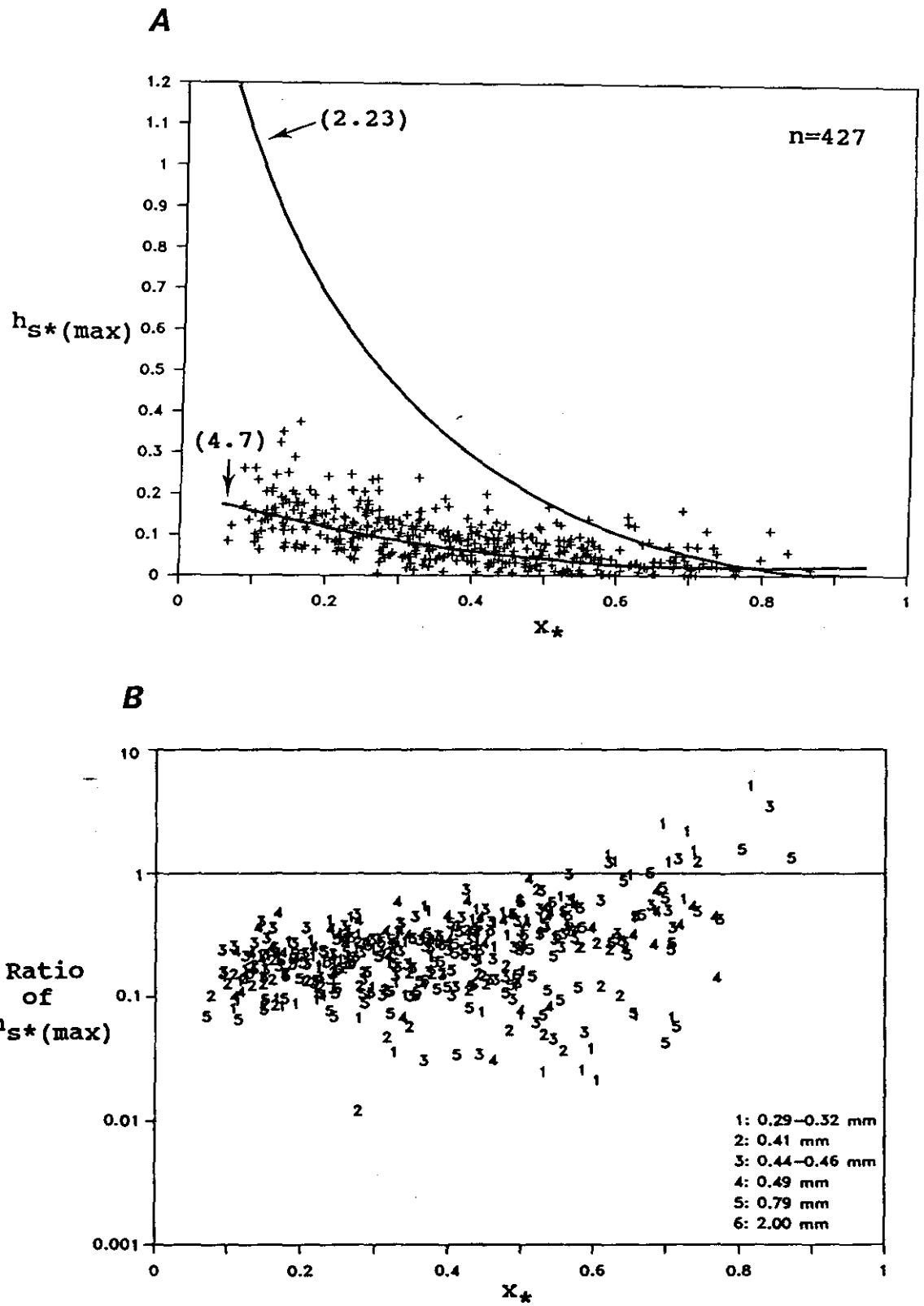

Figure 4.10: *(a)* Data from *Beach Type A* showing $h_{s*(max)}$ as a function of x_*. *(b)* Ratio of measured to predicted $h_{s*(max)}$, as a function of x_* and D.

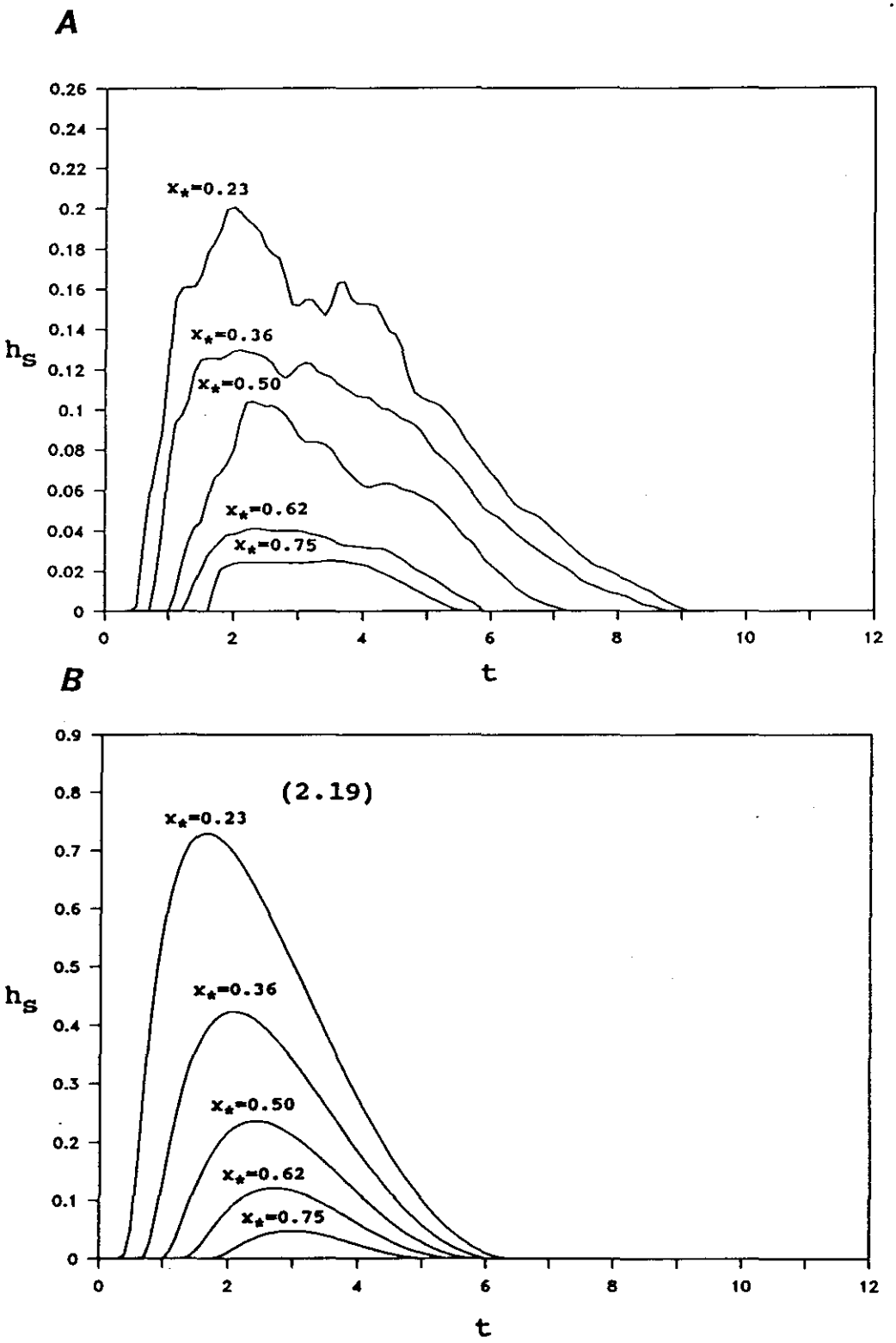

Figure 4.11: *(a)* Data from *Beach-Type A* showing $h_s(x,t)$ for a swash cycle with initial conditions u_o=4.93, β=0.1468, and D=0.00044. *(b)* Predicted $h_s(x,t)$ using (2.19), for a swash cycle with initial conditions u_o=4.93, and β=0.1468.

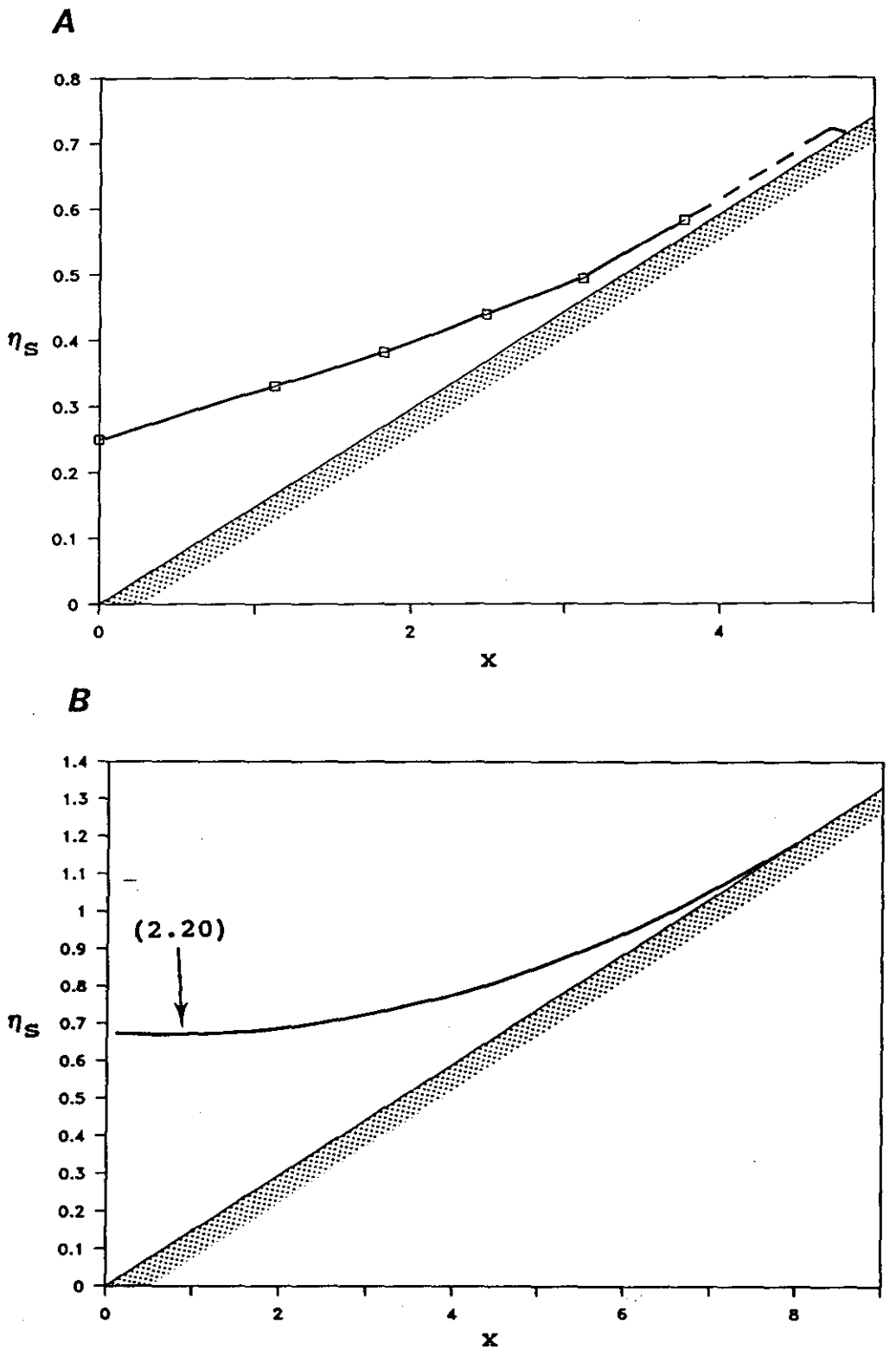

Figure 4.12: *(a)* Data from *Beach Type A* showing $\eta_s(x,t_{(max)})$ for a swash cycle with initial conditions u_o=4.93, β=0.1468, and D=0.00044. Open boxes indicate measurements and dashed line indicates inferred water surface profile at the leading edge. *(b)* Predicted $\eta_s(x,t_{(max)})$ using (2.20), for a swash cycle with initial conditions u_o=4.93, and β=0.1468.

the measurements from one swash cycle to the next. Although the gross shape of the $h_s(t)$ curves for both theory and data are similar, there are also several noteworthy differences (Fig. 4.11). As expected on the basis of all other data reported here, the measured h_s is over-predicted during the uprush. However, what is not expected is the pattern that emerges in the backwash. The measured backwash duration, and the magnitude of h_s near the end of the swash cycle are both larger than that expected from theory. The importance of these observations will become clear in Section 4.6, where the backwash is described in more detail.

The tendency for the water surface slope to approach β as the swash climbs the beach is apparent in Figure 4.12a, and is entirely consistent with the theory (Fig. 4.12b). The dashed line in Figure 4.12a, representing the water surface profile of the leading edge, does not asymptote the beach surface as suggested by theory. This inferred section of the profile is based on visual observations, and the data shown in Figure 4.13. The data are measurements of $h_{s*}(x)$ at 0.025 m increments from the front of the swash lens (see Section 3.5.3). It appears that in reality, the leading edge of the swash lens is blunt; strongly contrasting with the thin, acute profile shown in Figure 4.12b. Based on a numerical analysis which included bed friction, Freeman and LeMehaute (1964) argued that the profile should approximate a parabola. Thus a least squares regression model of the form $\eta_s=0.41x-1.96x^2$ ($r=0.95$) is fitted to the data. The appropriateness of this model is not clear due to the uncertainties inherent in obtaining the data (see Section 3.5.3), and the inability to combine measurements from several swash cycles to establish its statistical signifigance. However, other experimental do exist, which show a similar pattern to Figure 4.13 (Matsutomi, 1983). It is postulated therefore, that the true water depth immediately behind the shoreline is indeed greater than that expected from theory. This could lead to the measured h_s approaching the predicted h_s in the later stages of the uprush, and may explain the decrease in theoretical over-estimation shown in Figure 4.10b.

The data analysis presented in this Section shows that the non-linear shallow water theory qualitatively describes many features of bore uprush on a natural beach. There are some obvious discrepancies however, not the least of which is the consistent theoretical over-estimation of the data. This is discussed further in Section 4.7 as evidence for bed friction. The only theoretical under-

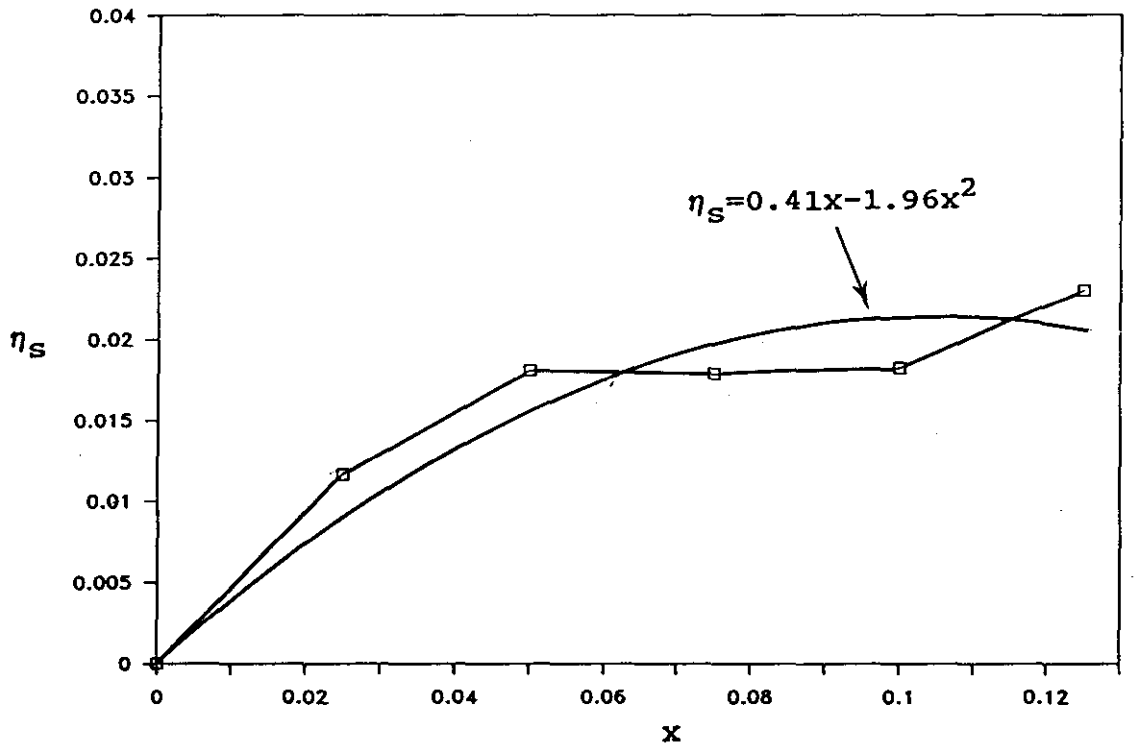

Figure 4.13: Data from *Beach Type A* showing the water surface profile of the leading 0.125 m of the swash lens.

estimation of the data occurred for h_{s*}, but there is some support for the idea that this too is a result of bed friction.

4.3 Uprush Following Wave Plunge At The Shoreline

4.3.1 Introduction.

The data reported in this Section were collected on *Beach Type B*. The relevant experimental conditions are listed in Table 3.1 in connection with Experiments 5, 7, 9, 10, 13, 14, 17 and 19.

4.3.2 Wave plunge at the shoreline.

The transformation of the wave profile from the point where the slope of the wave face becomes vertical to the beginning of uprush occurs over short spatial and temporal scales on *Type B* beaches. In the experiments reported here, this transformation usually occurred between the toe of the beach face and the initial shoreline.

Figure 4.14 shows a schematic of the transition from plunging breaker to swash, which summarizes observations made from the film records. As the wave travels shoreward it experiences some degree of shoaling due to the increasing slope of the bed (Fig. 4.14a). This shoaling effect immediately seaward of the initial shoreline has also been observed on *Beach Type* B_1 by Wright *et al.* (1986). Associated with the shoaling is a steepening of the wave face which is entirely consistent with predictions of the SWE (see Section 2.2; 2.4.5; Hedges and Kirkgoz, 1981). By the time the wave passes the toe of the beach, most of the wave face is vertical, and strong seaward velocities occur in front of the lower wave face. These observations compare well with the numerical study of breaker hydrodynamics by Peregrine *et al.* (1980). The seaward velocities are often enhanced by the preceding backwash, and occasionally provide sufficient instability to induce overturning. The presence of a beach step is common on *Beach Type B*, and appears to spatially fix the point where overturning begins. Figure 4.14b shows the wave at the time the plunging jet impacts on the beach, or the preceding backwash, and the associated splash forward of the impact point. Figure 4.14c shows the vortex collapsing, and the spray caused by the enclosed air that is forced out of the rear face of the wave. Once the vortex collapses the flow becomes more organised, and the swash lens begins to climb the beach in the manner described for bore uprush (Section 4.2.2).

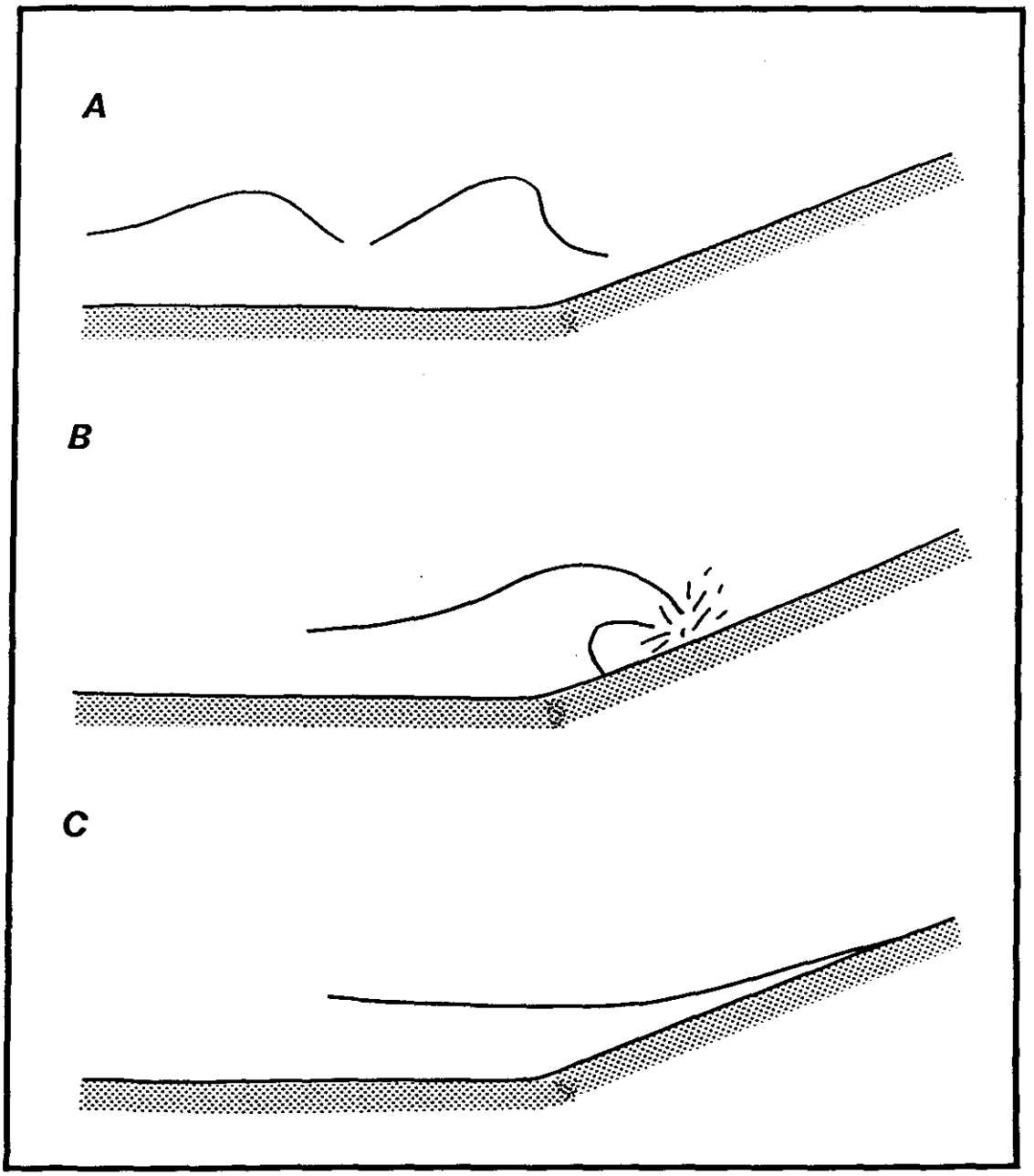

Figure 4.14: Schematic of the transition from plunging breaker to swash, which summarizes observations made from the film records.

An important difference between the transition process from bore to swash, and from plunging breaker to swash is the width of the transition zone. The zone is significantly wider in the case of the latter. Moreover, the transition is visually less continuous for plunging breakers; the plunging jet and collapse of the vortex seem to delay the beginning of uprush.

Since most of the swash cycle strongly resembles that described in the presence of bores, as might be expected on theoretical grounds (see Section 2.4.5), the predictions for swash following bore collapse are also compared to the data presented in this Section. The relationship between u_o and H_b is shown in Figure 4.15, together with the regression model

$$u_o = 5.03(H_b)^{0.19} \qquad (4.10)$$

(r=0.42, 44 df, 1 % level). Although the magnitude of the coefficients in (4.10) are similar to those found for bore collapse (*cf.* (4.1)), caution should be employed in such a comparison since η_b on *Beach Type A* and H_b on *Beach Type B* are not necessarily equivalent parameters. The range of k values for plunging breakers and their relationship to u_o are shown in Figure 4.16. Although the mean k value is marginally higher than that found for fully developed bores for a comparable range of wave heights, the modal value for both data sets are equal. It can be tentatively concluded, that for the two *Beach Types A* and *B*, η_b and H_b are equivalent quantities in terms of their effects on u_o. More data from *Beach Type B* are required to confirm this however.

4.3.3 Uprush.

The best least squares regression models of the data for swash following plunging breakers are listed in Table 4.2. The relationship between X_{s*} and t_* is shown in Figure 4.17a, together with the theoretical relationship (2.14) and the regression model (4.11). It is apparent from the data that the theory for swash following bore collapse is also successful in describing swash following plunging breakers; 93 % of the variance in X_{s*} is explained by t_*, and (4.11) is a quadratic as expected from theory. Interestingly, the degree of theoretical over-estimation is of the same order as that for bore uprush, and displays the same tendency to increase as $t_* \rightarrow 1$ (*cf.* Fig. 4.17b and 4.7b). Figure 4.17b shows no systematic arrangement of the data according to differences in grain size between experiments. As explained previously (Section 4.2.3), this does not necessarily indicate that the effects of grain size on the uprush are unimportant (see Section 4.7)

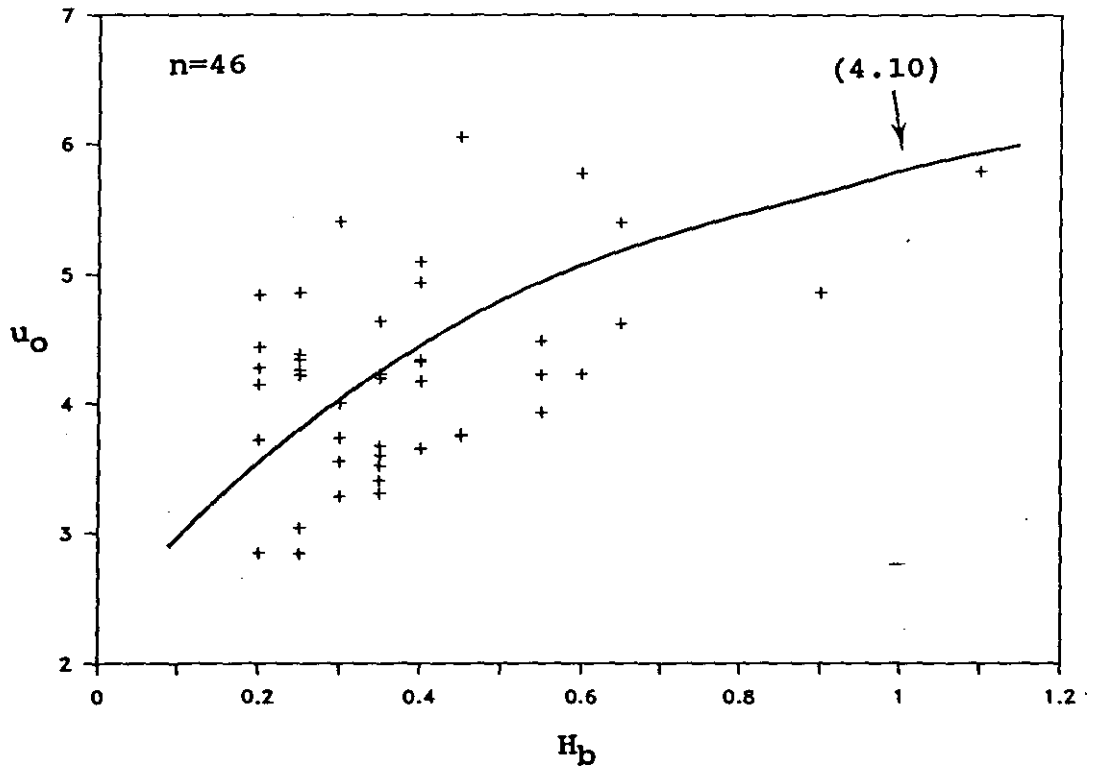

Figure 4.15: Data from *Beach Type B* showing u_o as a function of H_b.

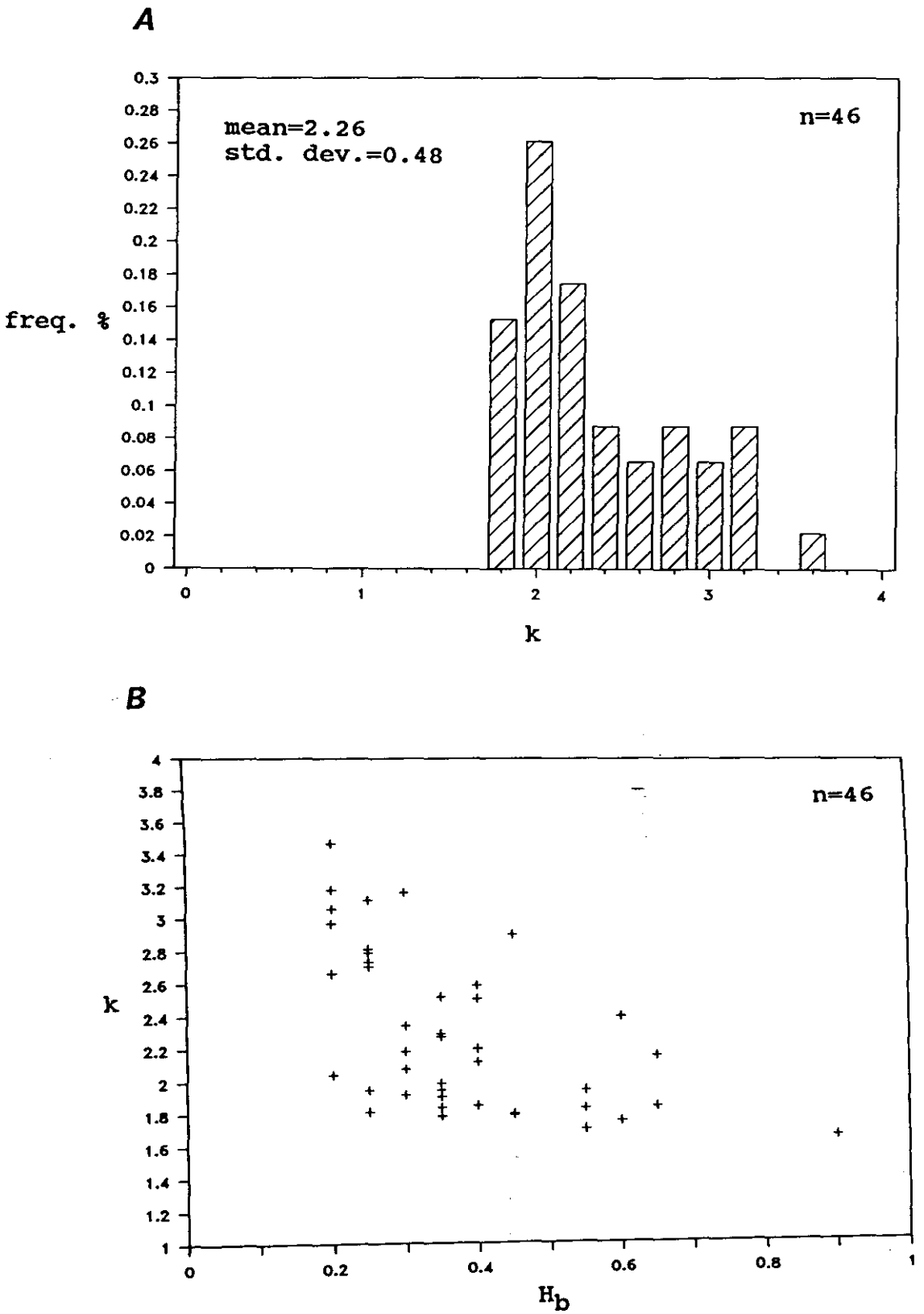

Figure 4.16: *(a)* Frequency histogram of k values measured on *Beach Type B*. *(b)* Values of k as a function of H_b.

TABLE 4.2
LEAST SQUARES REGRESSION MODELS DESCRIBING SWASH ON *BEACH TYPE B*

Model	Eq. no.	r	df	Level
$X_{s*} = 1.35t_* - 0.79(t_*)^2$	(4.11)	0.96	217	1 %
$Z_s = 0.047(u_o)^{1.61}$	(4.12)	0.78	44	1 %
$Z_s = 0.091 + 0.022(u_o)^2$	(4.13)	0.76	44	1 %
$\bar{U}_s = 0.37u_o$	(4.14)	0.69	45	1 %
$h_{s*(max)} = 0.13 - 0.32x_* + 0.22(x_*)^2$	(4.15)	0.62	166	1 %

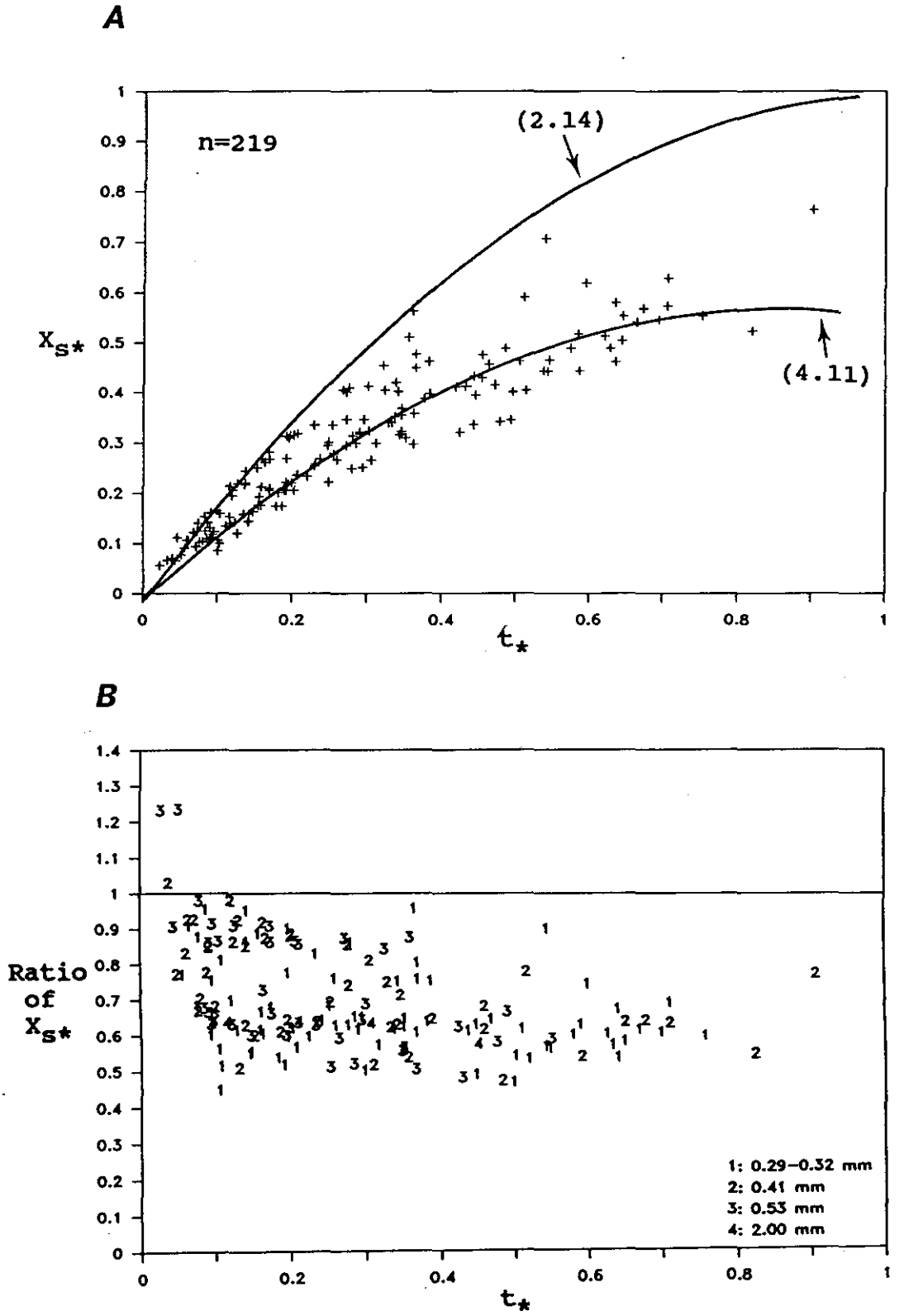

Figure 4.17: *(a)* Data from *Beach Type B* showing X_{s*} as a function of t_*. *(b)* Ratio of measured to predicted X_{s*}, as a function of t_* and D.

The relationship between Z_s and u_o is shown in Figure 4.18a, together with the theoretical relationship (2.17) and the regression model (4.12). Since according to theory Z_s is proportional to u_o^2, a regression model of the form (4.13) is also fitted to the data. The difference in variance explained between the two models is only 3 % (Table 4.2). The magnitude of theoretical over-estimation of the data, and its behaviour with increasing u_o are entirely consistent with that observed for bore uprush (*cf.* Fig. 4.18b and 4.8b).

The relationship between $\bar{U}_s$ and u_o is shown in Figure 4.19a, together the theoretical relationship (2.18) and the regression model (4.14). The best model for this data is of the theoretically expected linear form. Again, the degree of theoretical over-estimation is of the same order as that found for bore uprush (*cf.* Fig. 4.19b and Fig. 4.9b).

The relationship between $h_{s*(max)}$ and x_* is shown in Figure 4.20a, together with the theoretical relationship (2.23) and the regression model (4.15). Again, the relationship between the data is of the theoretically expected quadratic form, and the degree of theoretical over-estimation is the same as that found for bore uprush. Not surprisingly, measurements of $h_s(t)$ and $\eta_s(x)$ were very similar to those shown in Figures 4.11 and 4.12, and are therefore not repeated here.

The form of the regression models listed in Table 4.2 compare well with those found for bore uprush (Table 4.1). Moreover, they are qualitatively similar to the theoretical equations for bore uprush (Section 2.4.4). This implies that the processes described by the theory are equivalent on both *Beach Types*. The fact that the quantitative discrepancy between theory and data is similar for both *Beach Types* suggests further, that the processes not described by the theory are also equivalent (*e.g.* bottom friction).

4.4 Uprush Following Surging Waves

4.4.1 Introduction.

The results reported in this Section relate to data collected on *Beach Type C*. The relevant experimental conditions are listed in Table 3.1 in connection with Experiments 5, 7, 9, 10, 12, 13, 15, 16, 17, 18, and 19. A typical example of a surging wave as it passes over the step is shown in Figure 4.21. Notice that the wave front can display a very steep water surface slope as it climbs the beach, without subsequent overturning. The steep front, which

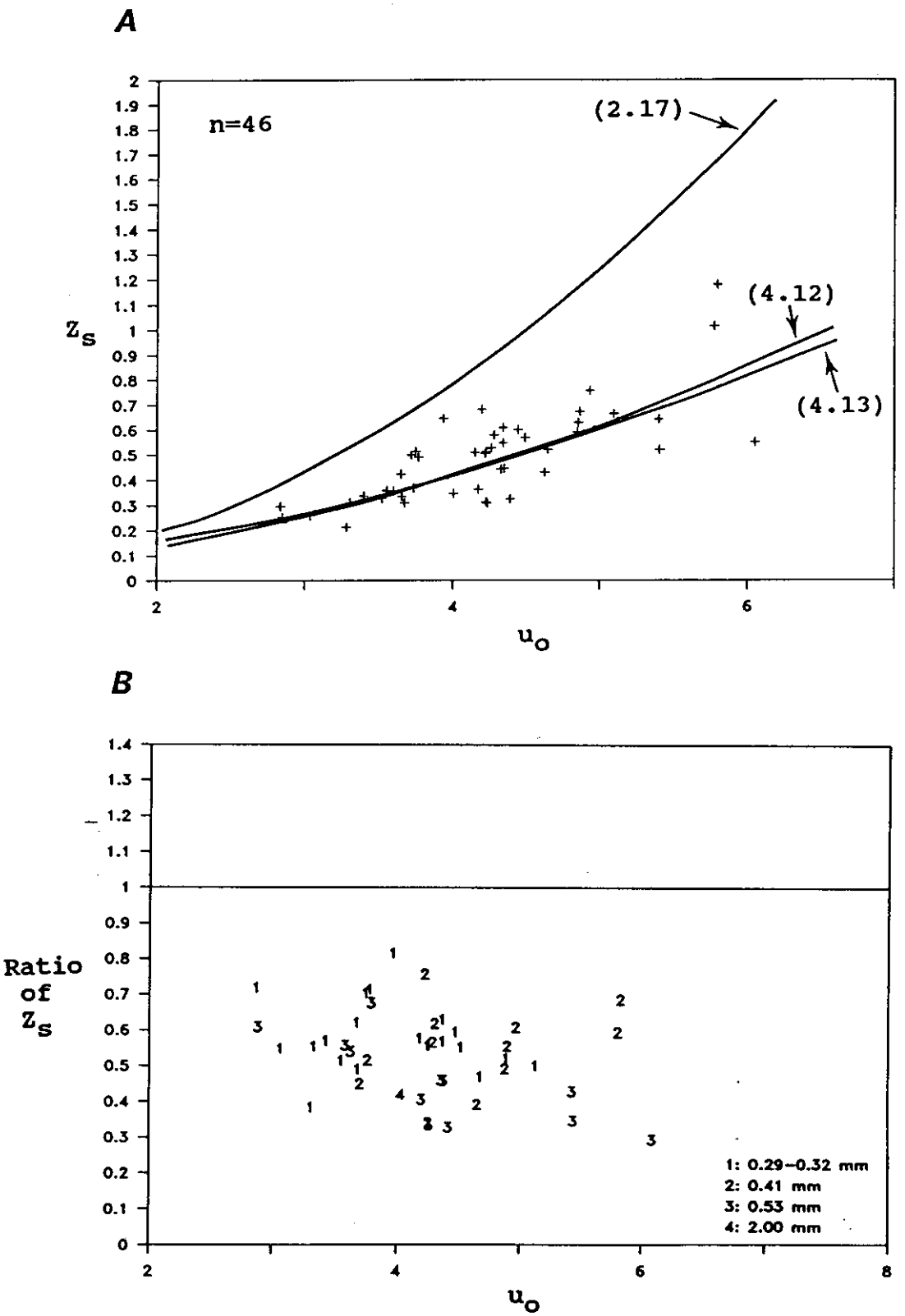

Figure 4.18: *(a)* Data from *Beach Type B* showing Z_s a function u_o. *(b)* Ratio of measured to predicted Z_s, as a function of u_o and D.

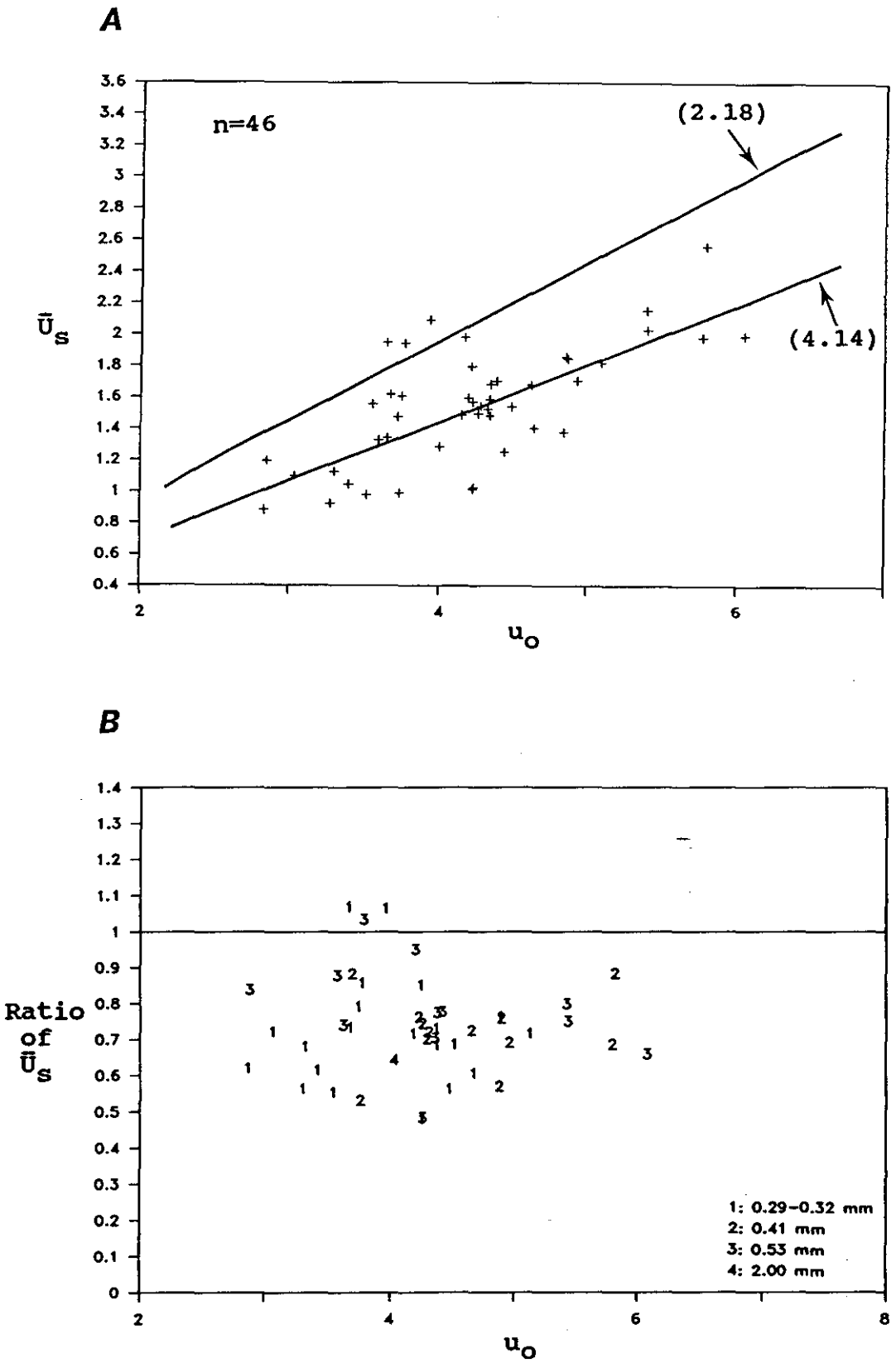

Figure 4.19: *(a)* Data from *Beach Type B* showing $\bar{U}_s$ as a function of u_o. *(b)* Ratio of measured to predicted $\bar{U}_s$, as a function of u_o and D.

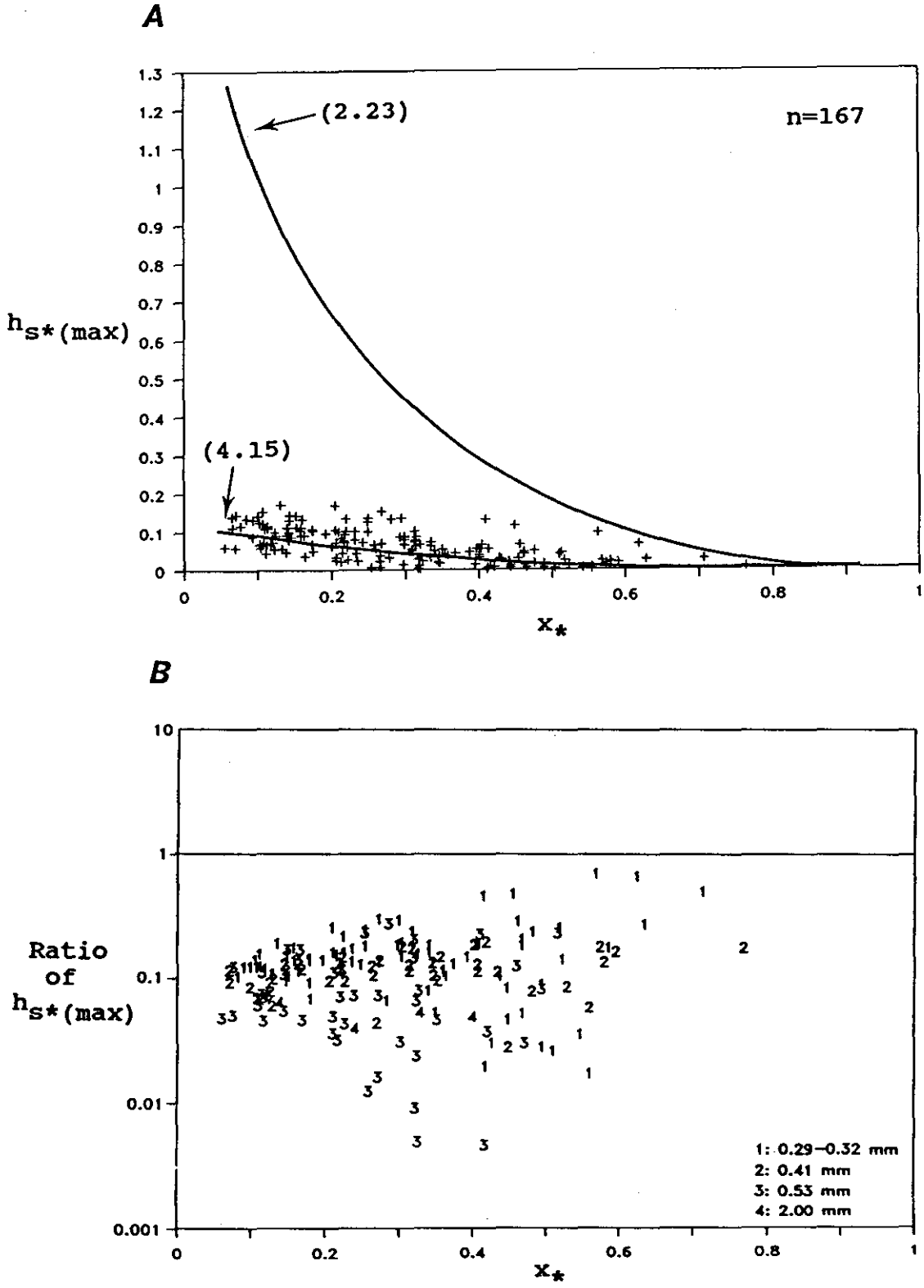

Figure 4.20: *(a)* Data from *Beach Type B* showing $h_{s*(max)}$ as a function of x_*. *(b)* Ratio of measured to predicted $h_{s*(max)}$, as a function of x_* and D.

Figure 4.21: **Photograph showing the steep water surface slope of a surging wave on *Beach Type C* (Photo by P. Cowell).**

probably contrasts with the laboratory waves discussed in Section 2.5.3 (also Gjevik and Pedersen, 1981; Pedersen and Gjevik, 1983), shows that at least part of the flow cannot be described by the SWE, thus introducing the possibility of a virtual bore. The concept of a virtual bore is considered appropriate, as the gross flow is still very different to the surf zone bores described in Section 2.4.3 (also Fig. 2.6). The understanding that all surging waves are not necessarily bore-free, but in some respects behave as if they contain a virtual bore is developed more thoroughly through the data presented in this Section, and the discussion of breaking and non-breaking waves contained in Section 4.5.

4.4.2 Surging waves.

Figure 4.22 shows a schematic of the transition from surging wave to swash, which summarizes observations made from the film records. Figure 4.22a shows the wave located over the beach step. By this time in the waves shoreward advance, it invariably displayed obvious slope assymetry. However, the toe of the wave front began to climb the beach before this assymetry could develop sufficiently for overturning to occur. Two scenarios were observed for the beginning of the swash cycle (Fig. 4.22b). The first was observed in the presence of relatively small waves and deep water over the beach step. In this case, the climbing swash lens retained some indication of the initial wave shape, that was in the form of a hump in the water surface profile. This feature is short-lived and appears to 'collapse' before the shoreline has advanced much more than the width of the wave crest. This hump can also be seen in some numerical (Gopalakrishnan and Tung, 1980; Kim et al., 1983; Pedersen and Gjevik, 1983) and laboratory studies (Pedersen and Gjevik, 1983; Synolakis, 1987a) of solitary wave run-up. The 'collapse' of the hump caused the shoreline to accelerate. Subsequent to this, the swash lens appeared to behave as a rarefaction wave, similar to that described in Sections 2.4.4 and 4.2.2 (Fig. 4.22c). The second scenario observed for the onset of uprush was associated with relatively larger waves, or shallower water depths over the step. In this case, the progress of the wave at the initial shoreline was momentarily restrained, and water seemingly piled up against the beach. This caused significant steepening of the wave face, almost to the vertical in some cases. Before the wave could break however, the shoreline began its ascent, while at the same time a wave was observed to propagate seaward (Fig. 4.22b). The height of this reflected wave was only a small fraction of the incident wave height. In contrast to the first scenario, the swash lens appeared as a

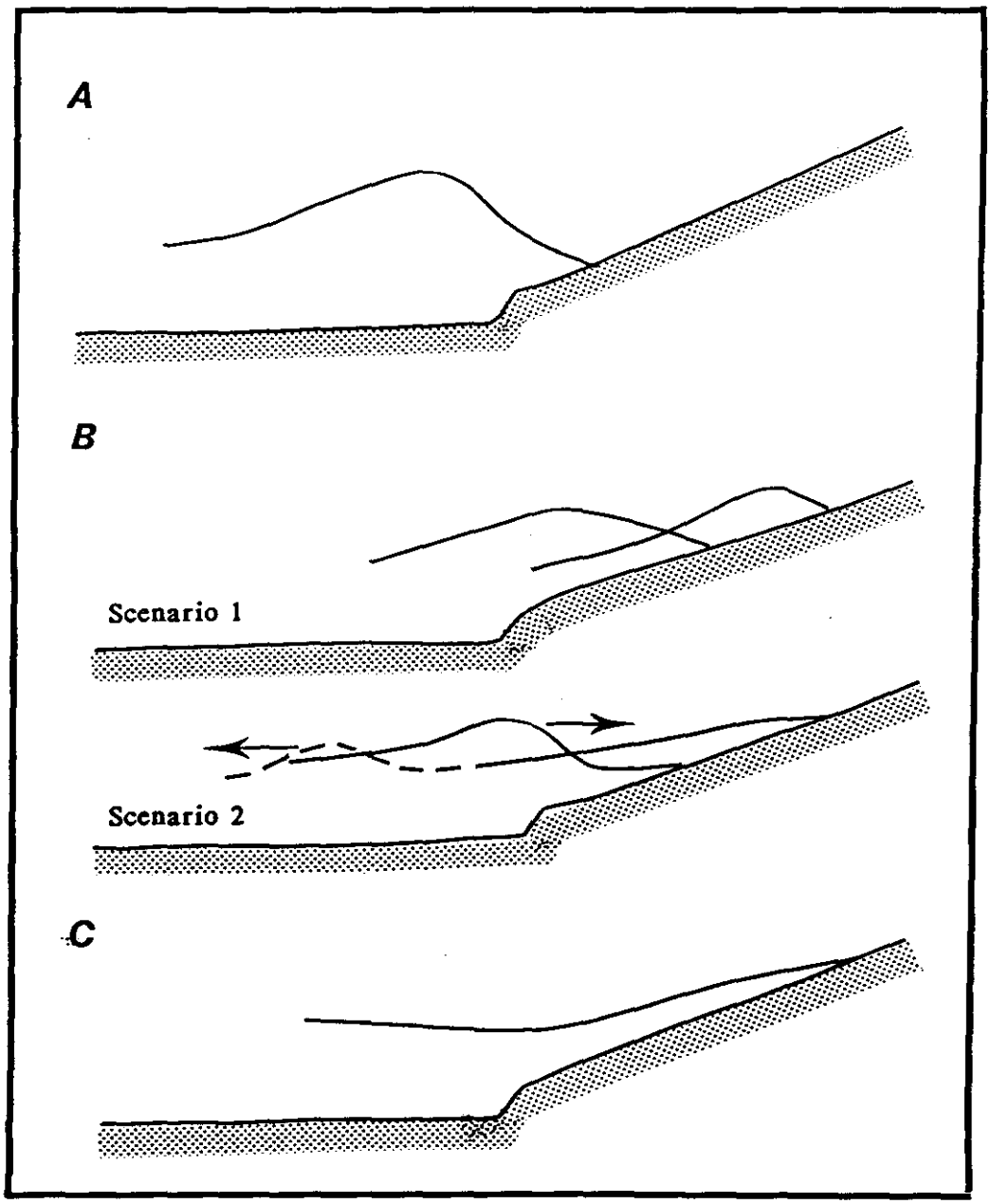

Figure 4.22: Schematic of the transition from surging wave to swash, which summarizes observations made from the film records.

rarefaction wave as soon as the shoreline began climbing the beach (Fig. 4.22c). This behaviour pattern for most of the uprush is entirely unexpected from theoretical considerations (*cf.* Section 2.5.3). Occasionally, the interaction of the toe of the wave front with the rough beach produced minor aeration in the swash lens. This was generally short-lived however, so that the swash lens lacked the extensive foam cover typical for breaking waves.

In order to apply the theoretical solutions for swash following non-breaking waves presented in Section 2.5.3, certain environmental conditions are required to ensure the mathematical validity of the solutions. For the standing wave solution of Carrier and Greenspan (1958), it is required that $\epsilon<1$ (Section 2.5.2). The range of ϵ measured in this study is shown in Figure 4.23a, and it can be seen that most of the data is greater than unity. Moreover, to apply the solitary wave solutions of Synolakis (1987a and b), it is a necessary condition that (2.36) is satisfied. It is clear from Figure 4.23b that none of the data satisfies this inequality. A partial explanation may lie in the difficulty involved with choosing an appropriate point on the beach profile to measure d. This difficulty arises due to the presence of a beach step and sloping nearshore profile that exist on natural beaches (Figure 2.3). Neither of these are present in Figure 2.14, where the theoretical conditions are defined. The estimate of d used here was the depth to the base of the step. It was found that the value of d needed to satisfy (2.36) had to be at least a factor 3 larger than this measure. It appears that the combination of swell waves and beach face profiles of the type shown in Figure 2.3c, are not complete analogs of the theoretical description indicated in Figure 2.14. This is clearly illustrated by the previous discussion of wave behaviour over the step (also Fig. 4.22).

Measurements of swash following non-breaking waves have been obtained in the presence of environmental conditions which do not satisfy the restrictions on the theoretical solutions. According to (2.36), the waves recorded here should have broken before reaching the step. These measurements are not unique in this respect; Synolakis (1987a) also found this phenomenon in some of his laboratory experiments. The example shown in Figure 4.24 clearly illustrates the theoretical profile overturning, whereas the measured data show the wave will climb the beach without breaking.

Theoretically, breaking inception is considered to occur when the wave face becomes vertical (Greenspan, 1958). It has long been recognized that the

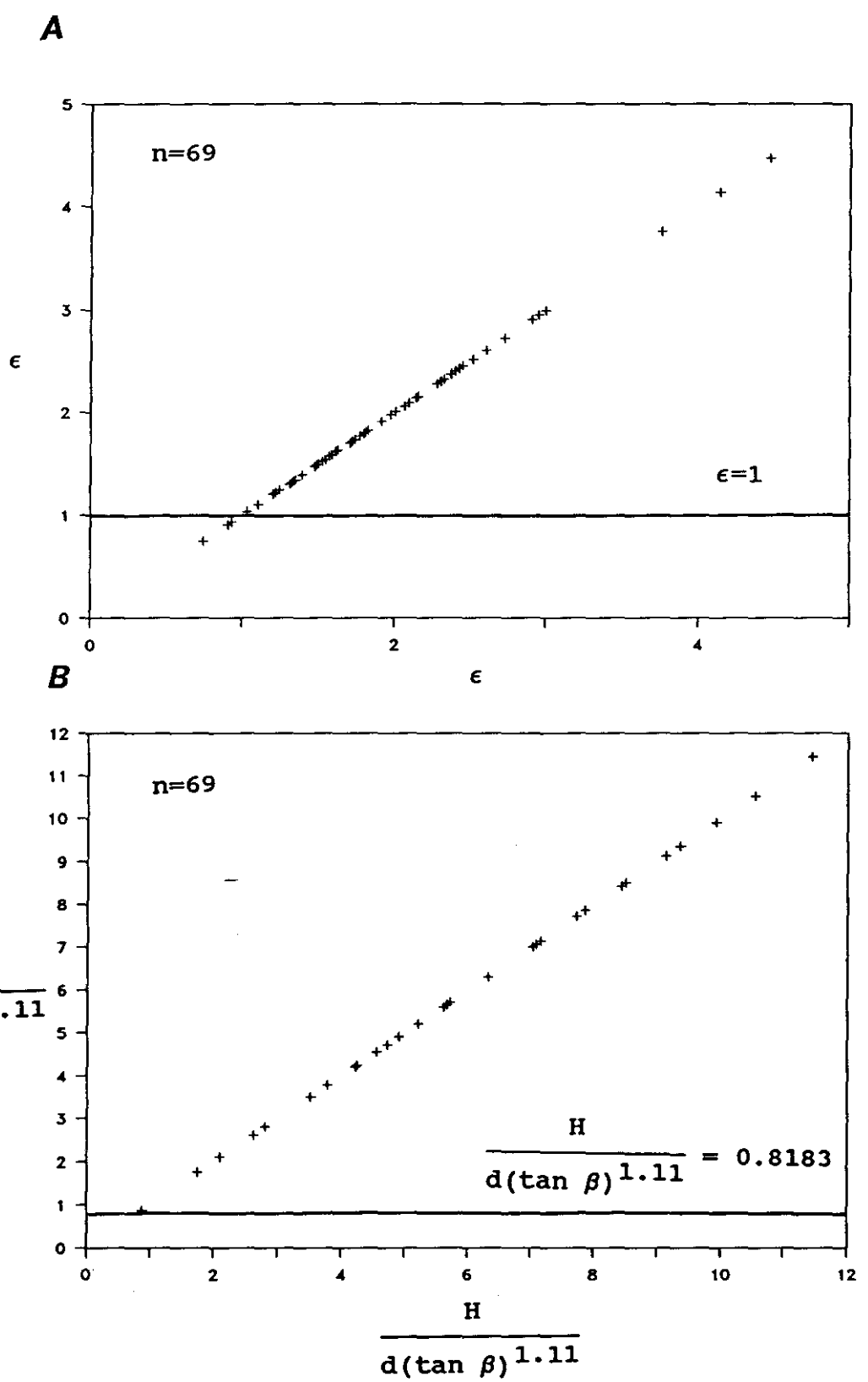

Figure 4.23: *(a)* Plot of ϵ values measured on *Beach Type C*, showing that most measurements did not satisfy the condition $\epsilon<1$ for Carrier and Greenspan's (1958) standing wave solution. *(b)* Plot of $H/[d(\tan\beta)^{1.11}]$ values measured on *Beach Type C*, showing that no measurements satisfied (2.36) for Synolakis' (1987a and b) solitary wave solution.

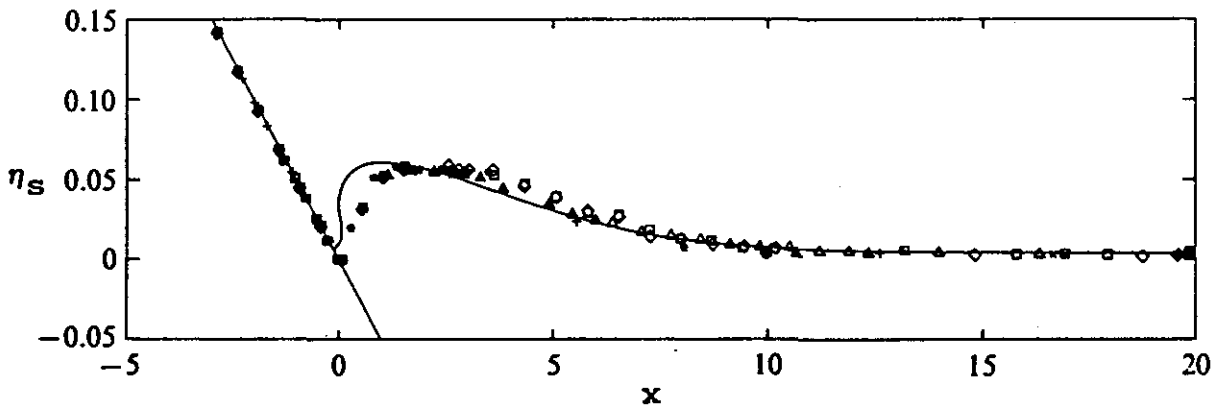

Figure 4.24: Predicted and measured $\eta_S(x)$ for a solitary wave with H/d=0.04 climbing a laboratory beach with β=0.05 (From Synolakis, 1987a).

SWE predict wave breaking too soon (see LeMehaute *et al.*, 1968). Thus it is not unlikely, that the theoretical criteria which predicts non-breaking waves is over-restrictive (*i.e.* (2.36)). The early prediction of breaker inception by the SWE is a manifestation of the 'long wave paradox', first discussed by Ursell (1953). The paradox is, that breaking is actually predicted for waves propagating over a flat bed. On low-gradient beaches, LeMehaute (1962) attempted to overcome this problem by introducing a non-saturated breaker stage between the unbroken wave and the bore (see Section 2.4.2). On the steeper *Beach Type C* however, a growth in slope assymetry from zero to infinity can occur over a single wave length (Cowell, 1982), thus precluding the possible introduction of a non-saturated breaker stage. The type of 'hydrodynamic hysteresis' observed in waves by Van Dorn and Pazan (1975) must also contribute to the early prediction of breaker inception.

Since the data measured on *Beach Type C* is outside the range of validity for the theoretical solutions in Section 2.5.3, they could not be compared. Such a comparison would lead to unreasonable theoretical estimates, sometimes an order of magnitude different to the data. The possibility that surging waves could exist, but could not be described by the bore-free solutions of the SWE has already been foreshadowed by the laboratory experiments of Guza and Bowen (1976). These experiments showed that surging waves exist for $\epsilon>1$; outside the range of theoretical validity (Section 2.5.2). Although it was not expected initially, much of the uprush appeared to behave like a rarefaction wave. Consequently, the remainder of this Section compares the data collected on *Beach Type C* with the predictions for swash following bore collapse. This may seem inappropriate at the outset, however, some justification lies in the apparent success of the comparison (Section 4.4.3). Also, as Meyer and Taylor (1972) point out, the division of theoretical research into bore and bore-free solutions of the SWE may be due more to a historical perspective, than any physical understanding of nature.

The relationship between u_o and H (measured over the step) is shown in Figure 4.25, together with the regression model

$$u_o = 5.42(H)^{0.25} \qquad (4.16)$$

(r=0.56, 67 df, 1 % level). The magnitude of the coefficients in (4.16) are larger than those found for breaking waves (*cf.* (4.1), (4.10)), as are the mean and mode of the k values (Fig. 4.26a and b). It is tentatively concluded therefore, that on *Beach Type C*, the effect of H on u_o is different to that

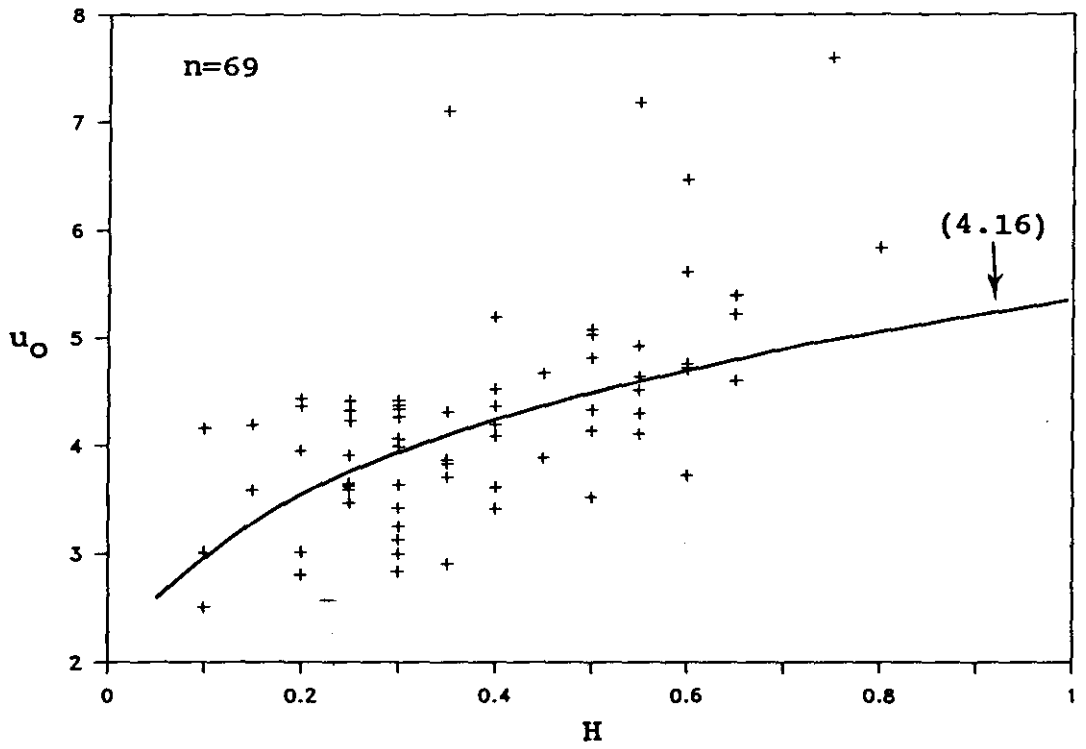

Figure 4.25: Data from *Beach Type C* showing u_o as a function of H.

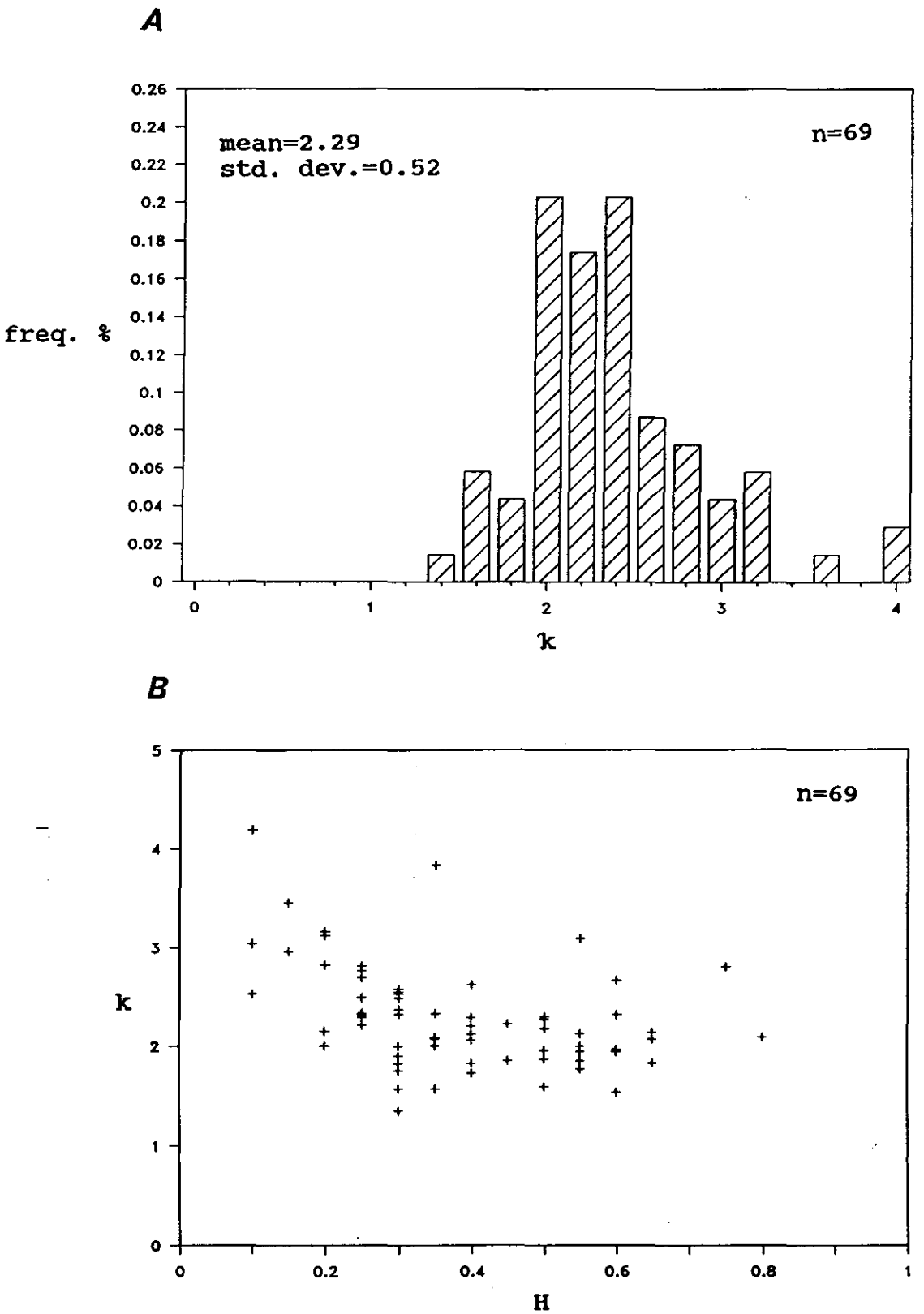

Figure 4.26: *(a)* Frequency histogram of k values measured on *Beach Type C.* *(b)* Values of k as a function of H.

found for breaking waves. Larger u_o values are expected for a given surging wave height, than for a similar bore height or plunging breaker height. This may demonstrate the effect of a hydrostatic head of water above the virtual bore height (*cf.* minor bore in Fig. 2.6), which is expected to increase the potential energy transferred to the swash (see Section 4.5). This head of water over and above the bore height is absent in the case of fully developed bores.

4.4.3 Uprush.

In this Section the theoretical solutions for swash following bore collapse are compared with the field data collected on *Beach Type C*. The best least squares regression models of the data are listed in Table 4.3. The relationship between X_{s*} and t_* is shown in Figure 4.27a, together with the theoretical relationship (2.14) and the regression model (4.17). It is apparent from the data that the theory for swash following bore collapse is also successful in describing swash following surging waves; 98 % of the variance in X_{s*} is explained by t_*, and (4.17) is a quadratic as expected from theory. Interestingly, the degree of theoretical over-estimation is of the same order as that found for breaking waves (*cf.* Fig. 4.27b, 4.7b,and 4.17b).

The relationship between Z_s and u_o is shown in Figure 4.28a, together with the theoretical relationship (2.17) and the regression model (4.18) (Table 4.3). Since according to theory Z_s is proportional to u_o^2, a regression model of the form (4.19) is also fitted to the data. The difference in variance explained between the two models amounts to 8 % (Table 4.3). The tendency for the theoretical over-estimation to increase with u_o, is again consistent with the results for breaking waves.

The remaining features of the swash, $\bar{U}_s$, and $h_{s*(max)}$ are compared with their theoretical counterparts in Figures 4.29 and 4.30 respectively (see also Table 4.3). Measurements of $h_s(t)$ and $\eta_s(x)$ were not seen to be significantly different from the examples presented for bore uprush, and are therefore not repeated here. The form of the regression models listed in Table 4.3 suggest that there is no apparent difference in the behaviour of the swash between *Beach Types*, for the range of conditions examined in this study. Furthermore, all of the processes considered here are found to be well described by those solutions of the shallow water theory which are specific to bore uprush. This implies that non-breaking waves may not necessarily be bore-free, and that the theoretical solutions for surging waves presented in Section

TABLE 4.3
LEAST SQUARES REGRESSION MODELS DESCRIBING SWASH ON *BEACH TYPE C*

Model	Eq. no.	r	df	Level
$X_{s*} = 1.18t_* - 0.50(t_*)^2$	(4.17)	0.96	326	1 %
$Z_s = 0.063(u_o)^{1.46}$	(4.18)	0.76	67	1 %
$Z_s = 0.22 + 0.017(u_o)^2$	(4.19)	0.71	67	1 %
$\bar{U}_s = 0.32u_o$	(4.20)	0.73	67	1 %
$h_{s*(max)} = 0.17 - 0.28x_* + 0.13(x_*)^2$	(4.21)	0.51	239	1 %

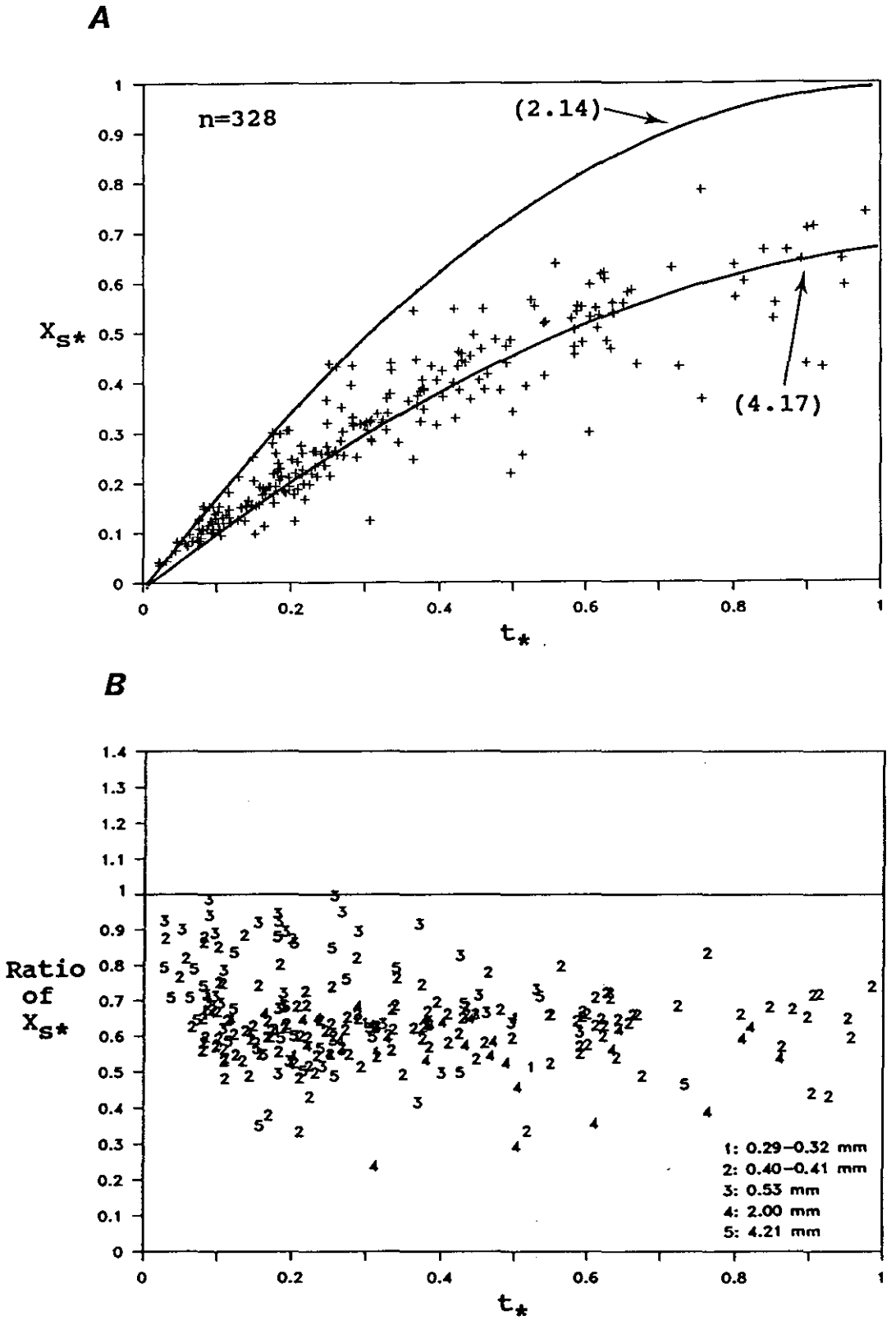

Figure 4.27: *(a)* Data from *Beach Type C* showing X_{s*} as a function of t_*. *(b)* Ratio of measured to predicted X_{s*}, as a function of t_* and D.

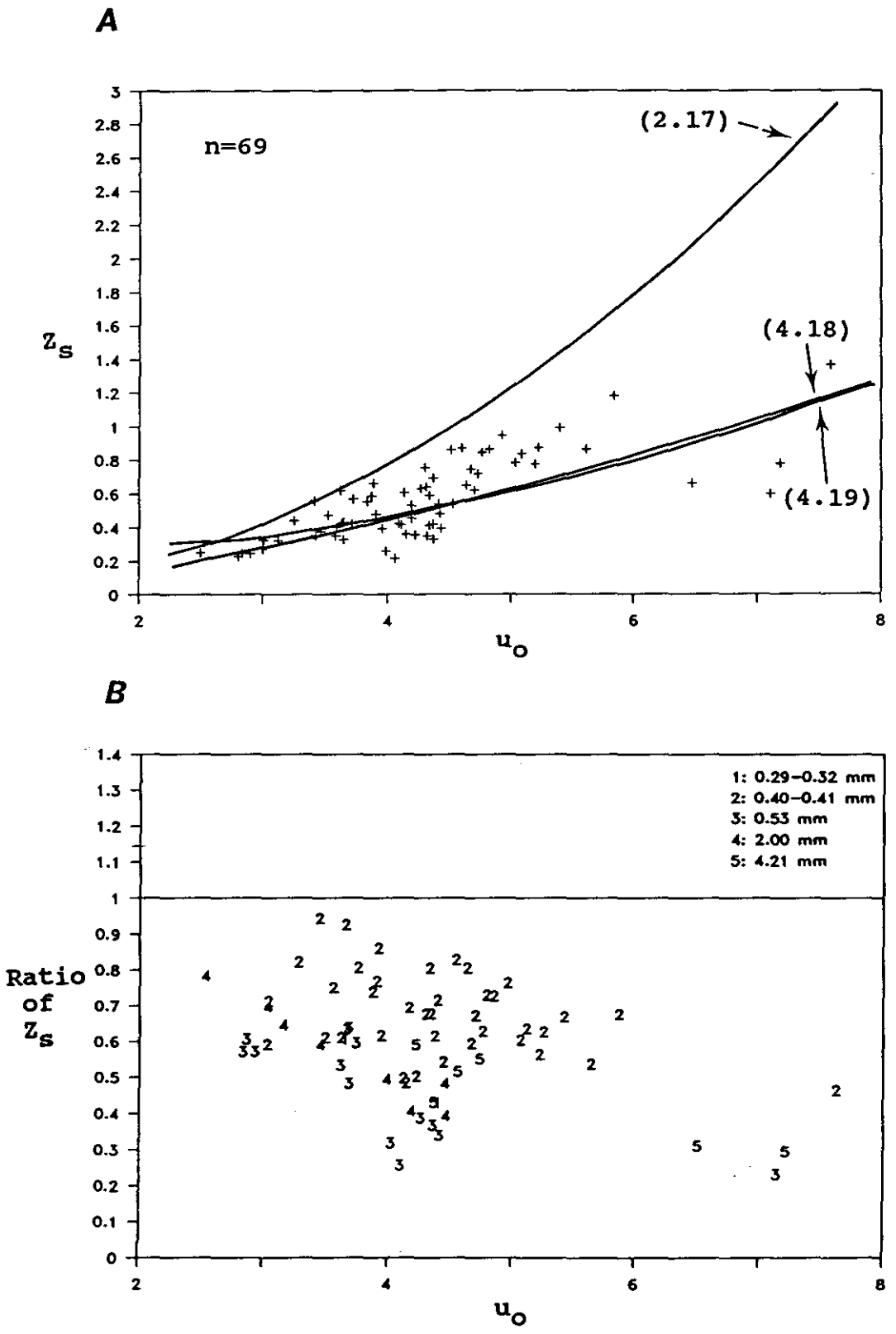

Figure 4.28: *(a)* Data from *Beach Type C* showing Z_s a function u_o. *(b)* Ratio of measured to predicted Z_s, as a function of u_o and D.

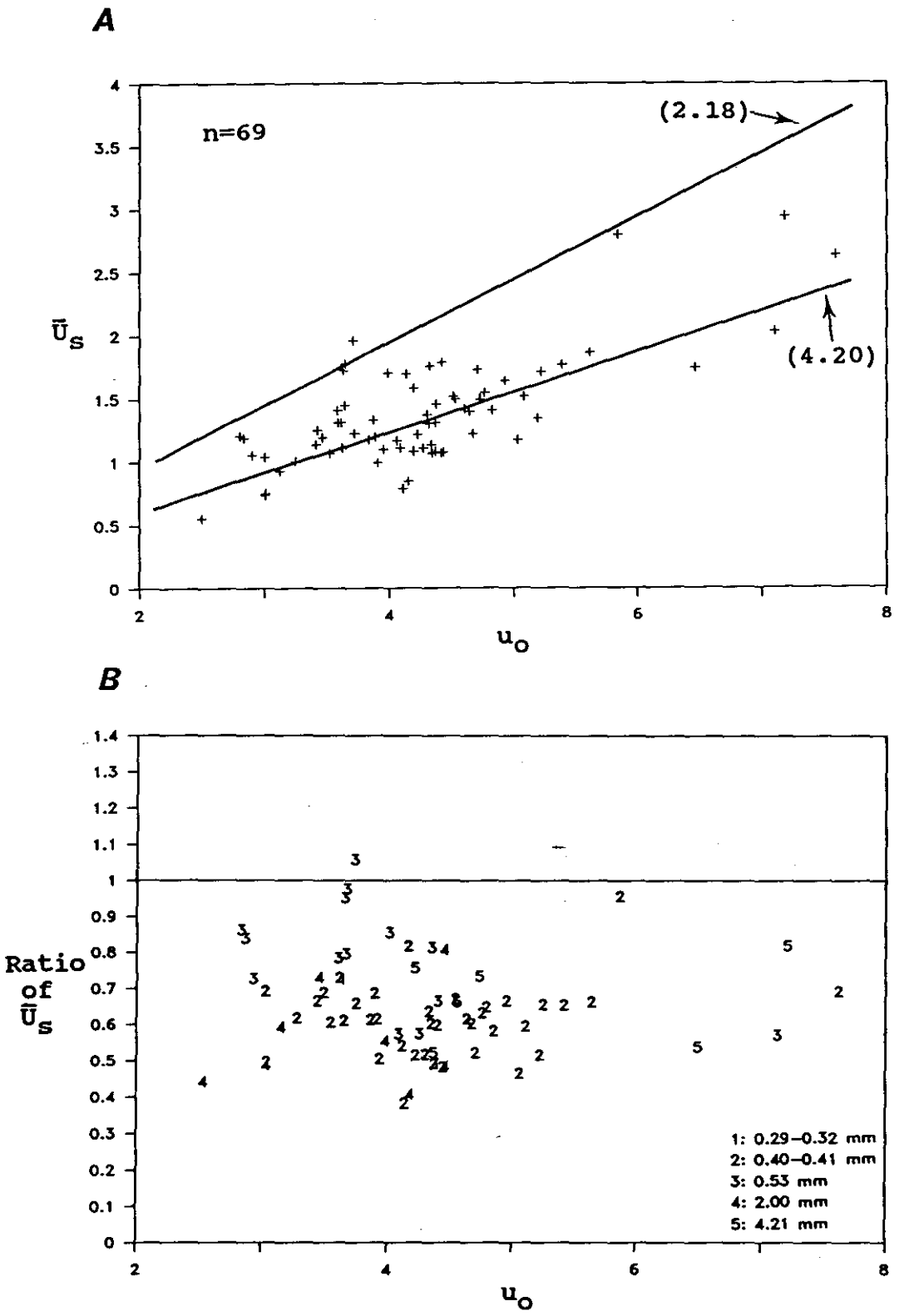

Figure 4.29: *(a)* Data from *Beach Type C* showing $\bar{U}_s$ as a function of u_o. *(b)* Ratio of measured to predicted $\bar{U}_s$, as a function of u_o and D.

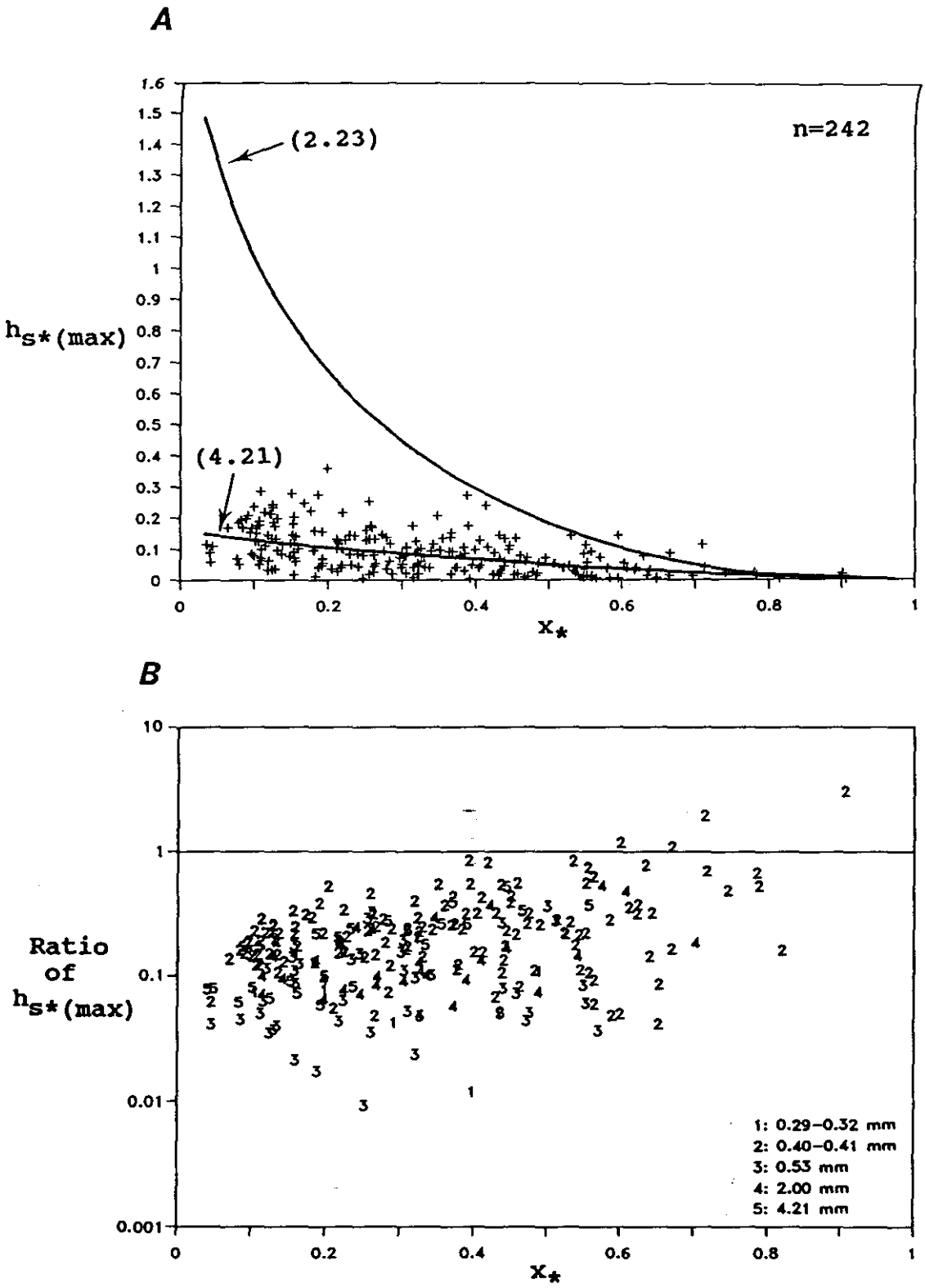

Figure 4.30: *(a)* Data from *Beach Type C* showing $h_{s*(max)}$ as a function of x_*. *(b)* Ratio of measured to predicted $h_{s*(max)}$, as a function of x_* and D.

2.5.3 may only rarely be suitable for application to swell waves on natural beaches. Their possible importance to infragravity waves and swash is discussed further in Section 7.2.

4.5 Comparison Of Swash Following Breaking And Non-breaking Waves

The purpose of this Section is to formally compare the data measuring swash following breaking and non-breaking waves. Visual comparison between the Figures shown in Sections 4.2.3, 4.3.3, and 4.4.3 indicates that several features of the swash behave similarly, regardless of the initial wave form. This is theoretically unexpected, and more quantitative evidence is presented here to establish this observation.

The regression models describing X_S, Z_S, $\bar{U}_S$, and $h_{S(max)}$ for each of the *Beach Types* are re-presented in Figure 4.31. Also shown are 2 standard error limits about the regression lines. Statistically, these limits are expected to contain 95 % of the total population from which the sample is drawn. It is clear for all the features presented, that the regression lines for each *Beach Type* lie within the error limits of the other *Types*. Two possible conclusions can be drawn. The first is that due to the scatter of the data, differences in swash following breaking and non-breaking waves are hidden by experimental error. The alternative conclusion is that the samples of data representing each of the initial wave conditions are drawn from the same population. This implies that in reality, there is no difference between swash following the breaking and non-breaking waves measured here. This second conclusion is the preferred choice for two reasons. First, the visual observations describing the swash cycle support this conclusion (*cf.* Sections 4.2.2, 4.3.2, and 4.4.2). Second, close coincidence of the error limits about the regression lines for $X_S(t)$, which have a very high level of signifigance on all *Beach Types* (Tables 4.1, 4.2, and 4.3), indicates that population differences are unlikely to be hidden by experimental error. Furthermore, the measured $X_S(t)$ for surging waves in no way resembles that predicted for a non-breaking solitary wave (*cf.* Fig. 4.27 and 2.16).

Additional support for the second conclusion lies with the shape of the $h_S(t)$ curves measured on the different *Beach Types*. By treating the swash depth at each digitized sample point as the frequency of occurrence of the particular time interval, the kurtosis of the $h_S(t)$ curve could be calculated. This parameter does not imply any physical phenomena, it is simply a sensitive,

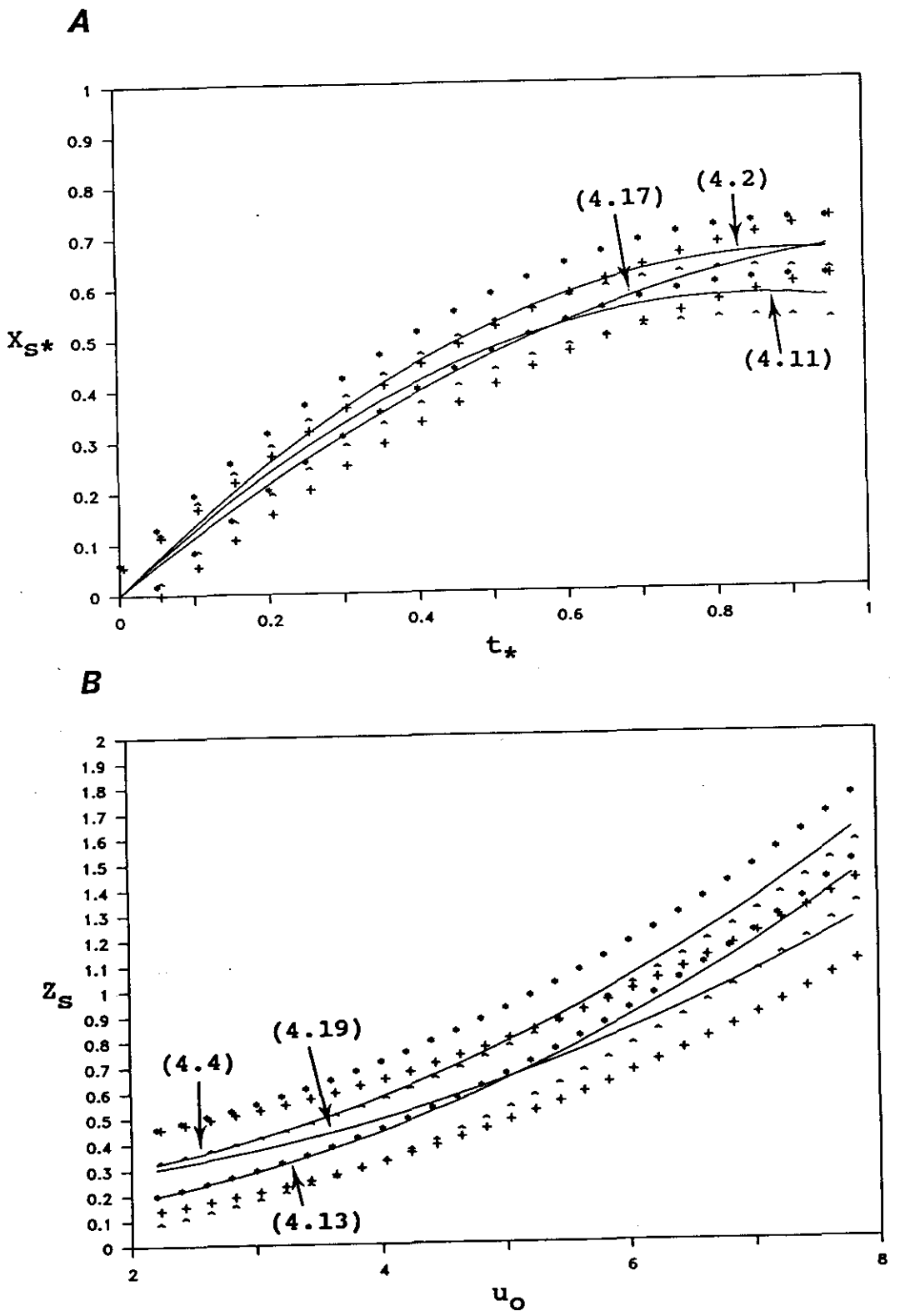

Figure 4.31: *(a)* Regression models showing two standard error limits for the data measuring X_{S*} as a function of t_*. The symbols *, ^, and + indicate the error limits for *Beach Types A*, *B*, and *C* respectively. *(b)* Regression models showing two standard error limits for the data measuring Z_S as a function of u_o.

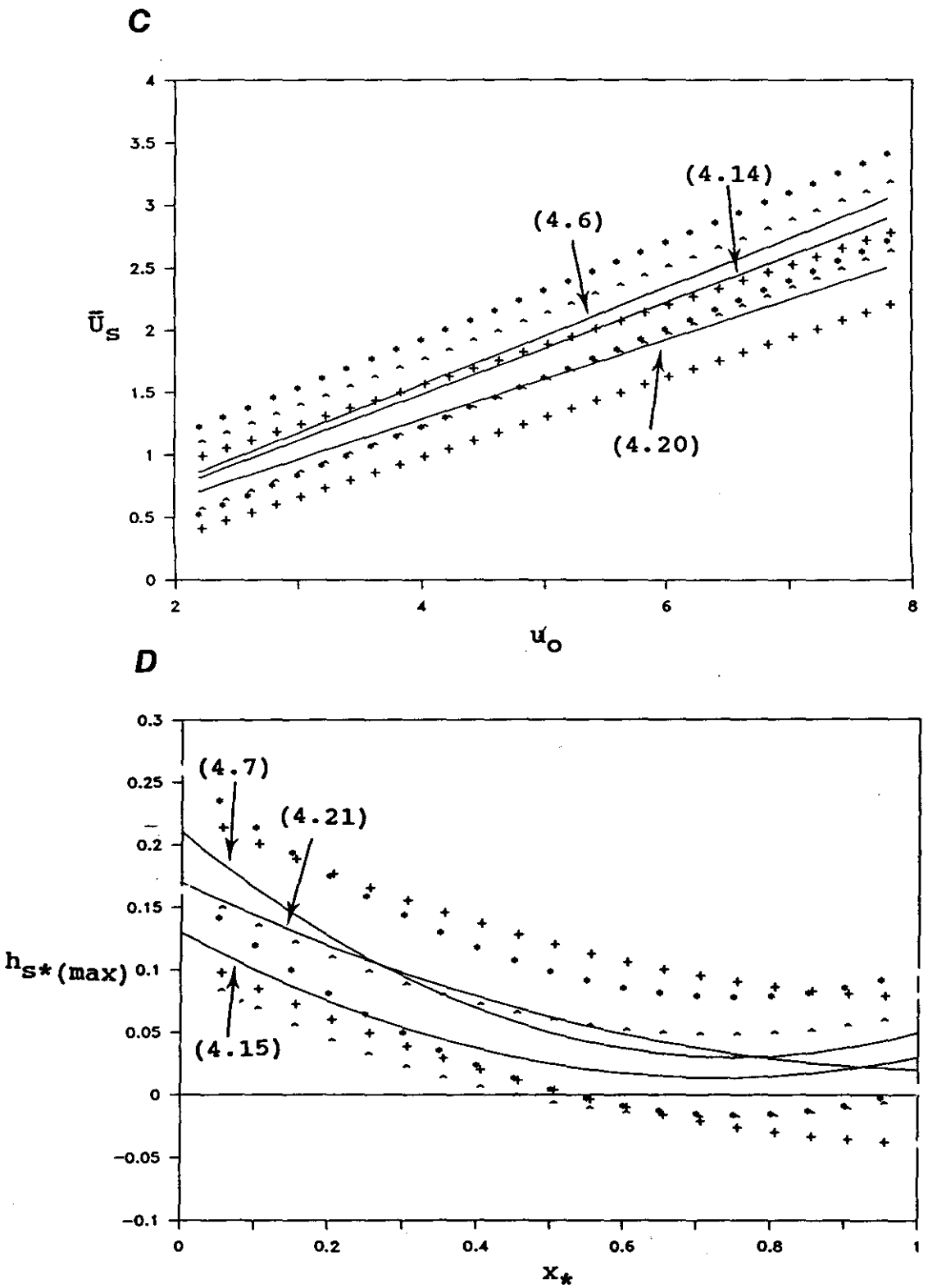

Figure 4.31 contd.: *(c)* Regression models showing two standard error limits for the data measuring $\bar{U}_S$ as a function of u_o. *(d)* Regression models showing two standard error limits for the data measuring $h_{S*(max)}$ as a function of x_*.

non-dimensional descriptor of the curve's shape. Since the kurtosis values are expected to change with distance up the beach (see Fig. 4.11b), it is required that the distribution of measurement locations across the beach is similar between experiments. Inspection of the data set confirms that this is indeed the case (Fig. 4.32). The frequency of occurrence of the shape parameter for both breaking and non-breaking waves is shown in Figure 4.33. The similarity between the distributions indicates that the $h_s(t)$ curves for both are very similar.

Substantial quantitative evidence has been presented in previous Sections to support the visual observation that uprush is equivalent for both the breaking and non-breaking waves measured here. Evidence has also been presented, that indicates the solutions of the SWE derived to describe bore uprush, are equally successful in the presence of surging waves. Since the conventional use of the theory implies that bore-free solutions will best describe surging waves (Section 2.6), this indicates that a new interpretation of the theory is necessary if it is to be applied to experimental data. In particular, this new interpretation must make use of the knowledge that non-breaking waves may behave as though they contain a virtual bore.

It is therefore proposed, that in order for the non-linear shallow water theory to provide a universal description of the swash, a continuum of swash types must be considered. The uprush of fully developed bores described in Section 2.4.4 and the uprush of surging waves described in Section 2.5.3 are the end-members of this continuum. They are theoretically described by the bore, and bore-free solutions of the SWE respectively. Along this continuum, the swash may display features of either solution, depending on its position relative to the end-members. The field data presented in this Chapter suggests that the solutions for bore uprush are capable of describing most field conditions, regardless of the initial wave conditions. The surging waves measured here had surface slopes sufficient to violate the first assumption of the SWE (Fig. 4.21; Section 2.2). Thus they may be considered to indicate a virtual bore inception, even though there was no subsequent overturning.

It is worth noting, that although most of the uprush behaved like a rarefaction wave, the transition process from incident wave to swash did appear to differ between the *Beach Types*. The transition zone increased in width as the initial wave condition changed from a turbulent bore to a surging

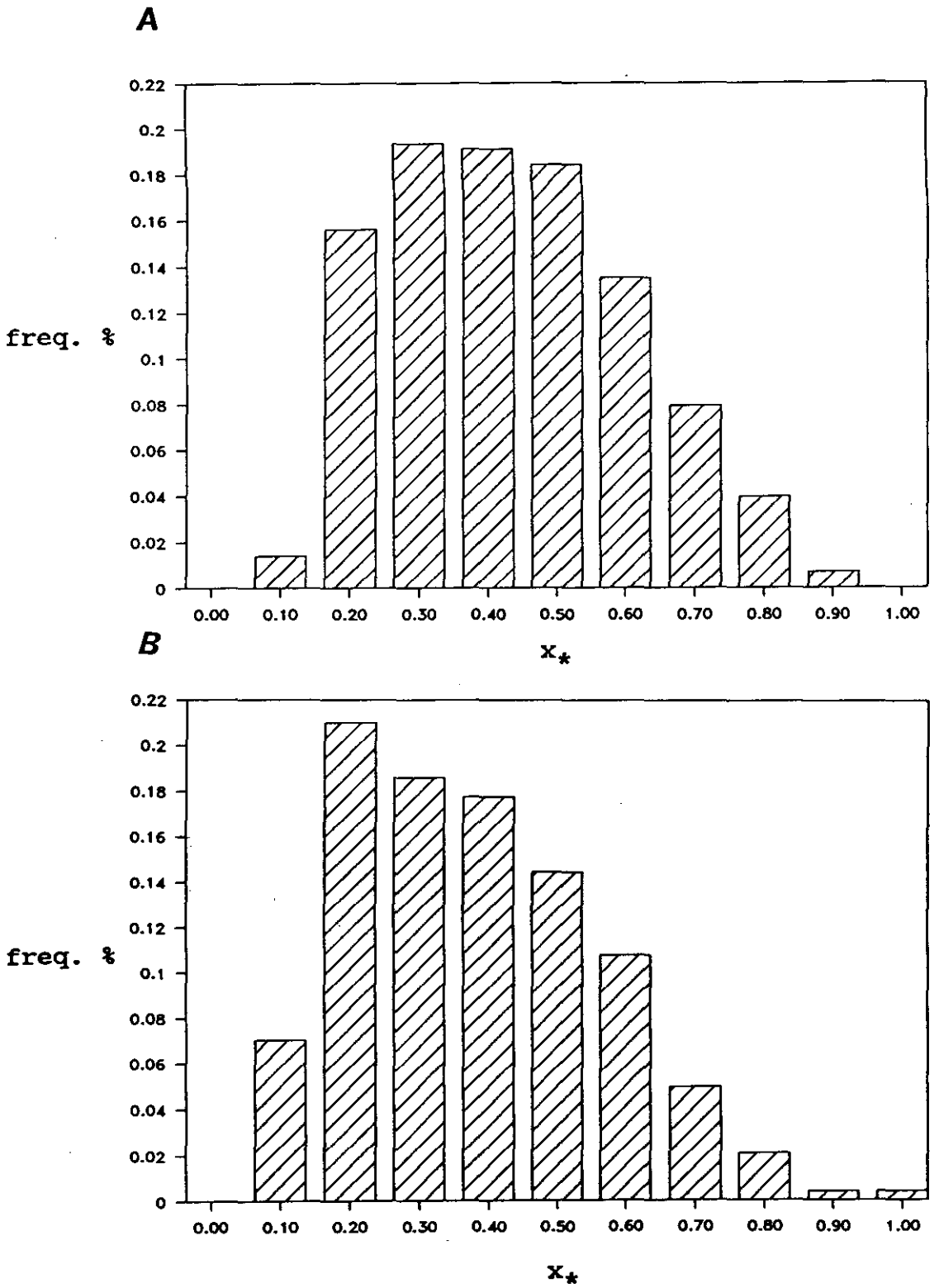

Figure 4.32: *(a)* Frequency histogram of the non-dimensional position of the probes during experiments on *Beach Types A* and *B*. *(b)* Frequency histogram of the non-dimensional position of the probes during experiments on *Beach Type C*. Comparison of the distributions suggests that the data coverage of the swash lens is similar for all *Beach Types*.

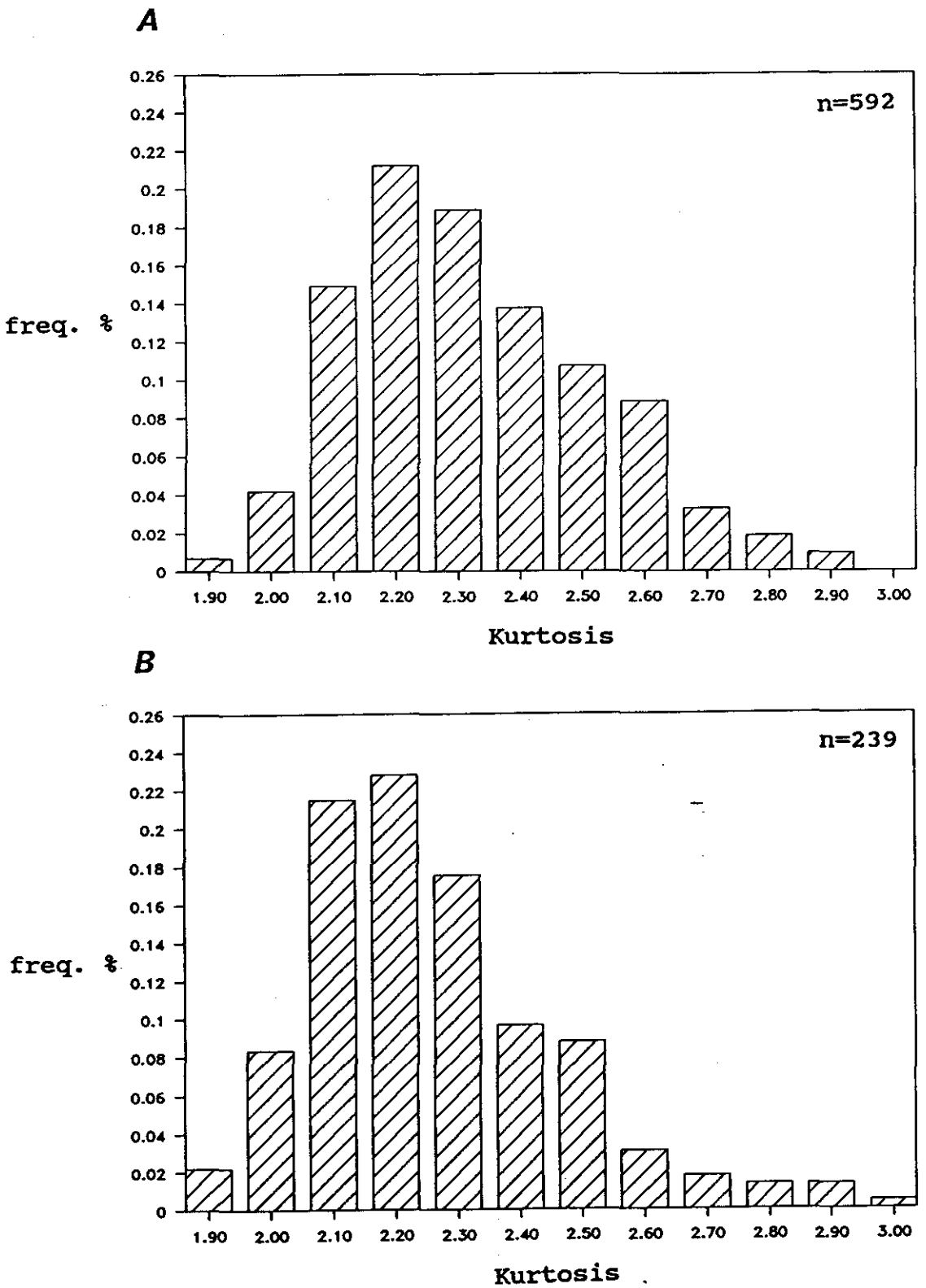

Figure 4.33: *(a)* Frequency histogram of the kurtosis values found for $h_s(t)$ curves measured on *Beach Types A* and *B*. *(b)* Frequency histogram of the kurtosis values found for $h_s(t)$ curves measured on *Beach Type C*.

wave (*cf.* Sections 4.2.2, 4.3.2, and 4.4.2). This can be easily explained in terms of the continuum concept described above. The width of the bore region in a fully developed bore is very narrow near the shoreline, consequently the region of the flow that cannot be described by the theory is small. Most of the flow on the beach face therefore appears as a rarefaction wave, and can be modelled by the solutions for bore uprush. As the non-breaking wave end of the continuum is approached the bore strength decreases, thus the bore width must increase (Section 4.2.2). This behaviour is evident in the similarity of appearance between minor bores and collapsing breakers (*cf.* Fig. 2.2 and 2.6). Due to the greater width of the bore, the transition zone also widens. Hence a smaller proportion of the flow on the beach can be described by the solutions for bore uprush. Eventually, deviations from small surface slopes become insignificant, the surging wave can be considered bore-free, and the bore-free solutions of the SWE can be applied.

Due to the choice of experimental design adopted in this study, continuous measurements of $X_s(t)$ in the transition zone were not possible. Such measurements can be obtained by either the resistance wires described in Guza and Thornton (1982), or the video recording method described in Aagaard (in press). Two sections of record from the latter method, kindly provided by T. Aagaard (University of Copenhagen, Denmark), are shown in Figure 4.34. Figure 4.34a shows the shoreline displacement for several swash cycles measured on Narrabeen Beach (Fig. 3.1) in the presence of surf zone bores. Since the initial acceleration of the shoreline due to bore collapse is nearly instantaneous, the entire shoreline path through time appears to be parabolic. Figure 4.34b is a section of record from Pearl Beach, where plunging breakers and surging waves were present at the shoreline (T. Aagaard, pers. comm.). This second record occasionally shows a smooth acceleration of the shoreline during the early stages of the uprush. This zone of acceleration is hypothesized here, to follow the arrival of a surging wave at the initial shoreline. In light of the above discussion this acceleration zone is expected for such conditions, and is believed to result from the larger time required for the virtual bore to 'collapse' and become swash. Consequently, less of the shoreline displacement on the beach can be described by the theory, as the SWE are not valid in this transition zone. Following the acceleration phase, the shoreline path appears parabolic (Fig. 4.34b), and is consistent with the data shown in Figure 4.27a.

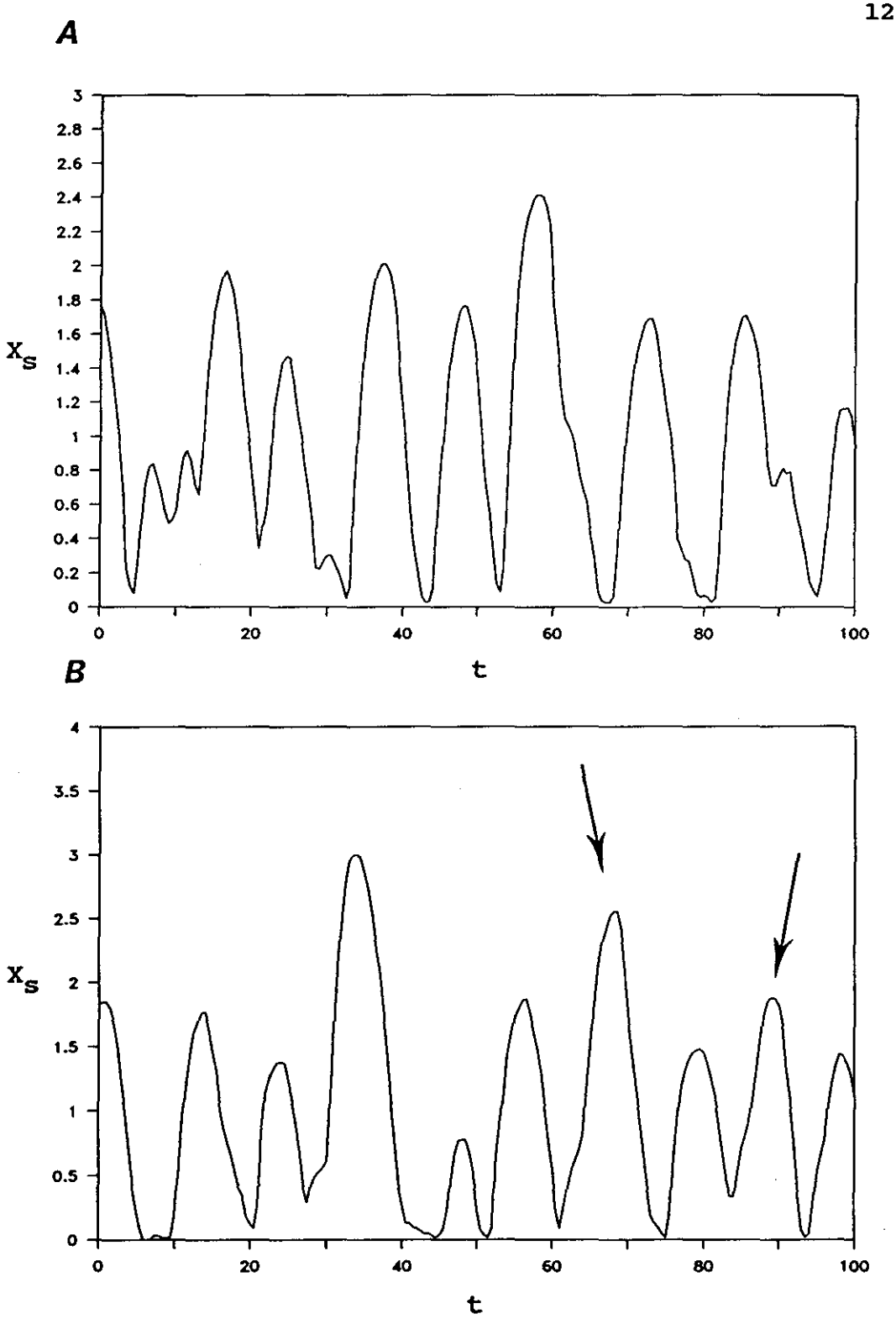

Figure 4.34: *(a)* Time series of shoreline displacement measured at Narrabeen beach, where surf zone bores were arriving at the initial shoreline. *(b)* Time series of shoreline displacement measured at Pearl beach, where plunging breakers and surging waves were arriving at the initial shoreline. Arrows indicate swash cycles showing a possible transition zone of shoreline acceleration in the early uprush (Data provided by T. Aagaard).

The discussion in this Section has demonstrated that the solutions for bore uprush describe all the data presented in this study, including non-breaking waves. A new exposition of the non-linear shallow water theory's application to swash has been presented. It is envisaged that a continuum of swash exists, that explains within the context of the theory, why swash following surging waves can be described by solutions for bores.

4.6 Backwash

This Section presents data relevant to the backwash stage of the swash cycle. Since the behaviour of the backwash was consistent for all experiments, the observations described below are generally applicable to all *Beach Types*. The discussion is more descriptive than analytical, because the data is principally in the form of $h_s(t)$ records that are best presented as illustrative examples.

Two types of backwash are evident in the data records, and are distinguished by the behaviour of the $h_s(t)$ curves for $t>t_{(max)}$. Examples of these are shown in Figure 4.35. The first shows the $h_s(t)$ curves approaching zero water depth in an obvious sequence (Fig. 4.35a). Notice that the curves are nearly parallel in the final stages of the backwash. This indicates physically, that the entire swash lens is decreasing in depth at a similar rate. Thus the wedge shape of the lens at the time of maximum uprush (Fig. 4.12) is maintained throughout the backwash. In contrast, the second example shows $h_s(t)$ curves that tend to approach zero water depth simultaneously, at least for the swash probes on the lower beach face (Fig. 4.35b). This represents the situation where the depth at the seaward end of the swash lens is decreasing at a faster rate than the landward end. Consequently, the swash lens is able to become uniformly shallow over much of its length. This type of backwash lens often contains small shock fountains due to the large fluid shear (see Fig. 4.36). The concomitant 'slurry' of sand and water renders the concept of an h_s meaningless, as the top several centimetres of the bed becomes mobile, and there is no clear fluid overlying.

It is the second backwash type that most closely resembles the theoretical behaviour described by (2.19) (*cf.* Fig. 4.35b and 4.11b). This agreement is probably fortuitous however, since the theoretical curves are for a smooth and rigid bed, and the measured curves are strongly influenced by the effects of a rough and movable bed. Most of the records displayed the behaviour shown in

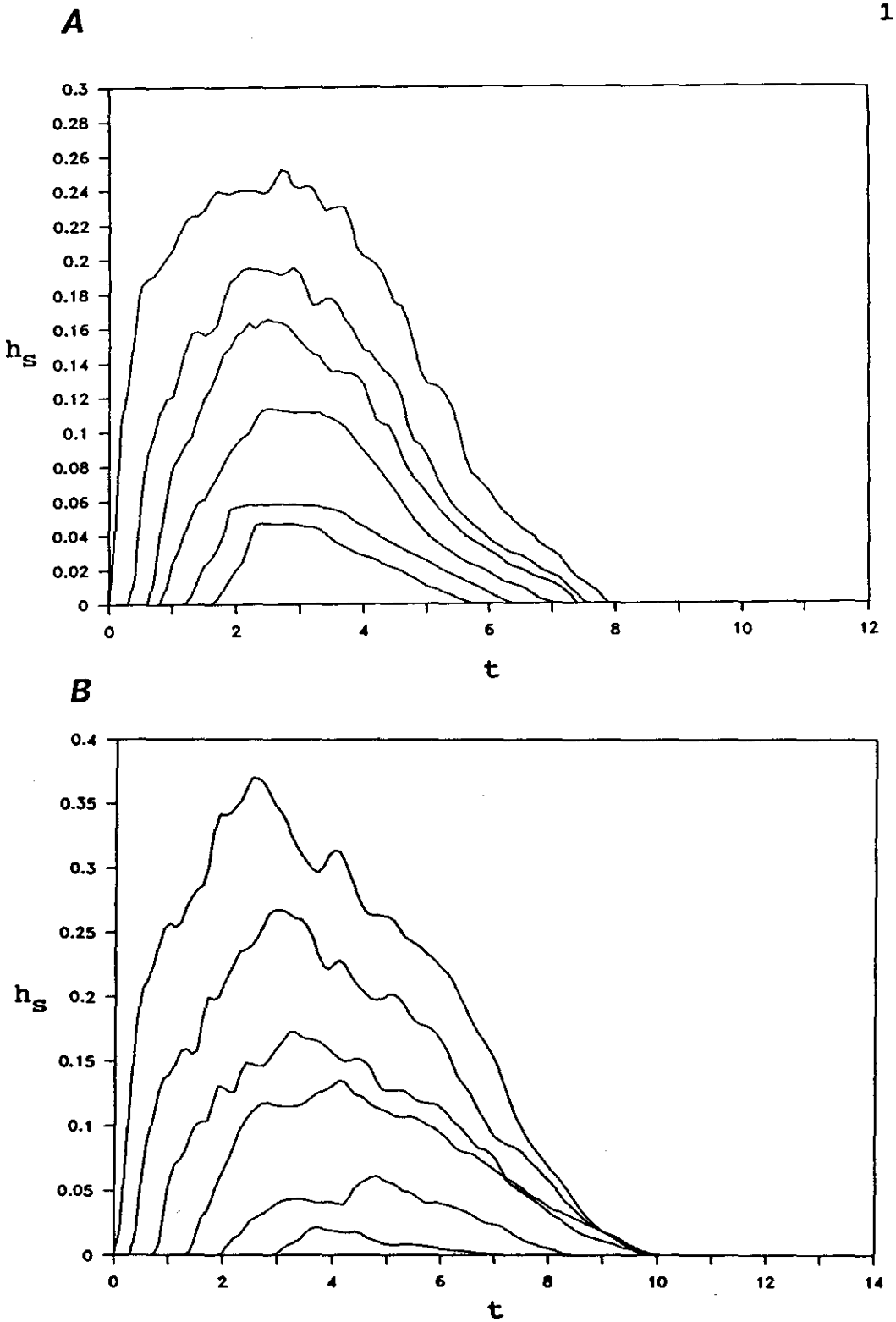

Figure 4.35: *(a)* Example of the first backwash type; initial conditions were u_o=4.91, β=0.1468, and D=0.00044. *(b)* Example of the second backwash type; initial conditions were u_o=5.05, β=0.1073, and D=0.00049.

Figure 4.36: **Photograph showing small shock fountains in the lower backwash. Also evident is the tendency for the fluid and bed to become indiscriminate as the water depth declines.**

Figure 4.35a, and indicate that the backwash on natural beaches cannot be described at all by (2.19). This is not completely unexpected, since the theory only claims to be valid until the appearance of a bore in the backwash.

It was mentioned in the discussion of Figure 4.11 that the measured backwash is significantly longer than that expected from theory. Furthermore, the depths in the backwash are consistently larger than those expected. These observations possibly indicate the presence of Shen and Meyer's backwash bore (Section 2.4.4). Previous field studies have interpreted this bore to be the stationary hydraulic jump which frequently forms near the *initial shoreline* (*e.g.* Ho *et al.*, 1963; Cowell, 1982). An interpretation more consistent with Shen and Meyer's prediction is the surface shear wave observed on relatively small slopes, since this type of bore forms up-beach in the interior of the flow (Peregrine, 1974b; *cf.* Fig. 4.37 and 2.13). This interpretation is still not entirely consistent however, because the shear wave is observed to propagate landward rather than seaward (see Peregrine, 1974b). Other wave forms in the backwash were observed on larger slopes, but were more transient than the phenomena shown in Figure 4.36. They tended to be smaller and narrower than the shear wave, often broke before disappearing, and moved seaward with the flow. Regardless of which of these wave types is most consistent with the expected behaviour of the backwash bore, they all have the effect of increasing the flow depth over that predicted by (2.19).

Although the backwash bore was frequently observed during the experiments, its representation in the chart records is poor. Secondary maxima in the $h_s(t)$ records are common, but they rarely occurred at more than one probe to establish the bore's propagation. This is probably due to the fact that the bore was restricted to the seaward end of the beach, and thus most of the probes were not in its path. Fortunately, on several occasions the occurrence of an unexpectedly large uprush meant that most of the probes were located, relative to the long backwash length, on the lower portion of the beach. One of these occasions is shown in Figure 4.38. The bore apparently formed somewhere landward of $x=2.18$ m, and grew in height as it moved down the beach. This example is consistent with the predictions shown in Figure 2.13 (see also Shen and Meyer, 1963), and is probably the second type of bore described above, rather than the surface shear wave.

Figure 4.37: Photograph showing surface shear waves or roll waves observed in the backwash. These may be one form of the backwash bore that was hypothesized by Shen and Meyer (1963).

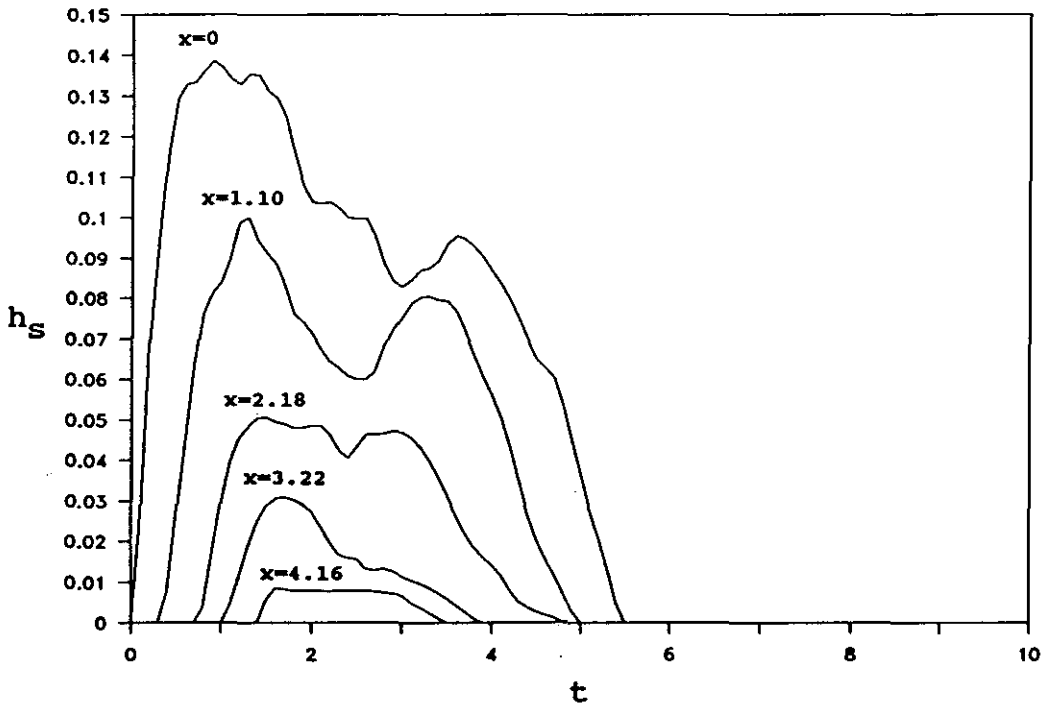

Figure 4.38: Measurements of $h_s(x,t)$ showing the development of a backwash bore up-beach from x=2.18, and its growth in height as it propagated seaward. Initial conditions for the swash were u_o=3.71, β=0.095, and D=0.00053.

The results in this Section indicate that the behaviour of $h_s(t)$ in the backwash contrasts significantly with the theoretical behaviour implied by (2.19). The difference is due to the unexpectedly large swash depths measured in the final stages of the backwash, which are believed to be caused by the backwash bore. The existence of this bore was foreshadowed by the theory, but is not quantitatively described by the theory (Section 2.4.4).

4.7 Evidence For Flow Resistance In The Swash Zone

Several previous studies have alluded to the possible effects of bottom friction in the swash zone, but until now the data collected in the field has been unable to establish its importance (Section 1.3). If the qualitative agreement between theory and data can be taken as an indication of the theory's ability to describe most of the physics, then some quantitative estimation of the effects of flow resistance are now available. The difference between the magnitude of the data measured, and the theoretical prediction is assumed to represent the total flow resistance induced by the bed. The individual contributions to this resistance by skin friction, sediment transport, and infiltration are discussed further in Section 5.3.

The shear stress created by flow over a rough, movable bed causes dissipation of energy in the flow, and a corresponding reduction in the water velocity (Yalin, 1977). Features of the swash lens that are influenced by the speed in which water moves up the beach include X_s, Z_s, $\bar{U}_s$, $h_{s(max)}$, and $h_s(t)$. Significantly, the measurements of these parameters are consistently over-estimated by the theory for the range of experimental conditions reported here (see Figures in Sections 4.2.3, 4.3.3, and 4.4.3).

Other features of the data that indicate friction effects include the following.

1. Over-estimation of X_s tends to increase with distance up the beach. This is expected if the effects of friction on a flow accumulate over the distance travelled.
2. Over-estimation of Z_s tends to increase with u_o. This follows from the previous observation, since larger u_o produces longer swash lengths.
3. The leading edge is blunt, in contrast to the acute edge expected from theory. Analysis by Freeman and LeMehaute (1964) predicts this type of profile in the presence of a bed friction that obeys the quadratic stress law.

4. Relatively high concentrations of sediment were observed to be mobilized by the flow, indicating at the very least, a critical amount of shear stress to initiate the motion.

The data presented in previous Sections show that X_s and Z_s measured on a natural, sandy beach may only reach 60-70 % of their predicted values due to the effects just described. Furthermore, the $h_{s(max)}$ might be reduced to 20 % of that predicted, although, not as much confidence can be placed in these latter measurements for two reasons. First, (2.19) is only proposed as an approximation near the shoreline. Second, there is a larger experimental error associated with these data.

The fact that variations in grain diameter between experiments had no obvious effect on the features measured here is not considered to be a serious contradiction to the inferred importance of friction. Most of the experimental grain diameters did not extend beyond the medium sand division of the Wentworth scale. The analysis presented in Section 5.5 shows that the effect on the friction factor in this range is small compared to other factors, such as the moving bed.

The evidence just described shows that the magnitude of flow resistance is sufficient to be measurable, and therefore needs to be incorporated into the theory for a more complete description of the swash on natural beaches. This is pursued further in Chapter 5.

4.8 Summary

In this Chapter original field measurements of swash on sandy beaches have been presented. These measurements constitute the first comprehensive data set designed to quantitatively test the theoretical solutions of the SWE.

The field data measuring uprush showed good qualitative agreement with the theoretical solutions for bores, on all three *Beach Types*. Although this was expected for uprush following breaking waves, there was no reason to expect it for surging waves. Confidence limits on the regression equations showed that there was no statistical difference in the data between breaking and non-breaking waves, for several features of the uprush. This indicated that the swash measured here was insensitive to the initial wave form, hence surging waves were found to behave as if they contained a virtual bore.

Despite the consistency in the data for most of the uprush, there were notable differences observed in the transition from incoming wave to swash. It was therefore proposed that there may be a continuum of swash behaviour, where fully developed bores and surging waves that satisfy $\epsilon<1$ are the end-members. The solutions of the SWE that describe these end-members are the bore and bore-free solutions presented in Section 2.4.4, and 2.5.3 respectively. Examples that lie between the end-members may display characteristics of both solutions. The important feature of this new exposition of the theory, is that it justifies the application of solutions for bore uprush to surging waves that do not satisfy the bore-free criterion. The implication from the data presented here is that Shen and Meyer's solutions are useful for describing most incident swash. The restriction is however, that as the bore-free end of the swash continuum is approached, the amount of shoreline displacement not described by the theory increases.

For the uprush data, all of the theoretically consistent regression models were easily significant at the 1 % level. Moreover, most of these models explained better than 60 % of the variance in the dependant variable. Exceptions to this were generally attributed to experimental error. This implies that the theory is capable of describing much of the underlying physics of the uprush. The backwash however, is not well described by the theory due to the presence of a backwash bore.

The theoretical assumption of a smooth and impermeable beach face precluded the possibility of a good quantitative match between theory and field data. Many previous studies have alluded to the probability that flow resistance in the swash zone will be significant. However, to date, the magnitude of these effects on natural beaches has remained unknown. If the qualitative success of the theory can be assumed to attest to its validity within the assumptions imposed, then the data presented in this Chapter provides the first quantitative measurements of the effects of flow resistance on natural beaches. The data support the previous contention that the magnitude of these effects is indeed significant. It is now possible to use the data presented here, to incorporate the effects of bottom friction into the theory.

CHAPTER 5
FLOW RESISTANCE IN THE SWASH ZONE

5.1 Introduction

Data presented in the previous Chapter show that the gross flow behaviour of the uprush on most sandy beaches is adequately described by the theory for swash following bore collapse (see Sections 4.2.3, 4.3.3, and 4.4.3). However, there is a significant discrepancy between the predictions of the theory and the actual magnitude of the data. The data available suggests that this discrepancy results from the theoretical assumption of a smooth and impermeable beach face (Section 4.7). In reality, some flow energy is dissipated due to the natural roughness of the bed, and thus precludes an exact match between theory and data. Now that the importance of this bed roughness has been established for the data, it is the aim of this Chapter to extend the inviscid theory, to provide a more quantitatively accurate description of swash on natural beaches.

Given the success of the inviscid equations for bore uprush in describing all of the field data, it seems most appropriate to extend these equations to include the effects of a rough and permeable beach. No field data is available to guide the extension of the bore-free solutions, and thus they are not pursued further. Only the uprush stage of the swash cycle is considered in this Chapter, since the existing theory does not satisfactorily describe the available backwash data (see Section 4.6). The equations for swash on a natural beach are derived in Section 5.2. The derivation begins by introducing a shear stress term into the existing equation of motion for the shoreline (*i.e.* (2.12)). This term defines the friction factor, which relates the bed roughness to the flow conditions. Once the equations for swash are derived, it only remains for this friction factor to be estimated, and then they can be tested against the field data. A conventional method for estimating the friction factor is presented in Section 5.3, and involves the summation of the bed roughness lengths due to skin friction, and a moving granular-fluid phase. The only remaining source of flow resistance considered to be important is the infiltration of the swash into the beach. There is no appropriate way of including these effects into the friction factor, and no information on their importance can be obtained from the data

set. The possible effects of infiltration are therefore excluded from the quantitative analysis presented here.

5.2 Equations For Swash On A Natural Beach

The problem considered here is that of the shoreline motion on a rough, permeable beach composed of cohesion-less sediment. The effect of the bed roughness, not previously considered in the theory, is to produce a shear stress that dissipates energy contained in the flow. More specifically, this stress is a force that acts parallel to the beach, and in the opposite direction to the uprush (Fig. 5.1). The magnitude of the shear stress τ is dependant on both the flow and the bed conditions and is often written as

$$\tau = 0.125\rho f u|u| \qquad (5.1)$$

(*e.g.* Sleath, 1984), where ρ is the fluid density, and f is the Darcy-Weisbach friction factor. Since only the uprush is considered here, the modulus can be removed and (5.1) can be re-written for the problem at hand;

$$\tau = 0.125\rho f \left[\frac{dX_s}{dt} \right]^2 \qquad (5.2).$$

The non-linear shallow water theory predicts that the uprush on a smooth and impermeable beach will behave as a rarefaction wave. Since no pressure is exerted on the leading edge of the wave from behind, its equation of motion can be derived by considering the balance of forces on a small 'fluid element' (see Section 2.4.4). The forces previously considered for the smooth beach case were the initial acceleration of the 'fluid element', and the gravitational acceleration. This description can now be extended to describe the natural beach, by including the bed shear stress as an additional force acting on the 'fluid element'.

From Figure 5.1, the equation of motion for the leading edge climbing a natural beach can be written as

$$m \frac{dX_s^2}{dt^2} + \tau\delta + mg(\sin\beta) = 0 \qquad (5.3),$$

where δ is the length of the leading edge. After substitution of (5.2) and dividing through by $m = \rho\delta h_\delta$, where h_δ is the swash depth a distance δ behind the shoreline, (5.3) can be re-written as

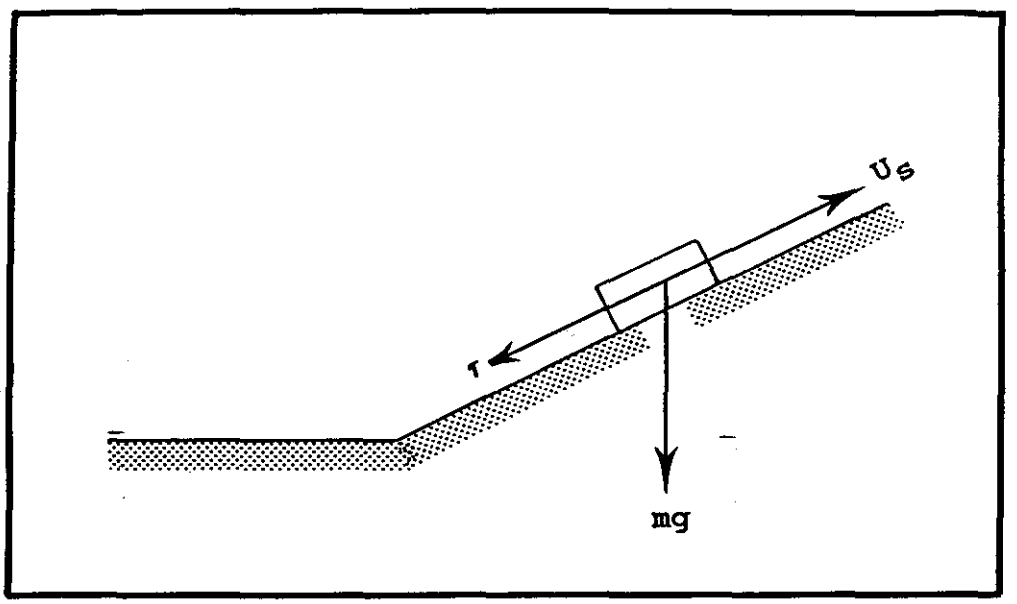

Figure 5.1: Definition sketch showing the balance of forces expected to be acting on a 'fluid element' climbing a natural beach.

$$\frac{d^2X_s}{dt^2} + \frac{f}{8h_\delta}\left[\frac{dX_s}{dt}\right]^2 + g(\sin\beta) = 0 \qquad (5.4).$$

If f, g, h_δ, and β are assumed to be constants, then (5.4) can be integrated using the separation of variables technique to yield

$$\frac{dX_s}{dt} = U_s(t) = \left[\frac{8gh_\delta(\sin\beta)}{f}\right]^{0.5} \tan(F+G) \qquad (5.5)$$

(see Appendix B for full derivation), where F and G are respectively

$$F = -t\left[\frac{gf(\sin\beta)}{8h_\delta}\right]^{0.5} \qquad G = \tan^{-1}\left[\frac{u_o\sqrt{f}}{\sqrt{[8gh_\delta(\sin\beta)]}}\right].$$

Furthermore, integration of (5.5) gives

$$X_s(t) = \frac{8h_\delta}{f}\ln\left[\frac{\cos(F+G)}{\cos G}\right] \qquad (5.6)$$

(Appendix B), and through trigonometry Z_s is found;

$$Z_s = \frac{-8h_\delta(\sin\beta)}{f}\ln\cos\left[\tan^{-1}\frac{u_o\sqrt{f}}{\sqrt{[8gh_\delta(\sin\beta)]}}\right] \qquad (5.7)$$

(Appendix B). These Equations are derived on the assumption that the presence of the bed shear stress does not alter the gross behaviour of the flow. More specifically, this assumption implies that the swash still behaves like a rarefaction wave on a natural beach, and that the 'fluid element' model of the leading edge motion remains appropriate. This assumption seems justified in view of the field data presented in Sections 4.2.3, 4.3.3, and 4.4.3.

It should be noted that (5.5) to (5.7) were initially derived by Kirkgoz (1981) using a Chezy coefficient formulation for f. The specific contribution this study makes is threefold. Firstly, it develops the available theoretical rationale upon which the derivation is based, to a level that enables the model shown in Figures 2.10 and 5.1 to be applied to field data (see Chapter 2). Secondly, this study provides a substantial data set that justifies the use of

this model, at least for describing the uprush part of the swash cycle (see Sections 4.2.3, 4.3.3, and 4.4.3). Thirdly, the analysis contained in the remainder of this Chapter constitutes the first attempt at testing (5.6) and (5.7) against field data.

Before (5.5) to (5.7) can be used to predict the behaviour of swash on natural beaches, estimates of h_δ and f are required. Since h_δ is taken as constant, the value of $h_{s(max)}$ at the mid swash (*i.e.* $L_s/2$) can be used as an estimate, representative of the entire uprush. The choice of $h_{s(max)}$ is convenient, because it can be calculated using (2.23) with no information other than u_o and β. Also, (2.23) has been found to provide a reasonable estimate of the true $h_{s(max)}$, at least near the mid swash (see Fig. 4.10a). The value of f depends on the relative roughness of the bed, and is discussed further in the following Section.

5.3 Estimating The Bed Friction Factor

5.3.1 Introduction.

Several types of bed roughness contribute to the value of f. Those most widely considered in the standard fluid mechanics texts include:

1) the roughness of the individual sediment grains,

2) the roughness created by sediment moving in the flow, and

3) the roughness created by perturbations in the bed surface (Raudkivi, 1976; Yalin, 1977).

These three types of bed roughness have been studied experimentally for both steady and oscillatory flows (see Yalin, 1977; Sleath, 1984 for summary). It is this long history of experimental work, rather than analytical description, that guides the estimation of f for most practical applications. The conventional approach used when calculating f, begins by assuming that f is related only to the relative roughness of the bed. This relative roughness is represented by the ratio of the total bed roughness length, to the flow depth. The former is usually calculated by a simple addition of the individual contributors listed above. Then some empirical relationship is used to relate the relative roughness to f.

For the data considered here, the third type of bed roughness can be conveniently ignored, since no bedforms were observed during the experiments. Although the critical Froude number for ripple development is usually exceeded during a single uprush, the duration of exceedance is apparently insufficient for the bed to respond completely (Nelson and Miller, 1974).

Broome and Komar (1979) have reported the formation of ripples beneath hydraulic jumps in the backwash, that may provide some form of roughness to subsequent uprush flows. However, these backwash ripples are restricted to flat, 'dissipative beaches' which are beyond the scope of this study (Section 1.2). Some measurements of small amplitude bedforms have been reported for the *Beach Types* considered here, but they have wave lengths far in excess of the swash length (*e.g* Sallenger and Richmond, 1984; Howd and Holman, 1987). The roughness contribution of this type of bedform can therefore be considered negligible, since the active beach face for any one swash cycle remains planar.

The following two Sub-sections present the most appropriate relationships available for calculating the bed roughness length due to skin friction, and movable bed effects. As an addendum, Section 5.3.4 speculates on the effects of infiltration on the uprush. Although there is no physical basis for incorporating these effects into the calculation of f, they must be considered since they are likely to be involved in the quantitative discrepancy between the inviscid theory and the data.

5.3.2 Roughness due to skin friction.

For a clear fluid flowing over a fixed bed, the only expected source of flow resistance is skin friction due to the roughness of individual grains composing the bed. If the flow is hydraulically rough and turbulent, which the swash is expected to be for most of its advance up the beach, then the velocity distribution in the flow should be well described by

$$\frac{u}{u_*} = 2.5 \ln\left[\frac{z}{z_o}\right] \qquad (5.8)$$

(Yalin, 1977), where Z is the elevation above the bed, z_o is the bed roughness length, and u_* is the shear velocity ($u_*=\sqrt{(\tau/\rho)}$). If it is assumed that the boundary layer in the leading edge occupies the entire flow depth, then (5.8) can be re-written using the notation of this study to yield u at the surface, and hence an approximation to U_s;

$$\frac{U_s}{U_{s*}} = 2.5 \ln\left[30\,\frac{h_\delta}{k_s}\right] \qquad (5.9).$$

The parameter k_s is known as the equivalent bed roughness length, and relates z_o to the mean grain diameter D (*N.B.* $z_o = k_s/30$; see Yalin, 1977).

It can be readily shown that the ratio on the left hand side of (5.8) is proportional to f^{-1}, if (5.1) is used to formulate u_*. Hence, when k_s is scaled by h_δ it uniquely determines f for the leading edge. Several laboratory studies indicate that for a fixed bed the value of k_s is constant for a given grain size, and should be of the order of twice D (see Yalin, 1977; van Rijn, 1982). The value adopted here is

$$k_{s(f)} = 2.5D \qquad (5.10).$$

The subscript (f) is intended to indicate k_s for the case of flow over a fixed bed.

The form of (5.9) suggests that f should be a function of the relative bed roughness only (*i.e.* $k_{s(f)}/h_\delta$). Since direct measurements of U_{s*} are unavailable, for the purpose of this analysis a more useful formulation for f is the Manning-Strickler equation. For the problem considered here, this equation can be written as

$$f = 0.122\left[\frac{k_{s(f)}}{h_\delta}\right]^{1/3} \qquad (5.11).$$

(After Sleath, 1984). For the range of relative roughness considered here, (5.11) and (5.9) are sufficiently equivalent to justify the use of the latter. Provided that D, u_o, and β are known, $h_\delta \equiv h_{s(max)}$ at the mid swash can be calculated using (2.23), $k_{s(f)}$ can be calculated using (5.10), and f for flow over a fixed bed can then be calculated using (5.11).

5.3.3 Roughness due to a movable bed.

If the bed is not fixed, then a two-phase flow exists, where a relatively clear fluid phase interacts with an underlying phase of moving fluid and granular material. The granular-fluid phase displays increasing sediment concentration with depth, and represents that part of the flow which is in contact with the stationary bed (Yalin, 1977). Even if the granular-fluid phase becomes dominated by inter-granular contact, it continues to display fluid-like behaviour, and is therefore still considered part of the flow (see Hanes and Inman, 1985; Hanes and Bowen, 1985; Wilson, 1988). The physics of this type of flow is more complex than that of a clear fluid over a fixed bed, hence there is

less consensus in the literature regarding its effect on f (*cf.* Hanes, 1984 and Wilson, 1988). The roughness created by the granular-fluid phase results from the turbulent wakes behind saltating grains, and the transfer of momentum from the flow due to the transported grains impacting with the bed (Owen, 1964; Grant and Madsen, 1982; Nielsen, 1985).

Cursory observations on natural beaches show that the bed shear stress is sufficient for the leading edge to transport sediment during most of the uprush. Moreover, the preservation of the swash mark on beaches testifies to the fact that transport continues almost to the point of maximum uprush, otherwise the mark would be destroyed by the subsequent backwash. Laboratory experiments conducted by Nelson and Miller (1974) substantiate these observations, and show that the principle modes of transport are traction and saltation. According to Owen (1964), who studied saltating grains in air, the roughness associated with this traction and saltation layer is proportional to the elevation reached by the saltating grains. Using Owen's hypothesis, and developing it for uni-directional flow of water, Smith and McLean (1977) obtained the following expression for the roughness length associated with a granular-fluid phase:

$$z_o = \alpha D\theta_c[(\theta'/\theta_c)-1] \qquad (5.12)$$

(*ibid.*). Thus the equivalent roughness $k_{s(m)}$, where the subscript (m) indicates the presence of a moveable bed, is

$$k_{s(m)} = 30\alpha D\theta_c[(\theta'/\theta_c)-1] \qquad (5.13).$$

In (5.13), θ_c is the critical Shield's parameter for the initiation of sediment transport, and θ' is the skin friction Shields parameter;

$$\theta' = \frac{0.125\rho f U_s^2}{\rho g D(S-1)} \qquad (5.14)$$

The numerator in (5.14) is the shear stress calculated using the skin friction formulation of f (see (5.1) and (5.11)). The parameter S is the ratio of sediment to fluid density, and can be taken as S=2.48. Also, since $\theta' >> \theta_c$, it can be assumed that θ_c=0.05 without any loss in accuracy. Smith and McLean's data for steady flow in a river provides α=26.3. The calculation of θ' requires some estimate of U_s. Since the level of analysis presented here assumes that f is constant for the entire uprush, a constant value for U_s that is representative for the uprush is sufficient. For the data analysis presented in Section 5.4 the following is adopted: $U_s \equiv \bar{U}_s = u_o/2$.

The total equivalent roughness for flow over a rough and movable bed, K_S, can now be written as

$$K_S = k_{S(f)} + k_{S(m)} \qquad (5.15).$$

This can then be substituted into (5.11) to yield the friction factor;

$$f = 0.122 \left[\frac{K_S}{h_\delta} \right]^{1/3} \qquad (5.16).$$

The procedure just described for calculating f presumes that the only contribution of the granular-fluid phase to the total flow, is to increase the roughness length of the bed. The main flow is assumed to continue to obey the 'Law of the Wall' (*i.e.* (5.8)). Several studies that present data where the measured f is greater than that expected for flow over a fixed bed, have found success in applying this approach (see Smith and McLean, 1977; Grant and Madsen, 1982; Nielsen, 1983). However, Wilson (1988) argues that when $\Theta > 0.8$ (*i.e.* sheet flow exists), the flow behaves according to its own Law. Notice that Θ is the Shield's parameter calculated using measured values of τ, and not the skin friction Shield's parameter Θ'. Wilson proposes that the velocity distribution in the presence of sheet flow will behave according to

$$\frac{U_S}{U_{S*}} = 2.5 \ln \left[53.2 \frac{h_\delta}{\delta_S} \right] \qquad (5.17)$$

(After Wilson, 1988), where δ_S is the thickness of the sheet flow layer. Wilson's laboratory experiments show that $\delta_S = 10\Theta D$. Equation (5.17) can be made compatible to (5.9) if the equivalent roughness length is taken to be about one half the sheet layer thickness. Hence,

$$k_S = K_S = 5\Theta D \qquad (5.18)$$

(Wilson, 1988). This adjustment enables the use of (5.18) with (5.16) to estimate f. It should be noted that Wilson measured the actual shear stress in his experiments, and was therefore able to calculate Θ. If Θ' is used as a surrogate for Θ in (5.18), then an under-estimation of f should be expected. Interestingly, from (5.18) Wilson observes that K_S is independent of grain size, since D also appears in the denominator of Θ.

In contrast to what is expected from the preceding equations, Gust and Southard (1983) report measured values of f in the presence of very weak bed-load transport, that were smaller than those measured for flow over a fixed bed. Furthermore, some recent experimental and theoretical studies have shown a similar reduction in f for sheet flow conditions (see Hanes, 1984; Hanes and Bowen, 1985). These contrasting results indicate the complexity of the processes, and introduce some degree of uncertainty into the analysis presented in Section 5.4.

5.3.4 Infiltration effects.

The loss of fluid into the permeable beach is expected to contribute to the total flow resistance, but in a different manner to the energy dissipation effects accounted for in the two previous Sub-sections. The loss of fluid from the leading edge alters the dimensions of the flow, and cannot in any obvious way be considered in terms of an equivalent roughness length. Thus it cannot be incorporated into (5.3) through the framework presented above. Fortunately, since only the uprush is considered here, there is some evidence which suggests that ignoring infiltration may lead to only minor errors.

Packwood (1983) used a numerical model to study the effects of infiltration, during a swash cycle which followed bore collapse on a fine-medium grade beach. His analysis was restricted to these grain sizes and a mild beach slope (β=0.035) so that Darcy's Law could be applied to the flow through the bed. For any given Z_s, the distance the swash travels over the permeable bed will be largest for gentle slopes. Thus, all other things being equal, the maximum potential for infiltration exists on gentler slopes. Since Packwood's range of D is comparable to this study and his β is significantly less, his results can be considered as an extreme case for the data collected in this study. Packwood's analysis shows that the effects of infiltration on Z_s are minimal, although, infiltration is found to have a significant effect on the backwash.

Although the model in Packwood (1983) still requires experimental confirmation, the results imply that only small errors in predicting the uprush might be expected if infiltration is ignored. Further support lies with the water table effluent zone that is frequently present on the beach face (Duncan, 1964). This saturated zone of beach must reduce the infiltration to zero for at least part of the uprush. It was not possible to calculate the importance of

infiltration in the uprush using the data collected in this study. Such an analysis would require measurements of the total volume of water in the bore, and the total volume in the swash lens at the time of maximum uprush. The infiltration loss would then be equal to the difference between the two volumes. Although estimates of the volume of water in the swash lens can be made from the $h_s(x,t)$ curves, no data is available for the volume of water contained in the bore. Given this lack of data to guide any further quantitative analysis, it is assumed that Packwood's results are valid, and the effect of infiltration is small relative to the bed friction. This enables the prediction of swash on natural beaches using only the bed shear stress to account for the flow resistance.

5.4 Comparison With Field Data

The ratio of measured Z_s to that predicted using (5.7) and the skin friction formulation of f (*i.e.* (5.11)), is plotted as a function of u_o in Figure 5.2. In this type of diagram, a perfect correspondence between the theory and measurements causes the points to lie on the horizontal line. Points that lie above the line suggest that the bed friction has been theoretically over-estimated, and *vice versa* for points that lie below the line. Before proceeding, it is worth noting that the initial wave type seems to have no effect on the behaviour of the data in any of these Figures. This supports similar observations made in Section 4.5. The location of the points in Figure 5.2 indicates that (5.11) does not completely account for the bed friction measured in the data. This result is demonstrated more clearly in Figure 5.3, where f is shown as a function of D/h_δ. The values of f were obtained by substituting measured values of Z_s, u_o, and β into (5.7). Thus they indicate the value required to make each point in Figure 5.2 lie on the line of perfect correspondence between theory and data. Figure 5.3 shows a clear pattern, where f is larger than expected for flow over a fixed bed. If the hypothesis that infiltration has little effect on the uprush is correct, then the roughness not accounted for is probably due to the presence of a movable bed in the experiments. It therefore appears, that the argument for decreased roughness in the presence of a granular-fluid phase proposed by Hanes (1984) and Gust and Southard (1983) is not appropriate for the swash zone.

The ratio of measured to predicted Z_s, using (5.15) and (5.16) to estimate f, is shown in Figure 5.4a. The tendency for most points to lie above the line suggests that K_s, and hence f, is over-estimated by (5.15). If a value

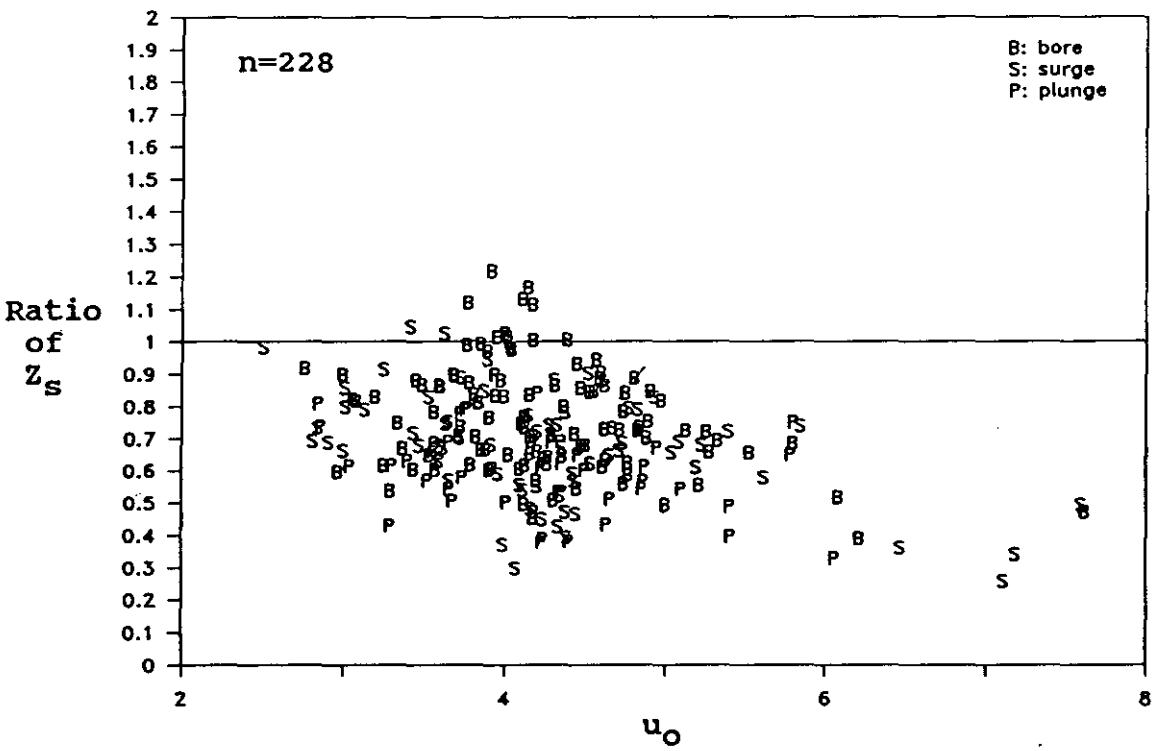

Figure 5.2: Ratio of measured to predicted Z_s as a function of u_o and the initial wave type. The predicted value was calculated using (5.7) and (5.11).

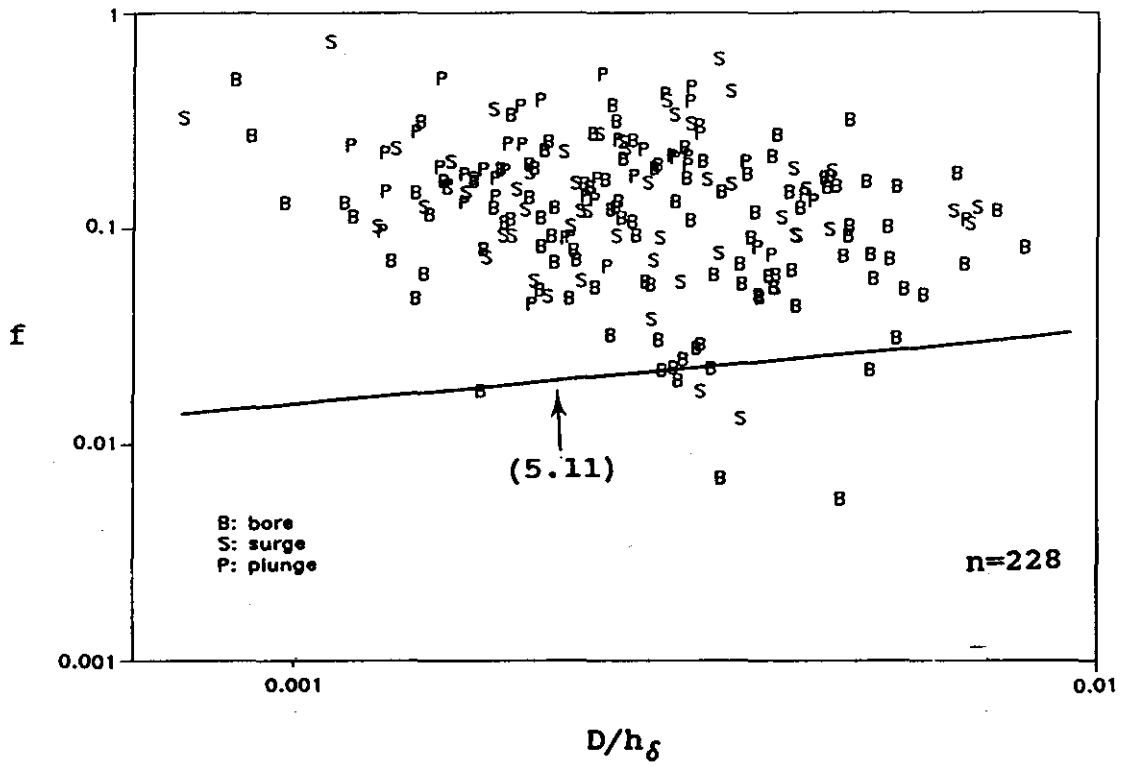

Figure 5.3: Apparent f as a function of initial wave type and relative bed roughness.

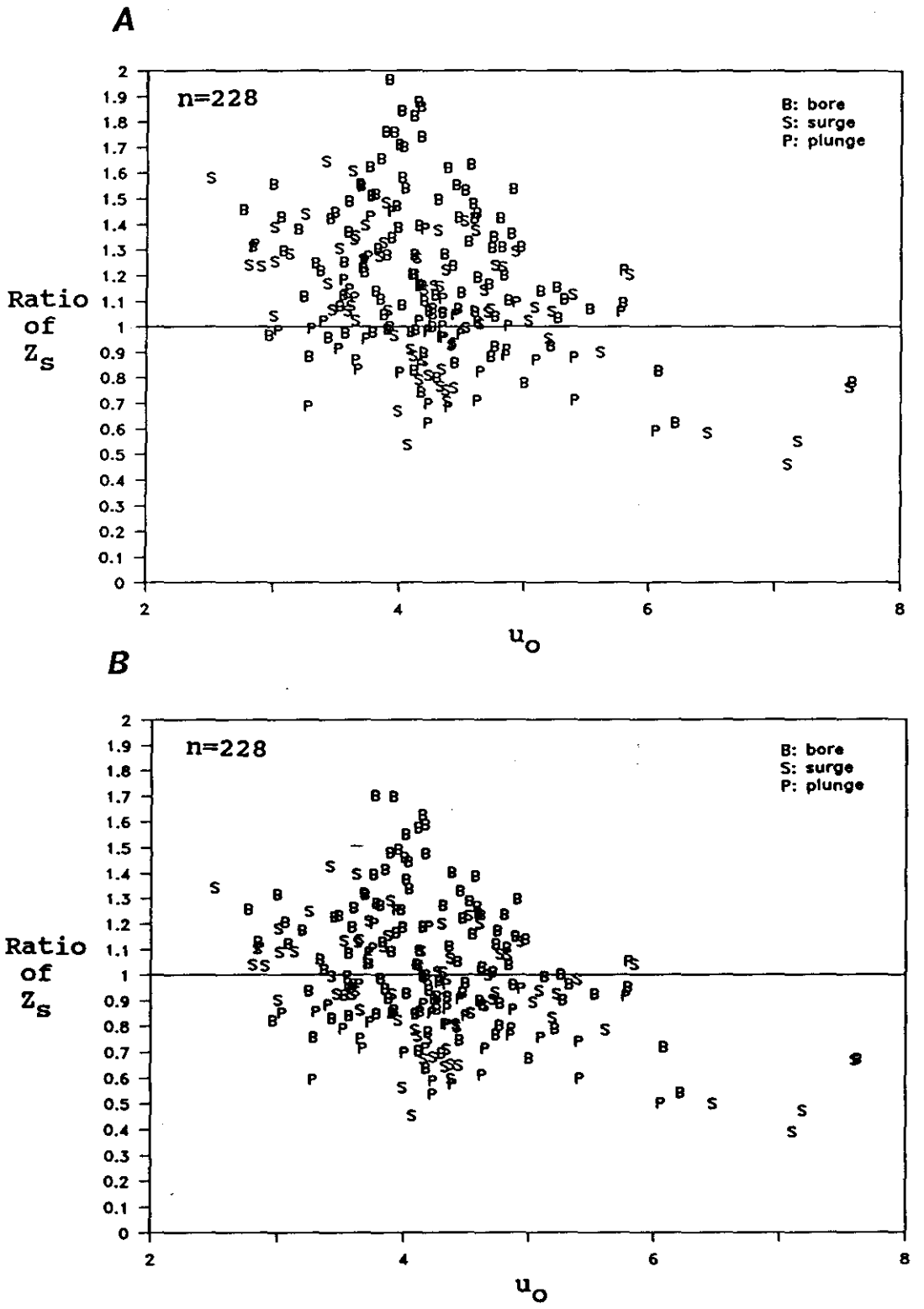

Figure 5.4: *(a)* Ratio of measured to predicted Z_s as a function of u_o and the initial wave type. The predicted value was calculated using (5.7), (5.15), (5.16) and α=26.3. *(b)* Ratio of measured to predicted Z_s as a function of u_o and the initial wave type. The predicted value was calculated using (5.7), (5.15), (5.16) and α=7.5.

of α=7.5 is used in (5.13) to calculate $k_s(m)$, then a better result is obtained (see Fig. 5.4b). However, no physical reason for such a reduction in α can be offered at this stage. Since Grant and Madsen (1982) calculated α=17 for measurements of $k_{s(m)}$ in oscillatory flow, the fact that the swash flow is unsteady is probably not a satisfactory explanation.

The ratio of measured to predicted Z_s, using (5.18) and (5.16) to calculate f, is shown in Figure 5.5a. Actual measurements of τ are unavailable from the experiments conducted during this study, so θ' was substituted for θ in (5.18). The effects of bed friction are again under-estimated, but this time it is expected since θ' only accounts for the skin friction contribution to τ (see Section 5.3.3). When using θ' in (5.18) a correction factor of 35 is required to account for the extra shear stress produced by the movable bed (see Fig. 5.5b). Hence, based on the range of data presented here, (5.18) can be re-written as

$$K_s = 175\theta' D \qquad (5.19).$$

It can easily be shown by substituting representative values for variables, that the required correction factor is not simply convenient, but is a physically sound quantity. For example, consider a typical case where u_o=4, D=0.0005, and h_δ is calculated to be 0.15. If the relevant substitutions are made into (5.11), (5.19) and (5.16), the values of f for the fixed and the natural bed are 0.025 and 0.15 respectively. This means that f is a factor 6, or almost an order of magnitude larger on the movable bed. This magnitude of increase in f for flow over a movable bed agrees well with measurements of f in oscillatory flow that are cited in Grant and Madsen (1982) and Nielsen (1983) (see their Fig. 3 and Fig. 10 respectively). It follows that the factor 35 needed to make $\theta' \equiv \theta$ is physically sound, as it produces results consistent with physical processes measured in a range of conditions broader than those considered here.

Since Wilson's (1988) conclusions are based on experiments in sheet flow conditions, the use of (5.19) to estimate f implies that θ>0.8 for most of the uprush. Figure 5.6 illustrates how θ' might be expected to behave during one uprush. The calculations were made using (5.14), and allowing U_s to vary with t. For the example shown, $U_s(t)$ is calculated using (2.13), and it is found that θ'>0.8 for more than 70 % of the time. It follows that θ>0.8 will be satisfied for at least the same amount of time, since any over-estimation

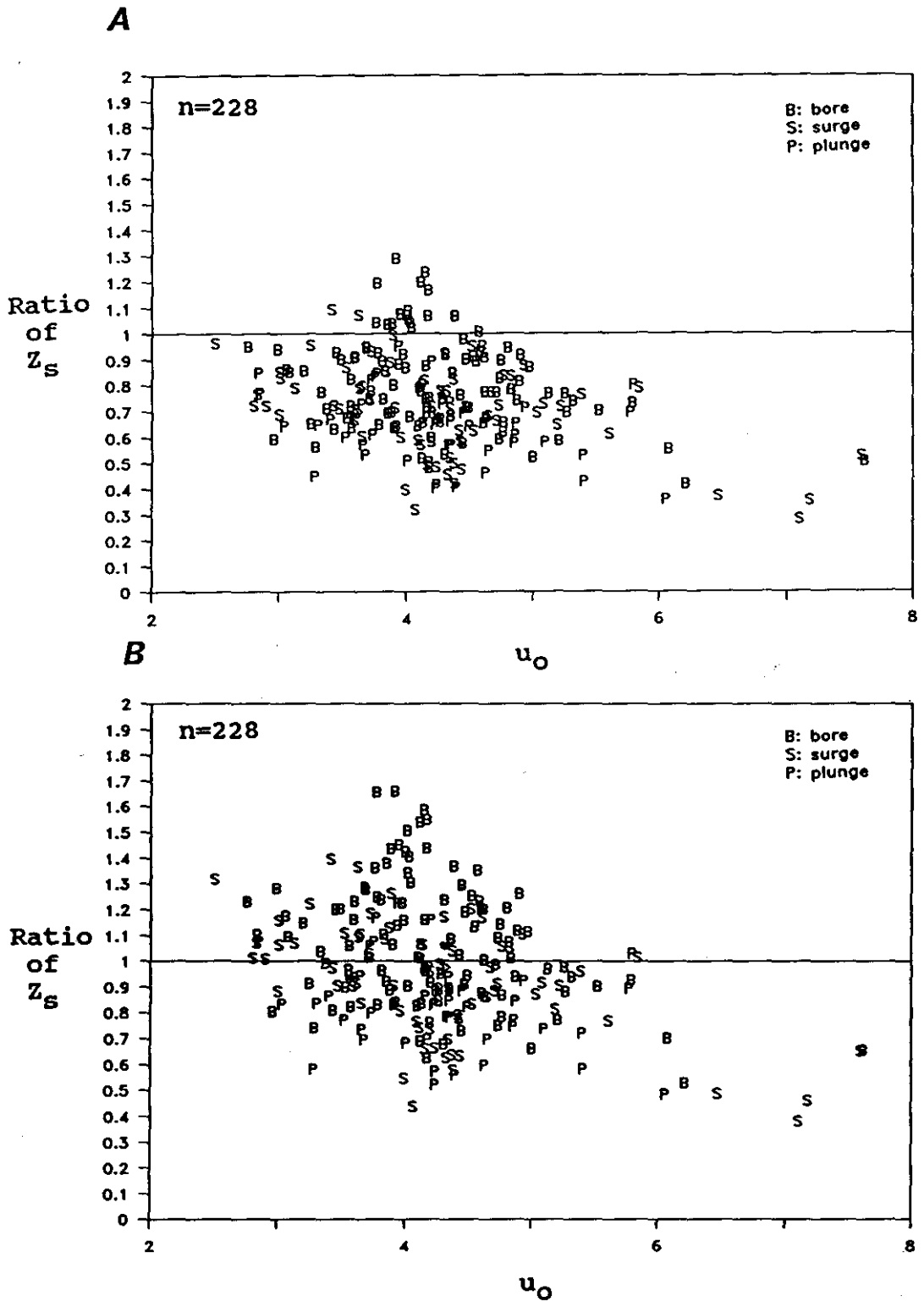

Figure 5.5: *(a)* Ratio of measured to predicted Z_s as a function of u_o and the initial wave type. The predicted value was calculated using (5.7), (5.16), and (5.18). *(b)* Ratio of measured to predicted Z_s as a function of u_o and the initial wave type. The predicted value was calculated using (5.7), (5.16), and (5.19).

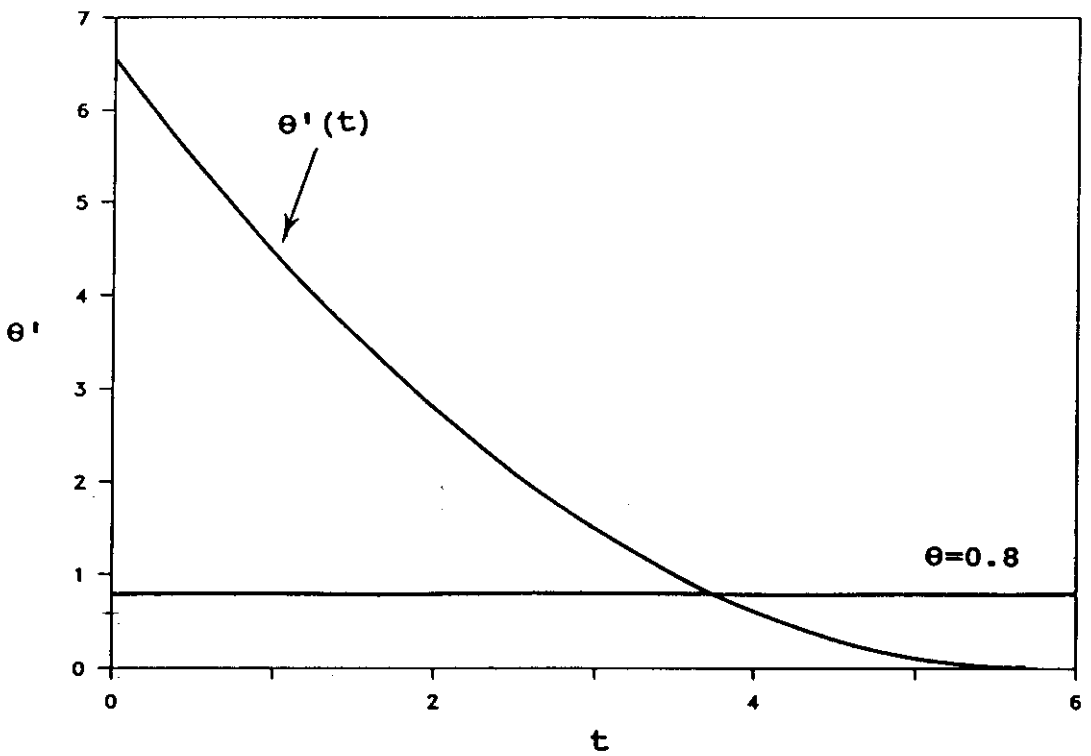

Figure 5.6: Predicted value of θ' using (5.14) for a swash cycle with initial conditions u_o=4, β=0.07, and D=0.0005. $U_s(t)$ was calculated using (2.13).

of $U_s(t)$ expected with (2.13) will be more than compensated by the fact that $\theta > \theta'$. It does not seem unreasonable therefore, to estimate a representative f for the swash zone using a model developed for sheet flow.

It must be conceded that there is a substantial amount of scatter in the data at the level of analysis illustrated in Figures 5.2 to 5.5. Thus the recommendation to use (5.19) and (5.16) to estimate f for any practical purpose, is based as much on their implied ability to describe the physics observed at the beach, as any demonstrated ability to explain the variance in the data. A great deal of the scatter may be due to the difficulties in isolating the expected weak trends in f, from the experimental error inherent in collecting data from natural sources. Despite these difficulties, Figure 5.7 shows that if (5.19) and (5.16) are used, then the equations for swash presented in Section 5.2 and Appendix B provide an excellent fit to the field measurements of X_s, Z_s, and $\bar{U}_s$ (Fig. 5.7a, b, and c). The matching for h_s during the uprush is improved to some degree, however, the unexpectedly large backwash duration is still not accounted for (Fig. 5.7d).

5.5 Discussion

In the derivation presented in Section 5.2, it was assumed that h_δ is constant so an exact solution to (5.4) could be obtained. Since it has been shown that h_s, and thus h_δ decreases with time during the uprush (Sections 2.4.4 and 4.2.3), this assumption requires further discussion. The expected variability in h_δ can be included into the derivation, but not without some difficulty. Although (2.19) is found to grossly over-estimate the measured h_s at the beginning of the uprush, by a magnitude that cannot be accounted for by the shear stress in the swash zone, it does at least describe the general behaviour of $h_s(t)$ (Fig. 4.11). If $x=\delta$ is substituted into (2.19), then $h_\delta(t)$ can be obtained. Upon substitution of (2.19) into (5.4), the equation of motion for the leading edge with time-dependant depth can be written as

$$\frac{d^2X_s}{dt^2} + \frac{9ft^2}{8(X_s-\delta)^2}\left[\frac{dX_s}{dt}\right]^2 + g(\sin\beta) = 0 \qquad (5.20).$$

An exact solution to (5.20) is not obvious. An approximate solution for X_s can be obtained through a perturbation approach, by assuming *a priori* that the inviscid equation (2.14) provides the first-order terms, and using f as the

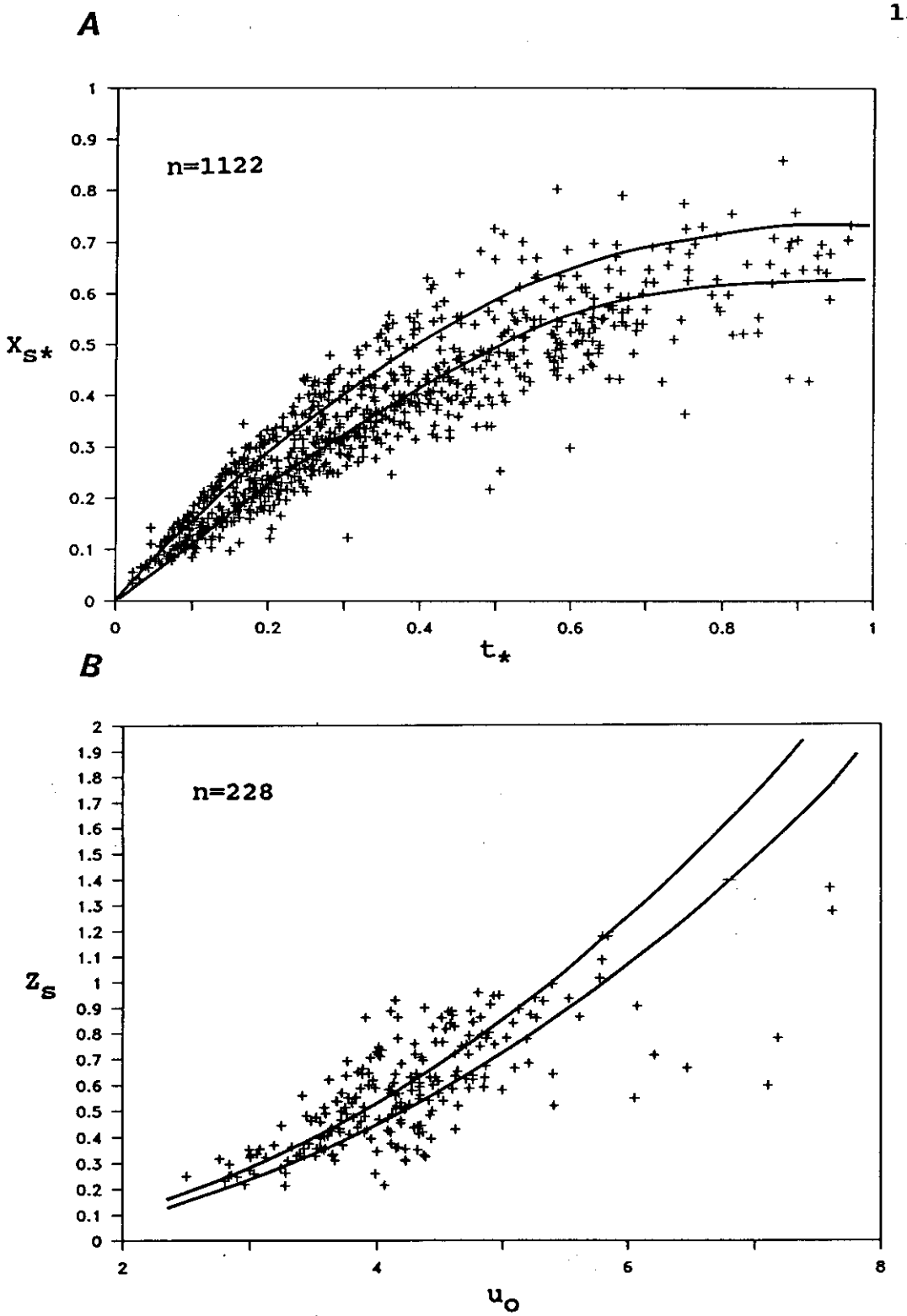

Figure 5.7: *(a)* X_{s*} as a function of t_*, showing all data and the theoretical prediction using (5.6), (5.16), and (5.19). The two predicted curves are for the extreme experimental slopes existing in the data set; β=0.0926 D=0.00046, and β=0.015 D=0.0004. *(b)* Z_s as a function of u_o, showing all data and the theoretical prediction using (5.7), (5.16), and (5.19).

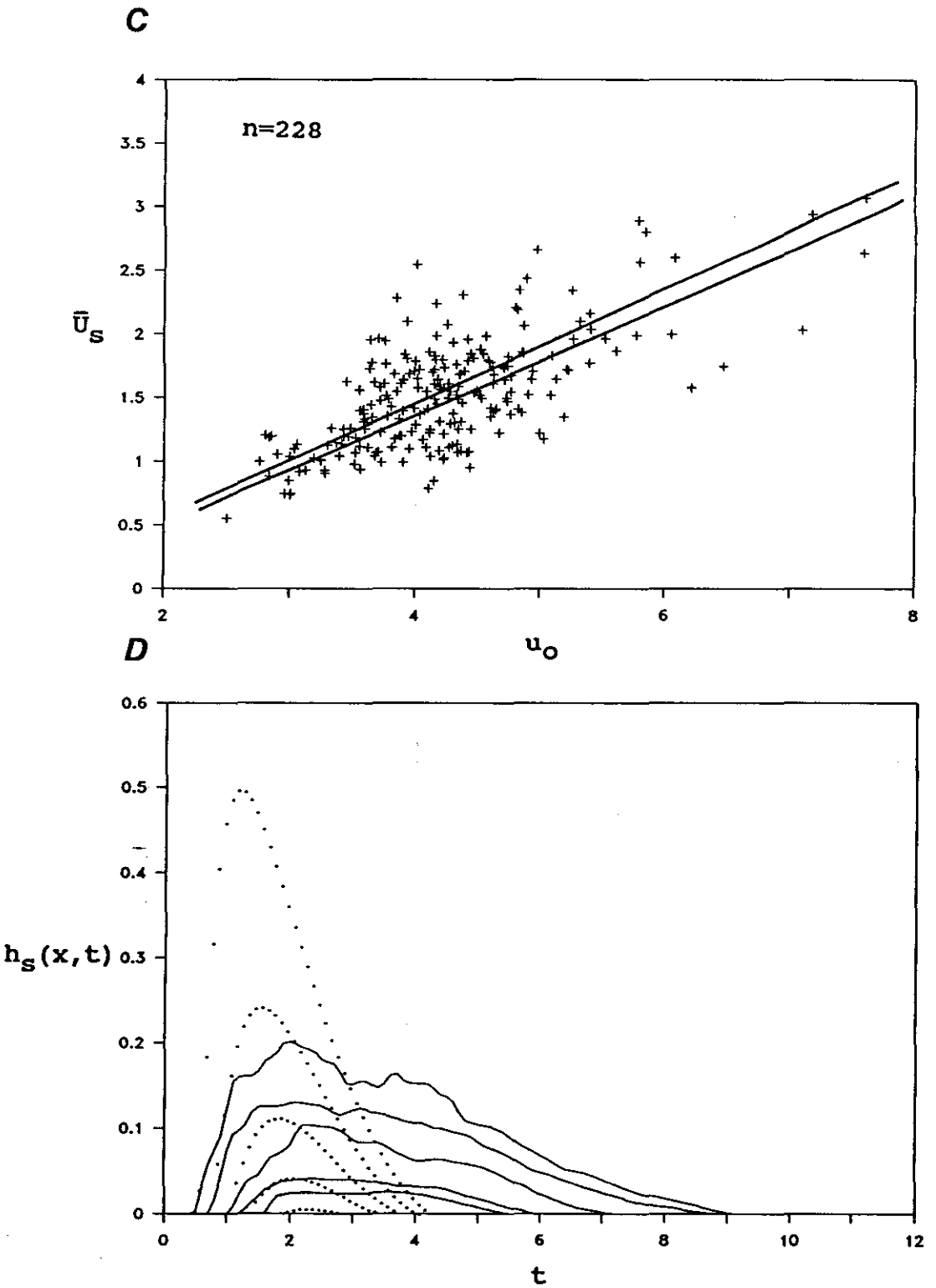

Figure 5.7 contd: (c) $\bar{U}_s$ as a function of u_o, showing all data and the theoretical prediction using (B.12), (B.15), (5.16), and (5.19). *(d)* Measured and predicted $h_s(x,t)$ for a swash cycle with initial conditions u_o=4.93, β=0.1468, and D=0.00044. Predicted curves are shown as dots and were calculated using (2.19); with (5.6), (5.16), and (5.19) to obtain $X_s(t)$. The locations of the measurements correspond with those shown in Figure 4.11.

small parameter in the derivation of higher-order terms (B. Boczar-Karakiewicz, pers. comm.). However, such a complex solution was not pursued here for several reasons. Even if the variation in h_δ can be accounted for in the equation of motion, f is considered a constant for the uprush, and requires a constant h_δ to be used in its calculation. Very little would be gained by only accommodating a varying h_δ for part of the analysis. The level of understanding surrounding the calculation of f does not permit at this stage, the possibility of a time-varying f. The possibility exists to simulate a time-dependant f, by calculating all the parameters at several time-steps during the uprush. However, the analysis then begins to lose its generality, and this concession is unecessary when the existing approach provides satisfactory results.

One further point should be made about treating h_δ as a constant. Figure 5.8 shows the predicted Z_s plotted against a range of h_δ that might be expected during the uprush. Clearly, large discrepancies in the predicted Z_s can result from the possible choices of h_δ. Based on the results presented in Figure 5.7, it is recommended that $h_{s(max)}$ at the mid swash be used to obtain realistic results.

It is instructive to speculate on the behaviour of Z_s, predicted by (5.7), for a range of morphological conditions. The predicted Z_s for a range of grain sizes is shown in Figure 5.9. Remember that Wilson's (1988) analysis suggested that f was independent of D, which implies Z_s should also be independent of D. The weak dependence of Z_s for small D shown in the Figure, only arises because θ' is used in (5.19). Interestingly, the effect of D remains insignificant for most sand sizes. This prediction corresponds very well with the observed insensitivity of the field measurements to variations in grain size between experiments (Sections 4.2.3, 4.3.3, and 4.4.3). This prediction also poses an interesting problem however. If the swash flow is mostly independent of D, what then is the mechanism which creates the frequently observed relationship between D and β (*e.g.* Bascom, 1951; Wiegel, 1964; Sunamura, 1984)? One possible solution is the effect of infiltration, which has been excluded here. The importance of infiltration as a negative feedback mechanism capable of determining equilibrium beach slopes is discussed further in Section 6.4.

The predicted Z_s for a range of β considered to be typical of sandy beaches is shown in Figure 5.10. The predicted Z_s has been scaled by the

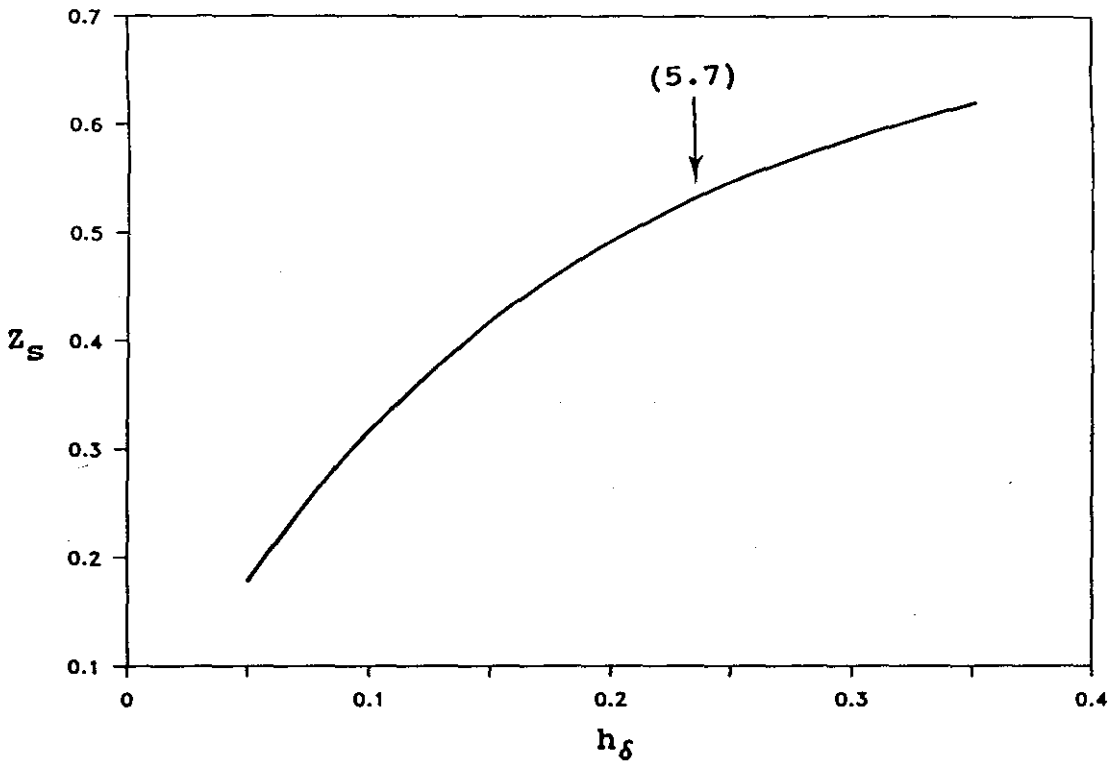

Figure 5.8: Predicted Z_S as a function of h_δ; using (5.7), u_o=4, β=0.07, and D=0.0005.

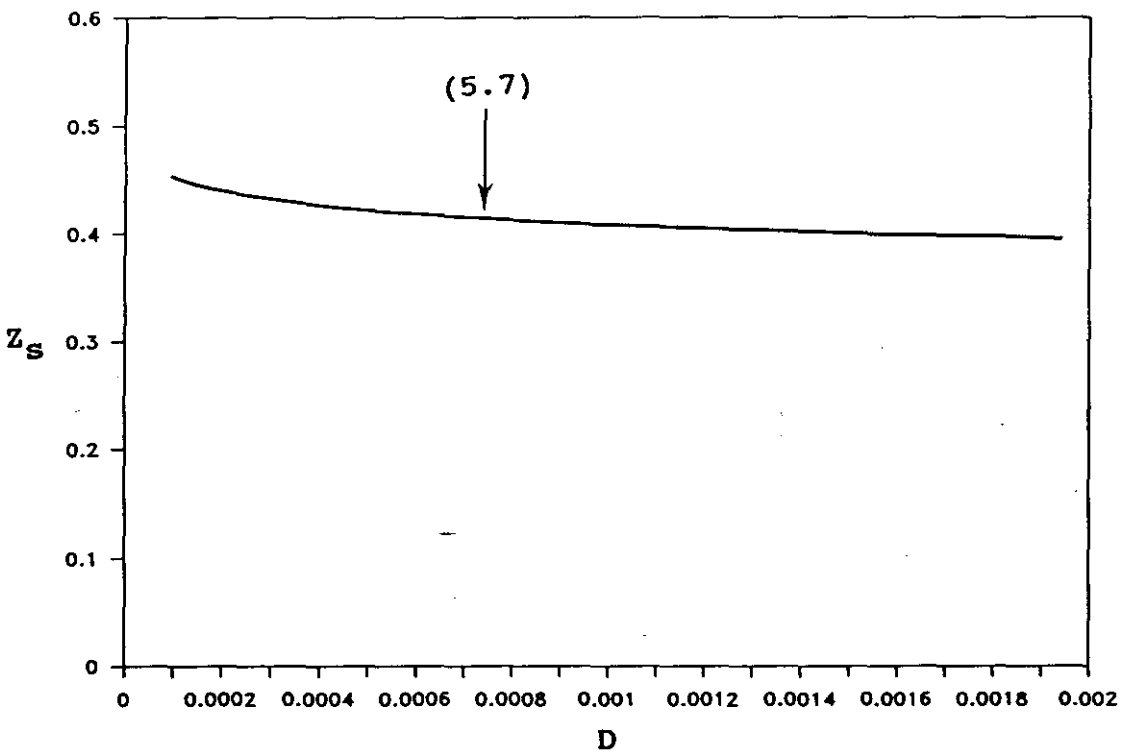

Figure 5.9: Predicted Z_S as a function of D; using (5.7), u_o=4, and β=0.07.

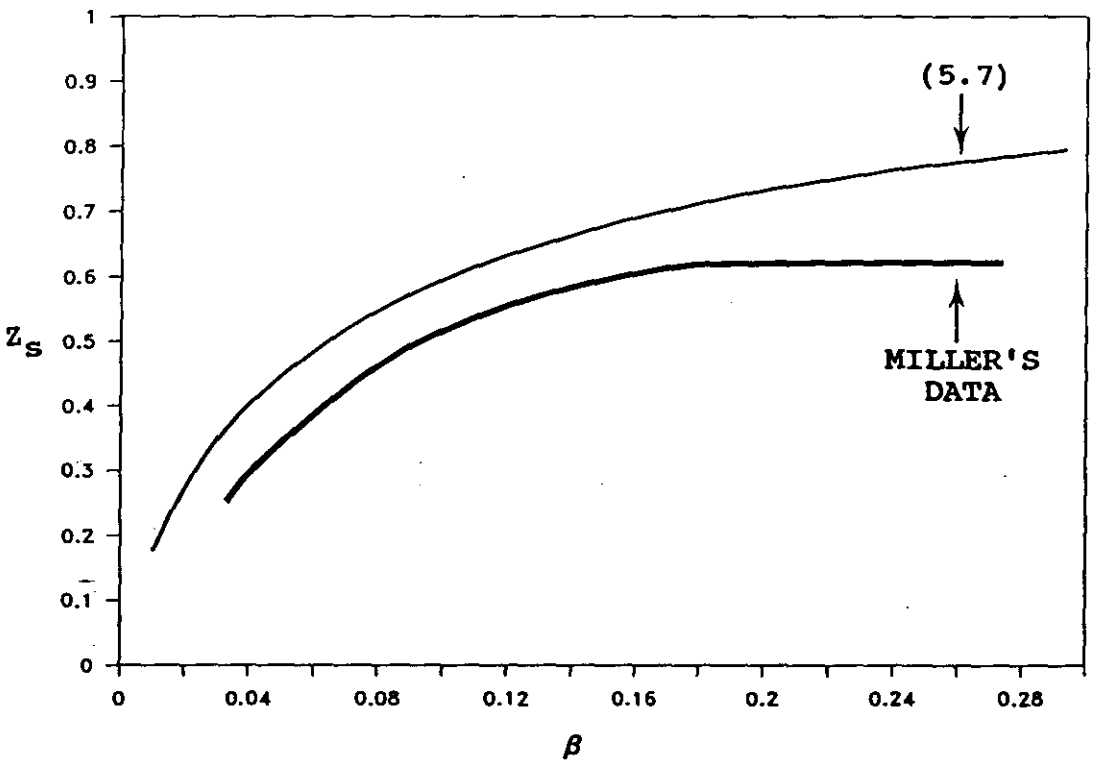

Figure 5.10: Predicted Z_S (scaled by (2.17)) as a function of β; using (5.7), u_o=4, and D=0.0005. Also shown are laboratory data summarized from Miller (1968).

inviscid result (*i.e.* (2.17)), so that laboratory data presented by Miller (1968) could also be examined. Interestingly, the improved theory and the data show that a positive relationship exists between Z_s and β. A relationship that Miller originally used to dismiss the applicability of the inviscid theory, since the predicted Z_s is independent of β (see (2.17)). The actual magnitude of the theoretical curve and the data set cannot be compared, because of unknown scale effects and the fact that Miller's data were measured on a fixed bed. However, it is noteworthy that the improved theory can now reproduce the measured effects of slope.

5.6 Summary

This Chapter has attempted to account for bed friction in the swash zone by extending the predictions of the inviscid, non-linear shallow water theory. The approach taken was to assume that the theory's description of the gross flow behaviour on a smooth beach, was also applicable to a natural beach. A shear stress term was then introduced into the existing equation of motion for the shoreline, and new equations describing the uprush were derived. These new equations necessarily assume that the shear stress does not prohibit the use of the small 'fluid element' description of the leading edge, and that the depth of the leading edge is constant during the uprush. The first assumption is well supported by the data presented in Chapter 4. The second assumption cannot be physically justified, but does not appear to produce unreasonable results.

Although caution should be exercised in drawing strong conclusions from the above analysis due to the scatter of the data, the following points are note-worthy.

1) The values of f required to achieve perfect correspondence between theory and data are higher than values expected for flow over a fixed bed. This supports the observation that the moving granular-fluid phase increases the bed roughness.

2) The exclusion of infiltration from the analysis did not lead to values of f that could not be accounted for by the expected sources of bed roughness. This is consistent with the numerical model results presented in Packwood (1983). However, it is expected that the effects of infiltration become important in some individual cases, particularly for the coarser grain sizes.

3) The effects of D and β on measurements of Z_s made in this and a previous study, that are not predicted at all by the inviscid theory, are now reproducible with (5.7).

Based on the analysis presented in the preceding Sections, uprush due to incident waves on a natural sandy beach can now be adequately predicted by calculating Θ' using (5.14) and taking $U_s \equiv \bar{U}_s = u_o/2$, calculating K_s using (5.19), calculating $h_\delta \equiv h_{s(max)}$ at the mid swash using (2.23), calculating f using (5.16), and substituting this calculated value of f into the desired equation in Section 5.2. This approach is very convenient, as the only initial measurements required are u_o, D, and β.

CHAPTER 6
IMPLICATIONS OF THE STUDY RESULTS FOR BEACH FACE PROFILES

6.1 Introduction

Field data presented in previous Chapters indicate that the non-linear shallow water theory can successfully describe several features of the swash cycle. It is now appropriate to consider the implications this theory holds for the study of beach face morphology. The development of a morphodynamic model which describes the creation of a seaward facing, equilibrium beach profile is the focus of this Chapter. Other swash created morphological features such as the berm and beach step can also be considered in the context of the study results (Section 7.2), however, they cannot be examined in detail until the underlying beach profile can be successfully modelled.

A beach profile slope is usually defined to be in equilibrium with the flow conditions when the net sediment transport everywhere on the profile is zero, thus the profile neither erodes or accretes (*e.g.* Bowen, 1980). This situation is generally unattainable in the coastal environment, as the time scales associated with morphological change are much longer than the time scales at which changes in flow conditions occur. Due to the irregular nature of incident wave heights, it is possible to observe successive swash cycles producing up-slope, down-slope, and zero net transport of sediment on a given profile without noticeably effecting its slope. A more realistic concept therefore, is a quasi-equilibrium beach slope; defined to be the slope at which zero net transport occurs when the sediment flux is averaged over several swash cycles. This definition requires that deviations from zero net transport for individual swash cycles must occur in both the onshore, and offshore direction so that a balance can eventually be achieved. The numerous data available that describe a relationship between beach slope, grain size, and wave conditions (*e.g.* Bascom, 1951; Wiegel, 1964; Sunamura, 1984) show that the quasi-equilibrium slope is not an elusive condition, but does indeed exist.

From a geomorphological perspective, the understanding of equilibrium beach slopes is important for two reasons. Firstly, such information is useful for predicting the magnitude of morphological change likely to occur due to a

large and sustained change in swash conditions. Secondly, the magnitude of the beach slope is believed to have some implicit significance to the beach profile's stability. The present understanding is that profiles which are steep relative to the wave steepness cause reflection and resonance of the incoming wave energy, thus enhancing the maximum swash height and potential for erosion (*e.g.* Wright, 1980; Bowen and Huntley, 1984).

The transport of sediment, and the creation of an equilibrium profile slope is achieved by the flow induced shear stress acting over a movable bed. A morphodynamic model that is able to predict the equilibrium slope of the profile should therefore contain two components: a description of the flow that includes the effect of shear stress, and a description of the sediment transport that includes beach slope. The non-linear shallow water theory can provide a suitable hydrodynamic description of the flow, as it now contains the necessary effects of shear stress (see Sections 5.2 and 5.4). Bagnold's (1963; 1966) model is chosen to provide a description of sediment transport, because it contains the necessary representation of beach slope.

The following Section presents the equations necessary for predicting water velocities and sediment transport in the swash zone. The combination of these equations represents the morphodynamic model. Since it is beyond the scope of this study to present original field data to test the component equations of the model (Section 1.2), they are compared with existing data to assess their suitability. Numerical results obtained from the model are contained in Section 6.3. These show that the model is presently unable to reproduce realistic profile slopes. Several explanations for this lack of success are discussed in Section 6.4.

6.2 The Morphodynamic Model

6.2.1 Equations for calculating sediment transport in the swash zone.

In order to keep the analysis as simple as possible only bedload transport is considered in the morphodynamic model. This is shown below to have no effect on the general conclusions drawn from the results.

Bagnold's (1963; 1966) model of bedload transport is based on the premiss that the rate of transport is proportional to the rate of energy dissipation in the shearing bedload layer. For the left-handed co-ordinate

system used throughout this thesis, the immersed weight sediment transport rate per unit width of flow, i_b, is given as

$$i_b = \frac{e_b \Omega}{\tan \Phi + \tan \beta} \qquad (6.1)$$

(Bagnold, 1963), where e_b is the bedload transport efficiency, Ω is the fluid power (*i.e.* $\Omega=\tau u$; Bagnold, 1966), and Φ is the internal friction angle of the sediment. For the problem at hand, (6.1) can be written more suitably as

$$i_b = \frac{0.125 e_b \rho f u_s^3}{\tan \Phi + \frac{u_s (\tan \beta)}{|u_s|}} \qquad (6.2),$$

where u_s is the water velocity within the swash lens. The form of the denominator in (6.2) is such that sediment is moved more easily down-slope with offshore flow ($u_s<0$), than up-slope with onshore flow ($u_s>0$). This is consistent with the down-slope effects of gravity on the sediment flux. The total immersed weight of sediment transported across the beach during one swash cycle, I_b, can be calculated from

$$\left.\begin{aligned} I_b &= \frac{0.125 e_b \rho f u_s^3 T_u}{\tan \Phi + \tan \beta} \qquad \text{for } u_s \geq 0 \\ I_b &= \frac{0.125 e_b \rho f u_s^3 T_d}{\tan \Phi - \tan \beta} \qquad \text{for } u_s < 0 \end{aligned}\right\} \qquad (6.3).$$

The parameters T_u and T_d are the duration times of onshore and offshore flows respectively.

Two assumptions are made in relation to (6.3) to simplify the analysis: transport occurs at all velocities so that there is no threshold for initiation of grain motion, and the parameters e_b and f are constant for the entire swash cycle. If these assumptions are satisfied, then (6.3) suggests that an onshore asymmetry of water velocity is required for zero net transport to occur. This asymmetry can be in the form of either a larger positive velocity, or a longer duration of positive velocity.

The simplest approach to determine the equilibrium beach slope for a given flow is to apply the condition of zero net transport, and solve (6.3) for

β. To proceed with this approach it is first necessary to provide a description of the water velocity in the swash.

6.2.2 Equations for calculating water velocities in the swash zone.

The behaviour of $u_s(t)$ is not explicitly available from the theory presented in Section 2.4.4, however, it can be obtained using the approximate method described below. This method is based on a manipulation of (2.19), which describes $h_s(x,t)$. It has previously been shown that (2.19), with (5.6) to calculate $X_s(t)$, provides a reasonably accurate description of $h_s(x,t)$ near the mid swash during the uprush (see Fig. 5.7d). However, its ability to describe the backwash is less than adequate. Not surprisingly therefore, the method described below is found to perform well in the uprush and poorly during the backwash.

In the following analysis the reference point for calculation of $u_s(t)$ is the mid swash. For a unit width of beach, the discharge of water passed the mid swash, Q_s, can be written as

$$Q_s = \frac{V_s}{t} = A_s u_s \qquad (6.4),$$

where V_s is the volume of water that has passed the mid swash, and A_s is the cross-sectional area of the flow. Since the swash flow is unsteady, all the parameters in (6.4) vary with time and thus preclude a simple solution for u_s. It is possible to obtain a simple, approximate solution however. It can be obtained by calculating the time-average value of each parameter for sequential time increments through the swash cycle. Upon re-arrangement of (6.4), the value of $u_s(t)$ averaged over a given time increment Δt can be calculated from

$$u_s(t) = \frac{\Delta V_s(t)}{A_s(t)\Delta t} \qquad (6.5),$$

where ΔV_s is the difference between V_s calculated at $t+0.5\Delta t$ and $t-0.5\Delta t$. All that is required now is some knowledge of $A_s(t)$ and $V_s(t)$.

Since only a unit width of beach is considered, $A_s \equiv h_s$, thus from (2.19);

$$A_s(t) = \frac{(X_s - x_m)^2}{(3t)^2} \qquad (6.6),$$

where x_m is the position of the mid swash relative to the initial shoreline. Also obtainable from (2.19) is the value of $V_s(t)$ between x_m and $X_s(t)$;

$$V_s(t) = \int_{x_m}^{X_s} \frac{(X_s-x)^2}{(3t)^2}\,dx = \left[\frac{(1/3)x^3+X_s{}^2x-X_sx^2}{(3t)^2}\right]_{x_m}^{X_s} \qquad (6.7).$$

Visually, (6.7) corresponds to the area bounded by x_m, $X_s(t)$, the $\eta_s(x)$ curve, and the bed surface (see Fig. 2.12f).

Now that A_s, V_s, and ΔV_s can be calculated, $u_s(t,x_m)$ can be obtained in the following manner. Calculations begin at the time the shoreline reaches the mid swash, which is when $t=t_m$. The value of $x_m=0.5L_s$ can be obtained from (B.15), and t_m can subsequently be obtained from (B.12). V_s is then calculated using (6.7) and (B.13) at times $t_m+0.5\Delta t$ and $t_m-0.5\Delta t$, thus providing ΔV_s. The value of A_s is then calculated from (6.6), and substituted into (6.5) with ΔV_s to yield $u_s(t)$. The process is then repeated for $t=t_m+\Delta t$, $t=t_m+2\Delta t$, and so on until the shoreline recedes beyond x_m. The accuracy of this method can be checked by calculating Q_s at each time step using (6.4), and adding it to the total present at the previous time step. For mass to be conserved, the value of this cumulative Q_s must be zero at the end of the swash cycle. The above method is found to provide a good estimate of $u_s(t)$ (*i.e.* the cumulative Q_s is zero), provided Δt is chosen small enough so that A_s does not change significantly between time steps. For the calculations made below, $\Delta t=0.05$.

An example of $u_s(t,x_m)$, $U_s(t)$, and the cumulative $Q_s(t,x_m)$ for one swash cycle is shown in Figure 6.1. The $U_s(t)$ curve was calculated using (5.5). The initial conditions are $u_o=4$, $\beta=0.07$, and $D=0.0005$. From (5.19) and (5.16) these yield $f=0.12$. The Figure shows that the cumulative Q_s increases when u_s is positive, decreases when u_s is negative, and equals zero once the shoreline has receded beyond the mid swash. Hence, mass is shown to be conserved throughout the calculation of $u_s(t)$. It is also evident from the Figure that upon arrival of the shoreline at the mid swash, the water velocity instantaneously accelerates to the value of the shoreline velocity, and then decreases to zero with a variable, but smooth deceleration. This contrasts markedly with the almost constant deceleration of the shoreline velocity. Interestingly, u_s is found to change sign before $U_s=0$. Physically, this

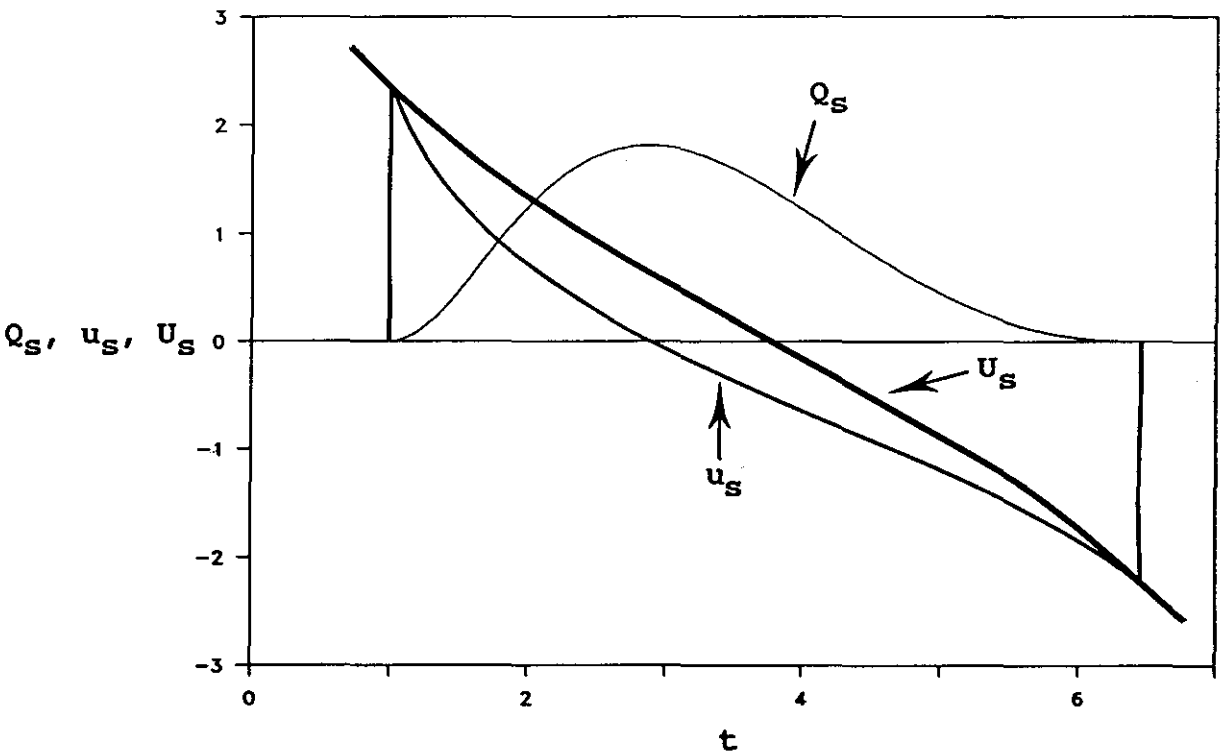

Figure 6.1: Predictions of the cumulative $Q_s(x_m,t)$, $u_s(x_m,t)$, and $U_s(t)$ for a swash cycle with initial conditions u_o=4, β=0.07, D=0.0005.

means that the water at the mid swash position begins flowing seaward when the shoreline is still climbing toward its point of maximum landward displacement. This theoretical behaviour is not unexpected, as it has also been observed in experimental measurements reported by Kemp (1975), and partly explains the tendency for the swash lens to thin rapidly in the latter stages of the uprush. During the backwash the water velocity increases to a maximum equal to the shoreline velocity, and drops to zero immediately after the shoreline recedes beyond the mid swash position.

Due to the experimental difficulties likely to be encountered in obtaining measurements of $u_s(t)$ (Section 3.3.2), very little data is available in the published literature. Some measurements selected from those available are reproduced in Figure 6.2 for comparison with the theoretical predictions. Only a qualitative comparison can be made here because the wave conditions at the initial shoreline are unknown. The theoretical behaviour of $u_s(t)$ during the uprush is observed to correspond well with the experimental data (*cf.* Fig. 6.1 and 6.2). As expected however, the theory performs poorly in the backwash. Despite this imbalance, it is still appropriate to apply the theory at its present level of development, to make explicit its limitations in the study of morphology.

6.3 Numerical Results

The cumulative $I_b(t)$ can be obtained from the model by replacing T_u and T_d with Δt in (6.3), and calculating I_b at each time step. Model predictions of $u_s(t)$ and $I_b(t)$ are shown in Figure 6.3 for the initial conditions u_o=4, β=0.14, D=0.0005, and e_b=0.12. The value of e_b was estimated from Figure 3 in Bagnold (1966). It is evident from comparing the cumulative $I_b(t)$ curve and $u_s(t)$ curve, that most of the onshore transport is predicted to occur in the early stages of the uprush, shortly after the arrival of the shoreline at the mid swash. The broad maxima in the cumulative $I_b(t)$ curve suggests that after this initial push of sediment, there is relatively little added for the remaining period of onshore flow. When the water velocity becomes negative the transport of sediment in the offshore direction begins, causing a downturn in the cumulative $I_b(t)$ curve. The rate of offshore transport starts slowly, but rapidly increases as the offshore velocity approaches its predicted maximum.

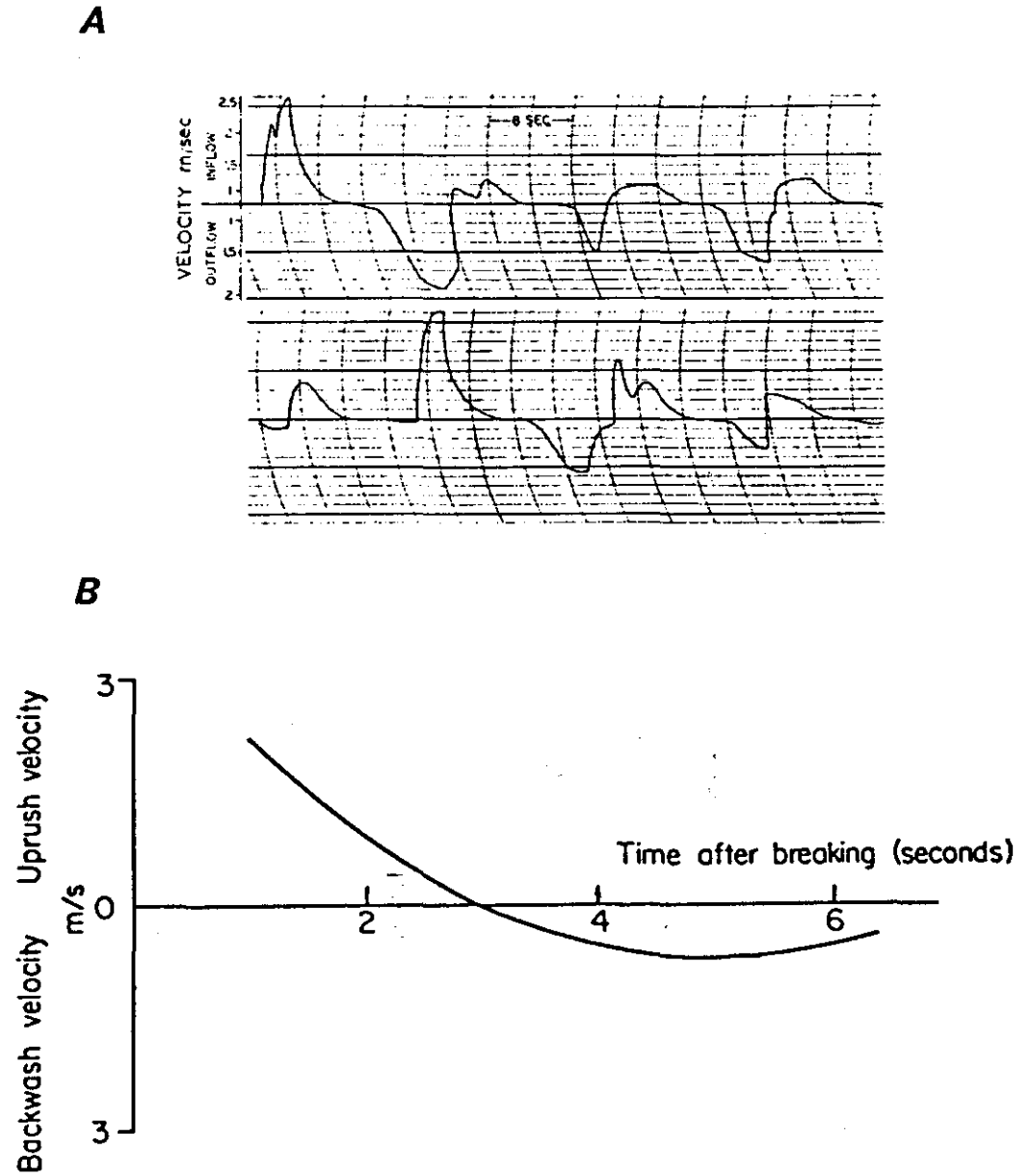

Figure 6.2: *(a)* Field measurements of $u_s(t)$ from Schiffman (1965). *(b)* Laboratory measurements of $u_s(t)$ from Kemp (1975).

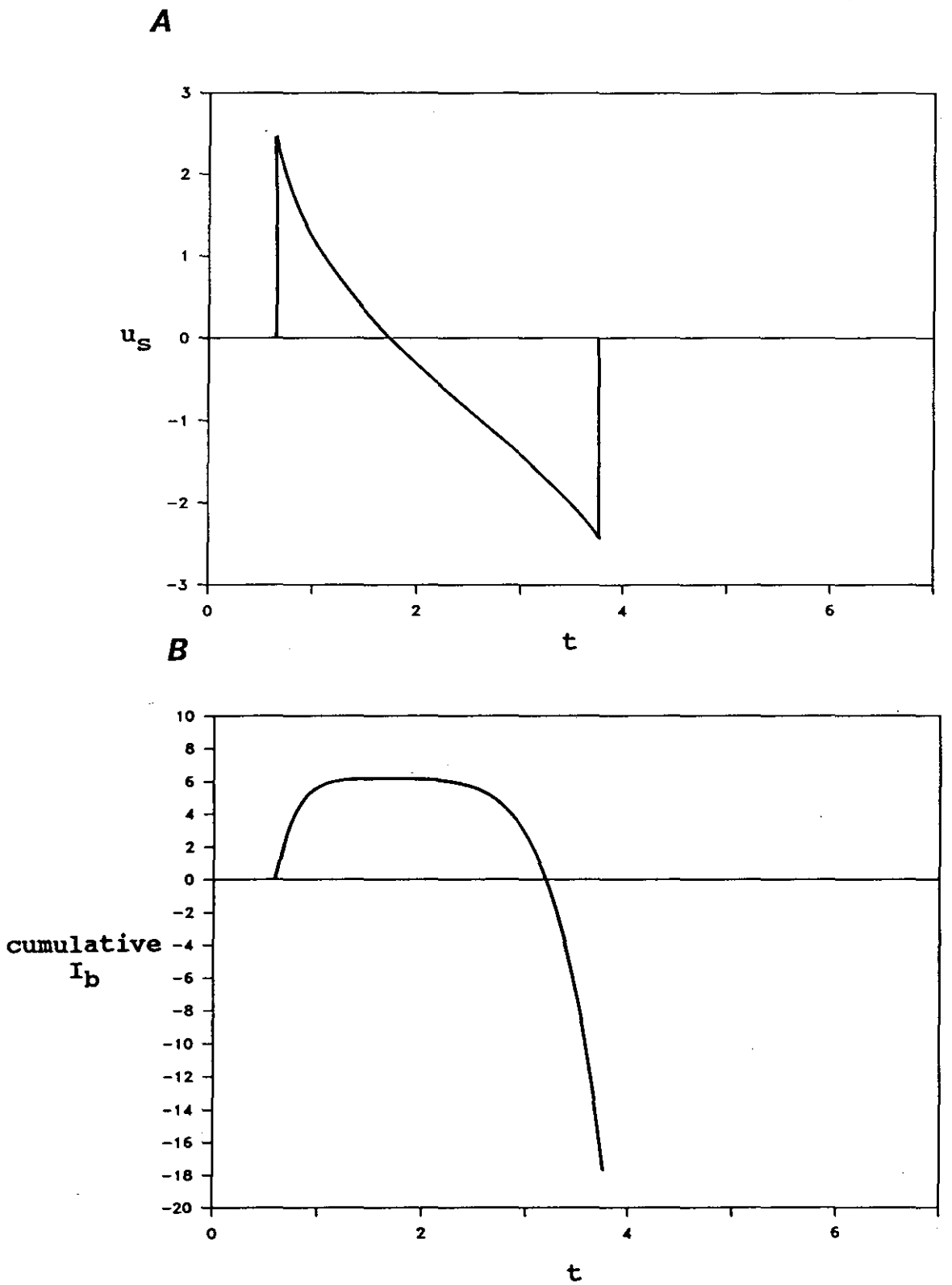

Figure 6.3: *(a)* Predicted $u_s(x_m,t)$ for a swash cycle with initial conditions u_o=4, β=0.14, D=0.0005. *(b)* Predictions of the cumulative $I_b(t)$ for a swash cycle with initial conditions u_o=4, β=0.14, D=0.0005.

To maintain a seaward facing beach slope, the morphodynamic model implies that an onshore asymmetry in velocity magnitude or duration must occur for most swash cycles (see (6.3)). Equivalently, the area under the $u_s(t)$ curve for $u_s>0$ must be larger than the area for $u_s<0$. It is apparent from Figure 6.3a that the velocity asymmetry for the given slope favours offshore flow. Not surprisingly therefore, the cumulative $I_b(t)$ curve becomes negative during the backwash, indicating more sediment is being moved offshore than was originally moved onshore.

The results obtained when the value of β is reduced to 0.07 are shown in Figure 6.4. Such a significant reduction in β apparently has no effect on the velocity asymmetry. The absolute magnitude of the positive and negative areas under the $u_s(t)$ curve change with β, but the relationship between the two areas on each slope are equivalent (*cf.* Fig. 6.3a and 6.4a). Therefore, the cumulative I_b at the end of the swash cycle is again negative. Calculation of the cumulative I_b for a number of cases showed that the pattern observed in Figure 6.3 and 6.4 remains unchanged for the full range of slopes typical of sandy beaches (*i.e.* $0.017<\beta<0.26$).

The only available field measurements of sediment transport during one swash cycle were made by Hardisty *et al.* (1984). They measured a dry sediment weight of 2.72 kg m^{-1} transported by an onshore flow with a velocity of 0.43 m s^{-1}. The corresponding immersed weight of the transported sediment is 1.63 kg m^{-1}. Since no indication of the experimental slope is given, or whether the velocity is the peak or average value it was not possible to attempt a theoretical prediction of their measurements. It is worth noting however, that the predicted I_b of 6.18 and 9.06 kg m^{-1} for peak onshore flows of 2.40 m s^{-1} seem quite reasonable when compared to this field data (Fig. 6.3 and 6.4). Particularly since the transport rate increases in proportion to the velocity cubed (see (6.2)). Based on this comparison, it is tentatively concluded that the approach presented here will provide a reasonable estimate of sediment transport during the uprush, but apparently substantially over-estimates transport during the backwash.

6.4 Discussion

In order to predict the quasi-equilibrium beach slope associated with a given flow condition, the morphodynamic model must be able to predict onshore, offshore, and zero net transport of sediment during one swash cycle

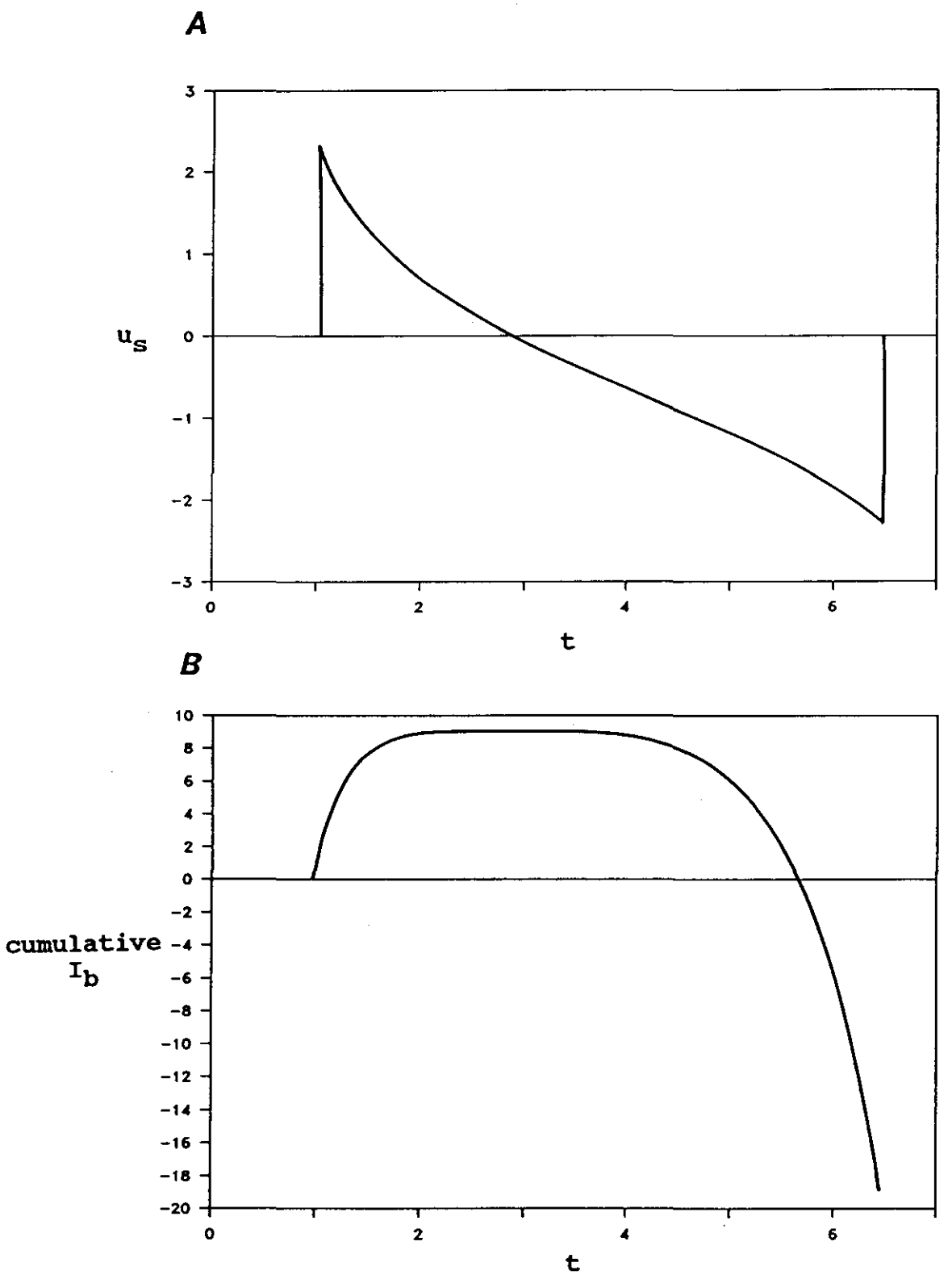

Figure 6.4: *(a)* Predicted $u_s(x_m,t)$ for a swash cycle with initial conditions u_o=4, β=0.07, D=0.0005. *(b)* Predictions of the cumulative $I_b(t)$ for a swash cycle with initial conditions u_o=4, β=0.07, D=0.0005.

(Section 6.1). The numerical results discussed in the previous Section indicate that the model is only capable of reproducing net offshore transport of sediment. This condition arises because the theory predicts that for all β, the peak magnitudes of positive and negative u_s are equal and T_u is less than T_d. The model is therefore unable to reproduce either an equilibrium beach slope, or a seaward facing beach slope.

Two hydrodynamic phenomena which occur during the swash cycle have not been included in the analysis: infiltration, and the backwash bore. Neither of these are understood sufficiently well to quantitatively incorporate into the model, however, their effect is expected to reduce the magnitude of offshore flow and sediment flux. The exclusion of these phenomena is therefore hypothesized to be the principal factor in the model's inability to reproduce natural beach slopes.

The data discussed in Section 5.4 offers support for Packwood's (1983) hypothesis that the effect of infiltration on the uprush is negligible, and probably explains why the morphodynamic model was able to predict reasonable estimates of the total weight of bedload transported during the uprush. It is worth remembering however, that Packwood's analysis showed the effects of infiltration becoming increasingly important during the backwash. The duration of offshore flow was found to be markedly reduced on a permeable beach, because much of the thin landward end of the swash lens is completely lost through infiltration (*ibid.*).

In the context of the morphodynamic model, a desired effect of infiltration is that the reduction in flow duration should increase with slope. This would enable the consistently predicted offshore transport of sediment to be counteracted. The well established, positive relationship between beach slope and grain diameter (see Bascom, 1951; Sunamura 1984) suggests how such an effect might be achieved. It is envisaged that a negative feedback mechanism exists where increases in beach slope and grain size, and the concomitant increase in porosity will enhance the effects of infiltration; thus reduce the rate of offshore transport. It is therefore hypothesized, that infiltration plays a principle role in determining the slope of a beach face profile.

The effect of a bore in the backwash is to increase the water depths over those predicted by (2.19). This results in an increase in the cross-

sectional area of the flow, and thus a decrease in the water velocity (see (6.5)). Hibberd and Peregrine (1979) used a finite-difference model to solve the SWE, and provide a numerical description of swash following bore collapse on a beach. Their results contain the presence of a backwash bore, and can therefore be used to demonstrate its effect on the water velocity and sediment flux. Figure 6.5 shows $\eta_s(x,t)$ and $u_s(x,t)$ at two positions in the backwash. These were obtained from the contours of η_s and u_s shown in Hibberd and Peregrine's Figures 8 and 10. The formation of the backwash bore and its effect on the cross-sectional area of the flow is clearly evident in Figure 6.5a. The $u_s(t)$ curve for the position on the upper beach, in the region where the bore's influence is absent, is very similar to the results obtained using the approximate method described in Section 6.2.3. However, for the position on the beach where the bore is influential, the value of u_s is reduced for much of the backwash. This results in a desirable, positive asymmetry in the magnitude of u_s.

Since a relatively large onshore asymmetry is necessary to achieve a steep slope, it is inferred that the size of the backwash bore will be positively related to slope if it is to have the desired effect. Of all the bore-like waves observed in the backwash during this study (see Section 4.6), the largest were the surface shear waves similar to those shown in Fig. 4.37. In contrast to the above inference, surface shear waves were restricted to the milder slopes. On the steeper slopes the bore-like waves in the backwash were smaller and more transient. This apparent anomaly to the relationship expected serves to emphasize the importance of infiltration during the backwash; Packwood's (1983) numerical results showed that a permeable beach reduced the size of the backwash bore over that predicted for an impermeable beach. It therefore seems probable, that infiltration will act as the principle mechanism for reducing the offshore sediment flux on steep slopes where the grain size and porosity is large. On smaller slopes where the porosity may be small, the backwash bore probably provides the principle mechanism.

There are assumptions made in the application of the model which may contribute to its poor performance, but they are considered of secondary importance in comparison to the effects of infiltration and the backwash bore. The assumption that no interaction occurs between successive swash cycles underpins both the hydrodynamic, and sediment transport models. If a second uprush occurred before a preceding backwash was complete, then it is likely

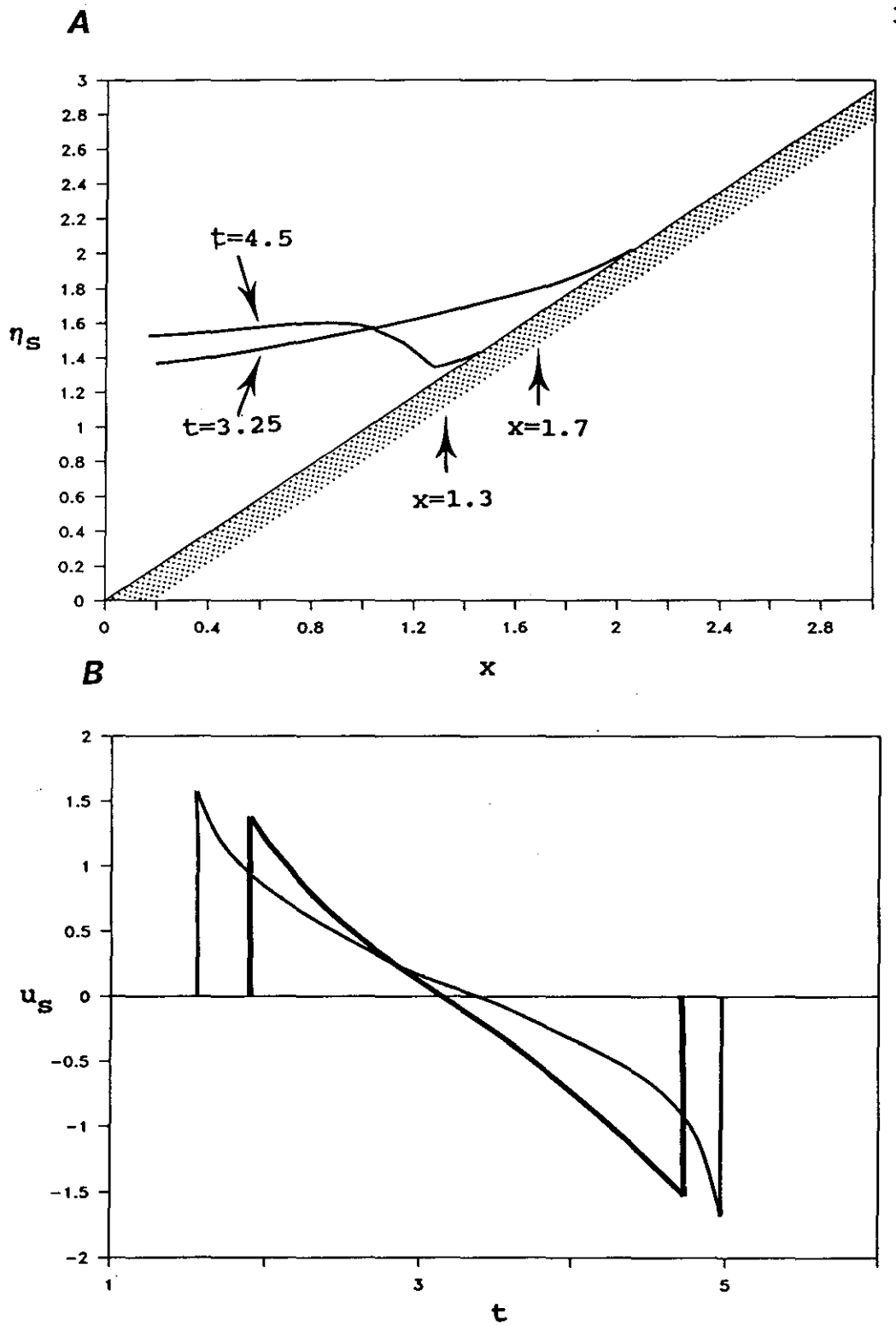

Figure 6.5: (a) Numerical model results of $\eta_s(x,t)$, measured from Figure 8 in Hibberd and Peregrine (1979). Arrows indicate the positions in the swash where the $u_s(t)$ curves shown in *(b)* were obtained. *(b)* Numerical model results of $u_s(t)$ measured from Figure 10 in Hibberd and Peregrine (1979). The bold line indicates results for x=1.7 and the fine line indicates results for x=1.3.

that a flow asymmetry that favours onshore transport would result. At its present level of development the hydrodynamic model cannot describe this type of interaction, and may provide an explanation for the inability of the model to reproduce natural beach profiles. However, this cannot be a complete explanation, since seaward facing slopes are sustained in swell wave environments where swash interaction is minimal.

It is expected that the direction of suspended sediment flux in the swash zone is always in the direction of the flow, since there are no bedforms of sufficient dimension to create the type of disequilibrium between flow and transport direction frequently observed in oscillatory flow over wave ripples (see Nielsen, 1988a for review). Thus, an onshore asymmetry of flow is also required to produce beach slopes in the presence of a suspended sediment load. For this reason, the exclusion of suspended load from the analysis will not effect the general conclusions drawn from the results above.

The assumption that transport occurs at all velocities probably underestimates the degree of imbalance in the sediment flux predicted in Figures 6.3b and 6.4b. For the range of slopes typical of sandy beaches, laboratory experiments conducted by Whitehouse and Hardisty (1988) show that the critical threshold for motion can be almost a factor two larger for up-slope flow, compared to flow down-slope. It follows, that if critical thresholds for motion are included in the analysis, then the duration of offshore transport will increase, thus enhancing the imbalance of transport.

The effect of assuming that e_b and f are constant throughout the swash cycle is not obvious. In reality it must be expected that they will both be largest during the backwash, since the rapidly decreasing depth increases the bed shear stress. Bagnold (1966) predicts that if the depth of flow decreases to the point where the bedload phase occupies the entire flow depth, which frequently occurs during the backwash (see Fig. 4.36), e_b could increase threefold, thus enhancing the offshore transport of sediment. However, some negative feedback to oppose this effect should exist, since the larger shear stress will tend to decrease the flow velocity. The combined effect of these two processes on the offshore transport of sediment is obviously complex, and not yet understood.

The assumptions discussed above will all need to be addressed at some stage, however, it is apparent from the model results that a more realistic description of velocities in the backwash is needed first. The inability of the shallow water theory to describe velocities in the backwash should not be seen as a failure. It is obvious even in a visual sense, that the backwash is a complex phenomena which must be studied with a sound understanding of the physics of highly concentrated, granular-fluid flows. A satisfactory description of water velocities in the backwash will probably never be achieved without such an integrated approach.

6.5 Summary

The morphodynamic model described above is presently unable to reproduce typically occurring beach profiles. However, the analysis has elucidated several salient processes that need to be included in the model before its further application to such morphological problems can be attempted. As expected, the inability to describe water velocities in the backwash proved fundamental to the lack of success in predicting natural beach slopes. Before progress can be made in this area, several features of the backwash require further understanding: the behaviour of $h_s(t)$ so that $u_s(t)$ can be approximated more accurately, and the effect of infiltration and a backwash bore on $u_s(t)$. It is already apparent from interpretation of the model results, that infiltration and a backwash bore will reduce the duration and magnitude of the offshore flow respectively. However, an understanding of the relationship between infiltration, the backwash bore, and beach slope still needs to be established. Further study into these hydrodynamic phenomena should also provide more insight into the nature of e_b and f in the backwash, and must therefore be considered a major research priority before beach face profiles can be successfully modelled (Section 7.2).

CHAPTER 7
SUMMARY AND CONCLUSIONS

7.1 Introduction

The purpose of this Chapter is to summarize the major points of discussion contained in previous Chapters, and to present the conclusions of the study. More specifically, the following Section demonstrates the scope and limitations of the study results, and highlights the processes requiring further research. Section 7.3 assesses the potential for applying the shallow water theory to problems beyond those specifically addressed here.

7.2 Discussion Of The Study Results

7.2.1 Comparison between the inviscid theory and field data.

This thesis has applied the non-linear shallow water theory to the study of swash related processes and morphology. The results of the study are specific to beaches where incident swash processes are dominant (Fig. 2.3), and where these processes satisfy certain criteria permitting the application of the theory (Sections 2.4.4 and 2.5.2).

The assumption that underpins the theory and analysis presented in previous Chapters is that no interaction occurs between successive swash cycles. The nature of the wave climate and the configuration of the coast line in the study region enabled the collection of data which satisfied this assumption. It is stressed that these data can only be considered directly representative of swash processes associated with swell waves arriving normal to the shoreline. On beaches where the wave period is highly irregular, or less than the swash period interaction between successive swash cycles becomes increasingly important.

A recent analysis of swash spectra by Mase (1988) contains some interesting insight into swash interaction, which is relevant to this study. Mase calculated the spectra of variations in shoreline position from a numerically simulated time series. The time series was constructed using a succession of truncated parabolas which corresponds to the pattern of shoreline displacement demonstrated in this study (*e.g* Section 4.2.3). Interestingly, the form of the calculated spectra matches well with the form measured in previous field

experiments (*e.g.* Huntley *et al.*, 1977). This seems to suggest, that despite the occasionally chaotic appearance of swash interaction, the processes studied here are of relevance even in the presence of highly irregular waves.

Two types of swash interaction are often observed when the wave period becomes less than the swash period. The first involves bores overrunning the swash lens during the uprush phase, and the second involves the collision between incoming bores and the backwash. It seems reasonable to expect from theoretical considerations, that once a bore crosses the leading edge of the swash lens it will experience bore collapse as it otherwise would at the initial shoreline. It is not clear however, what effect the moving swash lens will have on the initial velocity of the new shoreline. The whole problem of bore collapse at either a stationary or a moving shoreline requires further experimental study, since details of this phenomena are not explicitly available from the theory. The results reported here indicate that although energy dissipation in the bottom boundary layer of the bore can be ignored far from shore (see Svendsen, 1987), this source of dissipation becomes increasingly important near the shoreline (Section 4.2.2), and must be considered in any study of bore collapse.

The collision between the bore and the backwash frequently produces a hydraulic jump near the initial shoreline. Methods for calculating energy dissipation in the hydraulic jump can be found in most standard texts on fluid mechanics (*e.g.* Streeter and Wylie, 1981). Their application to a hydraulic jump containing large concentrations of suspended sediment still needs to be established however.

The general conclusion to be drawn from observations of wave action across the initial shoreline (Sections 4.2.2, 4.3.2, and 4.4.2), is that no existing theory is presently capable of modelling how energy is transferred from surf zone wave to swash. The data collected here show that wave height is not the only consideration. The relationship between wave height and shoreline velocity was found to also depend on the initial wave type (Sections 4.2.2, 4.3.2, and 4.4.2). In particular, a surging wave of given height was observed to be more efficient in transferring energy to the swash, than a similar breaking wave (*cf.* Fig. 4.6, 4.16, and 4.26). This is probably due to the energy dissipation associated with free-surface turbulence, present in bore collapse and wave plunge, but absent in surging waves.

Despite the uncertainties relating to wave behaviour at the initial shoreline, flow conditions in the swash zone are more completely described by the theory. There are two solution sets originating from the SWE, which are available for the study of swash. The first is generally applied to problems including wave breaking and relies on bore theory to describe the breaker's propagation. The second is applied to the study of non-breaking waves and is bore-free. These two approaches predict very different behavioural patterns for the swash lens.

The swash lens following bore collapse on a smooth and impermeable beach is predicted to behave as a rarefaction wave. This implies that the leading 'fluid element' of the lens is never passed by elements from behind, and enables the shoreline motion to be modelled through consideration of the leading element alone (Section 2.4.4). Most of the theoretical predictions for bore uprush were observed in the field data. Specifically, the following theoretical relationships were confirmed:

1) locus of shoreline displacement through time is parabolic,

2) maximum swash height as a function of initial shoreline velocity is quadratic,

3) mean shoreline velocity as a function of initial shoreline velocity is linear, and

4) maximum swash depth as a function of distance is quadratic.

All of these relationships are associated with the uprush phase of the swash cycle. Shoreline displacement during the backwash could not be accurately determined from the field techniques. A tendency for the decreasing swash depth near the shoreline to become increasingly loaded with sediment leads to uncertainty in distinguishing between the surface of the water and the beach (Fig. 4.36). Measurements of the water surface at other positions in the swash lens showed however, that the theory is unable to predict the dimensions of the backwash.

It was not possible to compare the bore-free solutions of the theory with the data presented here, as the waves measured did not satisfy the theoretical, non-breaking criterion. The opportunity for non-breaking waves to exist under conditions not described by the theory, had already been demonstrated by the laboratory results presented in Guza and Bowen (1976). In the experiments reported here, the presence of a sloping nearshore profile and a beach step

meant that the zone of theoretical breaking was narrow; significantly less than one wave length. The hydrodynamic hysterisis inherent in natural waves (Van Dorn and Pazan, 1975) enabled the experimental waves to propagate through these critical changes in depth and begin climbing the beach before overturning (Section 4.4.2).

Some features of the surging waves observed in the experiments were reminiscent of bore collapse. Particularly the tendency for the wave to become halted over the step, and the way in which it steepened before 'collapsing' and climbing the beach (Section 4.4.2). This observation prompted the hypothesis that the surging waves measured here contain a virtual bore. Comparison of the regression models for the data available showed that there was no statistical difference between the measurements of swash following bores and surging waves. On this basis, a new exposition of the theory's application to swash was proposed (Section 4.5).

A continuum of swash type seems to exist, where the bore and bore-free solutions of the SWE equations describe the end-members. Waves at the shoreline that are neither fully developed, hydrostatic bores or surging waves which satisfy $\epsilon \leq 1$, may produce a swash lens displaying features of both these end-members. The surging waves measured here happened to behave mostly like a rarefaction wave, as predicted for bore uprush (Fig. 2.12). They certainly did not display the predicted behaviour for non-breaking solitary wave uprush (Fig. 2.16). These observations are not meant to infer that waves do not exist on natural beaches at the bore-free end of the continuum, however, they do imply that the solutions for swash following bore collapse may describe most of the incident swash occurring on natural beaches.

The only restriction that seems to exist with applying the theoretical predictions for swash following bore collapse to other initial wave types, is that the proportion of the swash flow described by the theory is reduced towards the non-breaking wave end of the continuum. This may be due to the fact that any virtual bore which may exist in the wave is larger in width towards this end of the continuum (Section 4.5). Consider for example, the width of the bore region of a fully developed bore and a minor bore (Fig. 2.6). The bore region is not explicitly described by the theory, thus the proportion of swash not described is apparently inversely proportional to the bore strength.

7.2.2 Interaction of swash with the beach.

All of the regression models describing the data measured in this study were statistically significant at the 1 % level, and all were of a similar form to those expected from theory. However, the theory was found to consistently over-predict the magnitude of the data (Section 4.7). This study assumed that the total magnitude of over-prediction is due to factors relating to a natural bed, which are not described in the theory (Section 1.4). The factors considered are frictional dissipation due to bed shear, and the loss of momentum due to water infiltrating into the beach.

A set of equations for uprush on a natural beach were derived by including a shear stress term into the existing equation of motion for the shoreline (Section 5.2). The validity of this approach requires that the bed shear stress has only a passive effect on the gross flow characteristics, and that the rarefaction wave model of the swash provides a good description for natural beaches. The results presented in Chapter 4 suggest that this is a reasonable approach for the uprush, but probably not valid in the backwash, where the flow and the bed become indiscriminate (Section 4.2.3; Fig. 4.36).

Infiltration is also expected to contribute to the flow resistance, but in a different manner to the energy dissipation accounted for in the shear stress term. The loss of fluid into the beach is expected to alter the dimensions of the leading edge, in addition to reducing the over all swash length. The field techniques applied in this study could not be used to calculate absolute losses from the swash volume due to infiltration (Section 5.3.4). It is conceivable that (6.3) could be used to calculate the uprush and backwash discharge, which would provide the total loss over a single swash cycle. However, this would require accurate measurements of the water velocity which are difficult to obtain in the field (Section 3.3.2).

In comparing the predictions for uprush on a natural beach with the field data available, the apparent value of the friction factor was found to be larger than that expected from the empirically based, fixed bed models. It is not clear whether this is due entirely to the larger friction possible over a movable bed, or whether infiltration is more important.

A model for frictional dissipation in the presence of sheet flow was found to be suitable for predicting the apparent f required to match theory

with data. It still remains to be established whether the model contains all the necessary elements for describing the bed friction on a sandy beach, as it is implied that variations in grain size are not important (Section 5.3.3). This may be physically reasonable for sheet flow, where the entire bed down to a depth of several grain diameters is mobile, and the equivalent roughness length of the moving bed is much larger than the length associated with skin friction (Section 5.3). Given the scatter of the data however, some caution is necessary in applying the method. It is expected that as sediment diameter becomes larger than sand, skin friction effects will become more obvious, thus requiring a method for estimating f which depends on grain size. Moreover, flows that do not satisfy the sheet flow criterion for most of the uprush may also be found to more strongly reflect the importance of skin friction. With due regard to this cautionary note it can be concluded that the equations for swash presented in Section 5.2, combined with (5.16) and (5.19) to estimate f, provide a description of the shoreline behaviour on sandy beaches suitably accurate for most purposes.

Interestingly, if the sheet flow model for predicting the bed friction is established through further study, then the mechanism proposed by Komar and Wang (1984) for creating heavy mineral placers on beaches may need to be re-assessed. It is difficult to accept their hypothesis that the degree of grain protrusion into the flow is an important mechanism for entrainment, if a granular-fluid phase several grain diameters thick is moving along the bed.

Although a reasonable match between the measured and predicted behaviour of the shoreline was achieved using a friction factor to account for the total flow resistance, the possible importance of infiltration cannot be ignored. It was assumed on the basis of a numerical model developed by Packwood (1983), that infiltration had a negligible effect on the uprush. This assumption did not lead to unrealistic results for the friction factor. However, it still remains to be demonstrated that this is not fortuitous. The presence of the water table outcropping at the beach face provides one explanation, although, there are times during a tidal cycle when the water table lies well below the sand surface (Duncan, 1964). Some infiltration effects on the swash lens must be expected at these times. It is still possible however, that these effects remain second in importance to bed shear on sandy beaches. In contrast to the uprush phase, Packwood's model predicts that infiltration significantly

alters the flow behaviour in the backwash. The inferred importance of this result is discussed below.

A model was presented in Chapter 6, which was used to examine the morphodynamic behaviour of the beach slope. The model combined an approximate theory for water velocities in the swash with Bagnold's sediment transport equations. The analysis assumed that for a beach slope to be in equilibrium with the wave conditions, the net sediment flux averaged over several swash cycles has to be zero. In the presence of irregular waves, this requires that the model must be able to predict net transport in both onshore and offshore directions. The model was unable to achieve this, and was found to consistently predict disproportionately large transport in the offshore direction. This result arose from two intractable predictions relating to the water velocity: the peak magnitudes of onshore and offshore velocities are always equal, and the offshore flow duration is always the largest. Two features not considered in the model are infiltration and the backwash bore, which are inferred to have a significant effect on the water velocity and sediment flux in the backwash. Infiltration is expected to reduce the backwash duration. The backwash bore is expected to reduce the water velocity (Section 6.4).

The model results imply that a negative feedback mechanism may be responsible for the observed relationship between grain size and beach slope (Section 6.4). For a beach slope to steepen, it is required that the offshore flux of sediment be reduced. It is expected that the concomitant increase in porosity with grain size, means that infiltration will reduce the backwash flow on steeper beaches where the grain diameters are largest. Before the morphodynamic model presented in Chapter 5 can be expected to produce reasonable results the relationship between grain size, beach slope, infiltration and the backwash bore need to be the subject of more quantitative research. At this stage, the observations reported here suggest that infiltration and the backwash bore will be most important on steep and mild slopes respectively.

7.2.3 Geographic variability of swash.

This study has concentrated on one aspect of wave motion across the beach face. A complete approach for studying the geographical variability of swash zone morphology was beyond the scope of investigation. However, the framework used in this study does suggest a possible approach to the problem.

Given that the gross flow characteristics of incident swash appear to be independent of *Beach Type* (Section 4.5), an alternative explanation for the variability in beach face morphology relates to the relative importance of incident versus infragravity swash. Due to the nature of infragravity waves, specifically their large wave length relative to the scale of the beach morphology, they are expected to be almost universally reflected on natural beaches (Bowen and Huntley, 1984). Moreover, it is expected that $\epsilon<1$ will generally be satisfied.

The solutions for swash following bore collapse seem to describe all incident swash where $\epsilon>1$ (Chapter 5). If it can be demonstrated that the bore-free solutions of the SWE describe the behaviour of infragravity swash, then ϵ may be an important parameter for distinguishing between beach face morphology. An approach to quantifying the geographic distribution of swash might rely on the calculation of a frequency dependant ϵ from time series records of shoreline displacement. The specific nature of the swash zone could then be classified according to the relative proportions of energy existing for ϵ values smaller and larger than one. Along-shore variations in beach face morphology in phase with the surf zone morphology suggest possible gradients in the ϵ parameter, and differences in the relative importance of incident versus infragravity swash in the along-shore direction. The use of ϵ to quantify the geographic variability of surf zone morphologies by Wright and Short (1984) suggests some promise exists for such an approach.

7.3 Some Concluding Remarks

At their present level of development in the literature, the non-linear shallow water equations are theoretically capable of describing most incident swash on a smooth and impermeable beach. Methods for including friction and infiltration into the theoretical analysis exist, but have not until now been tested using field data. This study has applied the available theory to the study of incident swash on natural beaches. This exercise has demonstrated several important limitations of the theory. Some can be conceivably overcome with further experimental confirmation, and others may be impossible to investigate within the general framework of the theory. This leads to some final points worth considering, before further work is pursued using the approach developed in this study.

The effects of friction and infiltration on the swash have been demonstrated to be significant on the sandy beaches considered here. However, their relative importance is still unknown. A method used in this study for including frictional dissipation of energy into the theoretical framework seems to produce reasonable results. In addition, a numerical method based on the SWE is available to incorporate infiltration into the framework (Packwood, 1983). However, this is yet to be tested against field data. If the method is found to be satisfactory, then the non-linear shallow water theory is apparently capable of predicting the complete behaviour of swash on a natural beach, provided that no swash collisions occur.

Where swash collisions are important, Meyer and Taylor (1972) suggest that no new physics are introduced to the problem. However, the successful modelling of consecutive swash cycles which are interfering with incoming waves would require a sound understanding of the relationship between waves seaward of the initial shoreline and the parameter u_o. The observations reported in this study suggest that this process is exceedingly complex, and occurs over a range of spatial scales depending on the initial wave type. The shallow water theory does not provide the opportunity to study this transition zone between surf zone waves and swash.

Further laboratory experiments along the lines of those reported in Yeh and Ghazali (1986; 1988) may provide satisfactory empirical relationships between wave parameters and u_o. Given that such an empirical approach is required however, it may be equally instructive to simply determine stochastic relationships between wave height seaward of the initial shoreline and swash height. Such relationships would at the very least provide probabilities of the maximum swash height in the presence of irregular waves. Although this study has demonstrated that many swash related problems can be approached using the non-linear shallow water theory, it appears that a complete description of offshore waves and swash are beyond the scope of any one theory.

REFERENCES

AAGAARD, T., and Holm, J., (in press). Digitization of wave run-up using video records. *Journal of Coastal Research.*

AMEIN, M., 1966. A method for determining the behaviour of long waves climbing a sloping beach. *Journal of Geophysical Research*, 71: 401-410.

BAGNOLD, R.A., 1940. Beach formation by waves: Some model experiments in a wave tank. *Institute of Civil Engineers Journal*, Paper No. 5237: 27-49.

BAGNOLD, R.A., 1963. Mechanics of marine sedimentation. In: M. N. Hill (Editor), *The Sea, Volume 3*, Wiley-Interscience: 507-528.

BAGNOLD, R.A., 1966. An approach to the sediment transport problem from general physics. *Geological Survey Professional Paper 422-I*, 37 pp.

BASCOM, W.N., 1951. The relationship between sand size and beach face slope. *Transactions of the American Geophysical Union*, 32: 866-874.

BATTJES, J.A., 1974. Surf similarity. *Proceedings 14th Coastal Engineering Conference*, A.S.C.E.: 466-480.

BATTJES, J.A. and Janssen, J.P.F.M., 1978. Energy loss and set-up due to breaking of random waves. *Proceedings 16th Coastal Engineering Conference*, A.S.C.E.: 569-587.

BATTJES, J.A. and Stive, M.J.F., 1985. Calibration and verification of a dissipation model for random breaking waves. *Journal of Geophysical Research*, 90: 9159-9167.

BAUER, B.O., and Greenwood, B., 1988. Surf-zone Similarity. *The Geographical Review*, 78: 137-147.

BOWEN, A.J., 1980. Simple models of nearshore sedimentation: beach profiles and longshore bars. In: S.B. McCann (Editor), *Geological Survey of Canada, Paper 80-10*: 1-11.

BOWEN, A.J. and Huntley, D.A., 1984. Waves, long waves and nearshore morphology. In: B. Greenwood and R.A. Davis (Editors), Hydrodynamics and sedimentation in wave-dominated coastal environments. *Marine Geology*, 60: 1-13.

BRADSHAW, M.P., 1980. Topographic control of run-up variability. *Proceedings 17th Coastal Engineering Conference*, A.S.C.E.: 1091-1105.

BRADSHAW, M.P., 1982. *Bores and swash on natural beaches.* Coastal Studies Unit Technical Report No. 82/4, University of Sydney: 107 pp.

BROOME, R. and Komar, P.D., 1979. Undular hydraulic jumps and the formation of backwash ripples on beaches. *Sedimentology*, 26: 543-559.

CARRIER, G.F. and Greenspan, H.P., 1958. Water waves of a finite amplitude on a sloping beach. *Journal of Fluid Mechanics*, 4: 97-109.

COWELL, P.J., 1982. *Breaker stages and surf structure on beaches.* Coastal Studies Unit Technical Report No. 82/7, University of Sydney.

DALLY, W.R., Dean, R.G. and Dalrymple, R.A., 1985. Wave height variation across beaches of arbitrary profile. *Journal of Geophysical Research*, 90: 11917-11927.

DAVIES, J.L., 1980. *Geographical variation in coastal development.* Second Edition, Longman: 212 pp.

DEAN, R.G., 1977. *Equilibrium beach profiles: US Atlantic and Gulf Coasts.* Ocean Engineering Technical Report No. 12, University of Delaware: 45 pp.

DUNCAN, R.J., 1964. The effects of water table and tide cycle on swash backwash sediment distribution and beach profile development. *Marine Geology*, 2: 186-197.

EBERSOLE, B.A., 1987. Measurements and prediction of wave height decay in the surf zone. In: R.A. Dalrymple (Editor), *Coastal Hydrodynamics*, A.S.C.E.: 1-16.

FOX, W.T., Ladd, J.W. and Martin, M.K., 1966. A profile of four moment measures perpendicular to a shoreline, South Haven, Michigan. *Journal of Sedimentary Petrology*, 36: 1126-1130.

FREEMAN, J.C. and LeMehaute, B., 1964. Wave breakers on a beach and surges on a dry Bed. *Journal of the Hydraulics Division*, A.S.C.E., HY2: 187-216.

GALLAGHER, B., 1971. Generation of surf beat by non-linear wave interactions. *Journal of Fluid Mechanics*, 49: 1-20.

GALVIN, C.J., 1972. Wave Breaking in Shallow Water. In: R.E. Meyer (Editor), *Waves on beaches and resulting sediment transport.* Academic Press: 413-456.

GJEVIK, B. and Pedersen, G., 1981. *Run-up of long waves on an inclined plane.* Preprint series number 2, Department of Mathematics, University of Oslo, 27 pp.

GOPALAKRISHNAN, T.C. and Tung, C.C., 1980. Run-up of non-breaking waves - a finite-element approach. *Coastal Engineering*, 4: 3-22.

GRANT, W.D. and Madsen, O.S., 1982. Movable bed roughness in unsteady oscillatory flow. *Journal of Geophysical Research*, 87: 469-481.

GREENSPAN, H.P., 1958. On the breaking of water waves of finite amplitude on a sloping beach. *Journal of Fluid Mechanics*, 4: 330-334.

GUST, G. and Southard, J.B., 1983. Effects of weak bed load on the Universal Law Of The Wall. *Journal of Geophysical Research*, 88: 5939-5952.

GUZA, R.T., and Davis, R.E., 1974. Excitation of edge waves by waves incident on a beach. *Journal of Geophysical Research*, 79: 1285-1291.

GUZA, R.T. and Inman, D.L., 1975. Edge waves and beach cusps. *Journal of Geophysical Research*, 80: 2997-3012.

GUZA, R.T. and Bowen, A.J., 1976. Resonant interactions from waves breaking on a beach. *Proceedings 15th Coastal Engineering Conference*, A.S.C.E.: 560-579.

GUZA, R.T. and Thornton, E.B., 1981. Wave set-up on a natural beach. *Journal of Geophysical Research*, 86: 4133-4137.

GUZA, R.T. and Thornton, E.B., 1982. Swash oscillations on a natural beach. *Journal of Geophysical Research*, 87: 483-491.

HANES, D.M., 1984. Flow resistance due to intense bedload transport. *Proceedings 19th Coastal Engineering Conference*, A.S.C.E.: 1306-1310.

HANES, D.M. and Bowen, A.J., 1985. A granular-fluid model for steady intense bed-load transport. *Journal of Geophysical Research*, 90: 9149-9158.

HANES, D.M. and Inman, D.L., 1985. Observations of rapidly flowing granular-fluid materials. *Journal of Fluid Mechanics*, 150: 357-380.

HANES, D.M., Vincent, C.E., Huntley, D.A. and Clarke, T.L., 1988. Acoustic measurements of suspended sand concentration in the C^2S^2 experiment at Stanhope Lane, Prince Edward Island. *Marine Geology*, 81: 185-196.

HARDISTY, J., Collier, J., and Hamilton, D., 1984. A calibration of the Bagnold beach equation. Marine Geology, 61: 95-101.

HEDGES, T.S. and Kirkgoz, M.S., 1981. An experimental study of the transformation zone of plunging breakers. *Coastal Engineering* 4: 319-333.

HIBBERD, S. and Peregrine, D.H., 1979. Surf and run-up on a beach: a uniform bore. *Journal of Fluid Mechanics*, 95: 323-345.

HO, D.V. and Meyer, R.E., 1962. Climb of a bore on a beach: Part one uniform beach slope. *Journal of Fluid Mechanics*, 14: 305-318.

HO, D.V., Meyer, R.E. and Shen, M.C., 1963. Long surf. *Journal of Marine Research*, 21: 219-230.

HOLMAN, R.A., 1981. Infragravity energy in the surf zone. *Journal of Geophysical Research*, 86: 6442-6450.

HOLMAN, R.A., 1986. Extreme value statistics for wave run-up on a natural beach. *Coastal Engineering*, 9: 527-544.

HOLMAN, R.A. and Bowen, A.J., 1984. Long-shore structure of infragravity wave motions. *Journal of Geophysical Research*, 89: 6446-6452.

HOLMAN, R.A. and Sallenger, A.H., 1985. Set-up and swash on a natural beach. *Journal of Geophysical Research*, 90: 945-953.

HOLMAN, R.A., Huntley, D.A. and Bowen, A.J., 1978. Infragravity waves in storm conditions. *Proceedings 16th Coastal Engineering Conference*, A.S.C.E.: 268-284.

HORIKAWA, K. and Kuo, C.T., 1966. A study on wave transformation inside surf zone. *Proceedings 10th Coastal Engineering Conference*, A.S.C.E.: 217-233.

HOWD, P.A. and Holman, R.A., 1987. A simple model of beach foreshore response to long-period waves. *Marine Geology*, 78: 11-22.

HUGHES, M.G. and Cowell, P.J., 1987. Adjustment of reflective beaches to waves. *Journal Of Coastal Research*, 3: 153-167.

HUNTLEY, D.A. and Bowen, A.J., 1975. Comparison of the hydrodynamics of steep and shallow beaches. In: J. Hails and A. Carr (Editors), *Nearshore sediment dynamics and sedimentation*, Wiley: 69-109.

HUNTLEY, D.A., Guza, R.T. and Bowen, A.J., 1977. A universal form for shoreline run-up spectra? *Journal of Geophysical Research*, 82: 2577-2581.

HUNTLEY, D.A., Guza, R.T. and Thornton, E.B., 1981. Field observations of surf beat 1. Progressive edge waves. *Journal of Geophysical Research*, 86: 6451-6466.

IPPEN, A.T. and Kulin, G., 1954. The shoaling and breaking of the solitary wave. *Proceedings 5th Coastal Engineering Conference*, A.S.C.E.: 27-47.

KELLER, H.B., Levine, D.A. and Whitham, G.B., 1960. Motion of a Bore Over a Sloping Beach. *Journal of Fluid Mechanics*, 7: 302-316.

KEMP, P.H., 1975. Wave assymetry in the nearshore zone and breaker area. In J. Hails and A. Carr (Editors), *Nearshore sediment dynamics and sedimentation*, Wiley: 47-67.

KIM, S.K., Liu, P.L-F. and Liggett, J.A., 1983. Boundary integral equation solutions for solitary wave generation, propagation and run-up. *Coastal Engineering*, 7: 299-317.

KIRK, R.M., 1971. Instruments for investigating shore and nearshore processes. *New Zealand Journal of Marine and Freshwater Research*, 5: 358-375.

KIRKGOZ, M.S., 1981. A theoretical study of plunging breakers and their run-up. *Coastal Engineering*, 5: 353-370.

KISHI, T. and Saeki, H. 1966. The shoaling breaking and run-up of the solitary wave on impermeable rough slopes. *Proceedings 10th Coastal Engineering Conference*, A.S.C.E.: 322-349.

KOMAR, P.D., and Wang, C., 1984. Processes of selective grain transport and the formation of placers on beaches. *Journal of Sedimentary Petrology*, 92: 637-655.

LONGUET-HIGGINS, M.S. and Stewart, R.W., 1964. Radiation stresses in water waves; a physical discussion, with applications. *Deep-Sea Research*, 11: 529-562.

LEMEHAUTE, B., 1962. On non-saturated breakers and the wave run-up. *Proceedings 8th Coastal Engineering Conference*, A.S.C.E.: 77-92.

LEMEHAUTE, B., Koh, R.C.Y. and Li San Hwang, 1968. A synthesis on wave run-up. *Journal of the Waterways and Harbours Division*, A.S.C.E., HY2: 77-92.

MADSEN, P.A. and Svendsen, I.A., 1983. Turbulent bores and hydraulic jumps. *Journal of Fluid Mechanics*, 129: 1-25.

MASE, H., 1988. Spectral characteristics of random wave run-up. *Coastal Engineering*, 12: 175-189.

MATSUNAGA, N. and Honji, H., 1980. The backwash vortex. *Journal Of Fluid Mechanics*, 99: 813-815.

MATSUNAGA, N. and Honji, H., 1983. The steady and unsteady backwash vortices. *Journal Of Fluid Mechanics*, 135: 189-197.

MATSUTOMI, H., 1983. Numerical analysis of the run-up of tsunamis on dry bed. In: K. Ida and T. Iwasaki, *Tsunamis - Their Science and Engineering*, TERRAPUB: 479-493.

McLEAN, R.F. and Kirk, R.M., 1969. Relationship between grain size, size-sorting, and foreshore slope on mixed sand-shingle beaches. *New Zealand Journal of Geology and Geophysics*, 12: 138-155.

MEYER, R.E. and Taylor, A.D., 1972. Runup on beaches. In R.E. Meyer (Editor), *Waves on beaches and resulting sediment transport*. Academic Press: 357-412.

MICHE, A., 1951. Exposes a l'action de la houle. *Ann. Ponts Chaussees*, 121: 285-319.

MILLER, R.L., 1968. Experimental determination of run-up of undular and fully developed bores. *Journal of Geophysical Research*, 73: 4497-4510.

MIZUGUCHI, M., 1980. An heuristic model of wave height distribution in surf zone. *Proceedings 17th Coastal Engineering Conference*, A.S.C.E.: 278-289.

MUNK, W.H., 1949. Solitary wave theory and its applications to surf problems. *Annals New York Academy of Science*, 51: 376-424.

NELSON, C.L. and Miller, R.L., 1974. *The interaction of fluid and sediment on the foreshore*. Fluid Dynamics and Sediment Transport Laboratory Technical Report Number 15, University of Chicago: 176 pp.

NIELSEN, P., 1983. Analytical determination of nearshore wave height variation due to refraction shoaling and friction. *Coastal Engineering*, 7: 233-251.

NIELSEN, P., 1985. *A short manual of coastal bottom boundary layers and sediment transport*. Public Works Department N.S.W. Technical Memorandum 85/1: 56 pp.

NIELSEN, P., 1988. Three simple models of wave sediment transport. *Coastal Engineering*, 12: 43-62.

NIELSEN, P. and Cowell, P.J., 1981. *Calibration and data correction procedures for flow meters and pressure transducers commonly used by the Coastal Studies Unit*. Coastal Studies Unit Technical Report Number 81/1, University of Sydney: 33 pp.

OWEN, P.R., 1964. Saltation of uniform grains in air. *Journal of Fluid Mechanics*, 20: 225.

PACKWOOD, A.R., 1983. The influence of beach porosity on wave uprush and backwash. *Coastal Engineering*, 7: 29-40.

PEDERSEN, G. and Gjevik, B., 1983. Run-up of solitary waves. *Journal of Fluid Mechanics*, 135: 283-299.

PEREGRINE, D.H., 1966. Calculations of the development of an undular bore. *Journal of Fluid Mechanics*, 25: 321-330.

PEREGRINE, D.H., 1972. Equations for water waves and the approximations behind them. In R.E. Meyer (Editor), *Waves on beaches and resulting sediment transport*. Academic Press: 95-122.

PEREGRINE, D.H., 1974a. Water-wave interaction in the surf zone. *Proceedings 14th Coastal Engineering Conference*, A.S.C.E.: 500-517.

PEREGRINE, D.H., 1974b. Surface shear waves. *Journal of the Hydraulics Division*, A.S.C.E., HY9: 1215-1227.

PEREGRINE, D.H. and Svendsen, I.A., 1978. Spilling breakers, bores and hydraulic jumps. *Proceedings 16th Coastal Engineering Conference*, A.S.C.E.: 540-550.

PEREGRINE, D.H., Cokelet, E.D. and McIver, P., 1980. The fluid mechanics of waves approaching breaking. *Proceedings 17th Coastal Engineering Conference*, A.S.C.E.: 512-528.

RICHMOND, B.M. and Sallenger, A.H., 1984. Cross-shore transport of bi-modal sands. *Proceedings 19th Coastal Engineering Conference*, A.S.C.E.: 1997-2008.

RAUDKIVI, A.J., 1976. *Loose boundary hydraulics*. Pergamon Press: 397 pp.

SALLENGER, A.H. and Richmond, B.M., 1984. High-frequency sediment-level oscillations in the swash zone. In: B. Greenwood and R.A. Davis Jr. (Editors), Hydrodynamics and sedimentation in wave-dominated coastal environments. *Marine Geology*, 60: 155-164.

SALLENGER, A.H. and Holman, R.A., 1985. Wave energy saturation on a natural beach of variable slope. *Journal of Geophysical Research*, 90: 11939-11944.

SAWARAGI, T. and Iwata, K., 1974. On wave deformation after breaking. *Proceedings 14th coastal engineering Conference*, A.S.C.E.: 481-497.

SCHIFFMAN, A., 1965. Energy measurements in the swash-surf zone. *Limnology and Oceanography*, 10: 255-260.

SHEN, M.C. and Meyer, R.E., 1963. Climb of a bore on a beach: Part three run-up. *Journal of Fluid Mechanics*, 16: 113-125.

SHORT, A.D., 1984. Beach and nearshore facies: Southeast Australia. In: B. Greenwood and R.A. Davis, Jr. (Editors), Hydrodynamics and sedimentation in wave-dominated coastal environments. *Marine Geology*, 60: 261-282.

SHORT, A.D. and Wright, L.D., 1981. Beach systems of the Sydney region. *Australian Geographer*, 15: 8-16.

SLEATH, J.F.A., 1984. *Sea bed mechanics.* Wiley-Interscience: 335 pp.

SMITH, J.D. and McLean, S.R., 1977. Spatially averaged flow over a wavy surface. *Journal of Geophysical Research*, 82: 1735-1746.

SONU, C.J., Pettigrew, N. and Fredericks, R.G., 1974. Measurement of swash profile and orbital motion on the beach. *Proceedings of a Symposium on Ocean Wave Measurements and Analysis*: 621-638.

STOKER, J.J., 1957. *Water waves*: *The mathematical theory with applications.* Interscience: 567 pp.

STREETER, V.L., and Wylie, E.B., 1981. *Fluid mechanics.* McGraw-Hill: 562 pp.

SUHAYDA, J.N., 1974. Standing waves on beaches. *Journal of Geophysical Research*, 79: 3065-3071.

SUNAMURA, T., 1975. A study of beach ridge formation in laboratory. *Geographical Review Of Japan*, 48: 761-767.

SUNAMURA, T., 1984. Quantitative prediction of beach-face slopes. *Geological Society Of America Bulletin*, 95: 242-245.

SVENDSEN, I.A., 1984. Wave heights and set-up in a surf zone. *Coastal Engineering*, 8: 303-329.

SVENDSEN, I.A., 1987. Analysis of surf zone turbulence. *Journal of Geophysical Research*, 92: 5115-5124.

SVENDSEN, I.A. and Madsen, P.A., 1984. A turbulent bore on a beach. *Journal of Fluid Mechanics*, 148: 73-96.

SYNOLAKIS, C.E., 1987a. The runup of solitary waves. *Journal Of Fluid Mecahanics*, 185: 523-545.

SYNOLAKIS, C.E., 1987b. The runup and reflection of solitary waves. In: R.A. Dalrymple (Editor), *Coastal Hydrodynamics*, A.S.C.E.: 533-547.

TAKEDA, I. and Sunamura, T., 1983. A wave flume experiment of beach steps. *Annual Report Of The Institiute Of Geoscience University Of Tsukuba*, 9: 45-48.

THORNTON, E.B. and Guza, R.T., 1982. Energy saturation and phase speeds measured on a natural beach. *Journal of Geophysical Research*, 87: 9499-9508.

URSELL, F., 1953. The long wave paradox in the theory of gravity waves. *Proceedings of the Cambridge Philosophical Society*, 49: 685-692.

VAN DORN, W.G., 1976. Set-up and run-up in shoaling breakers. *Proceedings 15th Coastal Engineering Conference*, A.S.C.E.: 738-751.

VAN DORN, W.G., and Pazan, S.E., 1975. *Laboratory investigations of wave breaking Part II: Deep water waves.* Advanced Ocean Engineering Laboratory, Scripps Institution of Oceanography University of California, SIO Reference Number 75-21: 105 pp.

VAN RIJN, L.C., 1982. Equivalent roughness of alluvial bed. *Journal of the Hydraulics Division*, A.S.C.E.: 1215-1218.

WADDELL, E., 1973. *Dynamics of swash and implications to beach response.* Coastal Studies Institute Technical Report No. 139, Louisiana State University: 49 pp.

WHITEHOUSE, R.J.S., and Hardisty, J., 1988. Experimental assessment of two theories for the effect of bedslope on the threshold of bedload transport. *Marine Geology*, 79: 135-139.

WHITHAM, G.B., 1958. On the propagation of shock waves through regions of non-uniform area or flow. *Journal of Fluid Mechanics*, 4: 337-360.

WIEGEL, R.L., 1964. *Oceanographical Engineering.* Prentice-Hall: 532 pp.

WILSON, K.C., 1988. Frictional behaviour of sheet flow. *Progress report 67*, Institute of Hydrodynamic and Hydraulic Engineering, Technical University of Denmark: 11-22.

WRIGHT, L.D., 1976a. Nearshore wave-power dissipation and the coastal energy regime of the Sydney-Jervis Bay region, New South Wales: A comparison. *Australian Journal of Marine and Freshwater Research*, 27: 633-640.

WRIGHT, P., 1976b. A cine-camera technique for process measurement on a ridge and runnel beach. *Sedimentology*, 23: 705-712.

WRIGHT, L.D., 1980. Beach cut in relation to surf zone morphodynamics. *Proceedings 17th Coastal Engineering Conference*, A.S.C.E.: 978-996.

WRIGHT, L.D. and Short, A.D., 1984. Morphodynamic variability of surf zones and beaches: A synthesis. *Marine Geology*, 56: 93-118.

WRIGHT, L.D., Coffey, F.C. and Cowell, P.J., 1980. *Nearshore oceanography and morphodynamics of the Broken Bay - Palm Beach region, N.S.W.: Implications for offshore dredging.* Coastal Studies Unit Technical Report No. 80/1, University of Sydney: 210 pp.

WRIGHT, L.D., Guza, R.T. and Short, A.D., 1982. Dynamics of a high energy dissipative surf zone. *Marine Geology*, 45: 41-62.

WRIGHT, L.D., Nielsen, P., Shi, P. and List, J.H., 1986. Morphodynamics of a bar trough surf zone. *Marine Geology*, 70: 251-285.

YALIN, M.S., 1977. *Mechanics of sediment transport.* Pergamon Press: 298 pp.

YEH, H.H and Ghazali, A., 1986. Nearshore behaviour of bore on a uniformly sloping beach. *Proceedings 20th Coastal Engineering Conference*, A.S.C.E.: 877-888.

YEH, H.H and Ghazali, A., 1988. On bore collapse. *Journal of Geophysical Research*, 93: 6930-6936.

APPENDIX A

TABULATED FIELD DATA

TABLE A.1
TABULATED FIELD DATA

No.	Type	X_{s*}	t_*	u_o	D	β
1	B	0.00	0.00	2.99	0.49	0.107
2	B	0.25	0.26	2.99	0.49	0.107
3	B	0.49	0.58	2.99	0.49	0.107
4	B	0.76	1.12	2.99	0.49	0.107
5	B	0.00	0.00	4.31	0.49	0.107
6	B	0.12	0.07	4.31	0.49	0.107
7	B	0.24	0.14	4.31	0.49	0.107
8	B	0.37	0.25	4.31	0.49	0.107
9	B	0.50	0.39	4.31	0.49	0.107
10	B	0.64	0.59	4.31	0.49	0.107
11	B	0.00	0.00	3.77	0.49	0.107
12	B	0.15	0.13	3.77	0.49	0.107
13	B	0.31	0.29	3.77	0.49	0.107
14	B	0.48	0.53	3.77	0.49	0.107
15	B	0.65	0.91	3.77	0.49	0.107
16	B	0.00	0.00	3.71	0.49	0.107
17	B	0.16	0.14	3.71	0.49	0.107
18	B	0.32	0.32	3.71	0.49	0.107
19	B	0.50	0.64	3.71	0.49	0.107
20	B	0.00	0.00	4.56	0.49	0.107
21	B	0.11	0.10	4.56	0.49	0.107
22	B	0.21	0.19	4.56	0.49	0.107
23	B	0.33	0.29	4.56	0.49	0.107
24	B	0.44	0.38	4.56	0.49	0.107
25	B	0.57	0.54	4.56	0.49	0.107
26	B	0.00	0.00	3.69	0.49	0.107
27	B	0.16	0.14	3.69	0.49	0.107
28	B	0.32	0.31	3.69	0.49	0.107
29	B	0.50	0.33	3.69	0.49	0.107
30	B	0.68	0.93	3.69	0.49	0.107
31	B	0.00	0.00	3.06	0.49	0.107
32	B	0.23	0.24	3.06	0.49	0.107
33	B	0.47	0.49	3.06	0.49	0.107
34	B	0.00	0.00	4.17	0.49	0.107
35	B	0.13	0.11	4.17	0.49	0.107
36	B	0.25	0.22	4.17	0.49	0.107
37	B	0.39	0.34	4.17	0.49	0.107
38	B	0.53	0.52	4.17	0.49	0.107
39	B	0.68	0.76	4.17	0.49	0.107
40	B	0.00	0.00	4.60	0.49	0.107
41	B	0.10	0.13	4.60	0.49	0.107
42	B	0.22	0.23	4.60	0.49	0.107
43	B	0.33	0.34	4.60	0.49	0.107
44	B	0.46	0.59	4.60	0.49	0.107
45	B	0.00	0.00	3.60	0.49	0.107
46	B	0.17	0.09	3.60	0.49	0.107
47	B	0.34	0.21	3.60	0.49	0.107
48	B	0.53	0.51	3.60	0.49	0.107
49	B	0.71	0.87	3.60	0.49	0.107
50	B	0.00	0.00	4.16	0.49	0.107
51	B	0.13	0.07	4.16	0.49	0.107
52	B	0.25	0.16	4.16	0.49	0.107

TABLE A.1 (contd.)
TABULATED FIELD DATA

No.	Type	X_{s*}	t_*	u_o	D	β
53	B	0.39	0.30	4.16	0.49	0.107
54	B	0.53	0.61	4.16	0.49	0.107
55	B	0.00	0.00	3.95	0.49	0.107
56	B	0.14	0.21	3.95	0.49	0.107
57	B	0.28	0.33	3.95	0.49	0.107
58	B	0.44	0.43	3.95	0.49	0.107
59	B	0.59	0.57	3.95	0.49	0.107
60	B	0.76	0.82	3.95	0.49	0.107
61	B	0.00	0.00	4.03	0.49	0.107
62	B	0.14	0.08	4.03	0.49	0.107
63	B	0.27	0.18	4.03	0.49	0.107
64	B	0.42	0.33	4.03	0.49	0.107
65	B	0.57	0.49	4.03	0.49	0.107
66	B	0.73	0.76	4.03	0.49	0.107
67	B	0.00	0.00	4.42	0.49	0.107
68	B	0.11	0.08	4.42	0.49	0.107
69	B	0.24	0.20	4.42	0.49	0.107
70	B	0.36	0.33	4.42	0.49	0.107
71	B	0.49	0.50	4.42	0.49	0.107
72	B	0.00	0.00	3.68	0.49	0.107
73	B	0.16	0.16	3.68	0.49	0.107
74	B	0.32	0.30	3.68	0.49	0.107
75	B	0.50	0.59	3.68	0.49	0.107
76	B	0.68	0.95	3.68	0.49	0.107
77	B	0.00	0.00	3.85	0.79	0.123
78	B	0.17	0.09	3.85	0.79	0.123
79	B	0.32	0.20	3.85	0.79	0.123
80	B	0.48	0.28	3.85	0.79	0.123
81	B	0.67	0.50	3.85	0.79	0.123
82	B	0.00	0.00	4.23	0.79	0.123
83	B	0.22	0.13	4.23	0.79	0.123
84	B	0.36	0.28	4.23	0.79	0.123
85	B	0.48	0.46	4.23	0.79	0.123
86	B	0.00	0.00	4.17	0.79	0.123
87	B	0.22	0.14	4.17	0.79	0.123
88	B	0.37	0.24	4.17	0.79	0.123
89	B	0.49	0.32	4.17	0.79	0.123
90	B	0.64	0.41	4.17	0.79	0.123
91	B	0.80	0.67	4.17	0.79	0.123
92	B	0.00	0.00	4.44	0.79	0.123
93	B	0.20	0.12	4.44	0.79	0.123
94	B	0.32	0.19	4.44	0.79	0.123
95	B	0.44	0.28	4.44	0.79	0.123
96	B	0.56	0.46	4.44	0.79	0.123
97	B	0.70	0.63	4.44	0.79	0.123
98	B	0.00	0.00	4.58	0.79	0.123
99	B	0.19	0.16	4.58	0.79	0.123
100	B	0.30	0.28	4.58	0.79	0.123
101	B	0.41	0.42	4.58	0.79	0.123
102	B	0.53	0.63	4.58	0.79	0.123
103	B	0.66	0.73	4.58	0.79	0.123
104	B	0.00	0.00	4.00	0.79	0.123

TABLE A.1 (contd.)
TABULATED FIELD DATA

No.	Type	X_{s*}	t_*	u_o	D	β
105	B	0.24	0.17	4.00	0.79	0.123
106	B	0.40	0.30	4.00	0.79	0.123
107	B	0.54	0.40	4.00	0.79	0.123
108	B	0.69	0.60	4.00	0.79	0.123
109	B	0.87	0.89	4.00	0.79	0.123
110	B	0.00	0.00	4.76	0.79	0.123
111	B	0.17	0.13	4.76	0.79	0.123
112	B	0.28	0.23	4.76	0.79	0.123
113	B	0.38	0.32	4.76	0.79	0.123
114	B	0.49	0.51	4.76	0.79	0.123
115	B	0.00	0.00	3.33	0.79	0.123
116	B	0.35	0.34	3.33	0.79	0.123
117	B	0.57	0.66	3.33	0.79	0.123
118	B	0.00	0.00	3.19	0.79	0.123
119	B	0.38	0.40	3.19	0.79	0.123
120	B	0.62	0.87	3.19	0.79	0.123
121	B	0.00	0.00	4.12	0.79	0.123
122	B	0.23	0.21	4.12	0.79	0.123
123	B	0.37	0.43	4.12	0.79	0.123
124	B	0.51	0.61	4.12	0.79	0.123
125	B	0.65	0.93	4.12	0.79	0.123
126	B	0.00	0.00	4.11	0.79	0.123
127	B	0.15	0.13	4.11	0.79	0.123
128	B	0.28	0.21	4.11	0.79	0.123
129	B	0.42	0.47	4.11	0.79	0.123
130	B	0.00	0.00	4.61	0.79	0.123
131	B	0.18	0.14	4.61	0.79	0.123
132	B	0.30	0.24	4.61	0.79	0.123
133	B	0.40	0.37	4.61	0.79	0.123
134	B	0.52	0.51	4.61	0.79	0.123
135	B	0.65	0.71	4.61	0.79	0.123
136	B	0.00	0.00	4.19	0.79	0.123
137	B	0.22	0.16	4.19	0.79	0.123
138	B	0.36	0.31	4.19	0.79	0.123
139	B	0.49	0.51	4.19	0.79	0.123
140	B	0.00	0.00	5.21	0.79	0.123
141	B	0.14	0.05	5.21	0.79	0.123
142	B	0.23	0.14	5.21	0.79	0.123
143	B	0.32	0.24	5.21	0.79	0.123
144	B	0.41	0.40	5.21	0.79	0.123
145	B	0.00	0.00	4.49	0.79	0.123
146	B	0.19	0.16	4.49	0.79	0.123
147	B	0.32	0.28	4.49	0.79	0.123
148	B	0.43	0.45	4.49	0.79	0.123
149	B	0.55	0.67	4.49	0.79	0.123
150	B	0.00	0.00	3.85	0.79	0.123
151	B	0.26	0.18	3.85	0.79	0.123
152	B	0.43	0.28	3.85	0.79	0.123
153	B	0.58	0.42	3.85	0.79	0.123
154	B	0.00	0.00	4.15	0.79	0.123
155	B	0.23	0.14	4.15	0.79	0.123
156	B	0.37	0.23	4.15	0.79	0.123

TABLE A.1 (contd.)
TABULATED FIELD DATA

No.	Type	X_{s*}	t_*	u_o	D	β
157	B	0.50	0.38	4.15	0.79	0.123
158	B	0.64	0.56	4.15	0.79	0.123
159	B	0.00	0.00	3.99	0.79	0.123
160	B	0.24	0.21	3.99	0.79	0.123
161	B	0.40	0.38	3.99	0.79	0.123
162	B	0.54	0.55	3.99	0.79	0.123
163	B	0.69	0.89	3.99	0.79	0.123
164	B	0.00	0.00	7.61	0.79	0.123
165	B	0.07	0.04	7.61	0.79	0.123
166	B	0.11	0.08	7.61	0.79	0.123
167	B	0.15	0.11	7.61	0.79	0.123
168	B	0.19	0.16	7.61	0.79	0.123
169	B	0.24	0.21	7.61	0.79	0.123
170	B	0.00	0.00	4.47	0.79	0.123
171	B	0.19	0.17	4.47	0.79	0.123
172	B	0.32	0.28	4.47	0.79	0.123
173	B	0.43	0.42	4.47	0.79	0.123
174	B	0.55	0.55	4.47	0.79	0.123
175	B	0.69	0.74	4.47	0.79	0.123
176	B	0.00	0.00	4.73	0.79	0.123
177	B	0.17	0.10	4.73	0.79	0.123
178	B	0.28	0.19	4.73	0.79	0.123
179	B	0.38	0.27	4.73	0.79	0.123
180	B	0.49	0.43	4.73	0.79	0.123
181	B	0.62	0.59	4.73	0.79	0.123
182	B	0.00	0.00	3.97	0.79	0.123
183	B	0.25	0.23	3.97	0.79	0.123
184	B	0.40	0.41	3.97	0.79	0.123
185	B	0.54	0.70	3.97	0.79	0.123
186	B	0.70	0.94	3.97	0.79	0.123
187	B	0.00	0.00	3.90	0.79	0.123
188	B	0.26	0.19	3.90	0.79	0.123
189	B	0.42	0.36	3.90	0.79	0.123
190	B	0.56	0.62	3.90	0.79	0.123
191	B	0.00	0.00	4.26	0.79	0.123
192	B	0.21	0.18	4.26	0.79	0.123
193	B	0.35	0.38	4.26	0.79	0.123
194	B	0.47	0.58	4.26	0.79	0.123
195	B	0.00	0.00	3.53	0.79	0.123
196	B	0.31	0.29	3.53	0.79	0.123
197	B	0.51	0.63	3.53	0.79	0.123
198	B	0.00	0.00	4.02	0.79	0.123
199	B	0.24	0.20	4.02	0.79	0.123
200	B	0.39	0.39	4.02	0.79	0.123
201	B	0.53	0.69	4.02	0.79	0.123
202	B	0.00	0.00	3.48	0.79	0.123
203	B	0.32	0.33	3.48	0.79	0.123
204	B	0.53	0.83	3.48	0.79	0.123
205	B	0.71	0.97	3.48	0.79	0.123
206	B	0.00	0.00	4.17	0.41	0.128
207	B	0.13	0.07	4.17	0.41	0.128
208	B	0.27	0.18	4.17	0.41	0.128

TABLE A.1 (contd.)
TABULATED FIELD DATA

No.	Type	X_{s*}	t_*	u_o	D	β
209	B	0.42	0.34	4.17	0.41	0.128
210	B	0.60	0.68	4.17	0.41	0.128
211	B	0.00	0.00	4.11	0.41	0.128
212	B	0.13	0.11	4.11	0.41	0.128
213	B	0.28	0.24	4.11	0.41	0.128
214	B	0.43	0.42	4.11	0.41	0.128
215	B	0.62	0.65	4.11	0.41	0.128
216	B	0.00	0.00	3.29	0.41	0.128
217	B	0.20	0.18	3.29	0.41	0.128
218	B	0.44	0.60	3.29	0.41	0.128
219	B	0.00	0.00	4.83	0.41	0.128
220	B	0.09	0.07	4.83	0.41	0.128
221	B	0.20	0.16	4.83	0.41	0.128
222	B	0.31	0.26	4.83	0.41	0.128
223	B	0.45	0.41	4.83	0.41	0.128
224	B	0.58	0.64	4.83	0.41	0.128
225	B	0.00	0.00	5.52	0.41	0.128
226	B	0.07	0.04	5.52	0.41	0.128
227	B	0.16	0.11	5.52	0.41	0.128
228	B	0.24	0.18	5.52	0.41	0.128
229	B	0.34	0.27	5.52	0.41	0.128
230	B	0.44	0.34	5.52	0.41	0.128
231	B	0.00	0.00	4.34	0.41	0.128
232	B	0.12	0.06	4.34	0.41	0.128
233	B	0.25	0.17	4.34	0.41	0.128
234	B	0.39	0.37	4.34	0.41	0.128
235	B	0.55	0.65	4.34	0.41	0.128
236	B	0.00	0.00	4.15	0.41	0.128
237	B	0.13	0.07	4.15	0.41	0.128
238	B	0.27	0.17	4.15	0.41	0.128
239	B	0.42	0.36	4.15	0.41	0.128
240	B	0.60	0.70	4.15	0.41	0.128
241	B	0.00	0.00	4.62	0.41	0.128
242	B	0.10	0.08	4.62	0.41	0.128
243	B	0.22	0.21	4.62	0.41	0.128
244	B	0.34	0.34	4.62	0.41	0.128
245	B	0.49	0.52	4.62	0.41	0.128
246	B	0.63	0.76	4.62	0.41	0.128
247	B	0.00	0.00	3.56	0.41	0.128
248	B	0.17	0.15	3.56	0.41	0.128
249	B	0.37	0.34	3.56	0.41	0.128
250	B	0.57	0.68	3.56	0.41	0.128
251	B	0.00	0.00	3.76	0.41	0.128
252	B	0.16	0.14	3.76	0.41	0.128
253	B	0.33	0.24	3.76	0.41	0.128
254	B	0.51	0.38	3.76	0.41	0.128
255	B	0.74	0.78	3.76	0.41	0.128
256	B	0.00	0.00	4.17	0.41	0.128
257	B	0.13	0.10	4.17	0.41	0.128
258	B	0.27	0.28	4.17	0.41	0.128
259	B	0.00	0.00	3.92	0.41	0.128
260	B	0.14	0.12	3.92	0.41	0.128

TABLE A.1 (contd.)
TABULATED FIELD DATA

No.	Type	X_{s*}	t_*	u_o	D	β
261	B	0.31	0.26	3.92	0.41	0.128
262	B	0.47	0.52	3.92	0.41	0.128
263	B	0.00	0.00	3.72	0.41	0.128
264	B	0.16	0.14	3.72	0.41	0.128
265	B	0.34	0.32	3.72	0.41	0.128
266	B	0.53	0.62	3.72	0.41	0.128
267	B	0.00	0.00	3.90	0.41	0.128
268	B	0.14	0.12	3.90	0.41	0.128
269	B	0.31	0.27	3.90	0.41	0.128
270	B	0.48	0.58	3.90	0.41	0.128
271	B	0.00	0.00	3.81	0.29	0.134
272	B	0.14	0.11	3.81	0.29	0.134
273	B	0.28	0.26	3.81	0.29	0.134
274	B	0.43	0.45	3.81	0.29	0.134
275	B	0.60	0.67	3.81	0.29	0.134
276	B	0.00	0.00	4.09	0.29	0.134
277	B	0.12	0.06	4.09	0.29	0.134
278	B	0.25	0.15	4.09	0.29	0.134
279	B	0.38	0.26	4.09	0.29	0.134
280	B	0.52	0.43	4.09	0.29	0.134
281	B	0.65	0.76	4.09	0.29	0.134
282	B	0.00	0.00	4.12	0.32	0.139
283	B	0.11	0.10	4.12	0.32	0.139
284	B	0.22	0.18	4.12	0.32	0.139
285	B	0.32	0.27	4.12	0.32	0.139
286	B	0.44	0.44	4.12	0.32	0.139
287	B	0.53	0.58	4.12	0.32	0.139
288	B	0.00	0.00	3.56	0.32	0.139
289	B	0.15	0.10	3.56	0.32	0.139
290	B	0.29	0.15	3.56	0.32	0.139
291	B	0.43	0.25	3.56	0.32	0.139
292	B	0.59	0.44	3.56	0.32	0.139
293	B	0.70	0.77	3.56	0.32	0.139
294	B	0.00	0.00	2.96	2.00	0.129
295	B	0.24	0.24	2.96	2.00	0.129
296	B	0.43	0.55	2.96	2.00	0.129
297	B	0.00	0.00	4.03	0.44	0.147
298	B	0.20	0.13	4.03	0.44	0.147
299	B	0.33	0.24	4.03	0.44	0.147
300	B	0.44	0.34	4.03	0.44	0.147
301	B	0.56	0.43	4.03	0.44	0.147
302	B	0.67	0.54	4.03	0.44	0.147
303	B	0.00	0.00	5.12	0.44	0.147
304	B	0.13	0.07	5.12	0.44	0.147
305	B	0.20	0.11	5.12	0.44	0.147
306	B	0.28	0.16	5.12	0.44	0.147
307	B	0.35	0.24	5.12	0.44	0.147
308	B	0.42	0.33	5.12	0.44	0.147
309	B	0.00	0.00	4.19	0.44	0.147
310	B	0.19	0.10	4.19	0.44	0.147
311	B	0.30	0.19	4.19	0.44	0.147
312	B	0.41	0.42	4.19	0.44	0.147

TABLE A.1 (contd.)
TABULATED FIELD DATA

No.	Type	X_{s*}	t_*	u_o	D	β
313	B	0.52	0.74	4.19	0.44	0.147
314	B	0.00	0.00	3.59	0.44	0.147
315	B	0.25	0.15	3.59	0.44	0.147
316	B	0.41	0.28	3.59	0.44	0.147
317	B	0.56	0.45	3.59	0.44	0.147
318	B	0.70	0.67	3.59	0.44	0.147
319	B	0.00	0.00	4.76	0.44	0.147
320	B	0.14	0.11	4.76	0.44	0.147
321	B	0.23	0.18	4.76	0.44	0.147
322	B	0.32	0.27	4.76	0.44	0.147
323	B	0.40	0.44	4.76	0.44	0.147
324	B	0.48	0.59	4.76	0.44	0.147
325	B	0.00	0.00	4.55	0.44	0.147
326	B	0.16	0.09	4.55	0.44	0.147
327	B	0.26	0.15	4.55	0.44	0.147
328	B	0.35	0.17	4.55	0.44	0.147
329	B	0.44	0.25	4.55	0.44	0.147
330	B	0.53	0.35	4.55	0.44	0.147
331	B	0.00	0.00	3.43	0.44	0.147
332	B	0.28	0.26	3.43	0.44	0.147
333	B	0.45	0.47	3.43	0.44	0.147
334	B	0.00	0.00	4.73	0.44	0.147
335	B	0.15	0.12	4.73	0.44	0.147
336	B	0.24	0.18	4.73	0.44	0.147
337	B	0.32	0.31	4.73	0.44	0.147
338	B	0.40	0.38	4.73	0.44	0.147
339	B	0.49	0.64	4.73	0.44	0.147
340	B	0.00	0.00	4.46	0.44	0.147
341	B	0.16	0.10	4.46	0.44	0.147
342	B	0.27	0.20	4.46	0.44	0.147
343	B	0.36	0.29	4.46	0.44	0.147
344	B	0.46	0.39	4.46	0.44	0.147
345	B	0.55	0.63	4.46	0.44	0.147
346	B	0.00	0.00	2.76	0.44	0.147
347	B	0.43	0.51	2.76	0.44	0.147
348	B	0.70	1.04	2.76	0.44	0.147
349	B	0.00	0.00	4.59	0.44	0.147
350	B	0.16	0.09	4.59	0.44	0.147
351	B	0.25	0.17	4.59	0.44	0.147
352	B	0.34	0.22	4.59	0.44	0.147
353	B	0.43	0.27	4.59	0.44	0.147
354	B	0.52	0.35	4.59	0.44	0.147
355	B	0.00	0.00	3.08	0.44	0.147
356	B	0.35	0.42	3.08	0.44	0.147
357	B	0.56	0.64	3.08	0.44	0.147
358	B	0.00	0.00	5.27	0.44	0.147
359	B	0.12	0.07	5.27	0.44	0.147
360	B	0.19	0.11	5.27	0.44	0.147
361	B	0.26	0.15	5.27	0.44	0.147
362	B	0.33	0.19	5.27	0.44	0.147
363	B	0.39	0.26	5.27	0.44	0.147
364	B	0.00	0.00	5.00	0.44	0.147

TABLE A.1 (contd.)
TABULATED FIELD DATA

No.	Type	X_{s*}	t_*	u_o	D	β
365	B	0.13	0.08	5.00	0.44	0.147
366	B	0.21	0.19	5.00	0.44	0.147
367	B	0.29	0.25	5.00	0.44	0.147
368	B	0.36	0.46	5.00	0.44	0.147
369	B	0.44	0.66	5.00	0.44	0.147
370	B	0.00	0.00	3.87	0.44	0.147
371	B	0.22	0.19	3.87	0.44	0.147
372	B	0.35	0.34	3.87	0.44	0.147
373	B	0.48	0.52	3.87	0.44	0.147
374	B	0.60	0.79	3.87	0.44	0.147
375	B	0.00	0.00	4.28	0.44	0.147
376	B	0.18	0.20	4.28	0.44	0.147
377	B	0.29	0.30	4.28	0.44	0.147
378	B	0.39	0.38	4.28	0.44	0.147
379	B	0.49	0.48	4.28	0.44	0.147
380	B	0.60	0.64	4.28	0.44	0.147
381	B	0.00	0.00	4.87	0.44	0.147
382	B	0.14	0.10	4.87	0.44	0.147
383	B	0.22	0.13	4.87	0.44	0.147
384	B	0.30	0.18	4.87	0.44	0.147
385	B	0.38	0.26	4.87	0.44	0.147
386	B	0.46	0.38	4.87	0.44	0.147
387	B	0.00	0.00	4.02	0.44	0.147
388	B	0.20	0.12	4.02	0.44	0.147
389	B	0.33	0.21	4.02	0.44	0.147
390	B	0.45	0.29	4.02	0.44	0.147
391	B	0.56	0.39	4.02	0.44	0.147
392	B	0.68	0.56	4.02	0.44	0.147
393	B	0.00	0.00	4.29	0.44	0.147
394	B	0.18	0.14	4.29	0.44	0.147
395	B	0.29	0.27	4.29	0.44	0.147
396	B	0.39	0.46	4.29	0.44	0.147
397	B	0.00	0.00	4.44	0.44	0.147
398	B	0.17	0.14	4.44	0.44	0.147
399	B	0.27	0.28	4.44	0.44	0.147
400	B	0.37	0.35	4.44	0.44	0.147
401	B	0.46	0.53	4.44	0.44	0.147
402	B	0.00	0.00	3.78	0.44	0.147
403	B	0.23	0.20	3.78	0.44	0.147
404	B	0.37	0.38	3.78	0.44	0.147
405	B	0.51	0.59	3.78	0.44	0.147
406	B	0.00	0.00	4.80	0.31	0.135
407	B	0.17	0.10	4.80	0.31	0.135
408	B	0.27	0.16	4.80	0.31	0.135
409	B	0.36	0.22	4.80	0.31	0.135
410	B	0.46	0.30	4.80	0.31	0.135
411	B	0.54	0.36	4.80	0.31	0.135
412	B	0.00	0.00	6.21	0.31	0.135
413	B	0.10	0.11	6.21	0.31	0.135
414	B	0.16	0.12	6.21	0.31	0.135
415	B	0.22	0.22	6.21	0.31	0.135
416	B	0.27	0.32	6.21	0.31	0.135

TABLE A.1 (contd.)
TABULATED FIELD DATA

No.	Type	X_{s*}	t_*	u_o	D	β
417	B	0.32	0.44	6.21	0.31	0.135
418	B	0.00	0.00	4.97	0.31	0.135
419	B	0.16	0.11	4.97	0.31	0.135
420	B	0.25	0.16	4.97	0.31	0.135
421	B	0.34	0.20	4.97	0.31	0.135
422	B	0.43	0.28	4.97	0.31	0.135
423	B	0.50	0.36	4.97	0.31	0.135
424	B	0.00	0.00	4.09	0.31	0.135
425	B	0.24	0.20	4.09	0.31	0.135
426	B	0.37	0.35	4.09	0.31	0.135
427	B	0.50	0.59	4.09	0.31	0.135
428	B	0.00	0.00	5.79	0.31	0.135
429	B	0.12	0.09	5.79	0.31	0.135
430	B	0.18	0.14	5.79	0.31	0.135
431	B	0.25	0.16	5.79	0.31	0.135
432	B	0.31	0.21	5.79	0.31	0.135
433	B	0.37	0.27	5.79	0.31	0.135
434	B	0.00	0.00	4.38	0.31	0.135
435	B	0.21	0.13	4.38	0.31	0.135
436	B	0.32	0.21	4.38	0.31	0.135
437	B	0.43	0.33	4.38	0.31	0.135
438	B	0.55	0.39	4.38	0.31	0.135
439	B	0.64	0.46	4.38	0.31	0.135
440	B	0.00	0.00	4.36	0.31	0.135
441	B	0.21	-0.21	4.36	0.31	0.135
442	B	0.33	0.32	4.36	0.31	0.135
443	B	0.44	0.41	4.36	0.31	0.135
444	B	0.55	0.56	4.36	0.31	0.135
445	B	0.65	0.67	4.36	0.31	0.135
446	B	0.00	0.00	3.94	0.31	0.135
447	B	0.26	0.18	3.94	0.31	0.135
448	B	0.40	0.24	3.94	0.31	0.135
449	B	0.53	0.40	3.94	0.31	0.135
450	B	0.68	0.67	3.94	0.31	0.135
451	B	0.00	0.00	3.45	0.31	0.135
452	B	0.34	0.32	3.45	0.31	0.135
453	B	0.52	0.53	3.45	0.31	0.135
454	B	0.70	0.71	3.45	0.31	0.135
455	B	0.00	0.00	4.11	0.31	0.135
456	B	0.24	0.19	4.11	0.31	0.135
457	B	0.37	0.28	4.11	0.31	0.135
458	B	0.49	0.35	4.11	0.31	0.135
459	B	0.62	0.42	4.11	0.31	0.135
460	B	0.73	0.50	4.11	0.31	0.135
461	B	0.00	0.00	4.14	0.31	0.135
462	B	0.23	0.16	4.14	0.31	0.135
463	B	0.36	0.26	4.14	0.31	0.135
464	B	0.48	0.32	4.14	0.31	0.135
465	B	0.61	0.42	4.14	0.31	0.135
466	B	0.72	0.51	4.14	0.31	0.135
467	B	0.00	0.00	4.26	0.31	0.135
468	B	0.22	0.20	4.26	0.31	0.135

TABLE A.1 (contd.)
TABULATED FIELD DATA

No.	Type	X_{s*}	t_*	u_o	D	β
469	B	0.34	0.30	4.26	0.31	0.135
470	B	0.46	0.48	4.26	0.31	0.135
471	B	0.00	0.00	4.71	0.31	0.135
472	B	0.18	0.18	4.71	0.31	0.135
473	B	0.28	0.25	4.71	0.31	0.135
474	B	0.37	0.35	4.71	0.31	0.135
475	B	0.47	0.45	4.71	0.31	0.135
476	B	0.56	0.55	4.71	0.31	0.135
477	B	0.00	0.00	5.32	0.31	0.135
478	B	0.14	0.09	5.32	0.31	0.135
479	B	0.22	0.14	5.32	0.31	0.135
480	B	0.29	0.23	5.32	0.31	0.135
481	B	0.37	0.31	5.32	0.31	0.135
482	B	0.44	0.37	5.32	0.31	0.135
483	B	0.00	0.00	5.25	0.31	0.135
484	B	0.14	0.08	5.25	0.31	0.135
485	B	0.22	0.13	5.25	0.31	0.135
486	B	0.30	0.17	5.25	0.31	0.135
487	B	0.38	0.24	5.25	0.31	0.135
488	B	0.45	0.31	5.25	0.31	0.135
489	B	0.00	0.00	3.91	0.31	0.135
490	B	0.26	0.17	3.91	0.31	0.135
491	B	0.41	0.26	3.91	0.31	0.135
492	B	0.54	0.36	3.91	0.31	0.135
493	B	0.69	0.48	3.91	0.31	0.135
494	B	0.81	0.59	3.91	0.31	0.135
495	B	0.00	0.00	4.74	0.31	0.135
496	B	0.18	0.18	4.74	0.31	0.135
497	B	0.28	0.27	4.74	0.31	0.135
498	B	0.37	0.34	4.74	0.31	0.135
499	B	0.47	0.44	4.74	0.31	0.135
500	B	0.55	0.53	4.74	0.31	0.135
501	B	0.00	0.00	3.57	0.31	0.135
502	B	0.31	0.30	3.57	0.31	0.135
503	B	0.49	0.69	3.57	0.31	0.135
504	B	0.00	0.00	4.62	0.31	0.135
505	B	0.19	0.16	4.62	0.31	0.135
506	B	0.29	0.30	4.62	0.31	0.135
507	B	0.39	0.39	4.62	0.31	0.135
508	B	0.49	0.54	4.62	0.31	0.135
509	B	0.58	0.80	4.62	0.31	0.135
510	B	0.00	0.00	6.07	0.31	0.135
511	B	0.11	0.06	6.07	0.31	0.135
512	B	0.17	0.10	6.07	0.31	0.135
513	B	0.23	0.13	6.07	0.31	0.135
514	B	0.29	0.20	6.07	0.31	0.135
515	B	0.34	0.26	6.07	0.31	0.135
516	B	0.00	0.00	3.83	0.31	0.135
517	B	0.27	0.16	3.83	0.31	0.135
518	B	0.42	0.26	3.83	0.31	0.135
519	B	0.57	0.40	3.83	0.31	0.135
520	B	0.72	0.80	3.83	0.31	0.135

TABLE A.1 (contd.)
TABULATED FIELD DATA

No.	Type	X_{s*}	t_*	u_o	D	β
521	B	0.00	0.00	3.24	0.46	0.093
522	B	0.20	0.18	3.24	0.46	0.093
523	B	0.36	0.35	3.24	0.46	0.093
524	B	0.00	0.00	3.88	0.46	0.093
525	B	0.14	0.08	3.88	0.46	0.093
526	B	0.25	0.14	3.88	0.46	0.093
527	B	0.41	0.26	3.88	0.46	0.093
528	B	0.52	0.39	3.88	0.46	0.093
529	B	0.61	0.53	3.88	0.46	0.093
530	B	0.00	0.00	3.37	0.46	0.093
531	B	0.18	0.16	3.37	0.46	0.093
532	B	0.33	0.31	3.37	0.46	0.093
533	B	0.54	0.68	3.37	0.46	0.093
534	B	0.00	0.00	4.90	0.46	0.093
535	B	0.09	0.08	4.90	0.46	0.093
536	B	0.16	0.13	4.90	0.46	0.093
537	B	0.25	0.28	4.90	0.46	0.093
538	B	0.33	0.36	4.90	0.46	0.093
539	B	0.39	0.41	4.90	0.46	0.093
540	B	0.00	0.00	3.81	0.46	0.093
541	B	0.14	0.08	3.81	0.46	0.093
542	B	0.26	0.18	3.81	0.46	0.093
543	B	0.42	0.31	3.81	0.46	0.093
544	B	0.54	0.47	3.81	0.46	0.093
545	B	0.64	0.61	3.81	0.46	0.093
546	B	0.00	0.00	4.89	0.46	0.093
547	B	0.09	0.07	4.89	0.46	0.093
548	B	0.16	0.13	4.89	0.46	0.093
549	B	0.26	0.24	4.89	0.46	0.093
550	B	0.33	0.32	4.89	0.46	0.093
551	B	0.39	0.40	4.89	0.46	0.093
552	B	0.00	0.00	4.82	0.46	0.093
553	B	0.09	0.08	4.82	0.46	0.093
554	B	0.16	0.13	4.82	0.46	0.093
555	B	0.26	0.27	4.82	0.46	0.093
556	B	0.34	0.39	4.82	0.46	0.093
557	B	0.40	0.47	4.82	0.46	0.093
558	B	0.00	0.00	4.52	0.46	0.093
559	B	0.10	0.08	4.52	0.46	0.093
560	B	0.18	0.17	4.52	0.46	0.093
561	B	0.30	0.33	4.52	0.46	0.093
562	B	0.38	0.50	4.52	0.46	0.093
563	B	0.45	0.62	4.52	0.46	0.093
564	B	0.00	0.00	4.01	0.46	0.093
565	B	0.13	0.11	4.01	0.46	0.093
566	B	0.23	0.21	4.01	0.46	0.093
567	B	0.38	0.36	4.01	0.46	0.093
568	B	0.49	0.45	4.01	0.46	0.093
569	B	0.58	0.58	4.01	0.46	0.093
570	B	0.00	0.00	3.77	0.46	0.093
571	B	0.15	0.09	3.77	0.46	0.093
572	B	0.26	0.19	3.77	0.46	0.093

TABLE A.1 (contd.)
TABULATED FIELD DATA

No.	Type	X_{s*}	t_*	u_o	D	β
573	B	0.43	0.37	3.77	0.46	0.093
574	B	0.55	0.50	3.77	0.46	0.093
575	B	0.65	0.65	3.77	0.46	0.093
576	P	0.00	0.00	6.05	0.53	0.095
577	P	0.06	0.02	6.05	0.53	0.095
578	P	0.11	0.05	6.05	0.53	0.095
579	P	0.16	0.10	6.05	0.53	0.095
580	P	0.21	0.16	6.05	0.53	0.095
581	P	0.25	0.23	6.05	0.53	0.095
582	P	0.00	0.00	3.76	0.53	0.095
583	P	0.14	0.09	3.76	0.53	0.095
584	P	0.28	0.17	3.76	0.53	0.095
585	P	0.40	0.27	3.76	0.53	0.095
586	P	0.51	0.36	3.76	0.53	0.095
587	P	0.00	0.00	3.55	0.53	0.095
588	P	0.16	0.09	3.55	0.53	0.095
589	P	0.31	0.20	3.55	0.53	0.095
590	P	0.45	0.32	3.55	0.53	0.095
591	P	0.00	0.00	4.39	0.53	0.095
592	P	0.10	0.08	4.39	0.53	0.095
593	P	0.21	0.17	4.39	0.53	0.095
594	P	0.30	0.36	4.39	0.53	0.095
595	P	0.00	0.00	5.41	0.53	0.095
596	P	0.07	0.04	5.41	0.53	0.095
597	P	0.14	0.12	5.41	0.53	0.095
598	P	0.21	0.19	5.41	0.53	0.095
599	P	0.27	0.26	5.41	0.53	0.095
600	P	0.32	0.35	5.41	0.53	0.095
601	P	0.00	0.00	4.23	0.53	0.095
602	P	0.11	0.09	4.23	0.53	0.095
603	P	0.22	0.25	4.23	0.53	0.095
604	P	0.32	0.42	4.23	0.53	0.095
605	P	0.00	0.00	2.85	0.53	0.095
606	P	0.25	0.28	2.85	0.53	0.095
607	P	0.49	0.49	2.85	0.53	0.095
608	P	0.00	0.00	4.35	0.53	0.095
609	P	0.11	0.09	4.35	0.53	0.095
610	P	0.22	0.19	4.35	0.53	0.095
611	P	0.32	0.29	4.35	0.53	0.095
612	P	0.41	0.42	4.35	0.53	0.095
613	P	0.00	0.00	3.60	0.53	0.095
614	P	0.16	0.14	3.60	0.53	0.095
615	P	0.31	0.34	3.60	0.53	0.095
616	P	0.46	0.55	3.60	0.53	0.095
617	P	0.00	0.00	5.40	0.53	0.095
618	P	0.07	0.04	5.40	0.53	0.095
619	P	0.14	0.07	5.40	0.53	0.095
620	P	0.21	0.12	5.40	0.53	0.095
621	P	0.27	0.17	5.40	0.53	0.095
622	P	0.32	0.21	5.40	0.53	0.095
623	P	0.00	0.00	4.17	0.53	0.095
624	P	0.12	0.09	4.17	0.53	0.095

TABLE A.1 (contd.)
TABULATED FIELD DATA

No.	Type	X_{s*}	t_*	u_o	D	β
625	P	0.23	0.21	4.17	0.53	0.095
626	P	0.35	0.30	4.17	0.53	0.095
627	P	0.00	0.00	4.33	0.53	0.095
628	P	0.11	0.09	4.33	0.53	0.095
629	P	0.22	0.19	4.33	0.53	0.095
630	P	0.32	0.35	4.33	0.53	0.095
631	P	0.41	0.47	4.33	0.53	0.095
632	P	0.00	0.00	5.77	0.41	0.128
633	P	0.07	0.03	5.77	0.41	0.128
634	P	0.14	0.09	5.77	0.41	0.128
635	P	0.22	0.13	5.77	0.41	0.128
636	P	0.31	0.20	5.77	0.41	0.128
637	P	0.40	0.32	5.77	0.41	0.128
638	P	0.00	0.00	4.62	0.41	0.128
639	P	0.10	0.08	4.62	0.41	0.128
640	P	0.22	0.19	4.62	0.41	0.128
641	P	0.34	0.48	4.62	0.41	0.128
642	P	0.00	0.00	5.80	0.41	0.128
643	P	0.07	0.04	5.80	0.41	0.128
644	P	0.14	0.09	5.80	0.41	0.128
645	P	0.22	0.14	5.80	0.41	0.128
646	P	0.31	0.20	5.80	0.41	0.128
647	P	0.40	0.27	5.80	0.41	0.128
648	P	0.00	0.00	3.73	0.41	0.128
649	P	0.16	0.14	3.73	0.41	0.128
650	P	0.34	0.33	3.73	0.41	0.128
651	P	0.52	0.82	3.73	0.41	0.128
652	P	0.00	0.00	4.28	0.41	0.128
653	P	0.12	0.13	4.28	0.41	0.128
654	P	0.26	0.23	4.28	0.41	0.128
655	P	0.40	0.38	4.28	0.41	0.128
656	P	0.57	0.67	4.28	0.41	0.128
657	P	0.00	0.00	4.87	0.41	0.128
658	P	0.11	0.06	4.87	0.41	0.128
659	P	0.21	0.12	4.87	0.41	0.128
660	P	0.35	0.27	4.87	0.41	0.128
661	P	0.48	0.45	4.87	0.41	0.128
662	P	0.00	0.00	4.20	0.41	0.128
663	P	0.12	0.08	4.20	0.41	0.128
664	P	0.27	0.16	4.20	0.41	0.128
665	P	0.41	0.30	4.20	0.41	0.128
666	P	0.59	0.51	4.20	0.41	0.128
667	P	0.76	0.90	4.20	0.41	0.128
668	P	0.00	0.00	4.93	0.41	0.128
669	P	0.09	0.06	4.93	0.41	0.128
670	P	0.19	0.12	4.93	0.41	0.128
671	P	0.30	0.25	4.93	0.41	0.128
672	P	0.43	0.45	4.93	0.41	0.128
673	P	0.55	0.65	4.93	0.41	0.128
674	P	0.00	0.00	4.26	0.41	0.128
675	P	0.12	0.07	4.26	0.41	0.128
676	P	0.26	0.16	4.26	0.41	0.128

TABLE A.1 (contd.)
TABULATED FIELD DATA

No.	Type	X_{s*}	t_*	u_o	D	β
677	P	0.40	0.34	4.26	0.41	0.128
678	P	0.57	0.71	4.26	0.41	0.128
679	P	0.00	0.00	4.85	0.41	0.128
680	P	0.09	0.07	4.85	0.41	0.128
681	P	0.20	0.18	4.85	0.41	0.128
682	P	0.31	0.35	4.85	0.41	0.128
683	P	0.44	0.59	4.85	0.41	0.128
684	P	0.00	0.00	3.67	0.41	0.128
685	P	0.16	0.15	3.67	0.41	0.128
686	P	0.35	0.34	3.67	0.41	0.128
687	P	0.00	0.00	4.22	0.41	0.128
688	P	0.12	0.10	4.22	0.41	0.128
689	P	0.27	0.31	4.22	0.41	0.128
690	P	0.00	0.00	5.10	0.29	0.134
691	P	0.08	0.05	5.10	0.29	0.134
692	P	0.16	0.10	5.10	0.29	0.134
693	P	0.24	0.14	5.10	0.29	0.134
694	P	0.33	0.23	5.10	0.29	0.134
695	P	0.42	0.34	5.10	0.29	0.134
696	P	0.00	0.00	3.75	0.29	0.134
697	P	0.14	0.14	3.75	0.29	0.134
698	P	0.29	0.25	3.75	0.29	0.134
699	P	0.45	0.36	3.75	0.29	0.134
700	P	0.62	0.59	3.75	0.29	0.134
701	P	0.00	0.00	3.64	0.29	0.134
702	P	0.15	0.08	3.64	0.29	0.134
703	P	0.31	0.19	3.64	0.29	0.134
704	P	0.48	0.36	3.64	0.29	0.134
705	P	0.00	0.00	3.72	0.29	0.134
706	P	0.15	0.14	3.72	0.29	0.134
707	P	0.30	0.29	3.72	0.29	0.134
708	P	0.46	0.46	3.72	0.29	0.134
709	P	0.63	0.71	3.72	0.29	0.134
710	P	0.00	0.00	3.93	0.29	0.134
711	P	0.13	0.09	3.93	0.29	0.134
712	P	0.27	0.19	3.93	0.29	0.134
713	P	0.41	0.28	3.93	0.29	0.134
714	P	0.56	0.36	3.93	0.29	0.134
715	P	0.71	0.54	3.93	0.29	0.134
716	P	0.00	0.00	4.34	0.29	0.134
717	P	0.11	0.10	4.34	0.29	0.134
718	P	0.22	0.20	4.34	0.29	0.134
719	P	0.33	0.44	4.34	0.29	0.134
720	P	0.46	0.64	4.34	0.29	0.134
721	P	0.00	0.00	4.86	0.29	0.134
722	P	0.09	0.10	4.86	0.29	0.134
723	P	0.18	0.16	4.86	0.29	0.134
724	P	0.27	0.24	4.86	0.29	0.134
725	P	0.37	0.35	4.86	0.29	0.134
726	P	0.46	0.50	4.86	0.29	0.134
727	P	0.00	0.00	4.22	0.29	0.134
728	P	0.11	0.09	4.22	0.29	0.134

TABLE A.1 (contd.)
TABULATED FIELD DATA

No.	Type	X_{s*}	t_*	u_o	D	β
729	P	0.23	0.22	4.22	0.29	0.134
730	P	0.35	0.35	4.22	0.29	0.134
731	P	0.49	0.57	4.22	0.29	0.134
732	P	0.00	0.00	4.15	0.29	0.134
733	P	0.12	0.07	4.15	0.29	0.134
734	P	0.25	0.15	4.15	0.29	0.134
735	P	0.39	0.38	4.15	0.29	0.134
736	P	0.52	0.58	4.15	0.29	0.134
737	P	0.00	0.00	2.84	0.29	0.134
738	P	0.25	0.29	2.84	0.29	0.134
739	P	0.51	0.62	2.84	0.29	0.134
740	P	0.00	0.00	4.49	0.29	0.134
741	P	0.10	0.10	4.49	0.29	0.134
742	P	0.21	0.19	4.49	0.29	0.134
743	P	0.31	0.28	4.49	0.29	0.134
744	P	0.43	0.44	4.49	0.29	0.134
745	P	0.54	0.66	4.49	0.29	0.134
746	P	0.00	0.00	4.34	0.29	0.134
747	P	0.11	0.06	4.34	0.29	0.134
748	P	0.22	0.14	4.34	0.29	0.134
749	P	0.33	0.25	4.34	0.29	0.134
750	P	0.46	0.38	4.34	0.29	0.134
751	P	0.58	0.64	4.34	0.29	0.134
752	P	0.00	0.00	3.40	0.29	0.134
753	P	0.17	-0.19	3.40	0.29	0.134
754	P	0.36	0.36	3.40	0.29	0.134
755	P	0.55	0.69	3.40	0.29	0.134
756	P	0.00	0.00	4.44	0.29	0.134
757	P	0.10	0.09	4.44	0.29	0.134
758	P	0.21	0.17	4.44	0.29	0.134
759	P	0.32	0.29	4.44	0.29	0.134
760	P	0.44	0.54	4.44	0.29	0.134
761	P	0.55	0.75	4.44	0.29	0.134
762	P	0.00	0.00	4.22	0.29	0.134
763	P	0.11	0.09	4.22	0.29	0.134
764	P	0.23	0.22	4.22	0.29	0.134
765	P	0.35	0.35	4.22	0.29	0.134
766	P	0.49	0.63	4.22	0.29	0.134
767	P	0.00	0.00	4.64	0.29	0.134
768	P	0.09	0.07	4.64	0.29	0.134
769	P	0.19	0.16	4.64	0.29	0.134
770	P	0.29	0.27	4.64	0.29	0.134
771	P	0.40	0.51	4.64	0.29	0.134
772	P	0.00	0.00	3.30	0.32	0.139
773	P	0.17	0.18	3.30	0.32	0.139
774	P	0.34	0.33	3.30	0.32	0.139
775	P	0.50	0.64	3.30	0.32	0.139
776	P	0.00	0.00	3.04	0.32	0.139
777	P	0.20	0.20	3.04	0.32	0.139
778	P	0.40	0.50	3.04	0.32	0.139
779	P	0.00	0.00	3.65	0.32	0.139
780	P	0.14	0.12	3.65	0.32	0.139

TABLE A.1 (contd.)
TABULATED FIELD DATA

No.	Type	X_{s*}	t_*	u_o	D	β
781	P	0.28	0.26	3.65	0.32	0.139
782	P	0.41	0.43	3.65	0.32	0.139
783	P	0.00	0.00	3.52	0.32	0.139
784	P	0.15	0.12	3.52	0.32	0.139
785	P	0.30	0.31	3.52	0.32	0.139
786	P	0.44	0.54	3.52	0.32	0.139
787	P	0.00	0.00	3.28	0.32	0.139
788	P	0.18	0.16	3.28	0.32	0.139
789	P	0.34	0.49	3.28	0.32	0.139
790	P	0.00	0.00	4.00	2.00	0.129
791	P	0.13	0.11	4.00	2.00	0.129
792	P	0.24	0.21	4.00	2.00	0.129
793	P	0.32	0.30	4.00	2.00	0.129
794	P	0.39	0.45	4.00	2.00	0.129
795	S	0.00	0.00	2.80	0.53	0.095
796	S	0.26	0.25	2.80	0.53	0.095
797	S	0.51	0.58	2.80	0.53	0.095
798	S	0.00	0.00	3.64	0.53	0.095
799	S	0.15	0.09	3.64	0.53	0.095
800	S	0.30	0.18	3.64	0.53	0.095
801	S	0.43	0.26	3.64	0.53	0.095
802	S	0.54	0.36	3.64	0.53	0.095
803	S	0.00	0.00	4.22	0.53	0.095
804	S	0.12	0.09	4.22	0.53	0.095
805	S	0.23	0.18	4.22	0.53	0.095
806	S	0.34	0.32	4.22	0.53	0.095
807	S	0.00	0.00	4.32	0.53	0.095
808	S	0.11	0.08	4.32	0.53	0.095
809	S	0.22	0.18	4.32	0.53	0.095
810	S	0.32	0.31	4.32	0.53	0.095
811	S	0.00	0.00	7.10	0.53	0.095
812	S	0.04	0.02	7.10	0.53	0.095
813	S	0.08	0.05	7.10	0.53	0.095
814	S	0.12	0.10	7.10	0.53	0.095
815	S	0.15	0.15	7.10	0.53	0.095
816	S	0.18	0.19	7.10	0.53	0.095
817	S	0.00	0.00	3.71	0.53	0.095
818	S	0.15	0.08	3.71	0.53	0.095
819	S	0.30	0.18	3.71	0.53	0.095
820	S	0.44	0.25	3.71	0.53	0.095
821	S	0.57	0.52	3.71	0.53	0.095
822	S	0.00	0.00	3.59	0.53	0.095
823	S	0.16	0.18	3.59	0.53	0.095
824	S	0.32	0.30	3.59	0.53	0.095
825	S	0.47	0.46	3.59	0.53	0.095
826	S	0.00	0.00	2.83	0.53	0.095
827	S	0.25	0.15	2.83	0.53	0.095
828	S	0.49	0.45	2.83	0.53	0.095
829	S	0.00	0.00	3.63	0.53	0.095
830	S	0.15	0.10	3.63	0.53	0.095
831	S	0.30	0.18	3.63	0.53	0.095
832	S	0.43	0.28	3.63	0.53	0.095

TABLE A.1 (contd.)
TABULATED FIELD DATA

No.	Type	X_{s*}	t_*	u_o	D	β
833	S	0.55	0.42	3.63	0.53	0.095
834	S	0.00	0.00	2.90	0.53	0.095
835	S	0.24	0.18	2.90	0.53	0.095
836	S	0.47	0.49	2.90	0.53	0.095
837	S	0.00	0.00	4.06	0.53	0.095
838	S	0.12	0.09	4.06	0.53	0.095
839	S	0.25	0.36	4.06	0.53	0.095
840	S	0.00	0.00	4.37	0.53	0.095
841	S	0.11	0.08	4.37	0.53	0.095
842	S	0.21	0.24	4.37	0.53	0.095
843	S	0.32	0.40	4.37	0.53	0.095
844	S	0.00	0.00	3.65	0.53	0.095
845	S	0.15	0.08	3.65	0.53	0.095
846	S	0.31	0.20	3.65	0.53	0.095
847	S	0.45	0.44	3.65	0.53	0.095
848	S	0.00	0.00	3.99	0.53	0.095
849	S	0.13	0.10	3.99	0.53	0.095
850	S	0.26	0.26	3.99	0.53	0.095
851	S	0.00	0.00	5.84	0.41	0.128
852	S	0.06	0.04	5.84	0.41	0.128
853	S	0.14	0.10	5.84	0.41	0.128
854	S	0.21	0.13	5.84	0.41	0.128
855	S	0.31	0.19	5.84	0.41	0.128
856	S	0.39	0.28	5.84	0.41	0.128
857	S	0.00	0.00	4.09	0.41	0.128
858	S	0.13	0.11	4.09	0.41	0.128
859	S	0.28	0.31	4.09	0.41	0.128
860	S	0.44	0.67	4.09	0.41	0.128
861	S	0.00	0.00	4.14	0.41	0.128
862	S	0.13	0.08	4.14	0.41	0.128
863	S	0.28	0.21	4.14	0.41	0.128
864	S	0.42	0.34	4.14	0.41	0.128
865	S	0.61	0.63	4.14	0.41	0.128
866	S	0.00	0.00	4.11	0.41	0.128
867	S	0.13	0.11	4.11	0.41	0.128
868	S	0.28	0.34	4.11	0.41	0.128
869	S	0.43	0.92	4.11	0.41	0.128
870	S	0.00	0.00	3.61	0.29	0.134
871	S	0.15	0.14	3.61	0.29	0.134
872	S	0.32	0.29	3.61	0.29	0.134
873	S	0.48	0.50	3.61	0.29	0.134
874	S	0.00	0.00	4.37	0.32	0.139
875	S	0.10	0.08	4.37	0.32	0.139
876	S	0.19	0.20	4.37	0.32	0.139
877	S	0.29	0.31	4.37	0.32	0.139
878	S	0.39	0.52	4.37	0.32	0.139
879	S	0.00	0.00	3.72	0.40	0.150
880	S	0.17	0.22	3.72	0.40	0.150
881	S	0.35	0.38	3.72	0.40	0.150
882	S	0.60	0.61	3.72	0.40	0.150
883	S	0.00	0.00	4.37	0.40	0.150
884	S	0.12	0.12	4.37	0.40	0.150

TABLE A.1 (contd.)
TABULATED FIELD DATA

No.	Type	X_{s*}	t_*	u_o	D	β
885	S	0.25	0.29	4.37	0.40	0.150
886	S	0.43	0.42	4.37	0.40	0.150
887	S	0.62	0.62	4.37	0.40	0.150
888	S	0.00	0.00	5.22	0.40	0.150
889	S	0.08	0.08	5.22	0.40	0.150
890	S	0.18	0.16	5.22	0.40	0.150
891	S	0.30	0.27	5.22	0.40	0.150
892	S	0.43	0.39	5.22	0.40	0.150
893	S	0.55	0.59	5.22	0.40	0.150
894	S	0.00	0.00	3.41	0.40	0.150
895	S	0.20	0.22	3.41	0.40	0.150
896	S	0.41	0.54	3.41	0.40	0.150
897	S	0.71	0.90	3.41	0.40	0.150
898	S	0.00	0.00	3.84	0.40	0.150
899	S	0.16	0.15	3.84	0.40	0.150
900	S	0.33	0.31	3.84	0.40	0.150
901	S	0.56	0.64	3.84	0.40	0.150
902	S	0.00	0.00	5.03	0.40	0.150
903	S	0.09	0.07	5.03	0.40	0.150
904	S	0.19	0.16	5.03	0.40	0.150
905	S	0.33	0.32	5.03	0.40	0.150
906	S	0.47	0.63	5.03	0.40	0.150
907	S	0.60	0.95	5.03	0.40	0.150
908	S	0.00	0.00	3.47	0.40	0.150
909	S	0.19	0.17	3.47	0.40	0.150
910	S	0.40	0.42	3.47	0.40	0.150
911	S	0.00	0.00	4.64	0.40	0.150
912	S	0.11	0.10	4.64	0.40	0.150
913	S	0.22	0.18	4.64	0.40	0.150
914	S	0.38	0.37	4.64	0.40	0.150
915	S	0.55	0.61	4.64	0.40	0.150
916	S	0.00	0.00	3.87	0.40	0.150
917	S	0.15	0.15	3.87	0.40	0.150
918	S	0.32	0.31	3.87	0.40	0.150
919	S	0.55	0.59	3.87	0.40	0.150
920	S	0.00	0.00	4.27	0.40	0.150
921	S	0.13	0.13	4.27	0.40	0.150
922	S	0.26	0.23	4.27	0.40	0.150
923	S	0.45	0.44	4.27	0.40	0.150
924	S	0.65	0.89	4.27	0.40	0.150
925	S	0.00	0.00	7.59	0.40	0.150
926	S	0.04	0.02	7.59	0.40	0.150
927	S	0.08	0.05	7.59	0.40	0.150
928	S	0.14	0.10	7.59	0.40	0.150
929	S	0.20	0.15	7.59	0.40	0.150
930	S	0.26	0.21	7.59	0.40	0.150
931	S	0.00	0.00	3.91	0.40	0.150
932	S	0.15	0.13	3.91	0.40	0.150
933	S	0.31	0.28	3.91	0.40	0.150
934	S	0.54	0.64	3.91	0.40	0.150
935	S	0.00	0.00	5.19	0.40	0.150
936	S	0.09	0.08	5.19	0.40	0.150

TABLE A.1 (contd.)
TABULATED FIELD DATA

No.	Type	X_{s*}	t_*	u_o	D	β
937	S	0.18	0.18	5.19	0.40	0.150
938	S	0.31	0.33	5.19	0.40	0.150
939	S	0.44	0.49	5.19	0.40	0.150
940	S	0.56	0.86	5.19	0.40	0.150
941	S	0.00	0.00	4.31	0.40	0.150
942	S	0.12	0.14	4.31	0.40	0.150
943	S	0.26	0.24	4.31	0.40	0.150
944	S	0.44	0.43	4.31	0.40	0.150
945	S	0.64	0.80	4.31	0.40	0.150
946	S	0.00	0.00	3.59	0.40	0.150
947	S	0.18	0.17	3.59	0.40	0.150
948	S	0.37	0.40	3.59	0.40	0.150
949	S	0.00	0.00	4.93	0.40	0.150
950	S	0.10	0.11	4.93	0.40	0.150
951	S	0.20	0.23	4.93	0.40	0.150
952	S	0.34	0.33	4.93	0.40	0.150
953	S	0.49	0.48	4.93	0.40	0.150
954	S	0.62	0.63	4.93	0.40	0.150
955	S	0.00	0.00	4.73	0.40	0.150
956	S	0.10	0.10	4.73	0.40	0.150
957	S	0.21	0.19	4.73	0.40	0.150
958	S	0.37	0.33	4.73	0.40	0.150
959	S	0.53	0.58	4.73	0.40	0.150
960	S	0.00	0.00	4.19	0.40	0.150
961	S	0.13	-0.12	4.19	0.40	0.150
962	S	0.27	0.25	4.19	0.40	0.150
963	S	0.47	0.58	4.19	0.40	0.150
964	S	0.00	0.00	5.61	0.40	0.150
965	S	0.07	0.06	5.61	0.40	0.150
966	S	0.15	0.14	5.61	0.40	0.150
967	S	0.26	0.25	5.61	0.40	0.150
968	S	0.37	0.37	5.61	0.40	0.150
969	S	0.48	0.59	5.61	0.40	0.150
970	S	0.00	0.00	4.67	0.40	0.150
971	S	0.11	0.10	4.67	0.40	0.150
972	S	0.22	0.21	4.67	0.40	0.150
973	S	0.38	0.33	4.67	0.40	0.150
974	S	0.54	0.59	4.67	0.40	0.150
975	S	0.00	0.00	3.88	0.40	0.150
976	S	0.15	0.10	3.88	0.40	0.150
977	S	0.32	0.25	3.88	0.40	0.150
978	S	0.55	0.46	3.88	0.40	0.150
979	S	0.78	0.76	3.88	0.40	0.150
980	S	0.00	0.00	3.62	0.40	0.150
981	S	0.18	0.20	3.62	0.40	0.150
982	S	0.37	0.44	3.62	0.40	0.150
983	S	0.63	0.72	3.62	0.40	0.150
984	S	0.90	1.31	3.62	0.40	0.150
985	S	0.00	0.00	4.76	0.40	0.150
986	S	0.10	0.09	4.76	0.40	0.150
987	S	0.21	0.19	4.76	0.40	0.150
988	S	0.36	0.36	4.76	0.40	0.150

TABLE A.1 (contd.)
TABULATED FIELD DATA

No.	Type	X_{s*}	t_*	u_o	D	β
989	S	0.52	0.55	4.76	0.40	0.150
990	S	0.66	0.84	4.76	0.40	0.150
991	S	0.00	0.00	4.51	0.40	0.150
992	S	0.11	0.16	4.51	0.40	0.150
993	S	0.24	0.25	4.51	0.40	0.150
994	S	0.41	0.45	4.51	0.40	0.150
995	S	0.58	0.66	4.51	0.40	0.150
996	S	0.74	0.98	4.51	0.40	0.150
997	S	0.00	0.00	3.52	0.40	0.150
998	S	0.19	0.20	3.52	0.40	0.150
999	S	0.39	0.38	3.52	0.40	0.150
1000	S	0.67	0.87	3.52	0.40	0.150
1001	S	0.00	0.00	5.39	0.40	0.150
1002	S	0.08	0.07	5.39	0.40	0.150
1003	S	0.17	0.14	5.39	0.40	0.150
1004	S	0.28	0.27	5.39	0.40	0.150
1005	S	0.41	0.38	5.39	0.40	0.150
1006	S	0.52	0.54	5.39	0.40	0.150
1007	S	0.00	0.00	3.25	0.40	0.150
1008	S	0.22	0.23	3.25	0.40	0.150
1009	S	0.45	0.58	3.25	0.40	0.150
1010	S	0.78	1.18	3.25	0.40	0.150
1011	S	0.00	0.00	3.00	0.40	0.150
1012	S	0.26	0.26	3.00	0.40	0.150
1013	S	0.53	0.62	3.00	0.40	0.150
1014	S	0.00	0.00	4.30	0.40	0.150
1015	S	0.13	0.08	4.30	0.40	0.150
1016	S	0.26	0.18	4.30	0.40	0.150
1017	S	0.45	0.37	4.30	0.40	0.150
1018	S	0.64	0.56	4.30	0.40	0.150
1019	S	0.81	1.04	4.30	0.40	0.150
1020	S	0.00	0.00	3.01	0.40	0.150
1021	S	0.26	0.27	3.01	0.40	0.150
1022	S	0.53	0.61	3.01	0.40	0.150
1023	S	0.00	0.00	5.08	0.40	0.150
1024	S	0.09	0.08	5.08	0.40	0.150
1025	S	0.19	0.17	5.08	0.40	0.150
1026	S	0.32	0.28	5.08	0.40	0.150
1027	S	0.46	0.43	5.08	0.40	0.150
1028	S	0.58	0.66	5.08	0.40	0.150
1029	S	0.00	0.00	4.34	0.40	0.150
1030	S	0.12	0.20	4.34	0.40	0.150
1031	S	0.26	0.51	4.34	0.40	0.150
1032	S	0.44	0.90	4.34	0.40	0.150
1033	S	0.00	0.00	4.41	0.40	0.150
1034	S	0.12	0.09	4.41	0.40	0.150
1035	S	0.25	0.20	4.41	0.40	0.150
1036	S	0.42	0.40	4.41	0.40	0.150
1037	S	0.00	0.00	4.60	0.40	0.150
1038	S	0.11	0.10	4.60	0.40	0.150
1039	S	0.23	0.22	4.60	0.40	0.150
1040	S	0.39	0.38	4.60	0.40	0.150

TABLE A.1 (contd.)
TABULATED FIELD DATA

No.	Type	X_{s*}	t_*	u_o	D	β
1041	S	0.56	0.65	4.60	0.40	0.150
1042	S	0.71	0.91	4.60	0.40	0.150
1043	S	0.00	0.00	4.82	0.40	0.150
1044	S	0.10	0.09	4.82	0.40	0.150
1045	S	0.21	0.18	4.82	0.40	0.150
1046	S	0.35	0.37	4.82	0.40	0.150
1047	S	0.51	0.62	4.82	0.40	0.150
1048	S	0.65	0.95	4.82	0.40	0.150
1049	S	0.00	0.00	3.01	2.00	0.129
1050	S	0.24	0.25	3.01	2.00	0.129
1051	S	0.42	0.47	3.01	2.00	0.129
1052	S	0.57	0.80	3.01	2.00	0.129
1053	S	0.70	1.29	3.01	2.00	0.129
1054	S	0.00	0.00	3.13	2.00	0.129
1055	S	0.22	0.22	3.13	2.00	0.129
1056	S	0.38	0.43	3.13	2.00	0.129
1057	S	0.53	0.85	3.13	2.00	0.129
1058	S	0.00	0.00	3.43	2.00	0.129
1059	S	0.18	0.19	3.43	2.00	0.129
1060	S	0.32	0.32	3.43	2.00	0.129
1061	S	0.44	0.43	3.43	2.00	0.129
1062	S	0.54	0.64	3.43	2.00	0.129
1063	S	0.00	0.00	4.42	2.00	0.129
1064	S	0.11	0.09	4.42	2.00	0.129
1065	S	0.19	0.17	4.42	2.00	0.129
1066	S	0.26	0.26	4.42	2.00	0.129
1067	S	0.32	0.37	4.42	2.00	0.129
1068	S	0.39	0.46	4.42	2.00	0.129
1069	S	0.00	0.00	4.15	2.00	0.129
1070	S	0.12	0.31	4.15	2.00	0.129
1071	S	0.22	0.50	4.15	2.00	0.129
1072	S	0.30	0.60	4.15	2.00	0.129
1073	S	0.37	0.76	4.15	2.00	0.129
1074	S	0.00	0.00	2.50	2.00	0.129
1075	S	0.34	0.50	2.50	2.00	0.129
1076	S	0.60	0.81	2.50	2.00	0.129
1077	S	0.00	0.00	3.95	2.00	0.129
1078	S	0.14	0.11	3.95	2.00	0.129
1079	S	0.24	0.21	3.95	2.00	0.129
1080	S	0.33	0.28	3.95	2.00	0.129
1081	S	0.40	0.40	3.95	2.00	0.129
1082	S	0.48	0.63	3.95	2.00	0.129
1083	S	0.00	0.00	4.43	2.00	0.129
1084	S	0.11	0.08	4.43	2.00	0.129
1085	S	0.19	0.16	4.43	2.00	0.129
1086	S	0.26	0.23	4.43	2.00	0.129
1087	S	0.32	0.30	4.43	2.00	0.129
1088	S	0.38	0.48	4.43	2.00	0.129
1089	S	0.00	0.00	4.33	4.21	0.139
1090	S	0.10	0.15	4.33	4.21	0.139
1091	S	0.21	0.25	4.33	4.21	0.139
1092	S	0.33	0.42	4.33	4.21	0.139

TABLE A.1 (contd.)
TABULATED FIELD DATA

No.	Type	X_{s*}	t_*	u_o	D	β
1093	S	0.43	0.73	4.33	4.21	0.139
1094	S	0.00	0.00	4.70	4.21	0.139
1095	S	0.08	0.07	4.70	4.21	0.139
1096	S	0.18	0.12	4.70	4.21	0.139
1097	S	0.28	0.17	4.70	4.21	0.139
1098	S	0.37	0.25	4.70	4.21	0.139
1099	S	0.44	0.34	4.70	4.21	0.139
1100	S	0.00	0.00	4.52	4.21	0.139
1101	S	0.11	0.08	4.52	4.21	0.139
1102	S	0.21	0.20	4.52	4.21	0.139
1103	S	0.31	0.30	4.52	4.21	0.139
1104	S	0.38	0.38	4.52	4.21	0.139
1105	S	0.00	0.00	7.18	4.21	0.139
1106	S	0.04	0.02	7.18	4.21	0.139
1107	S	0.08	0.06	7.18	4.21	0.139
1108	S	0.12	0.11	7.18	4.21	0.139
1109	S	0.16	0.16	7.18	4.21	0.139
1110	S	0.19	0.21	7.18	4.21	0.139
1111	S	0.00	0.00	6.46	4.21	0.139
1112	S	0.04	0.03	6.46	4.21	0.139
1113	S	0.10	0.06	6.46	4.21	0.139
1114	S	0.15	0.12	6.46	4.21	0.139
1115	S	0.19	0.18	6.46	4.21	0.139
1116	S	0.23	0.23	6.46	4.21	0.139
1117	S	0.00	0.00	4.19	4.21	0.139
1118	S	0.10	0.08	4.19	4.21	0.139
1119	S	0.23	0.19	4.19	4.21	0.139
1120	S	0.35	0.27	4.19	4.21	0.139
1121	S	0.46	0.42	4.19	4.21	0.139
1122	S	0.55	0.53	4.19	4.21	0.139

Type refers to initial wave type: B=bore P=plunge S=surge
D is given in mm

TABLE A.2
TABULATED FIELD DATA

No.	Type	H	u_o	z_s	$\bar{U}_s$	D	β	$t_{(max)}$
1	B	0.10	2.99	0.35	0.85	0.49	0.107	3.85
2	B	0.30	4.31	0.72	1.93	0.49	0.107	3.47
3	B	0.30	3.77	0.55	1.36	0.49	0.107	3.80
4	B	0.40	3.71	0.43	1.07	0.49	0.107	3.75
5	B	0.45	4.56	0.89	1.98	0.49	0.107	4.17
6	B	0.35	3.69	0.54	1.07	0.49	0.107	4.70
7	B	0.35	3.06	0.34	1.14	0.49	0.107	2.75
8	B	0.30	4.17	0.78	1.80	0.49	0.107	4.05
9	B	0.35	4.60	0.58	1.35	0.49	0.107	4.05
10	B	0.45	3.60	0.49	1.26	0.49	0.107	3.65
11	B	0.35	4.16	0.52	1.83	0.49	0.107	2.65
12	B	0.25	3.95	0.70	1.68	0.49	0.107	3.90
13	B	0.30	4.03	0.71	1.72	0.49	0.107	3.85
14	B	0.45	4.42	0.63	1.96	0.49	0.107	3.00
15	B	0.35	3.68	0.54	1.04	0.49	0.107	4.85
16	B	0.30	3.85	0.65	2.28	0.79	0.123	2.33
17	B	0.30	4.23	0.51	1.74	0.79	0.123	2.40
18	B	0.55	4.17	0.86	2.24	0.79	0.123	3.15
19	B	0.30	4.44	0.82	1.84	0.79	0.123	3.65
20	B	0.25	4.58	0.84	1.79	0.79	0.123	3.82
21	B	0.45	4.00	0.73	1.79	0.79	0.123	3.33
22	B	0.40	4.76	0.64	1.67	0.79	0.123	3.12
23	B	0.35	3.33	0.36	1.26	0.79	0.123	2.35
24	B	0.35	3.19	0.37	1.03	0.79	0.123	2.93
25	B	0.45	4.12	0.58	1.25	0.79	0.123	3.80
26	B	0.40	4.11	0.37	1.22	0.79	0.123	2.50
27	B	0.40	4.61	0.83	1.75	0.79	0.123	3.87
28	B	0.35	4.19	0.52	1.56	0.79	0.123	2.71
29	B	0.40	5.21	0.68	1.72	0.79	0.123	3.25
30	B	0.35	4.49	0.61	1.55	0.79	0.123	3.23
31	B	0.45	3.85	0.44	1.55	0.79	0.123	2.30
32	B	0.45	4.15	0.64	1.72	0.79	0.123	3.05
33	B	0.30	3.99	0.59	1.41	0.79	0.123	3.40
34	B	0.70	7.61	1.28	3.07	0.79	0.123	3.40
35	B	0.45	4.47	0.77	1.81	0.79	0.123	3.45
36	B	0.45	4.73	0.79	1.75	0.79	0.123	3.70
37	B	0.25	3.97	0.62	1.23	0.79	0.123	4.10
38	B	0.40	3.90	0.52	1.40	0.79	0.123	3.02
39	B	0.45	4.26	0.52	1.61	0.79	0.123	2.65
40	B	0.30	3.53	0.35	1.18	0.79	0.123	2.45
41	B	0.40	4.02	0.47	1.58	0.79	0.123	2.42
42	B	0.40	3.48	0.46	1.26	0.79	0.123	3.00
43	B	0.55	4.17	0.57	1.64	0.41	0.128	2.70
44	B	0.50	4.11	0.57	1.86	0.41	0.128	2.40
45	B	0.30	3.29	0.26	0.90	0.41	0.128	2.27
46	B	0.65	4.83	0.79	2.35	0.41	0.128	2.65
47	B	0.60	5.52	0.94	1.97	0.41	0.128	3.73
48	B	0.60	4.34	0.56	1.25	0.41	0.128	3.50
49	B	0.55	4.15	0.56	1.61	0.41	0.128	2.72
50	B	0.55	4.62	0.72	1.61	0.41	0.128	3.50
51	B	0.20	3.56	0.39	1.40	0.41	0.128	2.20
52	B	0.40	3.76	0.64	1.77	0.41	0.128	2.82

TABLE A.2 (contd.)
TABULATED FIELD DATA

No.	Type	H	u_o	Z_s	$\bar{U}_s$	D	β	$t_{(max)}$
53	B	0.40	4.17	0.36	1.45	0.41	0.128	1.95
54	B	0.50	3.92	0.43	1.84	0.41	0.128	1.82
55	B	0.40	3.72	0.47	1.58	0.41	0.128	2.30
56	B	0.40	3.90	0.42	1.64	0.41	0.128	2.00
57	B	0.15	3.81	0.48	1.11	0.29	0.134	3.20
58	B	0.20	4.09	0.58	1.41	0.29	0.134	3.08
59	B	0.20	4.12	0.49	1.04	0.32	0.139	3.40
60	B	0.20	3.56	0.46	1.12	0.32	0.139	2.95
61	B	0.15	2.96	0.22	0.74	2.00	0.129	2.27
62	B	0.50	4.03	0.73	1.37	0.44	0.147	3.67
63	B	0.30	5.12	0.89	1.64	0.44	0.147	3.72
64	B	0.70	4.19	0.46	1.31	0.44	0.147	2.42
65	B	0.80	3.59	0.51	1.37	0.44	0.147	2.55
66	B	0.40	4.76	0.62	1.37	0.44	0.147	3.10
67	B	0.60	4.55	0.81	1.84	0.44	0.147	3.02
68	B	0.25	3.43	0.33	1.19	0.44	0.147	1.87
69	B	0.55	4.73	0.59	1.47	0.44	0.147	2.73
70	B	0.60	4.46	0.63	1.54	0.44	0.147	2.80
71	B	0.40	2.76	0.32	1.00	0.44	0.147	2.16
72	B	0.55	4.59	0.89	1.79	0.44	0.147	3.40
73	B	0.70	3.08	0.35	0.92	0.44	0.147	2.62
74	B	0.55	5.27	0.86	1.96	0.44	0.147	3.00
75	B	0.45	5.00	0.58	1.22	0.44	0.147	3.25
76	B	0.60	3.87	0.46	1.20	0.44	0.147	2.62
77	B	0.60	4.28	0.61	1.30	0.44	0.147	3.20
78	B	0.65	4.87	0.78	2.07	0.44	0.147	2.58
79	B	0.65	4.02	0.75	1.65	0.44	0.147	3.10
80	B	0.40	4.29	0.44	1.12	0.44	0.147	2.65
81	B	0.45	4.44	0.50	0.95	0.44	0.147	3.60
82	B	0.50	3.78	0.41	1.49	0.44	0.147	1.88
83	B	0.45	4.80	0.96	2.21	0.31	0.135	3.23
84	B	0.50	6.21	0.71	1.58	0.31	0.135	3.37
85	B	0.60	4.97	0.95	2.66	0.31	0.135	2.65
86	B	0.30	4.09	0.47	1.55	0.31	0.135	2.27
87	B	0.60	5.79	1.09	2.89	0.31	0.135	2.80
88	B	0.60	4.38	0.90	2.31	0.31	0.135	2.90
89	B	0.30	4.36	0.71	1.69	0.31	0.135	3.12
90	B	0.40	3.94	0.60	1.81	0.31	0.135	2.47
91	B	0.65	3.45	0.48	1.63	0.31	0.135	2.20
92	B	0.45	4.11	0.89	2.87	0.31	0.135	2.30
93	B	0.50	4.14	0.93	2.19	0.31	0.135	3.15
94	B	0.50	4.26	0.52	2.07	0.31	0.135	1.88
95	B	0.45	4.71	0.75	1.64	0.31	0.135	3.42
96	B	0.50	5.32	0.92	2.10	0.31	0.135	3.28
97	B	0.50	5.25	0.94	2.34	0.31	0.135	2.98
98	B	0.50	3.91	0.86	1.94	0.31	0.135	3.30
99	B	0.55	4.74	0.89	1.82	0.31	0.135	3.62
100	B	0.30	3.57	0.35	0.94	0.31	0.135	2.80
101	B	0.50	4.62	0.64	1.39	0.31	0.135	3.40
102	B	0.50	6.07	0.91	2.60	0.31	0.135	2.60
103	B	0.40	3.83	0.55	1.69	0.31	0.135	2.42
104	B	0.25	3.24	0.28	1.01	0.46	0.093	2.98

TABLE A.2 (contd.)
TABULATED FIELD DATA

No.	Type	H	u_o	Z_s	$\bar{U}_s$	D	β	$t_{(max)}$
105	B	0.30	3.88	0.64	1.61	0.46	0.093	4.30
106	B	0.40	3.37	0.33	1.15	0.46	0.093	3.10
107	B	0.55	4.90	0.91	1.52	0.46	0.093	6.47
108	B	0.40	3.81	0.53	1.43	0.46	0.093	4.00
109	B	0.45	4.89	0.80	2.43	0.46	0.093	3.57
110	B	0.45	4.82	0.75	2.19	0.46	0.093	3.70
111	B	0.35	4.52	0.77	1.88	0.46	0.093	4.40
112	B	0.40	4.01	0.72	2.54	0.46	0.093	3.05
113	B	0.45	3.77	0.69	1.51	0.46	0.093	4.95
114	P	0.45	6.05	0.55	2.00	0.53	0.095	2.90
115	P	0.45	3.76	0.49	1.95	0.53	0.095	2.65
116	P	0.30	3.55	0.36	1.56	0.53	0.095	2.42
117	P	0.25	4.39	0.32	1.71	0.53	0.095	2.00
118	P	0.30	5.41	0.52	2.03	0.53	0.095	2.70
119	P	0.35	4.23	0.31	1.03	0.53	0.095	3.15
120	P	0.20	2.85	0.25	1.20	0.53	0.095	2.23
121	P	0.25	4.35	0.44	1.68	0.53	0.095	2.78
122	P	0.35	3.60	0.36	1.33	0.53	0.095	2.82
123	P	0.65	5.40	0.64	2.16	0.53	0.095	3.13
124	P	0.40	4.17	0.36	1.98	0.53	0.095	1.92
125	P	0.40	4.33	0.44	1.52	0.53	0.095	3.05
126	P	0.60	5.77	1.02	1.99	0.41	0.128	4.00
127	P	0.65	4.62	0.43	1.68	0.41	0.128	2.00
128	P	1.10	5.80	1.18	2.56	0.41	0.128	3.60
129	P	0.30	3.73	0.37	0.99	0.41	0.128	2.90
130	P	0.20	4.28	0.58	1.55	0.41	0.128	2.93
131	P	0.90	4.87	0.67	1.85	0.41	0.128	2.85
132	P	0.35	4.20	0.68	1.60	0.41	0.128	3.33
133	P	0.40	4.93	0.76	1.71	0.41	0.128	3.47
134	P	0.25	4.26	0.53	1.50	0.41	0.128	2.75
135	P	0.20	4.85	0.59	1.38	0.41	0.128	3.35
136	P	0.35	3.67	0.31	1.62	0.41	0.128	1.50
137	P	0.60	4.22	0.31	1.57	0.41	0.128	1.55
138	P	0.40	5.10	0.67	1.83	0.29	0.134	2.72
139	P	0.45	3.75	0.51	1.61	0.29	0.134	2.38
140	P	0.40	3.64	0.42	1.95	0.29	0.134	1.62
141	P	0.20	3.72	0.50	1.48	0.29	0.134	2.52
142	P	0.55	3.93	0.65	2.10	0.29	0.134	2.30
143	P	0.40	4.34	0.55	1.49	0.29	0.134	2.75
144	P	0.25	4.86	0.63	1.86	0.29	0.134	2.53
145	P	0.25	4.22	0.51	1.80	0.29	0.134	2.10
146	P	0.20	4.15	0.51	1.49	0.29	0.134	2.55
147	P	0.25	2.84	0.30	0.88	0.29	0.134	2.50
148	P	0.55	4.49	0.57	1.55	0.29	0.134	2.75
149	P	0.40	4.34	0.61	1.59	0.29	0.134	2.85
150	P	0.35	3.40	0.34	1.05	0.29	0.134	2.40
151	P	0.20	4.44	0.60	1.25	0.29	0.134	3.57
152	P	0.55	4.22	0.51	1.02	0.29	0.134	3.75
153	P	0.35	4.64	0.52	1.41	0.29	0.134	2.75
154	P	0.35	3.30	0.31	1.13	0.32	0.139	1.98
155	P	0.25	3.04	0.26	1.10	0.32	0.139	1.70
156	P	0.40	3.65	0.34	1.34	0.32	0.139	1.80

TABLE A.2 (contd.)
TABULATED FIELD DATA

No.	Type	H	u_o	Z_s	$\bar{U}_s$	D	β	$t_{(max)}$
157	P	0.35	3.52	0.33	0.98	0.32	0.139	2.40
158	P	0.30	3.28	0.21	0.93	0.32	0.139	1.65
159	P	0.30	4.00	0.34	1.29	2.00	0.129	2.08
160	S	0.20	2.80	0.23	1.21	0.53	0.095	2.00
161	S	0.30	3.64	0.43	1.45	0.53	0.095	3.15
162	S	0.25	4.22	0.35	1.21	0.53	0.095	3.07
163	S	0.25	4.32	0.35	1.76	0.53	0.095	2.10
164	S	0.35	7.10	0.60	2.03	0.53	0.095	3.10
165	S	0.35	3.71	0.42	1.96	0.53	0.095	2.25
166	S	0.15	3.59	0.35	1.41	0.53	0.095	2.62
167	S	0.30	2.83	0.25	1.19	0.53	0.095	2.20
168	S	0.25	3.63	0.43	1.73	0.53	0.095	2.60
169	S	0.35	2.90	0.25	1.06	0.53	0.095	2.45
170	S	0.30	4.06	0.22	1.17	0.53	0.095	1.95
171	S	0.30	4.37	0.33	1.46	0.53	0.095	2.40
172	S	0.25	3.65	0.33	1.78	0.53	0.095	1.95
173	S	0.30	3.99	0.26	1.71	0.53	0.095	1.60
174	S	0.80	5.84	1.18	2.80	0.41	0.128	3.30
175	S	0.40	4.09	0.43	1.11	0.41	0.128	3.00
176	S	0.50	4.14	0.61	1.70	0.41	0.128	2.80
177	S	0.55	4.11	0.42	0.79	0.41	0.128	4.15
178	S	0.40	3.61	0.40	1.31	0.29	0.134	2.30
179	S	0.20	4.37	0.42	1.08	0.32	0.139	2.80
180	S	0.60	3.72	0.57	1.23	0.40	0.150	3.10
181	S	0.40	4.37	0.69	1.31	0.40	0.150	3.55
182	S	0.65	5.22	0.87	1.72	0.40	0.150	3.40
183	S	0.40	3.41	0.56	1.14	0.40	0.150	3.27
184	S	0.35	3.84	0.55	1.18	0.40	0.150	3.15
185	S	0.50	5.03	0.78	1.18	0.40	0.150	4.45
186	S	0.25	3.47	0.38	1.20	0.40	0.150	2.10
187	S	0.55	4.64	0.65	1.40	0.40	0.150	3.12
188	S	0.35	3.87	0.59	1.33	0.40	0.150	2.95
189	S	0.30	4.27	0.63	1.11	0.40	0.150	3.82
190	S	0.75	7.59	1.37	2.63	0.40	0.150	3.47
191	S	0.25	3.91	0.48	0.99	0.40	0.150	3.22
192	S	0.40	5.19	0.78	1.34	0.40	0.150	3.87
193	S	0.35	4.31	0.64	1.30	0.40	0.150	3.30
194	S	0.25	3.59	0.40	1.31	0.40	0.150	2.05
195	S	0.55	4.93	0.95	1.64	0.40	0.150	3.85
196	S	0.60	4.73	0.72	1.50	0.40	0.150	3.20
197	S	0.15	4.19	0.45	1.08	0.40	0.150	2.80
198	S	0.60	5.61	0.86	1.86	0.40	0.150	3.10
199	S	0.45	4.67	0.75	1.22	0.40	0.150	4.10
200	S	0.45	3.88	0.66	1.20	0.40	0.150	3.70
201	S	0.25	3.62	0.62	1.11	0.40	0.150	3.70
202	S	0.60	4.76	0.84	1.55	0.40	0.150	3.65
203	S	0.55	4.51	0.86	1.52	0.40	0.150	3.80
204	S	0.50	3.52	0.48	1.07	0.40	0.150	2.97
205	S	0.65	5.39	0.99	1.77	0.40	0.150	3.75
206	S	0.30	3.25	0.44	1.01	0.40	0.150	2.95
207	S	0.30	3.00	0.27	1.04	0.40	0.150	1.75
208	S	0.55	4.30	0.76	1.37	0.40	0.150	3.70

TABLE A.2 (contd.)
TABULATED FIELD DATA

No.	Type	H	u_o	z_s	$\bar{U}_s$	D	β	$t_{(max)}$
209	S	0.20	3.01	0.33	0.75	0.40	0.150	2.95
210	S	0.50	5.08	0.84	1.52	0.40	0.150	3.70
211	S	0.30	4.34	0.59	1.07	0.40	0.150	3.70
212	S	0.25	4.41	0.54	1.07	0.40	0.150	3.40
213	S	0.65	4.60	0.87	1.42	0.40	0.150	4.10
214	S	0.50	4.82	0.86	1.41	0.40	0.150	4.10
215	S	0.10	3.01	0.32	0.74	2.00	0.129	3.40
216	S	0.30	3.13	0.32	0.93	2.00	0.129	2.70
217	S	0.30	3.43	0.36	1.25	2.00	0.129	2.20
218	S	0.30	4.42	0.48	1.79	2.00	0.129	2.10
219	S	0.10	4.15	0.36	0.85	2.00	0.129	3.30
220	S	0.10	2.50	0.25	0.55	2.00	0.129	3.50
221	S	0.20	3.95	0.39	1.10	2.00	0.129	2.80
222	S	0.20	4.43	0.39	1.08	2.00	0.129	2.85
223	S	0.50	4.33	0.41	1.14	4.21	0.139	2.63
224	S	0.60	4.70	0.62	1.73	4.21	0.139	2.60
225	S	0.40	4.52	0.54	1.50	4.21	0.139	2.60
226	S	0.55	7.18	0.78	2.94	4.21	0.139	1.92
227	S	0.60	6.46	0.66	1.75	4.21	0.139	2.75
228	S	0.40	4.19	0.53	1.59	4.21	0.139	2.42

Type refers to initial wave type: B=bore P=plunge S=surge
D is given in mm

TABLE A.3
TABULATED FIELD DATA

No.	Type	$h_{s*(max)}$	x_*	u_o	D	β
1	B	0.1821	0.25	2.99	0.49	0.107
2	B	0.1194	0.49	2.99	0.49	0.107
3	B	0.0050	0.76	2.99	0.49	0.107
4	B	0.1468	0.12	4.31	0.49	0.107
5	B	0.1211	0.24	4.31	0.49	0.107
6	B	0.0961	0.37	4.31	0.49	0.107
7	B	0.0509	0.50	4.31	0.49	0.107
8	B	0.0214	0.64	4.31	0.49	0.107
9	B	0.2064	0.15	3.77	0.49	0.107
10	B	0.1489	0.31	3.77	0.49	0.107
11	B	0.0961	0.48	3.77	0.49	0.107
12	B	0.0264	0.65	3.77	0.49	0.107
13	B	0.1763	0.16	3.71	0.49	0.107
14	B	0.0989	0.32	3.71	0.49	0.107
15	B	0.0496	0.50	3.71	0.49	0.107
16	B	0.2332	0.11	4.56	0.49	0.107
17	B	0.1629	0.21	4.56	0.49	0.107
18	B	0.1393	0.33	4.56	0.49	0.107
19	B	0.0671	0.44	4.56	0.49	0.107
20	B	0.0475	0.57	4.56	0.49	0.107
21	B	0.1797	0.16	3.69	0.49	0.107
22	B	0.1197	0.32	3.69	0.49	0.107
23	B	0.0759	0.50	3.69	0.49	0.107
24	B	0.0183	0.68	3.69	0.49	0.107
25	B	0.2085	0.23	3.06	0.49	0.107
26	B	0.0913	0.47	3.06	0.49	0.107
27	B	0.2039	0.13	4.17	0.49	0.107
28	B	0.1609	0.25	4.17	0.49	0.107
29	B	0.1406	0.39	4.17	0.49	0.107
30	B	0.0731	0.53	4.17	0.49	0.107
31	B	0.0488	0.68	4.17	0.49	0.107
32	B	0.1015	0.10	4.60	0.49	0.107
33	B	0.0877	0.22	4.60	0.49	0.107
34	B	0.0271	0.33	4.60	0.49	0.107
35	B	0.0071	0.46	4.60	0.49	0.107
36	B	0.1756	0.17	3.60	0.49	0.107
37	B	0.1224	0.34	3.60	0.49	0.107
38	B	0.0874	0.53	3.60	0.49	0.107
39	B	0.0204	0.71	3.60	0.49	0.107
40	B	0.2121	0.13	4.16	0.49	0.107
41	B	0.1469	0.25	4.16	0.49	0.107
42	B	0.0887	0.39	4.16	0.49	0.107
43	B	0.0133	0.53	4.16	0.49	0.107
44	B	0.1742	0.14	3.95	0.49	0.107
45	B	0.1353	0.28	3.95	0.49	0.107
46	B	0.1113	0.44	3.95	0.49	0.107
47	B	0.0424	0.59	3.95	0.49	0.107
48	B	0.0163	0.76	3.95	0.49	0.107
49	B	0.3233	0.14	4.03	0.49	0.107
50	B	0.2088	0.27	4.03	0.49	0.107
51	B	0.1629	0.42	4.03	0.49	0.107
52	B	0.0739	0.57	4.03	0.49	0.107

TABLE A.3 (contd.)
TABULATED FIELD DATA

No.	Type	$h_{s*(max)}$	x_*	u_o	D	β
53	B	0.0254	0.73	4.03	0.49	0.107
54	B	0.1072	0.11	4.42	0.49	0.107
55	B	0.0883	0.24	4.42	0.49	0.107
56	B	0.0448	0.36	4.42	0.49	0.107
57	B	0.0150	0.49	4.42	0.49	0.107
58	B	0.3747	0.16	3.68	0.49	0.107
59	B	0.2403	0.32	3.68	0.49	0.107
60	B	0.1677	0.50	3.68	0.49	0.107
61	B	0.0329	0.68	3.68	0.49	0.107
62	B	0.1523	0.17	3.85	0.79	0.123
63	B	0.1222	0.32	3.85	0.79	0.123
64	B	0.0953	0.48	3.85	0.79	0.123
65	B	0.0718	0.67	3.85	0.79	0.123
66	B	0.0668	0.22	4.23	0.79	0.123
67	B	0.0481	0.36	4.23	0.79	0.123
68	B	0.0259	0.48	4.23	0.79	0.123
69	B	0.1440	0.22	4.17	0.79	0.123
70	B	0.1119	0.37	4.17	0.79	0.123
71	B	0.1139	0.49	4.17	0.79	0.123
72	B	0.0785	0.64	4.17	0.79	0.123
73	B	0.0398	0.80	4.17	0.79	0.123
74	B	0.1283	0.20	4.44	0.79	0.123
75	B	0.1124	0.32	4.44	0.79	0.123
76	B	0.0928	0.44	4.44	0.79	0.123
77	B	0.0546	0.56	4.44	0.79	0.123
78	B	0.0156	0.70	4.44	0.79	0.123
79	B	0.1588	0.19	4.58	0.79	0.123
80	B	0.1239	0.30	4.58	0.79	0.123
81	B	0.0970	0.41	4.58	0.79	0.123
82	B	0.0632	0.53	4.58	0.79	0.123
83	B	0.0351	0.66	4.58	0.79	0.123
84	B	0.1660	0.24	4.00	0.79	0.123
85	B	0.1193	0.40	4.00	0.79	0.123
86	B	0.0909	0.54	4.00	0.79	0.123
87	B	0.0479	0.69	4.00	0.79	0.123
88	B	0.0142	0.87	4.00	0.79	0.123
89	B	0.0719	0.17	4.76	0.79	0.123
90	B	0.0432	0.28	4.76	0.79	0.123
91	B	0.0373	0.38	4.76	0.79	0.123
92	B	0.0275	0.49	4.76	0.79	0.123
93	B	0.0400	0.35	3.33	0.79	0.123
94	B	0.0154	0.57	3.33	0.79	0.123
95	B	0.0923	0.38	3.19	0.79	0.123
96	B	0.0287	0.62	3.19	0.79	0.123
97	B	0.1145	0.23	4.12	0.79	0.123
98	B	0.0631	0.37	4.12	0.79	0.123
99	B	0.0448	0.51	4.12	0.79	0.123
100	B	0.0061	0.65	4.12	0.79	0.123
101	B	0.0795	0.15	4.11	0.79	0.123
102	B	0.0519	0.28	4.11	0.79	0.123
103	B	0.0217	0.42	4.11	0.79	0.123
104	B	0.1459	0.18	4.61	0.79	0.123

TABLE A.3 (contd.)
TABULATED FIELD DATA

No.	Type	$h_{s*(max)}$	x_*	u_o	D	β
105	B	0.0962	0.30	4.61	0.79	0.123
106	B	0.0784	0.40	4.61	0.79	0.123
107	B	0.0553	0.52	4.61	0.79	0.123
108	B	0.0367	0.65	4.61	0.79	0.123
109	B	0.0651	0.22	4.19	0.79	0.123
110	B	0.0475	0.36	4.19	0.79	0.123
111	B	0.0299	0.49	4.19	0.79	0.123
112	B	0.0667	0.14	5.21	0.79	0.123
113	B	0.0450	0.23	5.21	0.79	0.123
114	B	0.0307	0.32	5.21	0.79	0.123
115	B	0.0098	0.41	5.21	0.79	0.123
116	B	0.0975	0.19	4.49	0.79	0.123
117	B	0.0466	0.32	4.49	0.79	0.123
118	B	0.0323	0.43	4.49	0.79	0.123
119	B	0.0140	0.55	4.49	0.79	0.123
120	B	0.0965	0.26	3.85	0.79	0.123
121	B	0.0620	0.43	3.85	0.79	0.123
122	B	0.0454	0.58	3.85	0.79	0.123
123	B	0.1409	0.23	4.15	0.79	0.123
124	B	0.0841	0.37	4.15	0.79	0.123
125	B	0.0610	0.50	4.15	0.79	0.123
126	B	0.0192	0.64	4.15	0.79	0.123
127	B	0.0936	0.24	3.99	0.79	0.123
128	B	0.0490	0.40	3.99	0.79	0.123
129	B	0.0332	0.54	3.99	0.79	0.123
130	B	0.0026	0.69	3.99	0.79	0.123
131	B	0.0836	0.07	7.61	0.79	0.123
132	B	0.0642	0.11	7.61	0.79	0.123
133	B	0.0401	0.24	7.61	0.79	0.123
134	B	0.1506	0.19	4.47	0.79	0.123
135	B	0.1137	0.32	4.47	0.79	0.123
136	B	0.0896	0.43	4.47	0.79	0.123
137	B	0.0710	0.55	4.47	0.79	0.123
138	B	0.0388	0.69	4.47	0.79	0.123
139	B	0.1112	0.17	4.73	0.79	0.123
140	B	0.0765	0.28	4.73	0.79	0.123
141	B	0.0616	0.38	4.73	0.79	0.123
142	B	0.0496	0.49	4.73	0.79	0.123
143	B	0.0273	0.62	4.73	0.79	0.123
144	B	0.0955	0.25	3.97	0.79	0.123
145	B	0.0662	0.40	3.97	0.79	0.123
146	B	0.0470	0.54	3.97	0.79	0.123
147	B	0.0141	0.70	3.97	0.79	0.123
148	B	0.1235	0.26	3.90	0.79	0.123
149	B	0.0618	0.42	3.90	0.79	0.123
150	B	0.0466	0.56	3.90	0.79	0.123
151	B	0.0857	0.21	4.26	0.79	0.123
152	B	0.0378	0.35	4.26	0.79	0.123
153	B	0.0231	0.47	4.26	0.79	0.123
154	B	0.0468	0.31	3.53	0.79	0.123
155	B	0.0263	0.51	3.53	0.79	0.123
156	B	0.0612	0.24	4.02	0.79	0.123

TABLE A.3 (contd.)
TABULATED FIELD DATA

No.	Type	$h_{s*(max)}$	x_*	u_o	D	β
157	B	0.0367	0.39	4.02	0.79	0.123
158	B	0.0181	0.53	4.02	0.79	0.123
159	B	0.0758	0.32	3.48	0.79	0.123
160	B	0.0118	0.53	3.48	0.79	0.123
161	B	0.0031	0.71	3.48	0.79	0.123
162	B	0.1593	0.13	4.17	0.41	0.128
163	B	0.1414	0.27	4.17	0.41	0.128
164	B	0.0953	0.42	4.17	0.41	0.128
165	B	0.0305	0.60	4.17	0.41	0.128
166	B	0.1636	0.13	4.11	0.41	0.128
167	B	0.0779	0.28	4.11	0.41	0.128
168	B	0.0585	0.43	4.11	0.41	0.128
169	B	0.0247	0.62	4.11	0.41	0.128
170	B	0.0903	0.20	3.29	0.41	0.128
171	B	0.0389	0.44	3.29	0.41	0.128
172	B	0.1346	0.09	4.83	0.41	0.128
173	B	0.0901	0.20	4.83	0.41	0.128
174	B	0.0972	0.31	4.83	0.41	0.128
175	B	0.0308	0.45	4.83	0.41	0.128
176	B	0.0321	0.58	4.83	0.41	0.128
177	B	0.1199	0.07	5.52	0.41	0.128
178	B	0.1118	0.16	5.52	0.41	0.128
179	B	0.0915	0.24	5.52	0.41	0.128
180	B	0.0598	0.34	5.52	0.41	0.128
181	B	0.0366	0.44	5.52	0.41	0.128
182	B	0.1357	0.12	4.34	0.41	0.128
183	B	0.0941	0.25	4.34	0.41	0.128
184	B	0.0494	0.39	4.34	0.41	0.128
185	B	0.0054	0.55	4.34	0.41	0.128
186	B	0.1129	0.13	4.15	0.41	0.128
187	B	0.0612	0.27	4.15	0.41	0.128
188	B	0.0304	0.42	4.15	0.41	0.128
189	B	0.0133	0.60	4.15	0.41	0.128
190	B	0.1533	0.10	4.62	0.41	0.128
191	B	0.0764	0.22	4.62	0.41	0.128
192	B	0.0095	0.63	4.62	0.41	0.128
193	B	0.1182	0.17	3.56	0.41	0.128
194	B	0.0514	0.37	3.56	0.41	0.128
195	B	0.0326	0.57	3.56	0.41	0.128
196	B	0.1597	0.16	3.76	0.41	0.128
197	B	0.1300	0.51	3.76	0.41	0.128
198	B	0.0553	0.74	3.76	0.41	0.128
199	B	0.0061	0.27	4.17	0.41	0.128
200	B	0.1084	0.14	3.92	0.41	0.128
201	B	0.0499	0.31	3.92	0.41	0.128
202	B	0.0382	0.47	3.92	0.41	0.128
203	B	0.0683	0.16	3.72	0.41	0.128
204	B	0.0219	0.34	3.72	0.41	0.128
205	B	0.0082	0.53	3.72	0.41	0.128
206	B	0.0717	0.14	3.90	0.41	0.128
207	B	0.0203	0.31	3.90	0.41	0.128
208	B	0.0111	0.48	3.90	0.41	0.128

TABLE A.3 (contd.)
TABULATED FIELD DATA

No.	Type	$h_{s*(max)}$	x_*	u_o	D	β
209	B	0.1913	0.14	3.81	0.29	0.134
210	B	0.1362	0.28	3.81	0.29	0.134
211	B	0.0724	0.43	3.81	0.29	0.134
212	B	0.0024	0.60	3.81	0.29	0.134
213	B	0.1354	0.12	4.09	0.29	0.134
214	B	0.1118	0.25	4.09	0.29	0.134
215	B	0.0887	0.38	4.09	0.29	0.134
216	B	0.0577	0.52	4.09	0.29	0.134
217	B	0.0057	0.65	4.09	0.29	0.134
218	B	0.1324	0.11	4.12	0.32	0.139
219	B	0.1115	0.22	4.12	0.32	0.139
220	B	0.0537	0.32	4.12	0.32	0.139
221	B	0.0186	0.44	4.12	0.32	0.139
222	B	0.0041	0.53	4.12	0.32	0.139
223	B	0.1777	0.15	3.56	0.32	0.139
224	B	0.1129	0.29	3.56	0.32	0.139
225	B	0.0630	0.43	3.56	0.32	0.139
226	B	0.0045	0.59	3.56	0.32	0.139
227	B	0.0039	0.70	3.56	0.32	0.139
228	B	0.0667	0.24	2.96	2.00	0.129
229	B	0.0327	0.43	2.96	2.00	0.129
230	B	0.2426	0.20	4.03	0.44	0.147
231	B	0.1566	0.33	4.03	0.44	0.147
232	B	0.1256	0.44	4.03	0.44	0.147
233	B	0.0497	0.56	4.03	0.44	0.147
234	B	0.0391	0.67	4.03	0.44	0.147
235	B	0.1420	0.13	5.12	0.44	0.147
236	B	0.1226	0.20	5.12	0.44	0.147
237	B	0.1130	0.28	5.12	0.44	0.147
238	B	0.0640	0.35	5.12	0.44	0.147
239	B	0.0600	0.42	5.12	0.44	0.147
240	B	0.1454	0.19	4.19	0.44	0.147
241	B	0.1042	0.30	4.19	0.44	0.147
242	B	0.0676	0.41	4.19	0.44	0.147
243	B	0.0108	0.52	4.19	0.44	0.147
244	B	0.1528	0.25	3.59	0.44	0.147
245	B	0.1243	0.41	3.59	0.44	0.147
246	B	0.0844	0.56	3.59	0.44	0.147
247	B	0.0210	0.70	3.59	0.44	0.147
248	B	0.1209	0.14	4.76	0.44	0.147
249	B	0.0810	0.23	4.76	0.44	0.147
250	B	0.0772	0.32	4.76	0.44	0.147
251	B	0.0306	0.40	4.76	0.44	0.147
252	B	0.0195	0.48	4.76	0.44	0.147
253	B	0.1983	0.16	4.55	0.44	0.147
254	B	0.1834	0.26	4.55	0.44	0.147
255	B	0.1642	0.35	4.55	0.44	0.147
256	B	0.0598	0.44	4.55	0.44	0.147
257	B	0.0600	0.53	4.55	0.44	0.147
258	B	0.0685	0.28	3.43	0.44	0.147
259	B	0.0325	0.45	3.43	0.44	0.147
260	B	0.1396	0.15	4.73	0.44	0.147

TABLE A.3 (contd.)
TABULATED FIELD DATA

No.	Type	$h_{s*(max)}$	x_*	u_o	D	β
261	B	0.0678	0.24	4.73	0.44	0.147
262	B	0.0606	0.32	4.73	0.44	0.147
263	B	0.0350	0.40	4.73	0.44	0.147
264	B	0.0257	0.49	4.73	0.44	0.147
265	B	0.1371	0.16	4.46	0.44	0.147
266	B	0.1075	0.27	4.46	0.44	0.147
267	B	0.0893	0.36	4.46	0.44	0.147
268	B	0.0474	0.46	4.46	0.44	0.147
269	B	0.0369	0.55	4.46	0.44	0.147
270	B	0.0788	0.43	2.76	0.44	0.147
271	B	0.0299	0.70	2.76	0.44	0.147
272	B	0.2888	0.16	4.59	0.44	0.147
273	B	0.2062	0.25	4.59	0.44	0.147
274	B	0.0938	0.43	4.59	0.44	0.147
275	B	0.0885	0.52	4.59	0.44	0.147
276	B	0.1115	0.35	3.08	0.44	0.147
277	B	0.0637	0.56	3.08	0.44	0.147
278	B	0.2046	0.12	5.27	0.44	0.147
279	B	0.0703	0.33	5.27	0.44	0.147
280	B	0.0734	0.39	5.27	0.44	0.147
281	B	0.1520	0.13	5.00	0.44	0.147
282	B	0.0826	0.21	5.00	0.44	0.147
283	B	0.0511	0.29	5.00	0.44	0.147
284	B	0.0107	0.36	5.00	0.44	0.147
285	B	0.0086	0.44	5.00	0.44	0.147
286	B	0.1371	0.29	3.87	0.44	0.147
287	B	0.0969	0.45	3.87	0.44	0.147
288	B	0.0650	0.60	3.87	0.44	0.147
289	B	0.0144	0.77	3.87	0.44	0.147
290	B	0.1265	0.24	4.28	0.44	0.147
291	B	0.0978	0.37	4.28	0.44	0.147
292	B	0.0657	0.49	4.28	0.44	0.147
293	B	0.0312	0.63	4.28	0.44	0.147
294	B	0.0218	0.74	4.28	0.44	0.147
295	B	0.1318	0.18	4.87	0.44	0.147
296	B	0.1257	0.29	4.87	0.44	0.147
297	B	0.0994	0.38	4.87	0.44	0.147
298	B	0.0508	0.48	4.87	0.44	0.147
299	B	0.0400	0.57	4.87	0.44	0.147
300	B	0.2372	0.27	4.02	0.44	0.147
301	B	0.2011	0.42	4.02	0.44	0.147
302	B	0.1381	0.56	4.02	0.44	0.147
303	B	0.0707	0.71	4.02	0.44	0.147
304	B	0.0572	0.83	4.02	0.44	0.147
305	B	0.1298	0.24	4.29	0.44	0.147
306	B	0.0545	0.37	4.29	0.44	0.147
307	B	0.0468	0.49	4.29	0.44	0.147
308	B	0.0892	0.22	4.44	0.44	0.147
309	B	0.0385	0.34	4.44	0.44	0.147
310	B	0.0316	0.46	4.44	0.44	0.147
311	B	0.0063	0.58	4.44	0.44	0.147
312	B	0.0454	0.30	3.78	0.44	0.147

TABLE A.3 (contd.)
TABULATED FIELD DATA

No.	Type	$h_{s*(max)}$	x_*	u_o	D	β
313	B	0.0310	0.47	3.78	0.44	0.147
314	B	0.0262	0.63	3.78	0.44	0.147
315	B	0.1285	0.27	4.80	0.31	0.135
316	B	0.1078	0.36	4.80	0.31	0.135
317	B	0.0923	0.46	4.80	0.31	0.135
318	B	0.0770	0.54	4.80	0.31	0.135
319	B	0.0814	0.10	6.21	0.31	0.135
320	B	0.0761	0.16	6.21	0.31	0.135
321	B	0.0602	0.22	6.21	0.31	0.135
322	B	0.0336	0.27	6.21	0.31	0.135
323	B	0.0148	0.32	6.21	0.31	0.135
324	B	0.1710	0.16	4.97	0.31	0.135
325	B	0.1125	0.43	4.97	0.31	0.135
326	B	0.0804	0.50	4.97	0.31	0.135
327	B	0.1018	0.24	4.09	0.31	0.135
328	B	0.0735	0.37	4.09	0.31	0.135
329	B	0.0315	0.50	4.09	0.31	0.135
330	B	0.1590	0.12	5.79	0.31	0.135
331	B	0.0894	0.31	5.79	0.31	0.135
332	B	0.0721	0.37	5.79	0.31	0.135
333	B	0.1868	0.21	4.38	0.31	0.135
334	B	0.1306	0.43	4.38	0.31	0.135
335	B	0.0954	0.55	4.38	0.31	0.135
336	B	0.0829	0.64	4.38	0.31	0.135
337	B	0.1378	0.21	4.36	0.31	0.135
338	B	0.1358	0.33	4.36	0.31	0.135
339	B	0.0860	0.44	4.36	0.31	0.135
340	B	0.0670	0.55	4.36	0.31	0.135
341	B	0.0364	0.65	4.36	0.31	0.135
342	B	0.1189	0.26	3.94	0.31	0.135
343	B	0.1027	0.40	3.94	0.31	0.135
344	B	0.0849	0.53	3.94	0.31	0.135
345	B	0.0344	0.68	3.94	0.31	0.135
346	B	0.1099	0.34	3.45	0.31	0.135
347	B	0.0754	0.52	3.45	0.31	0.135
348	B	0.0741	0.70	3.45	0.31	0.135
349	B	0.2068	0.24	4.11	0.31	0.135
350	B	0.1698	0.37	4.11	0.31	0.135
351	B	0.1204	0.49	4.11	0.31	0.135
352	B	0.1214	0.62	4.11	0.31	0.135
353	B	0.0703	0.73	4.11	0.31	0.135
354	B	0.2478	0.23	4.14	0.31	0.135
355	B	0.1899	0.36	4.14	0.31	0.135
356	B	0.1455	0.61	4.14	0.31	0.135
357	B	0.1106	0.72	4.14	0.31	0.135
358	B	0.1063	0.22	4.26	0.31	0.135
359	B	0.0719	0.34	4.26	0.31	0.135
360	B	0.0591	0.46	4.26	0.31	0.135
361	B	0.1387	0.18	4.71	0.31	0.135
362	B	0.1357	0.28	4.71	0.31	0.135
363	B	0.0948	0.37	4.71	0.31	0.135
364	B	0.0672	0.47	4.71	0.31	0.135

TABLE A.3 (contd.)
TABULATED FIELD DATA

No.	Type	$h_{s*(max)}$	x_*	u_o	D	β
365	B	0.0534	0.56	4.71	0.31	0.135
366	B	0.1258	0.14	5.32	0.31	0.135
367	B	0.0505	0.44	5.32	0.31	0.135
368	B	0.1437	0.14	5.25	0.31	0.135
369	B	0.1212	0.22	5.25	0.31	0.135
370	B	0.0862	0.38	5.25	0.31	0.135
371	B	0.0783	0.45	5.25	0.31	0.135
372	B	0.2343	0.26	3.91	0.31	0.135
373	B	0.1604	0.69	3.91	0.31	0.135
374	B	0.1122	0.81	3.91	0.31	0.135
375	B	0.2083	0.18	4.74	0.31	0.135
376	B	0.1053	0.47	4.74	0.31	0.135
377	B	0.0700	0.55	4.74	0.31	0.135
378	B	0.0820	0.31	3.57	0.31	0.135
379	B	0.0245	0.49	3.57	0.31	0.135
380	B	0.0623	0.19	4.62	0.31	0.135
381	B	0.0562	0.29	4.62	0.31	0.135
382	B	0.0494	0.39	4.62	0.31	0.135
383	B	0.0138	0.49	4.62	0.31	0.135
384	B	0.0032	0.58	4.62	0.31	0.135
385	B	0.0918	0.11	6.07	0.31	0.135
386	B	0.0646	0.17	6.07	0.31	0.135
387	B	0.0623	0.23	6.07	0.31	0.135
388	B	0.0502	0.29	6.07	0.31	0.135
389	B	0.0403	0.34	6.07	0.31	0.135
390	B	0.1604	0.27	3.83	0.31	0.135
391	B	0.0876	0.42	3.83	0.31	0.135
392	B	0.0850	0.57	3.83	0.31	0.135
393	B	0.0321	0.72	3.83	0.31	0.135
394	B	0.1520	0.20	3.24	0.46	0.093
395	B	0.1032	0.36	3.24	0.46	0.093
396	B	0.3511	0.14	3.88	0.46	0.093
397	B	0.1074	0.41	3.88	0.46	0.093
398	B	0.1226	0.52	3.88	0.46	0.093
399	B	0.1260	0.61	3.88	0.46	0.093
400	B	0.1957	0.18	3.37	0.46	0.093
401	B	0.1586	0.33	3.37	0.46	0.093
402	B	0.0070	0.54	3.37	0.46	0.093
403	B	0.2610	0.09	4.90	0.46	0.093
404	B	0.1620	0.25	4.90	0.46	0.093
405	B	0.0837	0.39	4.90	0.46	0.093
406	B	0.1863	0.14	3.81	0.46	0.093
407	B	0.1746	0.26	3.81	0.46	0.093
408	B	0.0787	0.42	3.81	0.46	0.093
409	B	0.0452	0.54	3.81	0.46	0.093
410	B	0.0248	0.64	3.81	0.46	0.093
411	B	0.1691	0.09	4.89	0.46	0.093
412	B	0.0997	0.26	4.89	0.46	0.093
413	B	0.0938	0.33	4.89	0.46	0.093
414	B	0.0477	0.39	4.89	0.46	0.093
415	B	0.1714	0.09	4.82	0.46	0.093
416	B	0.1015	0.26	4.82	0.46	0.093

TABLE A.3 (contd.)
TABULATED FIELD DATA

No.	Type	$h_{s*(max)}$	x_*	u_o	D	β
417	B	0.0706	0.34	4.82	0.46	0.093
418	B	0.0497	0.40	4.82	0.46	0.093
419	B	0.2606	0.10	4.52	0.46	0.093
420	B	0.1335	0.30	4.52	0.46	0.093
421	B	0.0815	0.45	4.52	0.46	0.093
422	B	0.2450	0.13	4.01	0.46	0.093
423	B	0.1004	0.38	4.01	0.46	0.093
424	B	0.0815	0.49	4.01	0.46	0.093
425	B	0.0673	0.58	4.01	0.46	0.093
426	B	0.2507	0.15	3.77	0.46	0.093
427	B	0.1583	0.26	3.77	0.46	0.093
428	B	0.0510	0.43	3.77	0.46	0.093
429	B	0.0469	0.55	3.77	0.46	0.093
430	P	0.0604	0.06	6.05	0.53	0.095
431	P	0.0441	0.11	6.05	0.53	0.095
432	P	0.0356	0.16	6.05	0.53	0.095
433	P	0.0205	0.21	6.05	0.53	0.095
434	P	0.0068	0.25	6.05	0.53	0.095
435	P	0.1437	0.14	3.76	0.53	0.095
436	P	0.1338	0.28	3.76	0.53	0.095
437	P	0.0660	0.40	3.76	0.53	0.095
438	P	0.0411	0.51	3.76	0.53	0.095
439	P	0.1336	0.16	3.55	0.53	0.095
440	P	0.0871	0.31	3.55	0.53	0.095
441	P	0.0294	0.45	3.55	0.53	0.095
442	P	0.0599	0.10	4.39	0.53	0.095
443	P	0.0237	0.21	4.39	0.53	0.095
444	P	0.0141	0.30	4.39	0.53	0.095
445	P	0.0588	0.07	5.41	0.53	0.095
446	P	0.0465	0.14	5.41	0.53	0.095
447	P	0.0321	0.21	5.41	0.53	0.095
448	P	0.0083	0.27	5.41	0.53	0.095
449	P	0.0039	0.32	5.41	0.53	0.095
450	P	0.0677	0.11	4.23	0.53	0.095
451	P	0.0264	0.22	4.23	0.53	0.095
452	P	0.0021	0.32	4.23	0.53	0.095
453	P	0.1266	0.25	2.85	0.53	0.095
454	P	0.0164	0.49	2.85	0.53	0.095
455	P	0.0729	0.11	4.35	0.53	0.095
456	P	0.0442	0.22	4.35	0.53	0.095
457	P	0.0100	0.32	4.35	0.53	0.095
458	P	0.0013	0.41	4.35	0.53	0.095
459	P	0.1111	0.16	3.60	0.53	0.095
460	P	0.0613	0.31	3.60	0.53	0.095
461	P	0.0067	0.46	3.60	0.53	0.095
462	P	0.1444	0.07	5.40	0.53	0.095
463	P	0.0918	0.14	5.40	0.53	0.095
464	P	0.0719	0.21	5.40	0.53	0.095
465	P	0.0370	0.27	5.40	0.53	0.095
466	P	0.0275	0.32	5.40	0.53	0.095
467	P	0.0684	0.12	4.17	0.53	0.095
468	P	0.0424	0.23	4.17	0.53	0.095

TABLE A.3 (contd.)
TABULATED FIELD DATA

No.	Type	$h_{s*(max)}$	x_*	u_o	D	β
469	P	0.0173	0.35	4.17	0.53	0.095
470	P	0.1082	0.11	4.33	0.53	0.095
471	P	0.0730	0.22	4.33	0.53	0.095
472	P	0.0334	0.32	4.33	0.53	0.095
473	P	0.0104	0.41	4.33	0.53	0.095
474	P	0.1119	0.07	5.77	0.41	0.128
475	P	0.0990	0.14	5.77	0.41	0.128
476	P	0.0924	0.22	5.77	0.41	0.128
477	P	0.0746	0.31	5.77	0.41	0.128
478	P	0.0692	0.10	4.62	0.41	0.128
479	P	0.0589	0.22	4.62	0.41	0.128
480	P	0.0402	0.34	4.62	0.41	0.128
481	P	0.1395	0.07	5.80	0.41	0.128
482	P	0.1109	0.14	5.80	0.41	0.128
483	P	0.0768	0.22	5.80	0.41	0.128
484	P	0.0550	0.31	5.80	0.41	0.128
485	P	0.0383	0.40	5.80	0.41	0.128
486	P	0.1042	0.16	3.73	0.41	0.128
487	P	0.0506	0.34	3.73	0.41	0.128
488	P	0.0144	0.52	3.73	0.41	0.128
489	P	0.0853	0.12	4.28	0.41	0.128
490	P	0.0663	0.26	4.28	0.41	0.128
491	P	0.0558	0.40	4.28	0.41	0.128
492	P	0.0239	0.57	4.28	0.41	0.128
493	P	0.0665	0.11	4.87	0.41	0.128
494	P	0.0839	0.21	4.87	0.41	0.128
495	P	0.0354	0.35	4.87	0.41	0.128
496	P	0.0168	0.48	4.87	0.41	0.128
497	P	0.0904	0.12	4.20	0.41	0.128
498	P	0.0706	0.27	4.20	0.41	0.128
499	P	0.0553	0.41	4.20	0.41	0.128
500	P	0.0195	0.59	4.20	0.41	0.128
501	P	0.0062	0.76	4.20	0.41	0.128
502	P	0.0806	0.30	4.93	0.41	0.128
503	P	0.0298	0.43	4.93	0.41	0.128
504	P	0.0084	0.55	4.93	0.41	0.128
505	P	0.0727	0.12	4.26	0.41	0.128
506	P	0.0554	0.26	4.26	0.41	0.128
507	P	0.0337	0.40	4.26	0.41	0.128
508	P	0.0175	0.57	4.26	0.41	0.128
509	P	0.0877	0.09	4.85	0.41	0.128
510	P	0.0632	0.20	4.85	0.41	0.128
511	P	0.0499	0.31	4.85	0.41	0.128
512	P	0.0069	0.44	4.85	0.41	0.128
513	P	0.0914	0.16	3.67	0.41	0.128
514	P	0.0536	0.35	3.67	0.41	0.128
515	P	0.0553	0.12	4.22	0.41	0.128
516	P	0.0226	0.27	4.22	0.41	0.128
517	P	0.1169	0.08	5.10	0.29	0.134
518	P	0.0905	0.16	5.10	0.29	0.134
519	P	0.0729	0.24	5.10	0.29	0.134
520	P	0.0311	0.33	5.10	0.29	0.134

TABLE A.3 (contd.)
TABULATED FIELD DATA

No.	Type	$h_{s*(max)}$	x_*	u_o	D	β
521	P	0.0083	0.42	5.10	0.29	0.134
522	P	0.1306	0.14	3.75	0.29	0.134
523	P	0.1348	0.29	3.75	0.29	0.134
524	P	0.1144	0.45	3.75	0.29	0.134
525	P	0.0670	0.62	3.75	0.29	0.134
526	P	0.1423	0.15	3.64	0.29	0.134
527	P	0.1024	0.31	3.64	0.29	0.134
528	P	0.0501	0.48	3.64	0.29	0.134
529	P	0.0863	0.15	3.72	0.29	0.134
530	P	0.0880	0.30	3.72	0.29	0.134
531	P	0.0665	0.46	3.72	0.29	0.134
532	P	0.0259	0.63	3.72	0.29	0.134
533	P	0.1709	0.13	3.93	0.29	0.134
534	P	0.1539	0.27	3.93	0.29	0.134
535	P	0.1319	0.41	3.93	0.29	0.134
536	P	0.0958	0.56	3.93	0.29	0.134
537	P	0.0277	0.71	3.93	0.29	0.134
538	P	0.1223	0.11	4.34	0.29	0.134
539	P	0.1012	0.22	4.34	0.29	0.134
540	P	0.0631	0.33	4.34	0.29	0.134
541	P	0.0414	0.46	4.34	0.29	0.134
542	P	0.1339	0.09	4.86	0.29	0.134
543	P	0.1028	0.18	4.86	0.29	0.134
544	P	0.0687	0.27	4.86	0.29	0.134
545	P	0.0444	0.37	4.86	0.29	0.134
546	P	0.0118	0.46	4.86	0.29	0.134
547	P	0.1092	0.11	4.22	0.29	0.134
548	P	0.0797	0.23	4.22	0.29	0.134
549	P	0.0407	0.35	4.22	0.29	0.134
550	P	0.0179	0.49	4.22	0.29	0.134
551	P	0.1007	0.12	4.15	0.29	0.134
552	P	0.0998	0.25	4.15	0.29	0.134
553	P	0.0465	0.39	4.15	0.29	0.134
554	P	0.0245	0.52	4.15	0.29	0.134
555	P	0.1352	0.25	2.84	0.29	0.134
556	P	0.0452	0.51	2.84	0.29	0.134
557	P	0.1411	0.10	4.49	0.29	0.134
558	P	0.1058	0.21	4.49	0.29	0.134
559	P	0.0785	0.31	4.49	0.29	0.134
560	P	0.0275	0.43	4.49	0.29	0.134
561	P	0.0055	0.54	4.49	0.29	0.134
562	P	0.1543	0.11	4.34	0.29	0.134
563	P	0.1341	0.22	4.34	0.29	0.134
564	P	0.0720	0.33	4.34	0.29	0.134
565	P	0.0464	0.46	4.34	0.29	0.134
566	P	0.0222	0.58	4.34	0.29	0.134
567	P	0.0684	0.17	3.40	0.29	0.134
568	P	0.0371	0.36	3.40	0.29	0.134
569	P	0.1241	0.10	4.44	0.29	0.134
570	P	0.1001	0.21	4.44	0.29	0.134
571	P	0.0655	0.32	4.44	0.29	0.134
572	P	0.0208	0.44	4.44	0.29	0.134

TABLE A.3 (contd.)
TABULATED FIELD DATA

No.	Type	$h_{s*(max)}$	x_*	u_o	D	β
573	P	0.0025	0.55	4.44	0.29	0.134
574	P	0.1144	0.11	4.22	0.29	0.134
575	P	0.1019	0.23	4.22	0.29	0.134
576	P	0.0417	0.35	4.22	0.29	0.134
577	P	0.0056	0.49	4.22	0.29	0.134
578	P	0.1299	0.09	4.64	0.29	0.134
579	P	0.0962	0.19	4.64	0.29	0.134
580	P	0.0860	0.29	4.64	0.29	0.134
581	P	0.0557	0.40	4.64	0.29	0.134
582	P	0.1070	0.17	3.30	0.32	0.139
583	P	0.0511	0.34	3.30	0.32	0.139
584	P	0.0049	0.50	3.30	0.32	0.139
585	P	0.1692	0.20	3.04	0.32	0.139
586	P	0.0545	0.40	3.04	0.32	0.139
587	P	0.0807	0.14	3.65	0.32	0.139
588	P	0.0325	0.28	3.65	0.32	0.139
589	P	0.0056	0.41	3.65	0.32	0.139
590	P	0.1126	0.15	3.52	0.32	0.139
591	P	0.0674	0.30	3.52	0.32	0.139
592	P	0.0115	0.44	3.52	0.32	0.139
593	P	0.0505	0.18	3.28	0.32	0.139
594	P	0.0200	0.34	3.28	0.32	0.139
595	P	0.0564	0.13	4.00	2.00	0.129
596	P	0.0230	0.24	4.00	2.00	0.129
597	P	0.0217	0.32	4.00	2.00	0.129
598	P	0.0150	0.39	4.00	2.00	0.129
599	S	0.1761	0.26	2.80	0.53	0.095
600	S	0.0518	0.51	2.80	0.53	0.095
601	S	0.1450	0.15	3.64	0.53	0.095
602	S	0.0888	0.30	3.64	0.53	0.095
603	S	0.0703	0.43	3.64	0.53	0.095
604	S	0.0130	0.54	3.64	0.53	0.095
605	S	0.1113	0.12	4.22	0.53	0.095
606	S	0.0814	0.23	4.22	0.53	0.095
607	S	0.0396	0.34	4.22	0.53	0.095
608	S	0.0627	0.11	4.32	0.53	0.095
609	S	0.0399	0.22	4.32	0.53	0.095
610	S	0.0199	0.32	4.32	0.53	0.095
611	S	0.0578	0.04	7.10	0.53	0.095
612	S	0.0506	0.08	7.10	0.53	0.095
613	S	0.0332	0.12	7.10	0.53	0.095
614	S	0.0173	0.15	7.10	0.53	0.095
615	S	0.0125	0.18	7.10	0.53	0.095
616	S	0.1174	0.15	3.71	0.53	0.095
617	S	0.0721	0.30	3.71	0.53	0.095
618	S	0.0441	0.44	3.71	0.53	0.095
619	S	0.0050	0.57	3.71	0.53	0.095
620	S	0.0998	0.16	3.59	0.53	0.095
621	S	0.0413	0.32	3.59	0.53	0.095
622	S	0.0098	0.47	3.59	0.53	0.095
623	S	0.1601	0.25	2.83	0.53	0.095
624	S	0.0714	0.49	2.83	0.53	0.095

TABLE A.3 (contd.)
TABULATED FIELD DATA

No.	Type	$h_{s*(max)}$	x_*	u_o	D	β
625	S	0.0899	0.15	3.63	0.53	0.095
626	S	0.0504	0.30	3.63	0.53	0.095
627	S	0.0208	0.43	3.63	0.53	0.095
628	S	0.0092	0.55	3.63	0.53	0.095
629	S	0.0856	0.24	2.90	0.53	0.095
630	S	0.0111	0.47	2.90	0.53	0.095
631	S	0.0343	0.12	4.06	0.53	0.095
632	S	0.0052	0.25	4.06	0.53	0.095
633	S	0.0495	0.11	4.37	0.53	0.095
634	S	0.0278	0.21	4.37	0.53	0.095
635	S	0.0101	0.32	4.37	0.53	0.095
636	S	0.0710	0.15	3.65	0.53	0.095
637	S	0.0232	0.31	3.65	0.53	0.095
638	S	0.0173	0.45	3.65	0.53	0.095
639	S	0.0363	0.13	3.99	0.53	0.095
640	S	0.0193	0.26	3.99	0.53	0.095
641	S	0.1692	0.06	5.84	0.41	0.128
642	S	0.1137	0.14	5.84	0.41	0.128
643	S	0.1253	0.21	5.84	0.41	0.128
644	S	0.0775	0.31	5.84	0.41	0.128
645	S	0.0482	0.39	5.84	0.41	0.128
646	S	0.0969	0.13	4.09	0.41	0.128
647	S	0.0593	0.28	4.09	0.41	0.128
648	S	0.0351	0.44	4.09	0.41	0.128
649	S	0.1737	0.13	4.14	0.41	0.128
650	S	0.0934	0.28	4.14	0.41	0.128
651	S	0.0877	0.42	4.14	0.41	0.128
652	S	0.0396	0.61	4.14	0.41	0.128
653	S	0.1339	0.13	4.11	0.41	0.128
654	S	0.0365	0.28	4.11	0.41	0.128
655	S	0.0137	0.43	4.11	0.41	0.128
656	S	0.1203	0.15	3.61	0.29	0.134
657	S	0.0860	0.32	3.61	0.29	0.134
658	S	0.0229	0.48	3.61	0.29	0.134
659	S	0.0771	0.10	4.37	0.32	0.139
660	S	0.0543	0.19	4.37	0.32	0.139
661	S	0.0202	0.29	4.37	0.32	0.139
662	S	0.0038	0.39	4.37	0.32	0.139
663	S	0.2463	0.17	3.72	0.40	0.150
664	S	0.2058	0.35	3.72	0.40	0.150
665	S	0.1407	0.60	3.72	0.40	0.150
666	S	0.2136	0.12	4.37	0.40	0.150
667	S	0.1281	0.25	4.37	0.40	0.150
668	S	0.1434	0.43	4.37	0.40	0.150
669	S	0.0335	0.62	4.37	0.40	0.150
670	S	0.1679	0.08	5.22	0.40	0.150
671	S	0.0743	0.30	5.22	0.40	0.150
672	S	0.0283	0.43	5.22	0.40	0.150
673	S	0.0160	0.55	5.22	0.40	0.150
674	S	0.3586	0.20	3.41	0.40	0.150
675	S	0.2371	0.41	3.41	0.40	0.150
676	S	0.1130	0.71	3.41	0.40	0.150

TABLE A.3 (contd.)
TABULATED FIELD DATA

No.	Type	$h_{s*(max)}$	x_*	u_o	D	β
677	S	0.1404	0.16	3.84	0.40	0.150
678	S	0.0589	0.33	3.84	0.40	0.150
679	S	0.0136	0.56	3.84	0.40	0.150
680	S	0.2064	0.09	5.03	0.40	0.150
681	S	0.1020	0.33	5.03	0.40	0.150
682	S	0.0597	0.47	5.03	0.40	0.150
683	S	0.0060	0.60	5.03	0.40	0.150
684	S	0.1551	0.19	3.47	0.40	0.150
685	S	0.0971	0.40	3.47	0.40	0.150
686	S	0.1888	0.11	4.64	0.40	0.150
687	S	0.1279	0.22	4.64	0.40	0.150
688	S	0.1044	0.38	4.64	0.40	0.150
689	S	0.0342	0.55	4.64	0.40	0.150
690	S	0.2034	0.15	3.87	0.40	0.150
691	S	0.0956	0.32	3.87	0.40	0.150
692	S	0.1132	0.55	3.87	0.40	0.150
693	S	0.1849	0.13	4.27	0.40	0.150
694	S	0.1324	0.26	4.27	0.40	0.150
695	S	0.0525	0.45	4.27	0.40	0.150
696	S	0.0037	0.65	4.27	0.40	0.150
697	S	0.0881	0.04	7.59	0.40	0.150
698	S	0.0372	0.20	7.59	0.40	0.150
699	S	0.0258	0.26	7.59	0.40	0.150
700	S	0.2782	0.15	3.91	0.40	0.150
701	S	0.1735	0.31	3.91	0.40	0.150
702	S	0.0349	0.54	3.91	0.40	0.150
703	S	0.1091	0.31	5.19	0.40	0.150
704	S	0.0599	0.44	5.19	0.40	0.150
705	S	0.0087	0.56	5.19	0.40	0.150
706	S	0.2430	0.12	4.31	0.40	0.150
707	S	0.1734	0.26	4.31	0.40	0.150
708	S	0.0977	0.44	4.31	0.40	0.150
709	S	0.0137	0.64	4.31	0.40	0.150
710	S	0.0948	0.18	3.59	0.40	0.150
711	S	0.0384	0.37	3.59	0.40	0.150
712	S	0.1528	0.10	4.93	0.40	0.150
713	S	0.0924	0.34	4.93	0.40	0.150
714	S	0.0541	0.49	4.93	0.40	0.150
715	S	0.0392	0.62	4.93	0.40	0.150
716	S	0.1514	0.10	4.73	0.40	0.150
717	S	0.1202	0.21	4.73	0.40	0.150
718	S	0.0912	0.37	4.73	0.40	0.150
719	S	0.0463	0.53	4.73	0.40	0.150
720	S	0.1996	0.13	4.19	0.40	0.150
721	S	0.1449	0.27	4.19	0.40	0.150
722	S	0.0715	0.47	4.19	0.40	0.150
723	S	0.0791	0.26	5.61	0.40	0.150
724	S	0.0418	0.37	5.61	0.40	0.150
725	S	0.0241	0.48	5.61	0.40	0.150
726	S	0.1238	0.11	4.67	0.40	0.150
727	S	0.0983	0.22	4.67	0.40	0.150
728	S	0.0793	0.38	4.67	0.40	0.150

TABLE A.3 (contd.)
TABULATED FIELD DATA

No.	Type	$h_{s*(max)}$	x_*	u_o	D	β
729	S	0.0181	0.54	4.67	0.40	0.150
730	S	0.1803	0.15	3.88	0.40	0.150
731	S	0.1256	0.32	3.88	0.40	0.150
732	S	0.0857	0.55	3.88	0.40	0.150
733	S	0.0167	0.78	3.88	0.40	0.150
734	S	0.2220	0.18	3.62	0.40	0.150
735	S	0.1518	0.37	3.62	0.40	0.150
736	S	0.0763	0.63	3.62	0.40	0.150
737	S	0.0213	0.90	3.62	0.40	0.150
738	S	0.1252	0.10	4.76	0.40	0.150
739	S	0.0997	0.21	4.76	0.40	0.150
740	S	0.0910	0.36	4.76	0.40	0.150
741	S	0.0385	0.52	4.76	0.40	0.150
742	S	0.0132	0.66	4.76	0.40	0.150
743	S	0.2182	0.11	4.51	0.40	0.150
744	S	0.1264	0.41	4.51	0.40	0.150
745	S	0.0369	0.58	4.51	0.40	0.150
746	S	0.0224	0.74	4.51	0.40	0.150
747	S	0.2738	0.19	3.52	0.40	0.150
748	S	0.2717	0.39	3.52	0.40	0.150
749	S	0.0866	0.67	3.52	0.40	0.150
750	S	0.1854	0.08	5.39	0.40	0.150
751	S	0.1167	0.28	5.39	0.40	0.150
752	S	0.0459	0.41	5.39	0.40	0.150
753	S	0.0398	0.52	5.39	0.40	0.150
754	S	0.2155	0.22	3.25	0.40	0.150
755	S	0.1332	0.45	3.25	0.40	0.150
756	S	0.0221	0.78	3.25	0.40	0.150
757	S	0.1308	0.26	3.00	0.40	0.150
758	S	0.0300	0.53	3.00	0.40	0.150
759	S	0.2343	0.13	4.30	0.40	0.150
760	S	0.1693	0.26	4.30	0.40	0.150
761	S	0.1097	0.45	4.30	0.40	0.150
762	S	0.0302	0.64	4.30	0.40	0.150
763	S	0.0038	0.81	4.30	0.40	0.150
764	S	0.2528	0.26	3.01	0.40	0.150
765	S	0.1416	0.53	3.01	0.40	0.150
766	S	0.1979	0.09	5.08	0.40	0.150
767	S	0.0885	0.32	5.08	0.40	0.150
768	S	0.0195	0.46	5.08	0.40	0.150
769	S	0.0061	0.58	5.08	0.40	0.150
770	S	0.2120	0.12	4.34	0.40	0.150
771	S	0.1317	0.26	4.34	0.40	0.150
772	S	0.0454	0.44	4.34	0.40	0.150
773	S	0.1447	0.12	4.41	0.40	0.150
774	S	0.0789	0.25	4.41	0.40	0.150
775	S	0.0189	0.42	4.41	0.40	0.150
776	S	0.2845	0.11	4.60	0.40	0.150
777	S	0.1739	0.39	4.60	0.40	0.150
778	S	0.0919	0.56	4.60	0.40	0.150
779	S	0.0398	0.71	4.60	0.40	0.150
780	S	0.2368	0.10	4.82	0.40	0.150

TABLE A.3 (contd.)
TABULATED FIELD DATA

No.	Type	$h_{s*(max)}$	x_*	u_o	D	β
781	S	0.1361	0.35	4.82	0.40	0.150
782	S	0.0533	0.51	4.82	0.40	0.150
783	S	0.0076	0.65	4.82	0.40	0.150
784	S	0.1439	0.24	3.01	2.00	0.129
785	S	0.1051	0.42	3.01	2.00	0.129
786	S	0.0719	0.57	3.01	2.00	0.129
787	S	0.0116	0.70	3.01	2.00	0.129
788	S	0.1004	0.22	3.13	2.00	0.129
789	S	0.0301	0.38	3.13	2.00	0.129
790	S	0.0973	0.18	3.43	2.00	0.129
791	S	0.0544	0.32	3.43	2.00	0.129
792	S	0.0426	0.44	3.43	2.00	0.129
793	S	0.0238	0.54	3.43	2.00	0.129
794	S	0.0988	0.11	4.42	2.00	0.129
795	S	0.0667	0.19	4.42	2.00	0.129
796	S	0.0528	0.26	4.42	2.00	0.129
797	S	0.0456	0.32	4.42	2.00	0.129
798	S	0.1348	0.12	4.15	2.00	0.129
799	S	0.0488	0.22	4.15	2.00	0.129
800	S	0.0417	0.30	4.15	2.00	0.129
801	S	0.0201	0.37	4.15	2.00	0.129
802	S	0.1138	0.34	2.50	2.00	0.129
803	S	0.0550	0.60	2.50	2.00	0.129
804	S	0.0838	0.14	3.95	2.00	0.129
805	S	0.0413	0.24	3.95	2.00	0.129
806	S	0.0408	0.33	3.95	2.00	0.129
807	S	0.0397	0.40	3.95	2.00	0.129
808	S	0.0157	0.48	3.95	2.00	0.129
809	S	0.0715	0.11	4.43	2.00	0.129
810	S	0.0459	0.19	4.43	2.00	0.129
811	S	0.0447	0.26	4.43	2.00	0.129
812	S	0.0206	0.32	4.43	2.00	0.129
813	S	0.1668	0.10	4.33	4.21	0.139
814	S	0.1170	0.21	4.33	4.21	0.139
815	S	0.0728	0.33	4.33	4.21	0.139
816	S	0.0134	0.43	4.33	4.21	0.139
817	S	0.1916	0.08	4.70	4.21	0.139
818	S	0.1595	0.18	4.70	4.21	0.139
819	S	0.1367	0.28	4.70	4.21	0.139
820	S	0.1366	0.37	4.70	4.21	0.139
821	S	0.1335	0.44	4.70	4.21	0.139
822	S	0.1750	0.11	4.52	4.21	0.139
823	S	0.1326	0.21	4.52	4.21	0.139
824	S	0.1029	0.31	4.52	4.21	0.139
825	S	0.0841	0.38	4.52	4.21	0.139
826	S	0.1141	0.04	7.18	4.21	0.139
827	S	0.0705	0.08	7.18	4.21	0.139
828	S	0.0632	0.12	7.18	4.21	0.139
829	S	0.0590	0.16	7.18	4.21	0.139
830	S	0.0418	0.19	7.18	4.21	0.139
831	S	0.1090	0.04	6.46	4.21	0.139
832	S	0.0849	0.10	6.46	4.21	0.139

TABLE A.3 (contd.)
TABULATED FIELD DATA

No.	Type	$h_{s*(max)}$	x_*	u_o	D	β
833	S	0.0761	0.15	6.46	4.21	0.139
834	S	0.0695	0.19	6.46	4.21	0.139
835	S	0.0484	0.23	6.46	4.21	0.139
836	S	0.1748	0.10	4.19	4.21	0.139
837	S	0.1440	0.23	4.19	4.21	0.139
838	S	0.0965	0.35	4.19	4.21	0.139
839	S	0.0778	0.46	4.19	4.21	0.139
840	S	0.0558	0.55	4.19	4.21	0.139

Type refers to initial wave type: B=bore P=plunge S=surge
D is given in mm

APPENDIX B

DERIVATION OF THE EQUATIONS FOR SWASH ON A NATURAL BEACH

The problem at hand is to solve for X_s in (B.1), which is

$$\frac{d^2X_s}{dt^2} + \frac{f}{8h_\delta}\left[\frac{dX_s}{dt}\right]^2 + g(\sin\beta) = 0 \qquad \text{(B.1)}$$

If the constants a and b are defined as

$$a = f/(8h_\delta) \qquad \text{and} \qquad b = g(\sin\beta) \qquad \text{(B.2)}$$

and we let $d^2X_s/dt^2 = U_s$ then (B.1) can be written more conveniently as

$$\frac{dU_s}{dt} = -aU_s^2 - b \qquad \text{(B.3)}.$$

After separating the variables we have

$$\frac{-dU_s}{aU_s^2+b} = dt \qquad \text{(B.4)},$$

then we may integrate:

$$-\int \frac{dU_s}{aU_s^2+b} = \int dt = t+C \qquad \text{(B.5)},$$

$$-\frac{1}{a}\int \frac{dU_s}{U_s^2+(b/a)} = t+C \qquad \text{(B.6)},$$

The standard integral

$$\int \frac{dy}{x^2+y^2} = \frac{1}{x} \tan^{-1}\left[\frac{y}{x} + C\right]$$

can be used to yield

$$\frac{-1}{\sqrt{(ab)}} \tan^{-1}\left[\frac{U_s}{\sqrt{(b/a)}}\right] = t+C \qquad (B.7),$$

so

$$U_s = \sqrt{(b/a)} \tan\left[-\sqrt{(a/b)}(t+C)\right] \qquad (B.8).$$

When $t=0$ then $U_s=u_o$, thus

$$C = \frac{-\tan^{-1}[u_o/\sqrt{(b/a)}]}{\sqrt{(ab)}} \qquad (B.9).$$

Substitution of (B.9) and (B.2) into (B.8) yields

$$\frac{dX_s}{dt} = U_s(t) = \left[\frac{8gh_\delta(\sin\beta)}{f}\right]^{0.5} \tan(F+G) \qquad (B.10),$$

where

$$F = -t\left[\frac{gf(\sin\beta)}{8h_\delta}\right]^{0.5} \qquad G = \tan^{-1}\left[\frac{u_o\sqrt{f}}{\sqrt{[8gh_\delta(\sin\beta)]}}\right] \qquad (B.11).$$

When $U_s=0$ then $t=t_{(max)}$, thus from (B.10);

$$t_{(max)} = \frac{G}{\left[\frac{gf(\sin\beta)}{8h_\delta}\right]^{0.5}} \qquad (B.12).$$

Continuing the same approach as that shown in Section 2.4.4, the following are obtained:

$$X_s(t) = \frac{8h_\delta}{f} \ln\left[\frac{\cos(F+G)}{\cos G}\right] \qquad (B.13),$$

$$Z_s = \frac{-8h_\delta(\sin\beta)}{f} \ln\cos\left[\tan^{-1}\frac{u_o\sqrt{f}}{\sqrt{[8gh_\delta(\sin\beta)]}}\right] \qquad (B.14),$$

$$L_s = Z_s/(\sin\beta) \qquad (B.15).$$

(B.10) to (B.15) constitute in this study, the equations for swash on a natural beach.